

# **Oceanic Crust Evolution: Constraints From Integrated Core-Log Studies**

Thesis submitted for the degree of  
Doctor of Philosophy  
at the University of Leicester

by

**Sarah Louise Haggas**

(BSc Geology, Birmingham, 1994)

(MSc Geochemistry, Leeds, 1995)

Department of Geology

University of Leicester

June 1999

UMI Number: U125500

All rights reserved

INFORMATION TO ALL USERS

The quality of this reproduction is dependent upon the quality of the copy submitted.

In the unlikely event that the author did not send a complete manuscript and there are missing pages, these will be noted. Also, if material had to be removed, a note will indicate the deletion.



UMI U125500

Published by ProQuest LLC 2013. Copyright in the Dissertation held by the Author.  
Microform Edition © ProQuest LLC.

All rights reserved. This work is protected against  
unauthorized copying under Title 17, United States Code.



ProQuest LLC  
789 East Eisenhower Parkway  
P.O. Box 1346  
Ann Arbor, MI 48106-1346

*To my family*

## **Acknowledgements**

I would like to express my thanks to the following individuals:

Acknowledgements must first go to my supervisors Dr Tim Brewer and Dr Peter Harvey who have provided valuable input and support throughout my time at Leicester. The project was kindly funded by the University of Leicester. Thanks also to the staff and students of the University of Leicester, in particular all the members of Borehole Research, and to the participants of ODP Leg 176 for looking after a first-time sailor.

Additional thanks must be made to Dr Gerry Iturrino and all at Lamont-Doherty Earth Observatory for the assistance on many aspects of geophysical wireline logging.

I would also like to thank all my friends, many of whom are some distance away, for cheering me up during those writing-up months.

Special thanks must go to my mum, dad and sister, Victoria, who are the best family in the whole world and without whom none of this would be possible. And finally a big thank-you to Mitch who has had to put up with a very stressed person over the past few months.

## Table of Contents

List of Figures	v
List of Tables	ix
List of Plates	ix
<b>CHAPTER 1: Introduction</b>	<b>1-1</b>
1.1. Background	1-1
1.1.1. A brief history of ocean drilling	1-1
1.1.2. Drilling into oceanic basement	1-3
1.1.3. Downhole logging in basement boreholes	1-3
1.2. Aims of project	1-4
1.3. Format of remainder of thesis	1-5
<b>CHAPTER 2: A review of oceanic crustal structure and geochemistry</b>	<b>2-1</b>
2.1. Introduction	2-1
2.2. Ocean crust structure	2-1
2.2.1. Geophysical data	2-2
2.2.2.1. Seismic data	2-2
2.2.2.2. Gravity data	2-6
2.2.2. Ophiolite complexes	2-6
2.2.3. Dredging of the ocean floor	2-10
2.2.4. Drilling and downhole logging of boreholes	2-11
2.3. Basalt forms erupted at spreading centres	2-12
2.3.1. Pillow lavas	2-12
2.3.2. Sheet flows	2-15
2.3.3. Hyaloclastites and other breccias	2-15
2.3.4. Distribution of flow types on mid-ocean ridges	2-17
2.3.5. Factors affecting the morphology of submarine lava flows	2-18
2.3.5.1. Experimental modelling of lava flow morphologies	2-18
2.3.5.2. Effect of spreading rate on flow morphology	2-19
2.4. Morphology of spreading centres	2-21
2.4.1. Slow-spreading ridges	2-21
2.4.2. Fast-spreading ridges	2-23
2.4.3. Intermediate-spreading ridges	2-24
2.4.4. Seamounts	2-25
2.5. Mid-ocean ridge basalt (MORB) geochemistry	2-28
2.5.1. Origin of MORB	2-29
2.5.2. Regional variations in MORB geochemistry	2-32
2.5.3. Local variations in MORB geochemistry	2-32
2.5.4. Magma chamber models	2-33
2.5.4.1. The effect of spreading rate on magma chamber development	2-36

2.5.4.2. RTF magma chambers	2-41
2.5.5. Seamount Geochemistry	2-41
2.6. Summary	2-44
<b>CHAPTER 3 : Reconstructing the upper oceanic crust using core and log data: Case Study 1 : ODP Hole 896A</b>	<b>3-1</b>
3.1. Introduction	3-1
3.2. Geological Background	3-3
3.3. Core Recovery	3-3
3.4. Lithologies recovered from Hole 896A	3-5
3.4.1. Brecciated units in Hole 896A	3-7
3.4.1.1. Breccia Type A	3-8
3.4.1.2. Breccia Type B	3-8
3.4.1.3. Breccia Type C	3-10
3.4.2. Stratigraphical log of Hole 896A from core descriptions	3-12
3.4.2.1. Comparison with shipboard core descriptions	3-12
3.5. Logging tools deployed on Hole 896A	3-15
3.5.1. Construction of a stratigraphical log for Hole 896A using log data	3-15
3.5.2. Comparison of stratigraphical logs derived from FMS data and core descriptions	3-20
3.6. Lithological variability in ODP Hole 896A	3-26
3.6.1. Variations in lithology with distance from the ridge axis	3-27
3.6.2. Sedimentary, tectonic or volcanic breccias?	3-27
3.6.2.1. Possible presence of an active fault zone in Hole 896A	3-28
3.6.3. Variations in magnetic properties of the Hole 896A core	3-29
3.7. Mineralogy	3-30
3.7.1. Review of shipboard scientific party results	3-30
3.7.2. Results from this study	3-31
3.7.2.1. Primary mineralogy	3-31
3.7.2.2. Alteration	3-33
3.7.2.3. Variation in mineralogy with lithology	3-33
3.8. Geochemistry	3-34
3.8.1. Major element geochemistry	3-34
3.8.2. Trace element geochemistry	3-42
3.8.3. Alteration	3-45
3.8.4. Discussion	3-49
3.8.4.1. Division into chemical units	3-49
3.8.4.2. Comparison of geochemical and lithological variations	3-50
3.8.4.3. RTF magma chambers	3-52
3.8.4.4. The clinopyroxene “paradox”	3-53
3.9. Development of Hole 896A crustal section	3-54

3.9.1. Variations in depth of magma chamber	3-54
3.10. Summary	3-54
<b>CHAPTER 4: Reconstructing the upper oceanic crust using core and log data. Case Study 2: ODP Hole 504B</b>	<b>4-1</b>
4.1. Introduction	4-1
4.2. Previous legs	4-1
4.3. Lithological units	4-4
4.4. Log data	4-4
4.4.1. Construction of a lithostratigraphical log for Hole 504B	4-5
4.4.2. Comparison with lithostratigraphy with Hole 896A	4-9
4.5. Mineralogy	4-13
4.6. Geochemistry	4-14
4.6.1. Basalt types	4-15
4.6.2. Major element variations	4-15
4.6.3. Trace element variations	4-22
4.6.4. Alteration	4-26
4.6.5. Discussion	4-28
4.6.5.1. Origin of different basalt types in Hole 504B	4-28
4.6.5.2. Correlation of lithological and geochemical variations	4-28
4.6.5.3. Comparison of geochemistry and mineralogy with Hole 896A	4-28
4.7. Summary	4-35
<b>CHAPTER 5: Applications of downhole logs in basement cores with high core recovery. Case Study 3: ODP Hole 735B</b>	<b>5-1</b>
5.1. Introduction	5-1
5.2. Geological background	5-2
5.3. Summary of Leg 118 results	5-4
5.3.1. Lithological units	5-4
5.3.1.1. Redefinition of Leg 118 unit boundaries	5-5
5.3.2. Mineralogy	5-7
5.3.3. Geochemistry	5-10
5.3.4. Structural features and deformation in the Leg 118 core	5-10
5.3.5. Logging data	5-10
5.3.6. Models for crustal structure at Site 735B	5-11
5.4. Summary of Leg 176 results	5-13
5.4.1. Lithological units recovered on Leg 176	5-13
5.4.2. Structural geology of the Leg 176 core	5-15

5.4.3. Downhole logging on Leg 176	5-16
5.4.3.1. Logging results	5-17
5.4.3.2. FMS data	5-20
5.4.4. Core imaging	5-20
5.4.4.1. Imaging of Leg 118 core	5-27
5.4.4.2. Applications of the core image data and log data	5-27
5.4.5. Mineralogy	5-37
5.4.6. Geochemistry	5-39
5.4.6.1. Review of shipboard scientific party results	5-39
5.4.6.2. Results from this study	5-40
5.5. Summary	5-46
<b>CHAPTER 6: Conclusions and recommendations for future work</b>	<b>6-1</b>
6.1. Summary and conclusions	6-1
6.1.1. Lithological variability in the upper ocean crust	6-1
6.1.2. Core-log techniques in basement holes with relatively high core recovery	6-3
6.2. Suggested further work	6-4
Appendix A	
Appendix B	
Appendix C	
Appendix D	
Appendix E	
References	

## List of Figures

Figure 1.1	Location of ODP/DSDP drill sites, 1968-1998	1-2
Figure 2.1.	Location of major spreading centres	2-3
Figure 2.2.	Schematic oceanic crustal structure	2-5
Figure 2.3.	Comparison of the variation in bulk resistivity downhole, crustal velocity structure and lithostratigraphy in Hole 504B	2-7
Figure 2.4.	Schematic sections of various ophiolites	2-8
Figure 2.5.	Three-dimensional and cross-sectional views of a branching “pillow” lava	2-13
Figure 2.6.	Evolution of collapse features	2-16
Figure 2.7.	Areal ratio sheet basalt / pillow basalt versus spreading rate on axial zones of spreading ridges	2-20
Figure 2.8.	Deep tow profiles of fast-spreading, intermediate-spreading and slow-spreading ridges	2-22
Figure 2.9.	Cross-sectional ridge shapes of the East Pacific Rise	2-23
Figure 2.10.	Cross-section of the Galapagos Rift near 86°10', based on side-looking sonar and deep-tow data	2-26
Figure 2.11.	Schematic drawing of mantle pressure versus temperature and schematic cross-section of ocean crust and mantle	2-31
Figure 2.12.	Schematic diagram of a simplistic dome or “onion”-shaped magma chamber	2-34
Figure 2.13.	“Funnel”-shaped magma chamber model	2-34
Figure 2.14.	Model of a magma chamber along a fast-spreading ridge	2-35
Figure 2.15.	‘Infinite leek’ model of a subaxial magma chamber beneath a slow-spreading ridge	2-38
Figure 2.16.	Model in which the crust is constructed of seamounts and fissure-fed flows	2-40
Figure 2.17.	Two-element variation diagram showing the decoupling effect of evolution in a RTF magma chamber	2-42
Figure 3.1.	Location of ODP Holes 896A and 504B	3-2
Figure 3.2.	Lithostratigraphical log of Hole 896A derived from visual core descriptions	3-13
Figure 3.3.	Lithostratigraphical log of Hole 896A derived from FMS data	3-16
Figure 3.4.	Downhole resistivity data for Hole 896A	3-17
Figure 3.5.1.	FMS image showing massive basalt in Hole 896A	3-18

Figure 3.5.2.	FMS image showing pillow lavas in Hole 896A	3-20
Figure 3.5.3.	FMS image showing brecciated units in Hole 896A	3-21
Figure 3.5.4.	FMS image of a basalt flow	3-23
Figure 3.6.	Comparison between lithostratigraphical logs	3-24
Figure 3.7.	Variation of major oxides with depth in Hole 896A	3-35
Figure 3.8 (a)	Al <sub>2</sub> O <sub>3</sub> versus depth for Hole 896A	3-38
Figure 3.8 (b)	Al <sub>2</sub> O <sub>3</sub> versus MgO for Hole 896A	3-38
Figure 3.9 (a)	CaO versus depth for Hole 896A	3-39
Figure 3.9 (b)	CaO versus MgO for Hole 896A	3-39
Figure 3.10 (a)	TiO <sub>2</sub> versus depth for Hole 896A	3-41
Figure 3.10 (b)	TiO <sub>2</sub> versus MgO for Hole 896A	3-41
Figure 3.11.	Variations in selected trace elements with depth downhole	3-42
Figure 3.12 (a)	Ni versus depth for Hole 896A	3-44
Figure 3.12 (b)	Ni versus MgO for Hole 896A	3-44
Figure 3.13 (a)	Nb/Zr for Hole 896A samples	3-45
Figure 3.13 (b)	Nb/Y versus Zr/Y for Hole 896A samples	3-45
Figure 3.14 (a)	Variation in S with depth in Hole 896A	3-47
Figure 3.14 (b)	Variation in K <sub>2</sub> O with depth in Hole 896A	3-47
Figure 3.15.	Comparison of downhole variations in geochemistry with lithology in Hole 896A	3-50
Figure 3.16.	Zr versus Ni for Hole 896A basalts	3-52
Figure 4.1.	Drilling history and lithostratigraphy of ODP Hole 504B	4-2
Figure 4.2.	Example of FMS data from Hole 504B showing the relatively poor quality of the data obtained	4-6
Figure 4.3.	Caliper and resistivity downhole logs for Hole 504B	4-7
Figure 4.4.	Lithostratigraphical log of Hole 504B using log data and shipboard core descriptions	4-8
Figure 4.5.	Comparison of lithostratigraphical logs produced for this study and by Ayadi <i>et al.</i> (1998).	4-10
Figure 4.6.	Comparison of lithostratigraphical logs from ODP Holes 504B and 896A	4-11
Figure 4.7.	Zr vs. Nb for Hole 504B basalts	4-16
Figure 4.8.	Variation of Zr with depth for ODP Hole 504B	4-17
Figure 4.9.	Major elements versus depth downhole for Hole 504B	4-19
Figure 4.10.	Major elements versus depth downhole for Hole 504B	4-20
Figure 4.11.	Major oxides versus MgO for Hole 504B	4-21
Figure 4.12.a	TiO <sub>2</sub> versus depth downhole for Hole 504B	4-23

Figure 4.12.b	TiO <sub>2</sub> versus MgO for Hole 504B	4-23
Figure 4.13.a	Ni versus depth downhole for Hole 504B	4-24
Figure 4.13.b	Ni versus MgO for Hole 504B	4-24
Figure 4.14.	Zr / Y versus Nb / Y for Hole 504B basalts	4-25
Figure 4.15.	Variation of K <sub>2</sub> O with depth for ODP Hole 504B	4-27
Figure 4.16.	Comparison of lithostratigraphy with variation in MgO for Hole 504B	4-29
Figure 4.17.	Comparison of lithostratigraphy with variation in TiO <sub>2</sub> for Hole 504B	4-30
Figure 4.18.	Comparison of downhole geochemistry of Holes 504B and 896A	4-33
Figure 5.1.	Location of Site 735B	5-3
Figure 5.2.	Lithostratigraphy of Hole 735B drilled on Leg 118	5-6
Figure 5.3.	Models for crustal structure at Site 735B	5-12
Figure 5.4.	Lithostratigraphy of ODP Hole 735B	5-14
Figure 5.5.	Downhole logs for Hole 735B	5-18
Figure 5.6.	Downhole logs for the borehole section drilled during Leg 176	5-19
Figure 5.7.	FMS image showing a Fe-Ti oxide olivine gabbro layer within olivine gabbro	5-21
Figure 5.8.	FMS image showing modal layering in Fe-Ti oxide gabbros	5-22
Figure 5.9.	FMS image showing a conductive fracture in olivine gabbro	5-23
Figure 5.10.	Unrolled core image of massive olivine gabbro containing a 2 cm thick felsic vein	5-24
Figure 5.11.	Unrolled core image of laminated olivine gabbro with shallowly dipping bands of Fe-Ti oxide olivine clinopyroxenite and net-veined trondhjemite gabbro.	5-25
Figure 5.12.	Unrolled core image of disseminated Fe-Ti oxide olivine microgabbro containing a 0.2 - 0.6 mm thick plagioclase + amphibole veins and small-scale fractures	5-26
Figure 5.13.	Core 99R-4 from ODP Hole 735B prior to integration into core barrel lengths	5-28
Figure 5.14.	Reconstructed core barrel of Core 99R-4 from ODP Hole 735B using the DMT software CoreLog™	5-29
Figure 5.15.	Example of a reconstructed core piece from the Hole 735B core drilled on Leg 118 (Sample 118-735B-28R-1 #7)	5-30
Figure 5.16	Core 77R-2 from ODP Hole 735B	5-34
Figure 5.17.	FMS image showing a conductive fracture in olivine gabbro	5-35

Figure 5.18.	Orientation and location of the fractured piece in Core 77R-2 according to the information provided by the FMS data	5-36
Figure 5.19.	Downhole variations in major oxides for Hole 735B	5-41
Figure 5.20.	Downhole variation in trace elements for Hole 735B	5-43
Figure 5.21.	Comparison of downhole log data and geochemistry	5-47

### **List of Tables**

Table 1.1.	Principal applications of downhole logs	1-4
Table 2.1.	Seismic velocities of ocean crustal layers	2-4
Table 2.2.	Experimental morphologies of lava flows	2-20
Table 3.1.	Core recovery for ODP Hole 896A	3-4
Table 3.2.	Criteria for identification of lithological units from Hole 896A	3-7
Table 3.3.	Relative proportions of lithological units in ODP Hole 896A calculated from the shipboard core descriptions and the new core descriptions made for this study	3-14
Table 3.4.	Criteria for identification of lithological units using FMS images	3-18
Table 3.5.	Comparison of lithological logs for ODP Hole 896A	3-20
Table 4.1.	Summary of ODP Hole 504B drilling legs	4-3
Table 4.2.	Proportions of lithological units in the volcanic section of ODP Hole 504B	4-9
Table 4.3.	Chemical compositions of Hole 504B basalts	4-15
Table 4.4.	Comparison of Holes 504B and 896A	4-32
Table 5.1.1.	Core recovery in Hole 735B for Leg 118	5-31
Table 5.1.2.	Core recovery in Hole 735B for Leg 176	5-32

### **List of Plates**

Plate 3.1.	Small pillow lava from ODP Hole 896A (Sample 148-896A-11R-1 #1)	3-6
Plate 3.2.	Massive unit from Hole 896A (Sample 148-896A-16R-2 # 1)	3-6
Plate 3.3.	Hyaloclastite breccia (Type A) from Hole 896A (Sample 148-896A-14R-1 #5)	3-9
Plate 3.4.	“Jigsaw-puzzle” breccia (Type B) from Hole 896A (Sample 148-896A-18R-2 #3)	3-11
Plate 3.5.	Polymict, matrix-supported breccia (Type C) from Hole 896A (Sample 148-896A-27R-2 #5)	3-11

Plate 3.6.	Intergranular texture in a massive basalt from Hole 896A (Sample 896-19)	3-32
Plate 3.7.	Glomerocrysts of plagioclase in a pillow lava from Hole 896A (Sample 896-6)	3-32
Plate 5.1.	Thin-section photomicrograph in cross-polarised light of an olivine gabbro with ophitic texture (735-12)	5-9
Plate 5.2.	Thin-section photomicrograph in cross-polarised light of alteration and replacement by secondary minerals in a troctolite from ODP Hole 735B (735-13)	5-9
Plate 5.3.	Thin-section photomicrograph in cross-polarised light of a foliated microgabbro (HAG-15).	5-38
Plate 5.4.	Thin-section photomicrograph in cross-polarised light of the contact between a Fe-Ti oxide gabbro and an olivine gabbro (HAG-10)	5-38

# CHAPTER 1

---

## *Introduction*

### **1.1. Background**

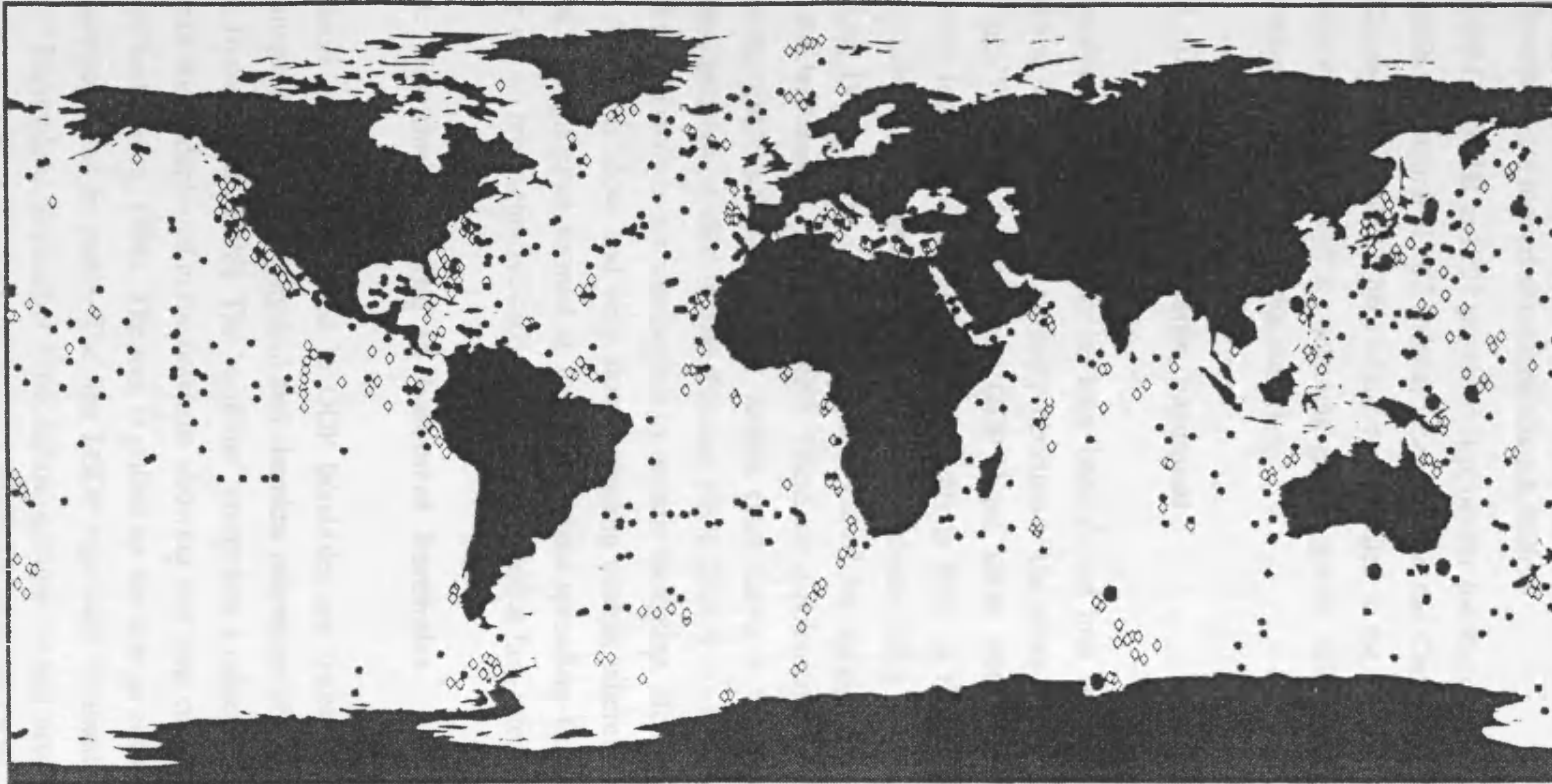
The ocean crust comprises greater than two-thirds of the surface of the Earth, however, investigation of the architecture of the ocean crust is complicated by the relative inaccessibility of its location in deep water, excluding most methods of direct sampling and observation.

Deep ocean drilling by the Deep Sea Drilling Project (DSDP) and Ocean Drilling Program (ODP) have enabled the recovery of *in situ* basement sections, allowing more detailed investigation into the processes operating at mid-ocean ridges. Unfortunately the usefulness of borehole drilling is restricted by the low core recovery experienced in the majority of basement boreholes. This severely restricts the interpretation of the ocean crust lithostratigraphy as many lithological units may be underrepresented in the core or not recovered at all. Even in cores with high core recovery, complications arise due to the fact that the recovered cores are unorientated with respect to grid North. Hence any veins, foliations or other structural features are unorientated, providing complications with the inference of tectonic setting for a particular borehole.

#### **1.1.1. A brief history of ocean drilling**

Most ocean crust drilling has been achieved by the Ocean Drilling Program (ODP) and its predecessor the Deep Sea Drilling Program (DSDP). The DSDP commenced in 1968 and in the period from 1968 to 1983 drilled 1092 boreholes, recovering approximately 112 km of core (ODP, 1998). It was succeeded in 1985 by the ODP, using a more technologically advanced vessel, the JOIDES Resolution (ODP, 1998). The sites of all the DSDP / ODP Holes drilled between 1968 and 1998 are indicated in Figure 1.1.

Notable discoveries made during the two program's long histories include the following examples:



- Deep Sea Drilling Project (DSDP) Sites
- ◊ Ocean Drilling Program (ODP) Sites
- Scheduled Legs FY'99 / FY'00

**Figure 1.1.** ODP and DSDP drill sites, 1968 - 1998, (after ODP, 1998).

- One of the most significant discoveries in ocean drilling occurred during DSDP Leg 3 in 1968 to 1969 (Maxwell *et al.*, 1970). This leg drilled 17 boreholes at 10 sites near to the Mid-Atlantic Ridge and found that the age of the crust increased systematically with distance from the ridge axis. This effectively proved Alfred Wegener's "continental drift" theory that the continents moved in relation to each other.
- ODP Leg 171B in 1997 provided support for the theory that a large meteorite impacted the Earth approximately 65 million years ago, at the Cretaceous / Tertiary boundary (Norris, Kroon *et al.*, 1998). Three of the cores drilled in the Atlantic Ocean during this leg contain layers of impact ejecta containing graded green, silica-rich, glassy globules, or tektites, derived from the meteorite impact.

### 1.1.2. Drilling into oceanic basement

The majority of ODP boreholes have been drilled into sediments, with basement boreholes providing samples of only a small proportion of the upper ocean crust. The deepest holes drilled into "true" oceanic basement are ODP Holes 504B, 896A, 332B, 395A, 418A and 735B, extensive logs and downhole measurements in three of these hole (Holes 395A, 504B and 418A) have led to them being regarded as reference holes for the upper ocean crust structure (Becker, 1990). Hole 332B cannot be revisited for logging, the re-entry cone has separated from the hole casing (Becker, 1990). These are supplemented by data from Hole 735B which penetrates gabbros from the lower oceanic crust (Layer 3) and represents the largest section of plutonic basement drilled to date (Becker, 1990; Dick *et al.*, 1997). Unfortunately the full range of spreading rates is not represented in oceanic basement, Holes 395A, 418A and 735B are in crust formed at slow and very slow-spreading centres whereas Holes 504B and 896A were drilled through crust formed at the intermediate-spreading Costa Rica Rift (Becker, 1990). There are no representative sections of crust formed at fast-spreading ridges.

### 1.1.3. Downhole logging in basement boreholes

The most common logs used in ODP boreholes are wireline logs which provide a nearly continuous record of the physical and chemical properties of the borehole walls (Worthington, 1994; Brewer *et al.*, 1998). The "wireline" comprises a cable which extends from the ship to a probe or sonde deployed in the borehole allowing real time communication from the tool to the ship (Worthington, 1994). The tool is pulled up the hole at constant speed, hence, continuous measurements can be made. The first DSDP logs were obtained from a borehole to the north-west of Bermuda in September 1968, natural gamma ray and neutron porosity logs were run in the drillpipe. The logging program was formalised when the ODP succeeded the DSDP in 1985 and the Formation Microscanner (FMS) was added to the standard logging suite in 1989.

Downhole logs are extremely valuable in ocean boreholes due to three main reasons (Worthington, 1994):

- in cores with low and / or erratic recovery, large sections of core may not be recovered. This is particularly a problem for hard sediments or igneous basement rocks which are too hard to be piston-cored and break relatively easily,
- borehole measurements are taken at *in situ* temperature and pressure whereas core measurements are made at surface conditions,
- downhole logging measurements are made at a greater scale than core measurements.

The applications of downhole logs are varied and summarised in Table 1.1. Applications include (a) global environmental change (for estimation of any changes a continuous downhole record is required so that cyclic variations in sediments can be seen, allowing palaeoclimatology and ocean circulation patterns to be investigated), (b) composition and structure of oceanic crust, particularly in basement boreholes with low core recovery, allowing investigation of the origin and evolution of the oceanic crust, (c) hydrogeology and (d) global stress regime (Worthington, 1994).

Principal Applications Downhole Measurement	Economic Geology	Geochemistry	Geothermics	Hydrogeology	Palaeoclimatology	Petrology / Sedimentology	Seismology	Stratigraphy	Structural Geology	Tectonics
Electrical Imaging					*	*			*	*
Acoustic Waveform					*	*	*	*	*	
Electrical Resistivity				*	*	*		*	*	
Neutron Porosity				*	*	*		*		
Temperature			*	*						
Natural Radioactivity	*	*			*	*		*		
Geochemical	*	*			*	*		*		
Susceptibility					*	*		*		

**Table 1.1.** Principal applications of downhole logging data, adapted from Worthington (1991).

Difficulties in calibration of downhole logs in basement boreholes, however, arise due to two main factors (Becker, 1990):

- the low core recovery experienced in many basement boreholes means that the position of many core pieces is uncertain. Hence, it is often difficult to correlate core and log properties,
- many of the logging tools used by the ODP were developed for use in sediments rather than oceanic basement, a particular complication for log interpretation in irregular boreholes.

## **1.2. Aims of project**

This research project has two main aims:

1) To supplement the core data in boreholes with poor core recovery with downhole logging data in order to reconstruct the lithological architecture of the crust. In many basement boreholes core recovery is low due to the resistant nature of igneous rocks, in these holes important lithological boundaries may not be recovered and many lithologies may be underrepresented in the core or be absent hence reconstruction of the lithological architecture cannot rely on core data alone. In this case integration of core and downhole logging data is essential for reconstruction of the borehole lithostratigraphy. Two case studies have been used for this purpose, ODP Holes 896A and 504B in the equatorial East Pacific, which penetrate 495 and 2111 m into upper oceanic basement respectively. In both holes core recovery is low (< 30 %) but good quality downhole logging data is available for Hole 896A, allowing the lithostratigraphy to be reconstructed and compared with the visual core descriptions. The reconstructed lithostratigraphy can then be compared to the geochemical and mineralogical core data in an attempt to constrain the lithological diversity observed in the upper oceanic crust.

2) In cores with relatively high core recovery, reconstruction of the lithostratigraphy is largely unnecessary. In the third case study in this thesis, some applications of log data in cores with high core recovery are presented. In particular, the correlation of core data and log data has been used to accurately locate and orientate a small number of core pieces within the Hole 735B core and a broad overview of the downhole geochemistry is compared with the log data.

## **1.3. Format of remainder of thesis**

The format of the remainder of this thesis is as follows. Chapter 2 provides a review of the available literature on oceanic crustal structure and geochemistry, concentrating on the methods used for investigating ocean crust structure, the morphology of mid-ocean ridges and the types of lava flow morphology erupted there and an overview of mid-ocean ridge basalt

geochemistry. Chapters 3 to 5 deal with case studies from three ocean crust basement boreholes in which core-log integration studies have been attempted. Chapter 3 is concerned with ODP Hole 896A, drilled through the volcanic section (Layer 2A). The first part of Chapter 3 details the reconstruction of the lithostratigraphy of ODP Hole 896A using core and log data, and discusses the processes responsible for this variation. The second part of Chapter 3 is concerned with the geochemistry and mineralogy of the Hole 896A core and its relationship to the observed lithological variations. Chapter 4 comprises a case study of ODP Hole 504B which comprises a complete volcanic section of the ocean crust. The lithostratigraphy of the core are discussed and the hole is compared to Hole 896A, both in terms of lithostratigraphy and geochemistry. Chapter 5 discusses the applications of core-log integration in ODP Hole 735B, a basement borehole with high core recovery. A method for accurate location and orientation of core pieces is presented. A summary of the work completed, with conclusions and suggestions for further investigations is provided in Chapter 6.

## CHAPTER 2

---

# *A Review of Oceanic Crustal Structure and Geochemistry*

### **2.1. Introduction**

This chapter provides a review of the available literature on the structure and geochemistry of the ocean crust formed at mid-ocean ridges.

The chapter can be loosely divided into three sections, section 2.2 discusses the various methods employed to study the architecture of the ocean crust and reviews some of the results obtained. Sections 2.3 and 2.4 are concerned with the morphology of mid-ocean ridges and the forms of basalt generated. The geochemistry of mid-ocean ridge basalts and some of the theories proposed as to their geochemical evolution are reviewed in Section 2.5.

### **2.2. Ocean crust structure**

There is still limited knowledge as to the architecture of the oceanic crust, and the processes through which it forms and evolves. The main obstacle to investigation of the ocean crust is its location in deep water which excludes most methods of direct sampling and observation. The earliest models for the structure of the oceanic crust were derived from two main sources; geophysical data (e.g. Raitt, 1956; Hill, 1957; Ewing and Ewing, 1959) and ophiolite complexes (e.g. Kidd, 1977; Christensen, 1978). Both these methods provide indirect means of investigating the crust.

New oceanic crust is generated at mid-ocean ridges. These can be very simply defined as constructive plate margins where two tectonic plates are moving apart. As the plates diverge the space formed between is filled by rising material from the mantle, the size and shape of which is unknown (Cann, 1974). Upper ocean crust formed at mid-ocean ridges is primarily composed of basalts, derived from partial melting of the underlying mantle peridotites (Lewis,

1983). On average, 3 km<sup>3</sup> of lava is estimated to erupt annually from mid-ocean ridges, comprising 60 to 70% of the annual global volcanic budget (Haymon *et al.*, 1993). The newly formed basaltic rocks are then moved away from the central ridge axis by means of sea-floor spreading due to horizontally spreading convection currents in the mantle (Christensen, 1970). The lower crust is believed to be formed from (Cann, 1974):

- (a) a lower layer of cumulates,
- (b) an upper layer of isotropic gabbro; produced by gradual cooling of the liquid in the magma chamber.

The constant replenishment of magma in the chamber from the asthenosphere has a limiting effect on fractional crystallisation in the magma chamber (Cann, 1974).

Mid-ocean ridges vary widely in their spreading rate and may be classified as fast, intermediate, slow-spreading or ultra-slow spreading according to their half-rate (Figure 2.1). Fast-spreading ridges have a half-rate of 6 to 7 cm / yr., an example being the East Pacific Rise (Macdonald, 1982). In contrast, a slow-spreading ridge, for example the Mid-Atlantic Ridge, generally has a half-rate of 1 to 2 cm / yr. (Macdonald, 1982), ridges with spreading rates < 1 cm / yr. are classified as ultra-slow spreading (e.g. South-West Indian Ridge; Dick *et al.*, 1992). Lying between these two end members are intermediate-spreading ridges. These have an average half-rate of 3 to 4 cm / yr., an example being the Galapagos Spreading Centre (Ballard *et al.*, 1979). Most models for ocean crustal structure suggest that the lithostratigraphy is very strongly influenced by spreading rate (e.g. Cann, 1974; Nisbett and Fowler, 1978; Smith and Cann, 1992). Reid and Jackson (1981) concluded through mathematical modelling that crustal thickness can be correlated with spreading rate. At slow-spreading ridges advection is slower than at fast-spreading ridges resulting in lower temperatures and consequently less migration of partial melt to the surface, hence thinner crust develops. In order to fully constrain the architecture of the ocean crust, it is essential to investigate each type of spreading centre, looking at the magmatic processes at each.

Where does our information on oceanic crustal structure come from? There are four main sources of information, direct sampling and dredging of the ocean crust, seismic surveys, ophiolite complexes and drilling / downhole logging of boreholes.

### **2.2.1. Geophysical Data**

#### *2.2.1.1. Seismic Data*

Seismic surveys provide evidence as to the velocity structure of the ocean crust and upper mantle. Early seismic surveys were conducted by Raitt (1956) in the central equatorial

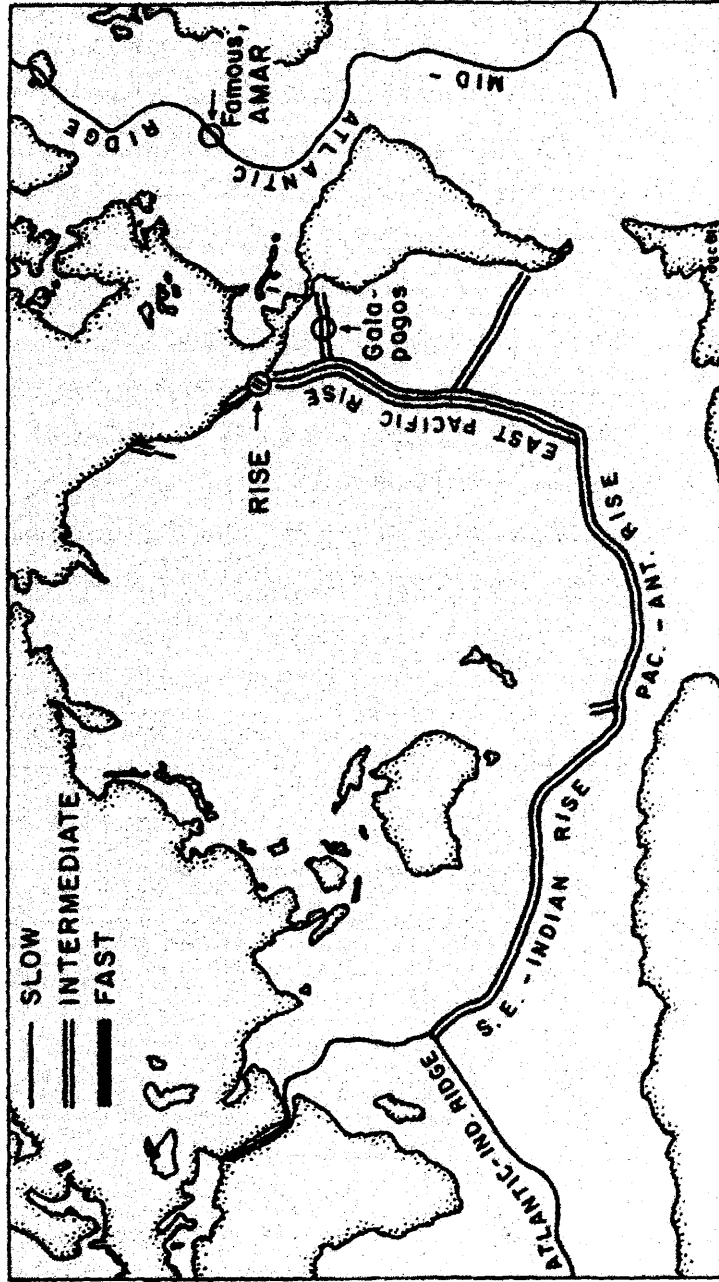


Figure 2.1. Location of major spreading centres (from Macdonald, 1982).

Pacific Ocean, and Ewing and Ewing (1959) on the Mid-Atlantic Ridge. The method employed requires two survey ships, one to fire the shots and the other to receive. The refracted seismic waves from the shots were received by a pressure sensitive hydrophone, suspended on surface buoys at a depth of approximately 200 feet (Raitt, 1956). From the data obtained by this method, the ocean crust was divided into three main seismic layers, with increasing average seismic velocity with increasing crustal depth (Table 2.1). The base of the crust was assigned to the depth where seismic refraction velocities increase to values in excess of 8.0 km/s. This seismic layering can be correlated with lithological units (Hill, 1957, Figure 2.2). The low velocity Layer 1 is thought to correlate with the sedimentary layer covering the ocean floor. This overlies Layer 2, the top of which is usually characterised by rough surface topography (Ludwig *et al.*, 1970). The average thickness of Layer 2 is approximately 2 to 3 km, with seismic velocities similar to both lithified sediments and extrusive igneous rocks (Ludwig *et al.*, 1970). Layer 3 is, on average, 8 to 10 km thick, its seismic velocities are consistent with massive basic igneous rocks (Ludwig *et al.*, 1970). Later work by Houtz and Ewing (1976) divides Layer 2 into three sub-layers: Layer 2A with velocities of  $3.6 \pm 0.4$  km/s corresponds to the extrusive pillow lavas, Layer 2B with velocities of  $5.2 \pm 0.4$  km/s has been interpreted as representing the transition layer between pillow lavas and the sheeted dyke complex and Layer 2C with velocities of  $6.1 \pm 0.2$  km/s corresponds to the sheeted dyke complex.

<u>Ocean Crust Layer</u>	<u>Seismic Velocity (km/s)</u>
Layer 1	2.15
Layer 2	$5.07 \pm 0.63$
Layer 3	$6.69 \pm 0.26$
Upper Mantle	$8.13 \pm 0.24$

**Table 2.1.** Seismic velocities of ocean crustal layers. After Raitt (1956) and Hill (1957).

An important question still to be addressed is whether the boundaries between the seismic layers represent lithological or physical properties changes in the ocean crust. The use of seismic data to constrain the architecture of the ocean crust is problematic, mainly because the seismic data defines the velocity structure of the crust which is not necessarily directly comparable to the lithological structure. Seismic velocities of basement rocks are influenced by many factors including fracturing and low temperature alteration of the crust. These factors can decrease velocities by up to 40% and 70% respectively (Christensen, 1978).

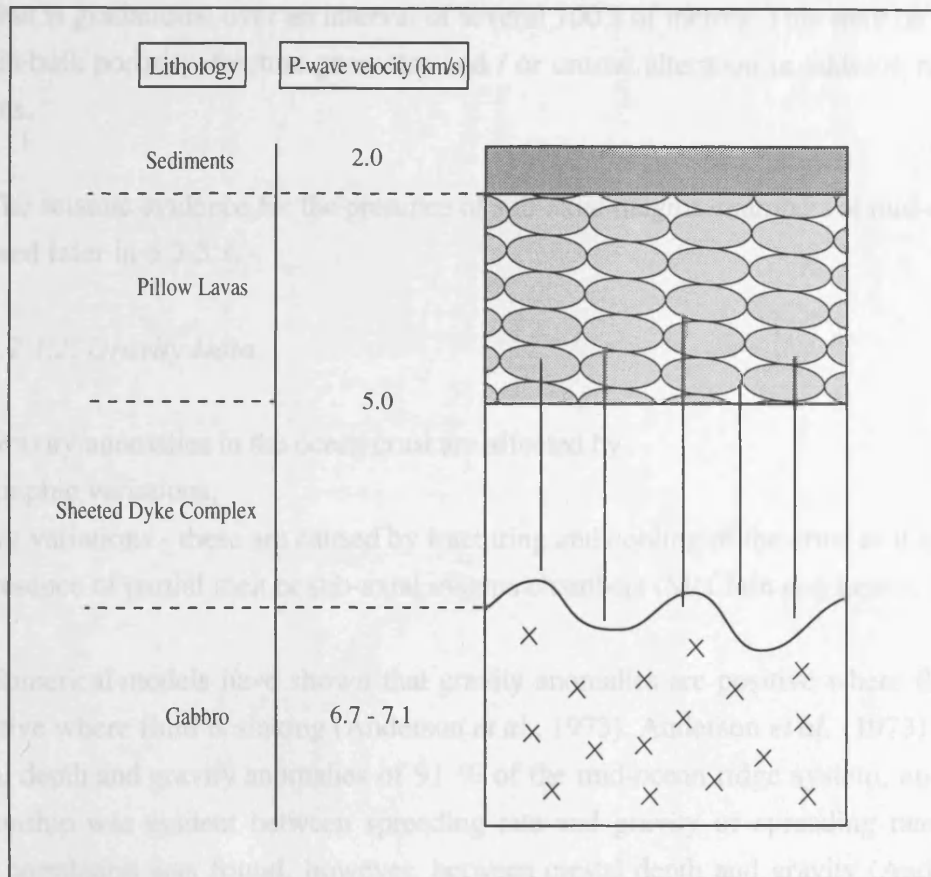


**Figure 2.2.** Schematic oceanic crustal structure, adapted from Brown and Musset (1993).

Christensen (1978) studied seismic velocities from ophiolites in an attempt to correlate the velocity structure of the crust with the lithostratigraphy. The first order seismic discontinuities in ophiolites is related to an increase in metamorphic grade from zeolites and greenschists to amphibolite facies (Christensen, 1978; Carlson and Herrick, 1990), and correlates with the proposed position of the Layer 2 / 3 boundary. These changes in metamorphic grade are believed to be closely connected to the lithostratigraphy (Christensen, 1978), hence, the Layer 2 / 3 boundary may represent both a lithological and metamorphic change in the ocean crust.

Detrick *et al.* (1994) investigated seismic and resistivity data from ODP Hole 504B in the eastern equatorial Pacific to attempt to constrain the position of the layer 2 / 3 boundary. Hole 504B is the deepest basement borehole drilled to date, and provides an *in situ* section of

upper ocean crust. Detrick *et al.* (1994) concluded that the boundary between the two layers is a transitional change in the physical properties of the crust (Figure 2.3). This does not occur sharply, but is gradational over an interval of several 100's of metres. This may be the result of changes in bulk porosity, fracture geometry and / or crustal alteration in addition to lithological constraints.

The seismic evidence for the presence of sub-axial magma chambers at mid-ocean ridges is discussed later in § 2.5.1.

#### *2.2.1.2. Gravity Data*

Gravity anomalies in the ocean crust are affected by :

- (a) topographic variations,
- (b) density variations - these are caused by fracturing and cooling of the crust as it ages,
- (c) the presence of partial melt or sub-axial magma chambers (McClain and Lewis, 1982).

Numerical models have shown that gravity anomalies are positive where fluid is rising and negative where fluid is sinking (Anderson *et al.*, 1973). Anderson *et al.* (1973) investigated the crestal depth and gravity anomalies of 91 % of the mid-ocean ridge system, and found that no relationship was evident between spreading rate and gravity or spreading rate and crestal depth. A correlation was found, however, between crestal depth and gravity (Anderson *et al.*, 1973). Sections deeper than average tend to have negative gravity anomalies whereas those shallower than average have positive gravity anomalies. These anomalies cannot be entirely accounted for by thicker crust as the lithosphere has insufficient strength to support the required mass excess (Anderson *et al.*, 1973) The anomalies must therefore arise from asthenospheric flow beneath the crust suggesting that shallow ridge sections represent areas of upwelling and deeper sections represent areas of downwelling (Anderson *et al.*, 1973)

#### **2.2.3. Ophiolite complexes**

Ophiolites are outcrops on land that possibly represent fragments of ancient oceanic crust. It has been theorised that ophiolites comprise obducted slabs of oceanic lithosphere which were emplaced on land rather than being subducted at destructive plate margins (Kidd, 1977). Ophiolites provide good evidence for the layered structure of the ocean crust, since many complexes have a three-layered structure similar to that predicted by seismic surveys (Fig. 2.4). Most ophiolite suites comprise a basaltic pillowed volcanic complex overlying a mafic sheeted dyke complex and a gabbro complex (Kidd, 1977). Studies of ophiolite complexes have produced similar seismic velocities to those recorded in the oceanic crust implying that the

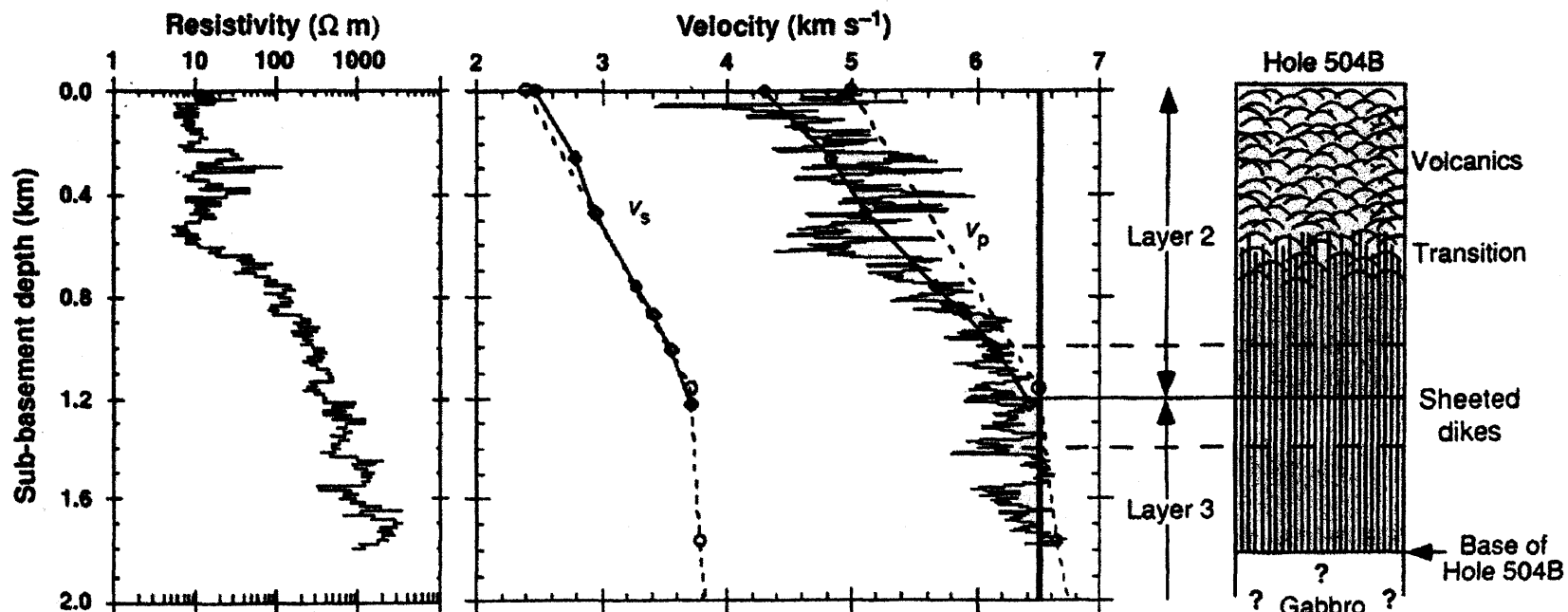


**Figure 2.3.** Comparison of the variation in bulk resistivity downhole, crustal velocity structure and lithostratigraphy in Hole 504B (from Detrick *et al.*, 1994). The change in vertical velocity gradient that defines the seismic layer 2/3 boundary is indicated,

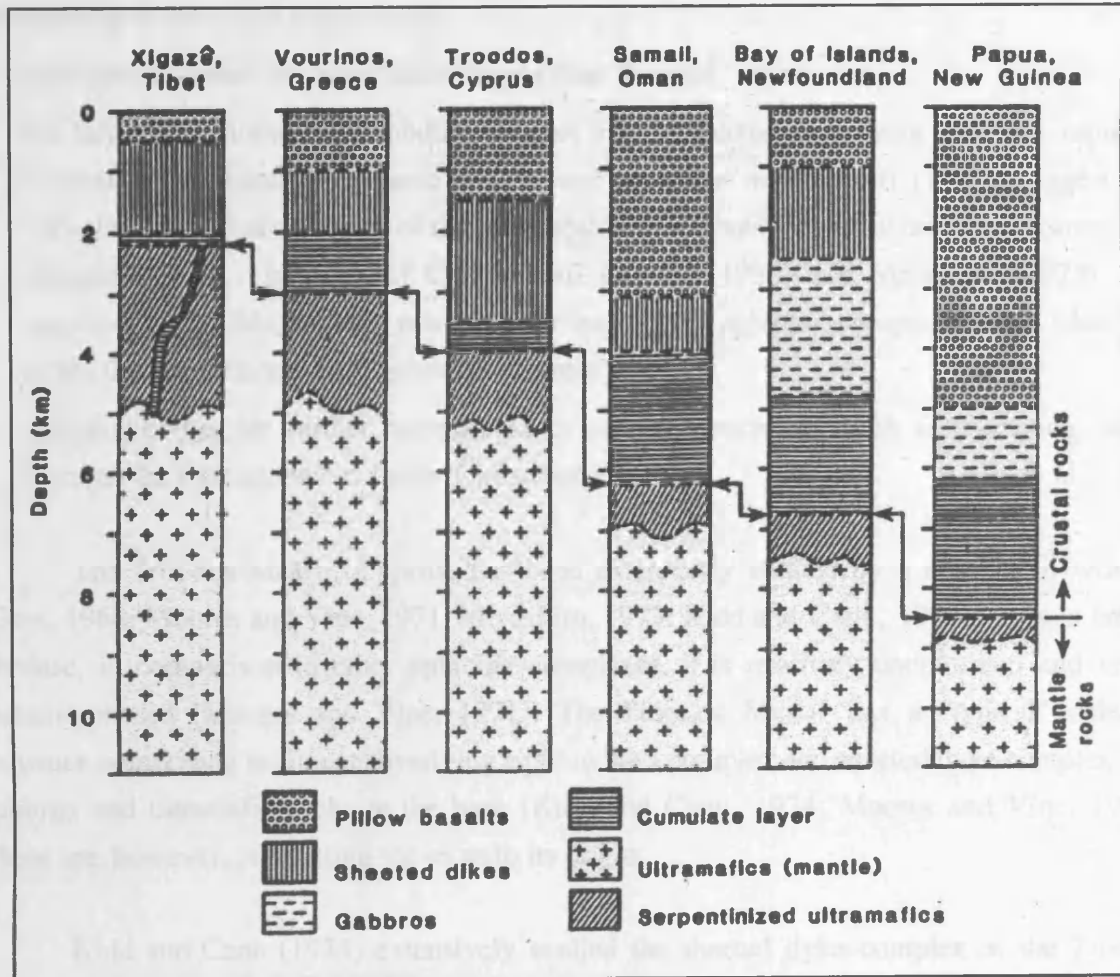


Figure 2.4. Schematic sections of various ophiolites (from Lewis, 1983).

structure of many ophiolites is analogous to ocean crust at least in terms of seismic structure (Christensen, 1978; Carlson and Herrick, 1990).

There are, however, three important disadvantages in using ophiolites to reconstruct the architecture of the *in situ* ocean crust :

- ophiolite segments are often much thinner than “normal” ocean crust,
- the fact that ophiolites were obducted rather than subducted may mean that they represent anomalous segments of oceanic lithosphere. Harrison and Bonatti (1981) suggest that ophiolites represent remnants of marginal basins which have been extensively deformed and metamorphosed. The work of Carlson and Herrick (1990) and Miyashiro (1973) is in agreement with this, and suggests that the majority of ophiolite complexes have island arc rather than mid-ocean ridge basalt geochemistry .
- ophiolite bodies are further complicated by tectonic processes, such as fracturing, which disrupts the stratigraphic column (Christensen, 1970).

The Troodos Massif, Cyprus, has been extensively studied by a number of workers (Gass, 1968; Moores and Vine, 1971; Miyashiro, 1973; Kidd and Cann, 1974). This is largely because, in comparison to other ophiolite complexes, it is relatively undeformed and is not metamorphosed (Moores and Vine, 1971). The Troodos Massif has a “typical” ophiolite sequence comprising sediments overlying a pillow lava complex and sheeted dyke complex with gabbros and ultramafic rocks at the base (Kidd and Cann, 1974; Moores and Vine, 1971). There are, however, conflicting views as to its origin.

Kidd and Cann (1974) extensively studied the sheeted dyke complex of the Troodos Massif. The large proportion of dykes with one predominant chilling direction led them to conclude that the complex was formed at a spreading centre. This is in contrast to the work of Miyashiro (1973), who analysed a number of basalts from the Troodos complex and concluded that the presence of calc-alkaline series basalts suggests that this ophiolite complex formed in an island-arc setting.

The presence of a sheeted dyke complex in some ophiolite complexes suggests they were formed in a seafloor spreading environment (Cann, 1974) but their geochemistry and petrology is rather different to MORB suggesting that they were not formed at M.O.R. (Alt *et al.*, 1998; Miyashiro, 1973). Current models for Tethyan ophiolites, such as the Troodos Massif, suggest that these complexes were formed in supra-subduction settings, in a spreading environment above a subduction zone (Schmincke *et al.*, 1983; Rautenschlein *et al.*, 1985; Alt *et al.*, 1998). Pearce (1975) concluded from trace element evidence that the lower pillow lava sections in the Troodos ophiolite had a spreading centre origin and the upper pillow lava

sections had an island arc origin. This is confirmed by Nd and Sr isotope data which suggests that the primitive Troodos lavas are closely related to boninites (high Mg, low Ti basalts), these rocks are subduction-related discounting formation of the ophiolite at M.O.R.s (McCulloch and Cameron, 1983). It is thought that Tethyan ophiolites were formed in the early stages of development of an island-arc in an extensional setting near to the point of seafloor spreading (Bloomer *et al.*, 1995; Pearce *et al.*, 1984; Schmincke *et al.*, 1983; Rautenschlein *et al.*, 1984). Production rates of crust in this setting will be higher than those on mature arcs but will be similar to those noted on ridges with low spreading rates (Bloomer *et al.*, 1995). Hence it is probable that though many ophiolites are representative of the generalised ocean crust stratigraphy, a number of examples may have formed in a rather different setting.

Whilst it is quite likely that the Troodos Massif formed in some form of seafloor spreading environment, the absence of similarly structured sheeted dyke complexes in a number of ophiolite complexes suggests they may have a slightly different origin. Ophiolite complexes formed in seafloor spreading environments may also reflect the spreading rate at which they formed. Cann (1974) proposes that the intrusion of dykes into the ocean crust varies according to spreading rate. As spreading rate increases the interval between dyke intrusions will be low, therefore, each dyke only has a very short time to cool before the next intrusion. This causes a decrease in thickness of the dyke swarm, consequently at very high spreading rates, there may be very few dykes (Cann, 1974). Hence, variations in the thickness of sheeted dyke complexes seen in ophiolites may be the result of variations in spreading rate. The well-developed dyke complex in the Troodos Massif suggests this ophiolite complex formed at relatively slow spreading rates (Cann, 1974).

### 2.2.1. Dredging of the ocean floor

Dredging of the ocean floor constitutes perhaps the simplest means of sampling of oceanic rocks and provided the earliest samples of oceanic crust from the deep ocean (e.g. Engel and Engel, 1964a,b; Nicholls *et al.*, 1964; Engel *et al.*, 1965). This method provides actual, physical samples of the ocean crust but these are not necessarily recovered *in situ*. Therefore, dredging and direct sampling only provide limited evidence as to the three-dimensional structure of the crust or its evolution with time.

Dredges have recovered a number of igneous lithologies from the ocean floor, including basalts, gabbros, peridotites and serpentinites (Engel *et al.*, 1970; Engel *et al.*, 1965; Kay *et al.*, 1970; Engel and Engel, 1964a,b; Nicholls *et al.*, 1964). What is perhaps surprising is that very similar lithologies have been recovered from the Atlantic, Pacific and Indian Oceans (Engel *et al.*, 1965), suggesting that the ocean crust is very similar over the entire surface of the Earth.

Dredging, however, does not provide an entirely accurate measure of the relative proportions of rock types present in the ocean crust, as some lithologies may be preferentially recovered with respect to others. This is reflected by the relatively low amounts of gabbro recovered in many dredge hauls, gabbro is much harder to break off outcrops than basalt or peridotite (Dick *et al.*, 1991b). Peridotites are usually extensively altered and basalt often occurs as poorly aggregated pillow lavas and breccias whereas, in contrast, outcrops of gabbro are generally massive and relatively unweathered (Dick *et al.*, 1991b).

The first manned submersible studies of mid-ocean ridges were made by the French submersible Archimede in 1973 which visited the Mid-Atlantic Ridge (Bellaiche *et al.*, 1974). Submersible expeditions, such as those by Alvin (e.g. Ballard *et al.*, 1975) and the diving saucer Cyana (Renard *et al.*, 1985) have also provided valuable information regarding the surface morphology of the ocean crust, discussed in § 2.4.

#### **2.2.4. Drilling and downhole logging of boreholes**

This is perhaps the most comprehensive method of sampling of the ocean crust. From the drilling of boreholes into the ocean floor, actual ocean crust samples can be compared with seismic and ophiolite evidence enabling a more accurate three-dimensional picture of the oceanic crustal structure to be constructed. Unfortunately, the complete crustal section has not yet been penetrated *in situ*. The deepest oceanic basement hole drilled to date is Ocean Drilling Program (ODP) Hole 504B, this has a total depth of 2111.0 metres below sea-floor (mbsf), with 1836.5 m of basement rocks, including volcanics and the sheeted dyke complex (Alt, Kinoshita *et al.*, 1993).

One of the disadvantages of borehole drilling is that core recovery from ocean crust boreholes is generally very low, on average, approximately 25% (Brewer *et al.*, 1998). This is due to the highly fragmentary and fractured nature of basement rocks, ensuring that main key lithologies may be misrepresented in ocean crust cores. This is particularly true of brecciated units in basement holes, the fragmentary nature of breccias allows circulation of seawater, resulting in alteration of the breccia clasts to clays. Lithologies such as massive basalts and gabbros are much more conducive to drilling (Brewer *et al.*, 1998).

The poor recovery in many basement boreholes severely complicates any interpretation of the ocean crust lithostratigraphy. Selective recovery of certain lithologies may ensure that many key lithological units are poorly represented in the core data or are not recovered at all. In many cases, no contacts between individual lithological units are recovered, complicating interpretation of the relationships between individual lithological units.

The use of downhole logging tools in boreholes provides geochemical and physical properties data to supplement the core data. This may aid reconstruction of the borehole stratigraphy in cases of poor core recovery, helping to effectively “fill in the gaps” and enable the true lithostratigraphy to be inferred. A selection of ODP logging tools are described in detail in Appendix B.

To fully interpret the lithostratigraphy of the ocean crust it is essential to integrate both core and log data because, at present, neither provides a fully reliable method of sampling of the crust.

### **2.3. Basalt forms erupted at spreading centres**

A variety of erupted basalt forms have been observed at mid-ocean ridges. These include lava lakes, sheet lavas, pillow lavas, so-called pavingstone lavas and hyaloclastite breccias (Bonatti and Harrison, 1988).

#### **2.3.1. Pillow lavas**

Pillow lavas are clusters of ellipsoidal lava masses resembling “pillows” in terms of general shape and size which form when hot lava is chilled by water contact (Moore, 1975). Furnes and Fridleifsson (1979) describe pillow lavas as the subaqueous equivalent of subaerially erupted pahoehoe lavas.

Early workers believed that pillow lavas comprised independent “sacks” of lava, however, later, more extensive investigations of ancient and modern pillow flows indicated that the majority of pillow lava units are composed of interconnected tubular masses (Moore, 1975; Vuagnat, 1975). Parallel to the flow plane, pillows can be seen to be tubular features, sinuous and of variable thickness (Vuagnat, 1975). In some instances the tubes branch producing more than one pillow. In cross-section these branched tubes will appear as isolated sacks (Figure 2.5).

Examples of basaltic pillows formed at mid-ocean ridges range from 10 cm to 7 m in diameter, however, they usually have diameters of less than 1 m (Macdonald, 1967). The most characteristic features of pillow lavas are the radial jointing, which may not always be evident, and the glassy crust, which is usually between 5 and 25 mm thick (Macdonald, 1967). The glass rim forms due to the extremely rapid chilling of the hot lava as it comes into contact with the cold seawater (Moore, 1975). Underneath the glassy crust of the pillow the presence of small vesicles can often be noted, these are usually 5 to 100 microns in diameter and very

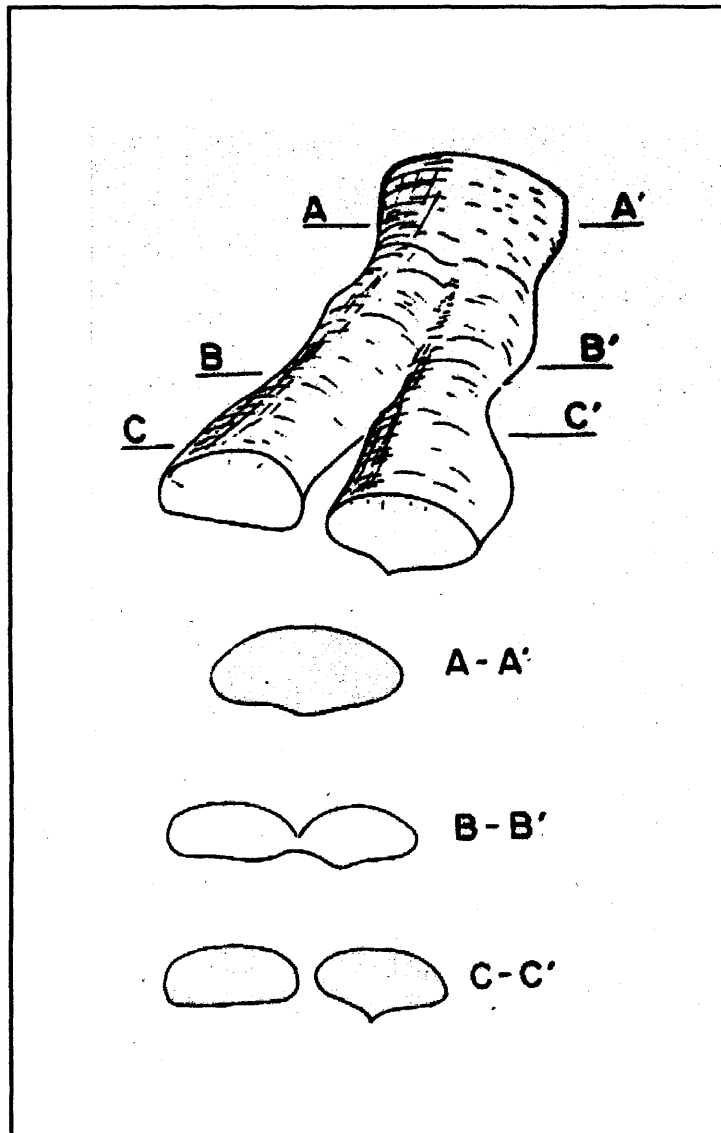


**Figure 2.5.** Three-dimensional and cross-sectional views of a branching “pillow” lava, from Vuagnat (1975).

sparsely distributed throughout the pillow (Wells *et al.*, 1979). The vesicles are formed by gases, released on crystallisation, which have been trapped beneath the rapidly chilled pillow surface (Bonatti, 1970).

The surface texture and form of pillow lavas is believed to be closely related to the rate of lava supply and the thickness of the surface crust developed during growth by cooling (Walker 1992; Chadwick and Embley, 1994; Kennish and Lutz, 1998). Walker (1992) identifies four main pillow-growth mechanisms:

- (a) Uniform stretching :- the chilled outer skin of the pillow stretches to allow new lava to be injected into it,
- (b) Localised stretching :- the chilled outer skin of the pillow breaks, new skin formed inside the rupture stretches,
- (c) Symmetrical spreading :- the chilled outer skin breaks, new skin forms at the edges of the break,
- (d) Toothpaste-like extrusion :- lava is extruded from front, top and sides of a pillow, new skin forms by asymmetric spreading.

Observations from camera tows and Alvin submersible dives on the Cleft Segment, Juan de Fuca Ridge have detected the presence of recent pillow lava mounds believed to have been erupted during the mid-1980s (Embley *et al.*, 1991; Chadwick *et al.*, 1991; Chadwick and Embley, 1994). These pillowed flows are aligned along a single fracture system and have similar morphologies and surface textures, therefore were probably erupted during the same volcanic episode (Chadwick and Embley, 1994). The pillow mounds contain numerous pillow lavas with two main types of surface textures (Chadwick and Embley, 1994) :

- (1) Elongate pillows with distinct surface striations. These pillow lavas are usually 1 to 2 m in diameter. The surface striations are aligned parallel to the long axis of the pillow.
- (2) Smooth-surfaced pillows. These are smaller in size than (1), on average, < 1 m in diameter. Roughly equal proportions of each pillow type occur intermingled suggesting contemporaneous formation.

The initial slow growth of the pillow lavas allows a thick crust to develop and smooth-surfaced pillows are formed (Chadwick and Embley, 1994). This thick crust eventually must be fractured for further growth to occur producing the striated pillow lavas. Smooth-surfaced pillows will be smaller than striated pillows because eventually the crust will be too thick to allow stretching. At faster growth rates a thinner, more stretchable skin may be formed (Chadwick and Embley, 1994).

### 2.3.2. Sheet flows

The term “sheet flow” was first used by Ballard *et al.* (1979) to describe smooth-surfaced submarine lava flows with relatively low relief. They are commonly found in the neovolcanic zones of fast-spreading (e.g. East Pacific Rise) and intermediate-spreading centres (e.g. Galapagos Rift; Kennish and Lutz, 1998). A variety of sheet flow subforms can be distinguished between (Kennish and Lutz, 1998; Ballard *et al.*, 1979):

(a) Smooth / Lobate - These are the most common forms seen at mid-ocean ridges. Lobate flows generally have a hummocky upper surface with relief of approximately 1 to 2 m. They usually possess a thick glassy crust, 5 to 15 cm thick.

(b) Ropy - This type of sheet flow has a “folded” surface morphology. The flows often grade into more or less deformed flow morphologies. The “ropy” or “folded” surface of these flows is formed as the molten lava drags the cooling crust along with it (Lonsdale, 1977).

(c) Whorly - In these flows the folded surface features occur in circular patterns. Each whorl is 1 to 10 m in diameter. These surface coils of lava form at shear zones at the edges of lava flows (Lonsdale, 1977).

(d) Hackly / Jumbled - These have irregular surfaces with thin glassy crusts usually < 0.5 cm thick. They are found associated with hydrothermal vents, fissures and collapse features.

The variations in morphology of sheet flows observed are probably the result of four main factors (Lonsdale, 1977): (i) viscosity; (ii) crystallinity; (iii) temperature; (iv) effusion rate. The factors affecting the morphologies of submarine lava flows are discussed in § 2.3.4.

Collapse features are often found associated with sheet flows at mid-ocean ridges (Francheteau *et al.*, 1979; Hon *et al.*, 1994, Figure 2.6). These are believed to be the remnants of a collapsed lava lake (Gente *et al.*, 1986) and develop due to the drain-back of lava (Hon *et al.*, 1994). The collapse features often contain pillars which vary in diameter from 0.5 to 2 m widening upwards (Francheteau *et al.*, 1979). The pillars are believed to form as seawater trapped in the crust beneath the lava pool rises as it is heated, the rising liquid rises in conduits the walls of which are quenched forming a hollow column of rock.

### 2.3.3 Hyaloclastites and other breccias

The proportion of submarine volcanoclastic rocks (approximately 8 to 10 %) is small in comparison to pillow lavas and sheet flows (Fisher and Schmincke, 1984). The actual percentage of brecciated units, however, is probably greater than suggested by deep-sea drilling cores because unconsolidated material is very difficult to recover (Fisher and Schmincke, 1984).

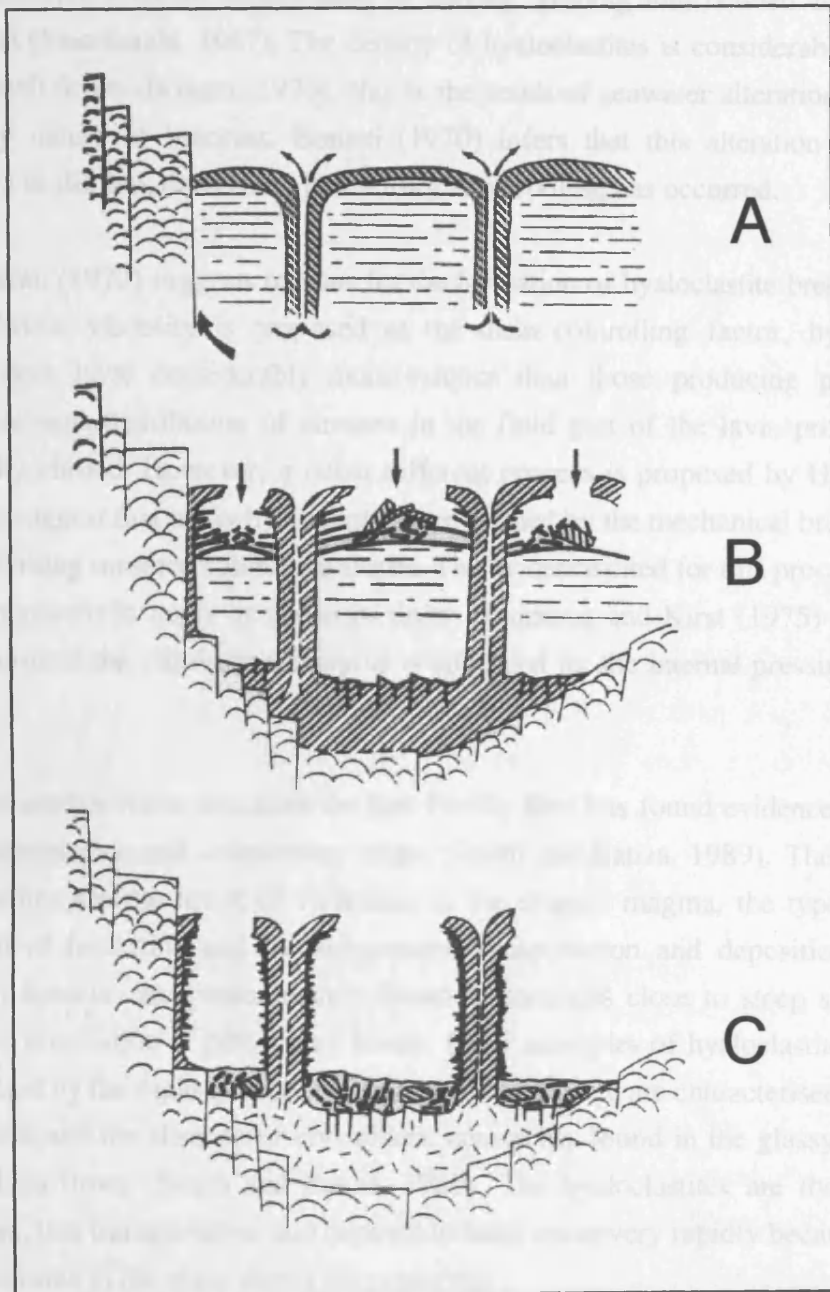


**Figure 2.6.** Evolution of collapse features, from Francheteau *et al.* (1979).  
 (A) filling of lava pool, (B) lava pool withdrawal results in roof collapse  
 (C) final stage leaving isolated pillars.

Hyaloclastites comprise aggregates of glass and basalt fragments in a clay carbonate matrix which are thought to be produced by rapid chilling and shattering when basic / intermediate lava flows or extrudes into water (Furnes and Freidleifsson, 1979). Hyaloclastites are often massive with no stratification or sorting, grading into bedded materials of similar composition (Macdonald, 1967). The density of hyaloclastites is considerably less than that of massive basalt flows (Bonatti, 1970), this is the result of seawater alteration, facilitated by the fragmentary nature of breccias. Bonatti (1970) infers that this alteration occurs whilst the erupted lava is still hot, decreasing in intensity after cooling has occurred.

Bonatti (1970) suggests reasons for the formation of hyaloclastite breccias in preference to pillow lavas, viscosity is proposed as the main controlling factor, hyaloclastites being generated from lavas considerably more viscous than those producing pillows. The high viscosity prevents distribution of stresses in the fluid part of the lava, promoting shattering when rapidly chilled. However, a rather different process is proposed by Honnorez and Kirst (1975) who suggest that many hyaloclastites are formed by the mechanical breakdown of pillow lava rims forming on steep submarine slopes. The evidence cited for this process is the presence of pillow fragments in many hyaloclastite units. Honnorez and Kirst (1975) also conclude that the granulation of the pillow lava margins is enhanced by the internal pressure of the growing lava tube.

Submersible Alvin data from the East Pacific Rise has found evidence for hyaloclastites of both hydrovolcanic and sedimentary origin (Smith and Batiza, 1989). The contrasting types of hyaloclastites are the result of variations in the erupted magma, the type of eruption, the environment of formation and the subsequent transportation and deposition of the breccia. Sedimentary breccias are predominantly found in locations close to steep slopes, suggesting formation by brecciation of pillow lava fronts. Other examples of hyaloclastites are more likely to have formed by the rapid quenching of erupted lavas, these are characterised by an abundance of glass shards and the absence of crystallites, commonly found in the glassy margins of most submarine lava flows (Smith and Batiza, 1989). The hyaloclastites are then transported by density flows, this transportation and deposition must occur very rapidly because in many cases delicate structures in the glass shards are preserved.

#### **2.3.4. Distribution of flow types on mid-ocean ridges**

Francheteau and Ballard (1983) note that on fast and intermediate-spreading ridges, there is a decrease in the ratio of sheet flows : pillow lavas with increasing distance from the ridge axis. The crest of the ridge on the East Pacific Rise has sheet flows extruded in a relatively narrow zone, these start to grade into pillows where the lava starts to flow downslope (Francheteau and Ballard, 1983). Francheteau and Ballard (1983) suggest sheet flows are preferentially erupted at

the axis because this provides the shortest route from the magma chamber to the surface, allowing rapid eruption of high temperature lavas. At a distance from the axis, conduit networks will be longer, giving the lava time to cool and resulting in slower effusion rates, therefore pillow lavas will be formed.

### **2.3.5. Factors affecting the morphology of submarine lava flows**

It is perhaps easiest to assume that the same processes generate both subaerial and subaqueous eruptions. If this is the case, then a number of factors such as, large volumes of magma, high effusion rates, elevated eruption temperatures accompanied by an extensive transport system and a relatively low topographic gradient are required for the production of submarine lava fields (Fornari *et al.*, 1985). Explosive eruptions on the seafloor are largely restricted by the hydrostatic pressure of the overlying ocean and the low volatile content of mid-ocean ridge basalts, which inhibit vesiculation (Haymon *et al.*, 1993). Unfortunately direct observations of submarine basalt eruption are rarely observed, therefore it is extremely difficult to know the exact conditions of emplacement of each flow type.

There are usually no compositional differences between pillow lavas and sheet flows, however, the glassy rind on pillow lavas is generally thinner than observed on sheet flows (Kennish and Lutz, 1998). Pillow lavas tend to contain more crystals, which suppress formation of the glassy rind. Bonatti and Harrison (1988) suggest that the factors determining the form of basalt erupted are:

- temperature
- viscosity - which is dependant on temperature and composition
- eruption rate - which is related to viscosity.

A number of workers suggest that the variety of basalt forms erupted at spreading centres may be explained by variations in the effusion rates of the erupted lava (Ballard *et al.* 1979; Walker, 1973). Walker (1973) studied a number of modern lava flows comparing the length of a flow to the effusion rate. He concluded that at high effusion rates the lava flows quickly away from the vent, forming a simple flow constructed of a single flow unit (analogous to sheet flows). At lower effusion rates the erupted lava accumulates around the vent forming several flow units known as a compound lava flow (analogous to pillowed flows).

#### *2.3.5.1. Experimental modelling of lava flow morphologies*

Laboratory experiments using polyethylene glycol wax extruded into a sucrose solution have been used to relate lava morphology to extrusion rate and cooling rates (Griffiths and Fink, 1992; Fink and Griffiths, 1992; Gregg and Fink, 1995). The wax provides a good analogue for

lava because as it cools the surface solidifies and deforms over a molten interior (Chadwick and Embley, 1994). As lava is extruded it cools and solidifies as a result of radiative or convective heat loss (Griffiths and Fink, 1992). A thin layer at the flow's surface solidifies first. The formation of this surface crust is an important process in determining the surface morphology of the erupted lava flow. Griffiths and Fink (1992) found that formation of pillow lavas is associated with flow rates of  $< 1 \text{ m}^3\text{s}^{-1}$ . At higher effusion rates ( $< 100 \text{ m}^3\text{s}^{-1}$ ) sheet flows will form with either smooth or mm-scale striated surface morphologies. If flow rates are increased further ( $< 300 \text{ m}^3\text{s}^{-1}$ ) folded or ropy sheet flows will develop. The results of Griffiths and Fink (1992) are summarised in Table 2.1., similar morphologies are produced whether the lava is extruded from a point or a line source (Fink and Griffiths, 1992).

One eruption may be capable of producing all the flow morphologies observed at mid-ocean ridge axes. Sheet flows may be produced at the initially high effusion rates at the onset of an eruption, these will grade into more pillowed flows at the flow margins where effusion rates are lower (Gregg and Fink, 1995). This is similar to the model proposed by Ballard *et al.* (1979) after studies of lava flow morphologies at the Galapagos Rift. Ballard *et al.* (1979) suggest that sheet flows are the product of high effusion rate eruptions in the early stages of an eruptive sequences whereas pillow lavas form at lower effusion rates after an extensive conduit system has developed.

#### *2.3.5.2. Effect of spreading rate on flow morphology*

Bonatti and Harrison (1988) note a relationship between lava flow morphology and spreading rate (Figure 2.7). At slow-spreading ridges pillow lavas are the dominant flow form whereas as spreading rate increases the proportion of lava lakes and sheet flows also increases. For example, at the fast-spreading East Pacific Rise, within the axial graben the lava flows comprise 72 % sheet flows and 28 % pillow lavas whereas at the slow spreading Mid-Atlantic Ridge the axis comprises 88 % pillow lavas, with only 12 % sheet flows (Bonatti and Harrison, 1988). Bonatti and Harrison (1988) propose that this relationship is due to the depth of a subaxial magma chamber supplying the lava to the surface and the nature of the conduits transporting the lava. At fast-spreading ridges, a relatively shallow magma chamber is more likely to occur (§2.5.4) with shallow, wide conduits transporting the magma to the surface, producing predominantly sheet flows. Smaller, deeper magma chambers are expected at slow-spreading ridges therefore lava will be transported to the surface in longer, narrower conduits, at lower effusion rates, producing pillow lava flows.

Laboratory morphology	Submarine morphology	Cooling rate	Slope	Flow rate
pillows	pillows	↑	↓	↓
	lobate sheets			
rifts	lineated sheets			
folds	ropy sheets			
levees	jumbled sheets			

**Table 2.1.** Correlation between laboratory and submarine flow morphologies (adapted from Gregg and Fink, 1995).

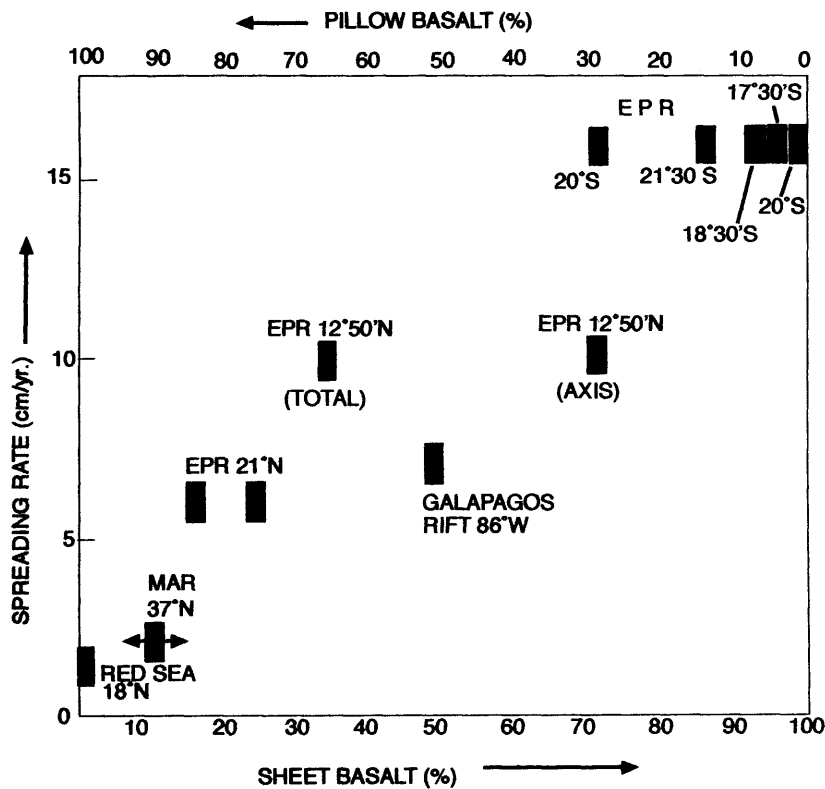


**Figure 2.7.** Areal ratio sheet basalt / pillow basalt versus spreading rate on axial zones of spreading ridges (adapted from Bonatti and Harrison, 1988).

## **2.4. Morphology of spreading centres**

The actual crustal architecture at mid-ocean ridges is considerably more complicated than the simple three-layer structure previously outlined. Manned submersible studies during the 1970's provided the first glimpse of the structure and morphology of spreading centres (Ballard *et al.*, 1975; Bellaiche *et al.*, 1974). The morphology of a spreading centre is believed to be related to the depth of the magma source supplying the ridge and can be closely correlated with spreading rate (Allmendinger and Riis, 1979). A comparison of cross-sections from mid-ocean ridges with different spreading rates is shown in Figure 2.8.

### **2.4.1. Slow-spreading ridges**

A slow-spreading ridge, such as the Mid-Atlantic Ridge, generally has an axial valley, 30 to 45 km wide and 1 to 2 km deep (Smith and Cann, 1993). This median valley consists of an inner valley floor, 5 to 12 km wide, bordered by faulted valley walls. The inner valley floor is the main area of lava extrusion. Volcanic activity produces a ridge with a pronounced rift valley usually 1.5 to 3.0 km wide, cross-cut by small transform faults (Macdonald, 1982). These axial ridges are believed to be almost entirely volcanic in origin and are largely unaffected by faulting, they are therefore probably the primary sites for crustal accretion at slow-spreading ridges (Smith and Cann, 1992). Some flank eruptions do occur, however, these are of significantly lower volumes of lava than the axial eruptions (Macdonald and Luyendyk, 1977). The axial ridge consists of rugged hills (volcanoes), the flanks of which are characterised by broad lobate flows (Ballard *et al.*, 1975). On the upper surfaces of the axial ridge hummocky pillow lava forms are usually observed. The majority of the structural processes on the ridge occur in a 20 to 25 km wide area perpendicular to the ridge axis (Allmendinger and Riis, 1979).

Project FAMOUS (French - American Undersea Study) provided the first detailed topographic picture of the axial zone of the Mid-Atlantic Ridge (Luyendyk and Macdonald, 1977; Macdonald and Luyendyk, 1977). Macdonald and Luyendyk (1977) divided the median valley of the Mid-Atlantic Ridge (M.A.R) into four provinces: (a) inner floor, (b) inner walls, (c) terraces, and (d) outer walls. The outer walls represent the boundary between the median valley and the outer rift mountains. The inner walls often have an asymmetric structure. In the FAMOUS area of the Mid-Atlantic Ridge (latitude 37°N) the western wall is steeper than the eastern wall. Faulting is considerably more abundant on the east side than the west. This is consistent with greater extension to the east than the west, associated with the asymmetrical spreading rates on this segment of the M.A.R (Macdonald and Luyendyk, 1977). Along the length of the Mid-Atlantic Ridge (M.A.R.), it can be divided into a number of spreading segments, divided by transform and non-transform discontinuities (Sempere *et al.*, 1993; Sempere *et al.*, 1990).

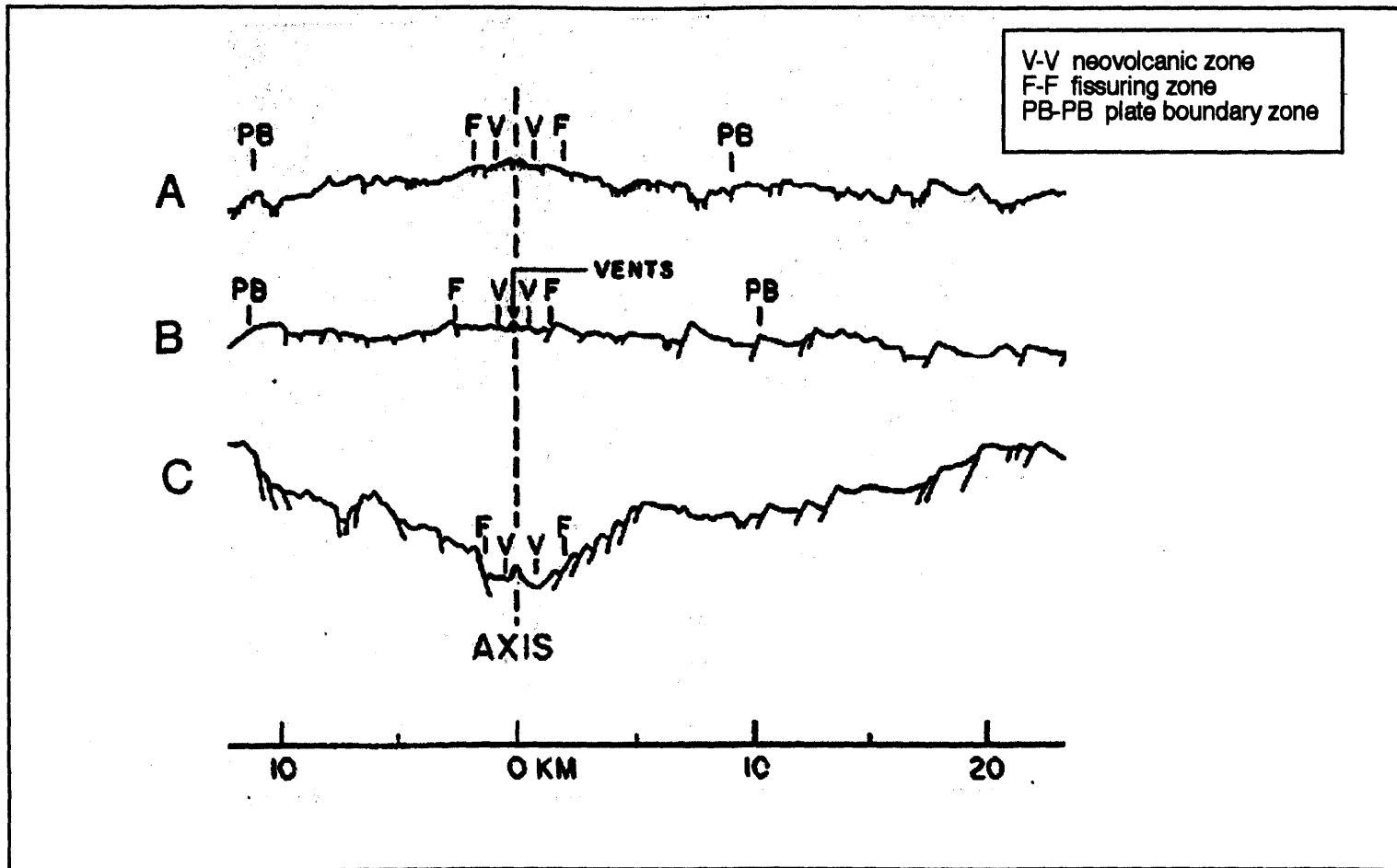


**Figure 2.8.** Deep-tow profiles of (A) fast-spreading, (B) intermediate-spreading and (C) slow-spreading ridges, from Macdonald (1982).

### 2.4.2. Fast-spreading ridges

In contrast to slow-spreading ridges, a fast-spreading ridge, with a shallow large source, tends to have an axial high, 1 to 2 km wide with considerably less rugged topography (Allmendinger and Riis, 1979). Macdonald and Fox (1988) noted that three different cross-sectional ridge shapes occur on the East Pacific Rise (E.P.R.) (Figure 2.9):

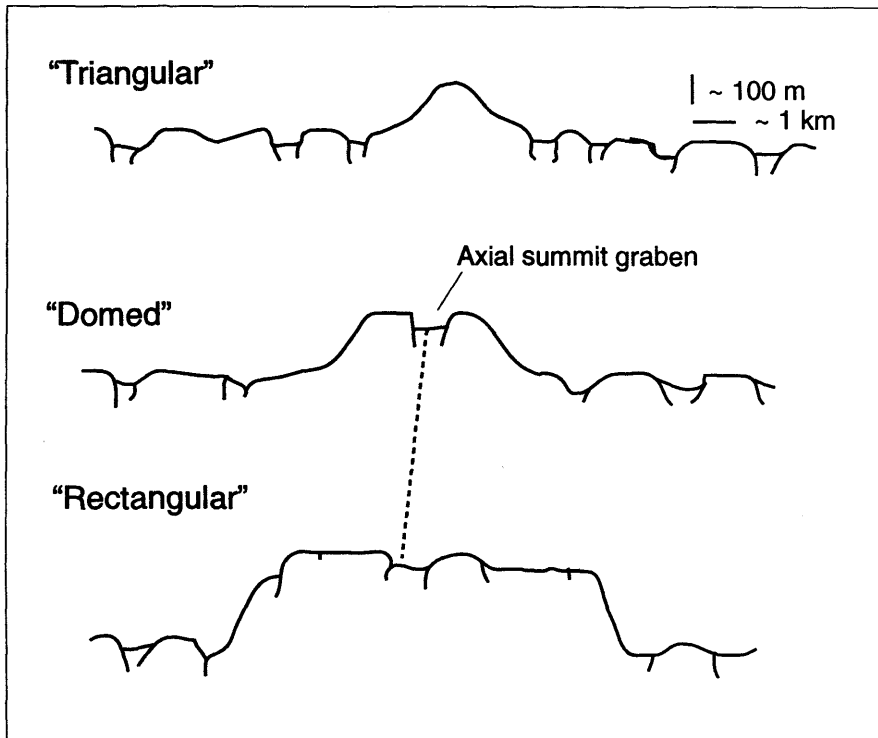


**Figure 2.9.** Cross-sectional shapes of the East Pacific Rise axis (from Macdonald and Fox, 1988).

(1) Rectangular :- This has a flat summit 4 to 8 km wide at the top and < 12 km wide at the base. An example of this morphology is seen on the E.P.R at 13°N, here, the axial crest of the ridge is a wide, flat-topped structure rising several hundreds of metres above the seafloor (Gente *et al.*, 1996).

(2) Domed :- Here, the summit is 1 to 2 km wide at the top and 4 to 8 km wide at the base

(3) Triangular :- These sections have very narrow summits, only 10s to 100 metres wide with a 1 to 4 km base.

An axial graben, approximately 50 m deep, is often present at the top of the ridge on rectangular and dome shaped cross-sections. This graben progressively shallows southwards.

The inner valley floor of the graben has relatively constant width and structure. Macdonald and Fox (1988) suggest that the development of the axial summit graben is related to the volume of melt in a subaxial magma reservoir (§2.5.3), its formation is somewhat analogous to volcanic calderas. Subsequent to an eruption magma levels may fall, causing the roof of a subaxial magma chamber to collapse. An alternative mode of formation is suggested by Gente *et al.* (1986). They propose that the axial summit graben is formed by progressive collapse of wall slabs. This is a three-stage process summarised below :

- (1) generation and enlargement of fissures forms wall slabs
- (2) tilting and collapse of slabs forms inner steps
- (3) the walls of the graben are disrupted, producing talus piles at the foot of the walls

The axial summit graben on fast-spreading ridges is very different to the rift valleys observed at slow and intermediate-spreading ridges. Slow-spreading ridge rift valleys are much wider (6 to 30 km) and deeper (> 1 km) than the axial summit grabens on the E.P.R (Macdonald and Fox, 1988). These are unlikely to be formed by collapse of a magma reservoir roof, as this would suggest the presence of larger magma reservoirs at slow-spreading ridges, largely excluded by seismic data and thermal models (§2.5.3)

Volcanism on fast-spreading ridges is dominated by low-relief lava flows (Smith and Cann, 1993). Manned submersible studies by the diving saucer Cyana observed relatively recent volcanic activity on the axial crest of the E.P.R at 17°30'S (Renard *et al.*, 1985). The summit of the ridge in this area is covered by relatively fresh lobate sheet flows which gradually grade into more pillowed flows on the flanks of the crest (Renard *et al.*, 1985). Haymon *et al.* (1993) suggest that there is a cycle of volcanism and tectonism at fast-spreading mid-ocean ridge crests which starts with dyke intrusion and volcanic eruption, followed by magma drainage and collapse. Tectonic activity then fractures the crust forming the axial graben.

### **2.4.3. Intermediate-spreading ridges**

Van Andel and Ballard (1979) describe the rift system morphology of the intermediate-spreading Galapagos Rift as very simple, consisting of a rift valley bordered by steep slopes. These lead to a crestral range which rises 100 to 250 m above the valley floor. This is a stark contrast to the slow-spreading Mid-Atlantic Ridge (M.A.R.) where the difference in height between the inner floor and the ridge crest is 1500 to 2500 m (van Andel and Ballard, 1979). The rift valley of the Galapagos rift can be divided into four main structural and volcanic zones (Allmendinger and Riis, 1979) :

- central zone
- lava plains

- marginal zone
- inner walls

The small-scale morphology of the Galapagos Rift is broadly similar to the slow-spreading Mid-Atlantic Ridge (Lonsdale, 1977). However, the Galapagos Rift has an axial rise rather than a rift valley (Figure 2.10). The lava plains of the Galapagos Rift vary from 2 to 4 km in width and contain an axial volcanic ridge (Lonsdale, 1977). This is similar to ridges observed on the Mid-Atlantic Ridge but is considerably more continuous and less elevated. The location of the main extrusive zone of the ridge, the volcanic axis, moves slowly and continuously over time (Allmendinger and Riis, 1979).

Macdonald (1982) suggests a number of reasons why axial rift valleys develop at slow-spreading centres and not at fast-spreading centres:

- (a) Hydraulic head loss :- Viscous forces beneath the ridge are sufficient to cause a loss in hydraulic head. This results in the formation of a topographic depression.
- (b) Thinning of a ductile layer beneath the rift valley
- (c) Imbalances in supply of new material versus crustal acceleration.

The exact geometry of mantle flow beneath mid-ocean ridges is not fully understood. Seismic evidence suggests that the crust is at its full thickness within a few kilometres of the ridge axis, therefore any off-axis additions should be relatively small (Batiza *et al.*, 1992).

#### **2.4.4. Seamounts**

Seamounts often develop on the flanks of mid-ocean ridges. These chains of volcanic edifices may be aligned parallel to the absolute plate motion direction, parallel to the relative plate motion direction or oblique to both (Allan *et al.*, 1989). Seamounts may be roughly circular or elongate in plan view, usually with steep sides and conical or flattened tops (Abers *et al.*, 1988). Seamount shape appears to be controlled by a number of factors including (a) the age of the underlying lithosphere (b) the thickness of the overlying sediment cover, (c) the geometry of lava conduits supplying the seamount, (d) the fracture pattern in the local area and (e) the plate velocity with respect to the asthenosphere (Smith, 1988; Batiza, 1982). The flattened summits of some seamounts probably develop due to the infilling of a central crater accompanied by circumferential growth along ring fracture conduits (Abers *et al.*, 1988). Volumes of observed seamounts range from  $< 1 \text{ km}^3$  to approximately  $600 \text{ km}^3$ .

Seamounts are thought to represent the surface expression of off-axis mantle upwelling (Shen *et al.*, 1993). They are much more abundant on the flanks of the Mid-Atlantic Ridge than the East Pacific Rise, Smith and Cann (1990) identified 481 seamounts from the median valley

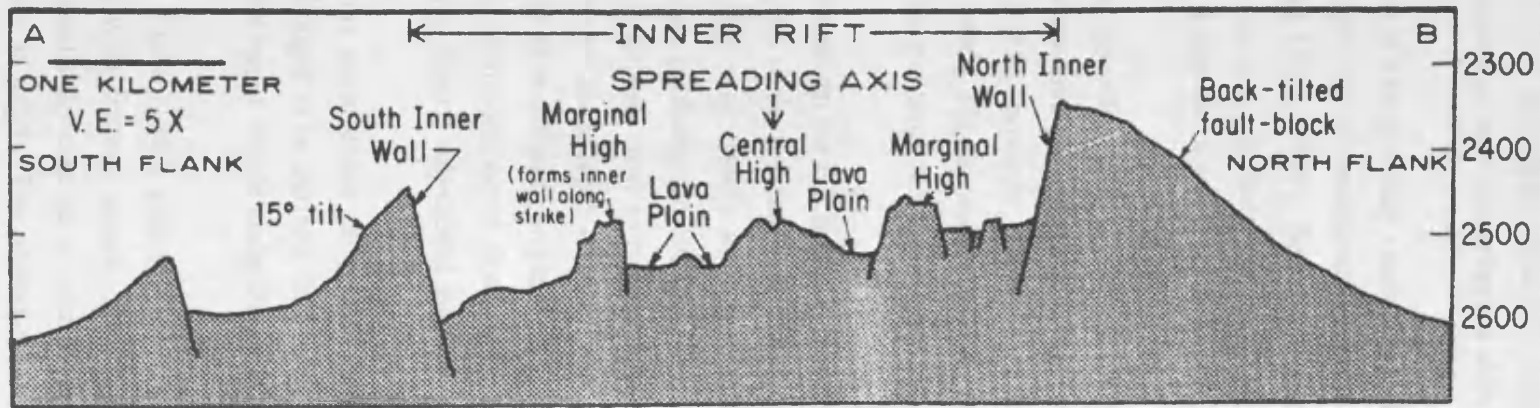


**Figure 2.10.** Cross-section of the Galapagos Rift near  $86^{\circ} 10'$  based on side-looking sonar and deep-tow data, (from Lonsdale, 1977).

floor of the Mid-Atlantic Ridge between 24 and 30°N. This gives a density of approximately 800 seamounts per 1000 km<sup>2</sup>. In addition, the entirety of the axial volcanic ridge in this area appears to be constructed of coalesced seamounts. The presence of large numbers of these volcanic edifices at slow-spreading ridges may suggest that seamount volcanism is an important process in the formation of new lithosphere at slow-spreading ridges (Smith and Cann, 1990).

The absence of a large steady - state, long - lived magma chamber beneath the M.A.R (§ 2.5.1.2.) would ensure that any eruptions would be small localised events from isolated magma pockets (Smith and Cann, 1990). Seamounts produced at the M.A.R may represent point source eruptions from small isolated magma chambers or intermediate-sized magma chambers capable of feeding a number of small seamounts.

On the fast-spreading East Pacific Rise, the density of seamounts is much lower, approximately 9 seamounts per 1000 km<sup>2</sup> (Smith and Cann, 1990). The heights of individual seamounts at the E.P.R, however, are characteristically greater than observed at the M.A.R (Smith and Cann, 1990). This is probably due to the relatively thin crust of the M.A.R median valley floor, which is too weak to support very large volcanic structures.

Most seamounts on the E.P.R. occur between 6 and 20 km from the ridge axis implying that the magma supply to the seamounts is related to some form of upwelling system below the mid-ocean ridge (Shen *et al.*, 1993). Activity of this upwelling system decreases with increasing distance from the axis, probably largely due to the increasing thickness of the lithosphere. Even seamounts formed relatively close to one other may have different modes of origin. Fornari *et al.* (1988) describe two main types of seamount from the Lamont chain close to the E.P.R. These are thought to have differing origins :

- (1) Small low-relief seamounts occur close to the ridge crest, geochemically these lavas appear to have been derived from a sub-crestal magma system such as that described by Shen *et al.*, (1993).
- (2) Large seamounts occur either as isolated edifices or as chains extending away from the ridge. These are thought to be derived from melt anomalies, areas of higher temperature and partial melting in the upper mantle under thinned lithosphere (Fornari *et al.*, 1988).

Batiza and Vanko (1983) note that most seamounts occur in groups or clusters and are closely associated with fracture zones. They interpret this observation as suggesting that seamounts preferentially develop on or near fracture zones. The fracture zones probably serve as magma conduits at depth. The seamounts themselves are produced at oblique fracture networks (Batiza and Vanko, 1983).

Shen *et al.* (1993) suggest three possible origins for seamounts on mid-ocean ridges:

- crust / mantle density anomalies which result in small-scale convection near the ridge axis
- upwelling of mantle between thinned lithosphere
- mini-hotspots with fixed deep mantle sources.

Lonsdale (1983) concludes that some seamounts result from combinations of intrusive and extrusive processes. He suggests that the precursor to development of a seamount is the formation of a laccolith by magma intrusion. As the dome develops, fracturing and collapse occur allowing for extrusion of lava and the development of a lava cone.

Lava flows found on seamounts are very similar to those located on mid-ocean ridge axes, however, a greater abundance of hyaloclastite breccias are found on seamount slopes. Pillow lavas are also common on the flanks of seamounts whereas the summit regions are more likely to be represented by sheet flows (Batiza *et al.*, 1989). This is similar to the distribution of lava types observed on the axial crest of the East Pacific Rise (Renard *et al.*, 1985). Dredge hauls from the Lamont seamount chain, close to the E.P.R., recovered a wide variety of lithologies including ponded sheet flows, lobate flows, pillow lavas, hyaloclastites and massive flow interiors (Allan *et al.*, 1989).

Most seamounts appear to show a trend in evolution of eruptive styles, morphology and petrology, progressing from pillow lavas to sheet flows to hyaloclastites (Batiza *et al.*, 1989). This may reflect changes in the eruptive rate of the seamount lavas. Binard *et al.* (1992) suggest the variation in flow type observed on some seamount slopes is related the depth below seafloor of the eruption, at greater depths, “quiet” eruptions of sheet flows and pillow lavas occur. As the seamount grows, at shallower water depths, more “reactive” eruptions can take place, producing hyaloclastites and auto-brecciated lavas.

## 2.5. Mid-Ocean Ridge Basalt (MORB) Geochemistry

Dredge hauls in the 1960's and 70's provided the first evidence of the nature of mid-ocean ridge basalts (MORB) (e.g. Engel *et al.*, 1965, 1970; Kay *et al.*, 1970). Ocean crust rocks are dominated by low-K olivine tholeiite basalts with a relatively narrow range of chemical compositions (Engel *et al.*, 1965, 1970; Kay *et al.*, 1970). They have high Al and are dominated by olivine and plagioclase mineral assemblages (O'Hara, 1968).

Sun *et al.*, (1979) divide MORB into three chemical groups:

- (i) **Plume** or 'enriched' MORB - rich in incompatible elements (U, Th, Rb, K, Cs, Ba, Nb), (La / Sm) N < 1.
- (ii) **Normal** or 'depleted' MORB - depleted in incompatible elements, (La / Sm) N > 1.
- (iii) **Transition** MORB - intermediate between (i) and (ii).

Melting experiments have shown no correlation between the degree of melting and (i), (ii) or (iii) (Sun *et al.*, 1979).

The suboceanic mantle is probably not heterogeneous, as suggested by trace element and isotope studies and the fact that many suites of MORB cannot be produced from a single parent composition (Langmuir and Hanson, 1980). Most large-scale heterogeneities in MORB are believed to be the result of plumes of enriched material ascending from the deep mantle (Macdougall and Lugmair, 1985). The complementary relationship between MORB and plume sources suggest that MORB becomes depleted in incompatible elements through the migration of enriched liquids (Anderson, 1981). Anderson (1981) states that continental crust is also complementary to MORB therefore is probably also related in some way to the depletion of MORB source.

Two of the most important processes affecting MORB compositions are shallow-level fractional crystallisation and magma mixing. Probably all MORB has experienced some degree of shallow-level fractional crystallisation, changing the abundances of major elements from the parental magma (Klein and Langmuir, 1987). Miyashiro *et al.* (1970) found that an increase in FeO\*/MgO in MORB is related to a decrease in the anorthite (An) content of plagioclase, this is consistent with fractional crystallisation. This is also suggested by the large range of FeO\*/MgO values seen in MORB (0.32 to 2.84 wt. %). Most MORB tholeiites have similar features to the eutectic system fosterite - anorthite - diopside at 1 atm, suggesting that fractional crystallisation of these basalts occurs at low pressure (Miyashiro *et al.*, 1970).

Fisk *et al.*, (1995) state that MORB is assumed to be largely free of significant oceanic crust contamination. This is due to the tensional environment of mid-ocean ridges. An envelope of fresh basalt and cumulates protects the crust, this is difficult to assimilate due to its high melting temperature (Fisk *et al.*, 1995).

### **2.5.1. Origin of MORB**

The composition, location and volume of the source of MORB is still rather uncertain (Anderson, 1981). The source of MORB is believed to be depleted mantle lherzolite in the spinel - plagioclase facies, the overall range of MORB compositions may be generated by between approximately 8 and 20% partial melting of a lherzolite source (Viereck *et al.*, 1989).

There has been a great deal of debate and controversy over the composition and depth of origin of MORB (e.g. Presnall and Hoover, 1987; Stolper, 1980; O'Hara, 1965). Models of MORB genesis can be divided into two main groups:

(a) Presnall and Hoover (1987) and Fujii and Bougault (1983) suggest that the most primitive MORB compositions represent primary magmas with compositions similar to liquids generated

by partial melting of the mantle beneath a mid-ocean ridge. These have been relatively unmodified by fractional crystallisation and magma mixing since segregation from the mantle.

(b) O' Hara (1968); Green *et al.* (1979) and Elthon (1979) suggest that primitive MORB compositions do not represent primary compositions and are derived from primary magmas by the fractional crystallisation of olivine and other mineral phases. This occurs at lower pressure than segregation of the primary melt from the mantle. In order to produce the lava compositions erupted at mid-ocean ridges the primary magma must be rich in MgO, approximately 20 wt % (Stolper, 1980). However, there are conflicting theories as to the depth at which these MgO-rich primary magmas are generated:

- O' Hara (1968) suggested that these primary magmas are generated by partial melting at 25 to 30 kbar. This leaves residual olivine + orthopyroxene + clinopyroxene + garnet in the mantle.
- Green *et al.* (1979) concluded through experimental methods that the primary magmas are generated at 20 kbar, leaving residual olivine + orthopyroxene spinel in the mantle. Experimental work by Stolper (1980) reached almost identical conclusions to Green *et al.* 1979 with only very slight pressure differences
- Elthon (1979) suggested that MgO-rich primary magmas are generated by partial melting a 5 to 10 kbar. This leaves olivine + orthopyroxene residue in the mantle.

The main argument against picritic melt as the parent of primitive MORB is the lack of picritic melts found erupted at the surface (Presnall *et al.*, 1979). Sparks *et al.* (1980) suggest that density variations are very important in explaining the absence of picritic parental melts erupted at the surface. They propose that picritic parents do exist but are prevented from eruption due to their high densities. Hypothetical parental picritic melts will be denser than fractionated basalts, largely due to their relative enrichment in Fe. If these picritic melts are injected into a sub-axial magma chamber, density stratification will occur with the dense picritic melts pooling at the base of the magma chamber and not mixing with the overlying fractionated magmas (Sparks *et al.*, 1980). This new influx of melt will inflate the magma chamber and increase fluid pressure, possibly pushing some of the fractionated lava out of the magma chamber as an eruption. If olivine precipitates from the picritic melt the density will increase but if large amounts of olivine precipitate the liquid will become buoyant, eventually rising and mixing with the more fractionated basalts. Sparks *et al.* (1980) suggest that this process may be partially responsible for the formation of the dunite layers found at the base of ophiolite cumulate sequences, providing a complementary mechanism to crystal settling.

Klein and Langmuir (1989) provide a model integrating both shallow and deep partial melting to explain the diversity of mid-ocean ridge basalts. They envisage that partial melts are pooled together from throughout melting columns of variable length (Figure 2.11). Trends in

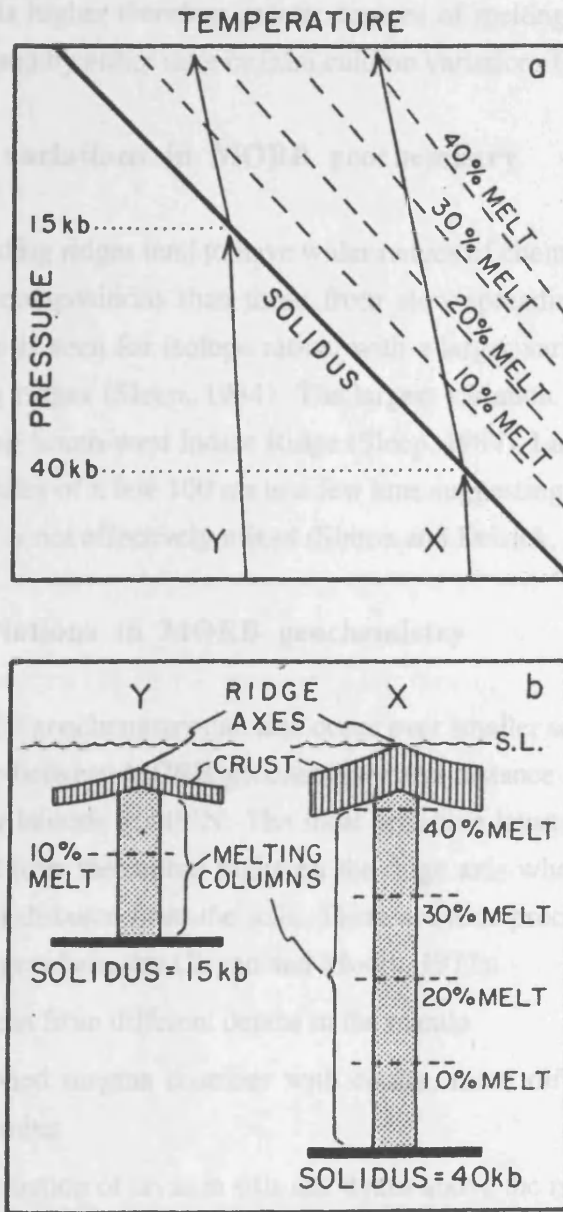


**Figure 2.11.** (a) Schematic drawing of mantle pressure versus temperature. X is a hotter batch of mantle which intersects the solidus at greater depths and undergoes greater extents of melting; Y represents a cooler melt which intersects the solidus at shallower depths and undergoes less melting on ascent. (b) Schematic cross-section of ocean crust and mantle resulting from the paths of X and Y, (from Klein and Langmuir, 1989).

MORB compositions can arise as the result of variations within such a melt column, in column Y melting of cooler mantle occurs, this has a lower mean pressure of melting and hence lower extents of partial melting occur whereas in column X, which represents a much longer melt column, pressure is higher therefore greater degrees of melting occur. Trends in geochemical data can occur caused by either inter or intra column variations (Klein and Langmuir, 1989).

### **2.5.2. Regional variations in MORB geochemistry**

Lavas at fast-spreading ridges tend to have wider ranges of chemical compositions and extend to more fractionated compositions than those from slow-spreading ridges (Sinton and Detrick, 1992). The reverse is seen for isotope ratios, with a larger variation at slow-spreading ridges than fast-spreading ridges (Sleep, 1984). The largest variation in isotope ratios occurs on the ultra slow-spreading South-west Indian Ridge (Sleep, 1984). Lava compositions may also vary along a ridge on scales of a few 100 ms to a few kms suggesting that subaxial magma chambers are not continuous or not effectively mixed (Sinton and Detrick, 1992; Batiza *et al.* 1988).

### **2.5.3. Local variations in MORB geochemistry**

Variations in MORB geochemistry can also occur over smaller scales. Bryan and Moore (1977) noted a relationship between MORB geochemistry and distance from the ridge axis on the Mid Atlantic Ridge near latitude 30°49'N. The most primitive lavas with high MgO, low TiO<sub>2</sub> and K<sub>2</sub>O were retrieved from the central highs on the ridge axis whereas the most evolved samples were recovered at a distance from the axis. There are four processes that may account for this spatial zonation of geochemistry (Bryan and Moore, 1977):

- tapping of magma from different depths in the mantle
- tapping of a zoned magma chamber with cooler, more differentiated magma in the outer parts of the chamber
- shallow differentiation of lavas in sills and dykes above the magma chamber
- differentiation during a lava flow

Bryan and Moore (1977) favour the second of these processes, however, this model does not account for the wide diversity in REE variations. It is probably more likely that the flank lavas were erupted from different melt batches than those on the axis (Nisbet and Fowler, 1978) (§2.5.4.3).

It has been proposed that magma chambers are situated beneath some mid-ocean ridge axes. The existence of such features may account for the layered structure and geochemical variations of the oceanic crust. Initially it was believed that ocean basalts represented essentially unmodified primary melts from the mantle (Robson and Cann, 1982), however, work by

O'Hara (1977) and others showed distinct petrological evidence that ocean basalts are unlikely to be primary melts. This is confirmed by studies of the East Pacific Rise (Robson and Cann, 1982) here, two generations of phenocryst are found within basalt samples, suggesting that the basalt is a mixture of primitive and evolved melts. These were perhaps mixed in a subaxial, crustal magma chamber undergoing fractional crystallisation (Robson and Cann, 1982).

#### **2.5.4. Magma chamber models**

It is now widely accepted that some form of magma chamber may be present beneath mid-ocean ridge axes (e.g. Cann, 1970, 1974; Bryan and Moore, 1977; Pallister and Hopson, 1981). The dimensions, shape and longevity of such features however, has been the subject of much debate for the past 20 to 30 years. Early workers envisaged that sub-axial magma chambers were large, dome-shaped reservoirs containing predominantly molten material (Figure 2.12) (Cann 1970, 1974; Bryan and Moore, 1977). The upper crust is formed as magma is erupted at the sea-floor through fissures, these lavas cut through previously erupted lavas, producing a layer of entirely volcanic rocks (Cann, 1974). The lower crust is believed to be formed due to solidification of the sub-axial magma chamber. It consists of two main components (Cann, 1974):

- (a) A lower layer comprised of cumulates. This is formed as crystals settle to the floor of the magma chamber,
- (b) An upper layer comprising isotropic gabbro, formed by gradual cooling of the magma chamber. This layer is cooled by seawater circulation in the upper crust.

This simple magma chamber model produces the classic three-layered crustal structure predicted by ophiolites and is often called the "infinite onion" model as crust continuously peels off the edges of the chamber whilst the chamber is fed by new liquid from below (Nisbet and Fowler, 1978).

Pallister and Hopson (1981) investigated plutonic sequences from the Samail ophiolite in Oman and produced a "funnel" rather than "onion" shaped magma chamber (Figure 2.13). This contains a "sandwich" horizon formed by the convergence of downward crystallisation from the roof and upward crystallisation from the floor.

All these early models assumed the interior of the magma chamber was predominantly molten. However, a number of workers suggest that the interior of the magma chamber has only a thin layer of melt with the bulk of the magma chamber interior containing a mush of crystals and interstitial liquid (Figure 2.14) (Sleep, 1975; Dewey and Kidd, 1977; Sinton and Detrick, 1993). This melt lens is assumed to be < 1 to 2 km wide and a few tens to hundreds m thick (Sinton and Detrick, 1993). The low velocity zone (§ 2.5.1.2) imaged beneath some fast-spreading ridges is represented by the "mush zone".

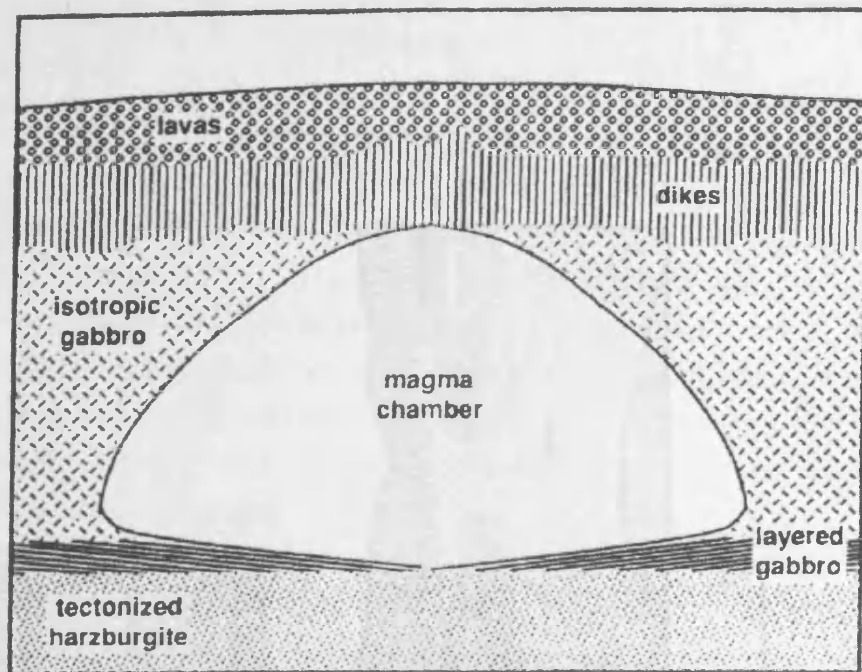


Figure 2.12. Schematic diagram of a simplistic dome or "onion"-shaped magma chamber (from Sinton and Detrick, 1992).

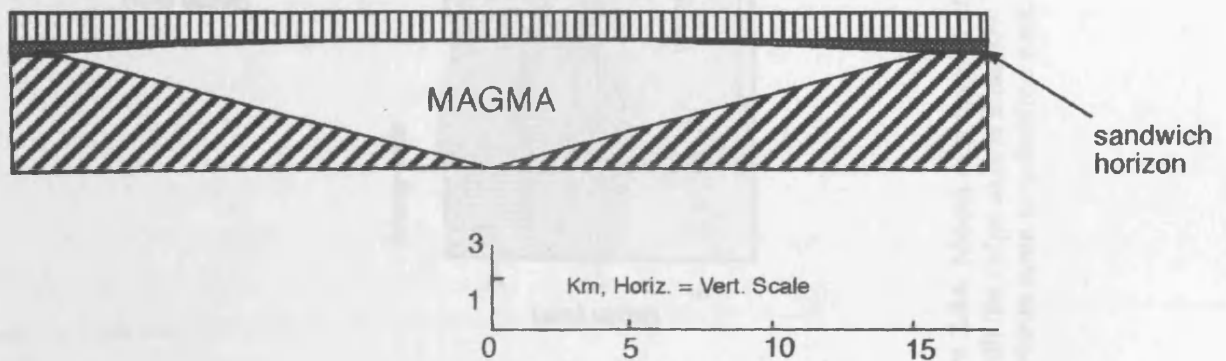
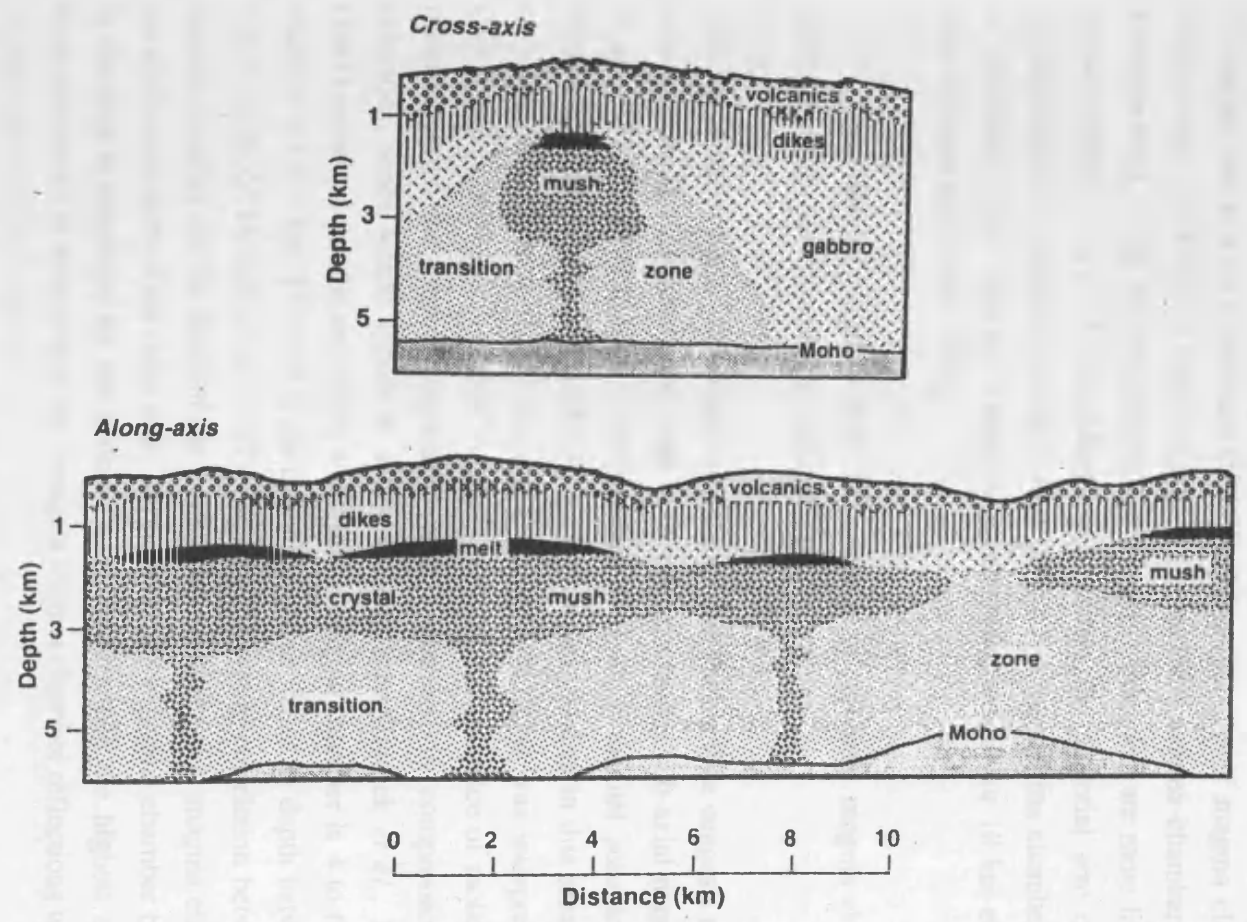


Figure 2.13. "Funnel"-shaped magma chamber model (adapted from Pallister and Hopson, 1981).



**Figure 2.14.** Model of a magma chamber along a fast-spreading ridge, from Sinton and Detrick (1992). Beneath the ridge axis is a narrow body of melt that grades down into a “mush” zone surrounded by a transition zone to solidified rock.

Magma chambers may be either open or closed systems (Robson and Cann, 1982). At mid-ocean ridges magma chambers are more likely to be open systems because the asthenosphere is continuously uprising. Depth to the magma chamber will increase off-axis due to the thickening of the lithosphere (Haymon *et al.*, 1993).

#### *2.5.4.1. The effect of spreading rate on magma chamber development*

Spreading rate is a very important factor in the production of magma chambers beneath mid-ocean ridges. Dick *et al.* (1992) suggest that long-lived magma chambers are present beneath fast-spreading ridges whereas shorter-lived magma chambers are more likely to occur beneath slow-spreading ridges. As spreading rate increases the potential size of a magma chamber expands, at half-spreading rates of 0.45 to 0.9 cm / yr. no magma chamber can exist, however, at a half-rate of 6.0 km / yr. a magma chamber may extend for 10 km either side of the ridge axis (Robson and Cann, 1982).

Two lines of evidence as to the presence of sub-axial magma chambers beneath fast-spreading ridges are provided by seismic data:

(1) Low Velocity Zone:- Seismic data from the East Pacific Rise suggests the presence of a low velocity zone (LVZ) beneath the ridge axis, interpreted as a sub-axial magma chamber (Detrick *et al.*, (1987)). Detrick *et al.* (1987) undertook a multi-channel seismic survey of the East Pacific Rise between 8°50' N and 13°30' N. The seismic data in this area implies the presence of a low-velocity zone (LVZ) beneath the ridge axis. This was interpreted by Detrick *et al.* (1987) as representing a sub-axial magma chamber. The presence of molten or partially molten material within the crust is associated with a decrease in compressional and shear-wave velocities, hence would appear as a low velocity zone (Detrick *et al.*, 1990). Detrick *et al.* (1987) estimated that the maximum width of this magma chamber is 4 to 6 km with an average width of < 3 to 4 km. The roof of the magma chamber varies in depth between 1.2 and 2.4 km below sea-floor. Detrick *et al.* (1987) also found a strong correlation between the depth of the magma chamber and the depth of the ridge axis, the shallowest magma chambers are found on the shallowest parts of the ridge axis. The presence of a magma chamber beneath the ridge axis in this area is supported by the geochemistry, basalts with the highest eruption temperatures were discovered in areas where the strongest magma chamber reflections were observed.

(2) High amplitude subhorizontal upper crustal reflector associated with the top of the LVZ (Herron *et al.*, 1980; Hale *et al.*, 1982; Detrick *et al.*, 1987). This has been interpreted as representing the top of a sub-axial magma chamber (Detrick *et al.*, 1987). This axial magma chamber reflector is located approximately 2 km below sea-floor (Herron *et al.*, 1980). Herron *et al.* (1980) could not detect the sides of the magma chamber, implying that the magma

chamber sides are very steep or the seismic velocity difference is too gradational. Herron *et al.* (1980) also noted a correlation between the width of the ridge crest and the apparent width of the top of the subaxial magma chamber, in areas with a narrow ridge crest, the magma chamber reflector is also narrow.

Hale *et al.* (1982) reprocessed and remigrated the data obtained by Herron *et al.* (1980) and reached similar conclusions. They interpreted a dipping reflector 2.4 km below sea-floor as the top of a subaxial magma chamber. This magma chamber is asymmetrical about the axis, extending 650 to 4.5 km to the west of the axis and apparently mostly absent on the east side of the ridge.

Seismic surveys have so far failed to locate a magma chamber along the Mid-Atlantic Ridge but the geochemical evidence shows low pressure evolution of magmas has occurred. This may suggest that a magma chamber exists in the area but is limited in space and time (Smith and Cann, 1992). Thermal models place constraints on the size and shape of magma chambers that can develop at slow-spreading ridges (Dewey and Kidd, 1977; Sleep, 1975; Kuszniir and Bott, 1976). Slow-spreading ridges tend to be more fractured than fast-spreading ridges therefore are cooled more effectively by hydrothermal circulation, suggesting narrower magma chambers would develop (Dewey and Kidd, 1977).

Nisbet and Fowler (1978) proposed that at slow-spreading ridges the “infinite onion” model is unlikely to occur due to five main factors:

- seismic evidence suggests the presence of magma chambers greater than approximately 2 km in width is unlikely
- thermal constraints restrict the development of a large magma chamber at slow-spreading ridges
- the presence of mantle xenocrysts in many erupted lavas suggests that the lavas cannot have resided for long periods in shallow sub-axial magma chambers
- it is very difficult for a magma chamber to periodically let parental liquids pass through and still maintain the chemistry of low pressure melt equilibria
- the Rayleigh number for a magma chamber 1 to 6 km wide would be approximately  $10^{18}$  to  $10^{23}$ . This implies very vigorous convection therefore the zoned magma chamber suggested by Bryan and Moore (1977) would be very unlikely to develop.

As an alternative, Nisbet and Fowler (1978) suggest an “infinite leek” model in which partial melt segregating from the mantle is trapped beneath the base of the crust at a depth of approximately 6 to 8 km below sea-floor (Figure 2.15). As this pool of melt grows a crack is nucleated in the crust above it. As the crack expands the melt ascends into it. When the base of

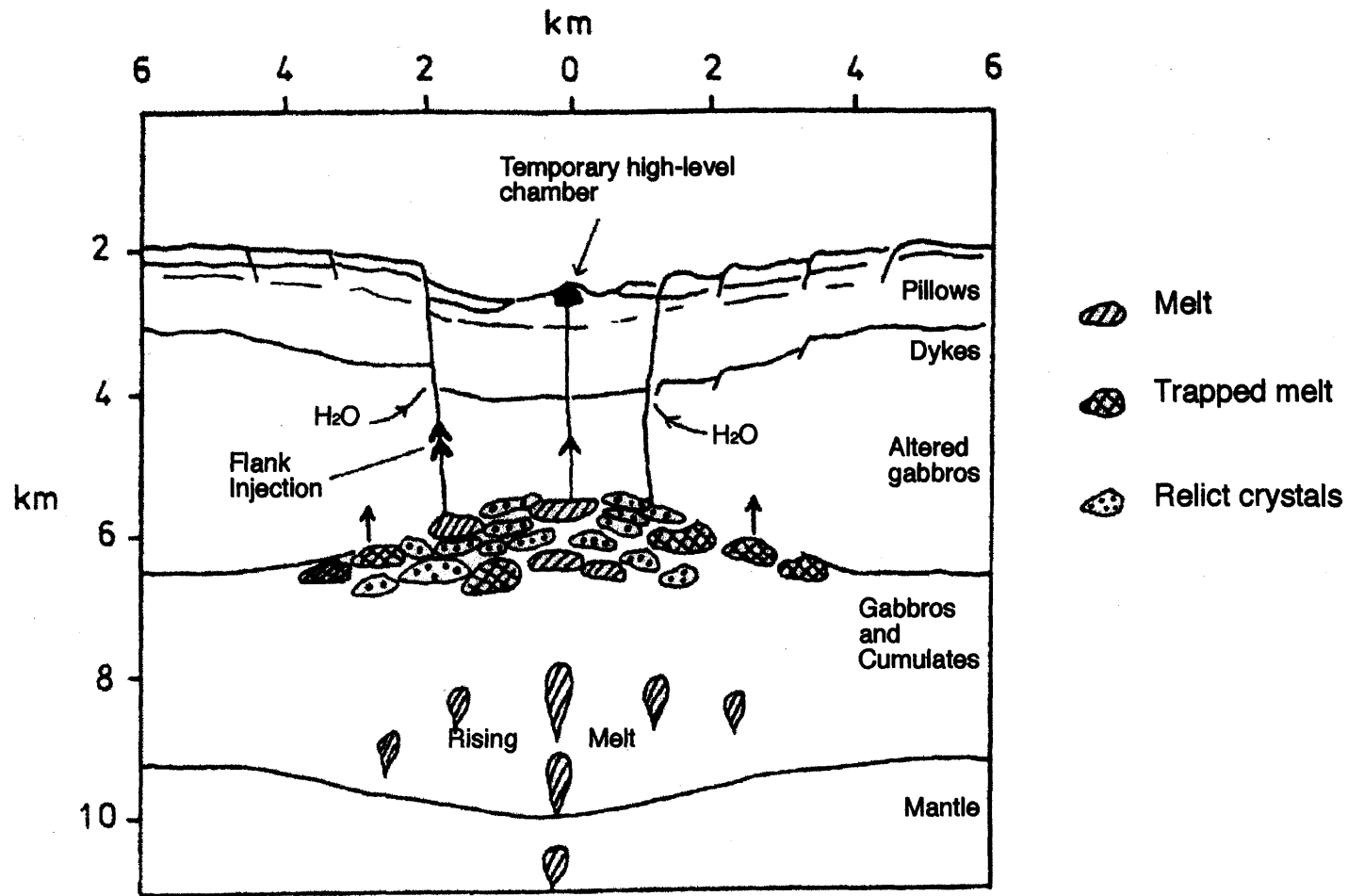


**Figure 2.15.** 'Infinite leak' model of a subaxial magma chamber beneath a slow-spreading ridge. The rising melt is trapped at the base of the elastic crust; it may be injected to the surface or crystallise out as gabbro (from Nisbet and Fowler, 1978).

the crack becomes sealed the magma rises rapidly to the surface and a small volcano is developed.

Nisbet and Fowler (1978) uses this model to explain the more evolved lavas often noted on the flanks of the M.A.R inner valley floor. Liquids rising from the mantle at a distance from the ridge axis are more likely to become trapped beneath the crust, therefore, when they eventually escape to the surface they will erupt more evolved lavas than seen at the ridge axis.

Stakes *et al.* (1984) claim that steady-state magma chambers can develop at slow-spreading ridges. Their studies of the Mid-Atlantic Ridge (36°47'N) suggest the limited range of glass compositions in this area requires the presence of some form of steady-state magma chamber, a wider range of chemical compositions would be expected for small ephemeral magma bodies. Stakes *et al.* (1984) propose that a steady-state magma chamber exists beneath their studied section of the Mid-Atlantic Ridge however it is less than 2 km in diameter. They suggest that this magma chamber only exists in its steady-state at the centre of a ridge segment, with more ephemeral bodies at the segment ends where the rift valley terminates at fracture zones. If these bodies are connected to the main steady-state magma chamber they will expand and contract in response to the magma supply.

More recent models for magma chamber development at slow-spreading ridges favour the existence of small melt batches. A similar model to that of Nisbet and Fowler (1978) is suggested by Smith and Cann (1993) however, they propose that the batches of magma ascend within the crust rather than being trapped at its base (Figure 2.16). The ascending melts rise until they reach the base of the brittle lid (caused by hydrothermal circulation in the upper crust) and form small bodies of magma.

Magma chambers may also be absent or discontinuous beneath some fast-spreading ridges. Gravity and seismic data collected by McClain and Lewis (1982) on the Juan de Fuca Ridge (spreading rate 3 cm / yr.) at 47°N shows no evidence for the presence of a sub-axial low velocity / density zone in this area. The area has significantly different seismic wave propagation and density structure than observed on the E.P.R. McClain and Lewis (1982) conclude that :

- (a) accretion at fast-spreading ridges may not always be a continuous process but an episodic one,
- (b) cooling is probably quicker than was previously modelled and probably extends to the base of the crust.
- (c) even with the absence of a LVZ the crust at the Juan de Fuca Ridge is a similar thickness as described elsewhere therefore the crust - mantle boundary is probably not a petrological boundary. It therefore more than likely represents the depth of penetration of hydrothermal alteration.

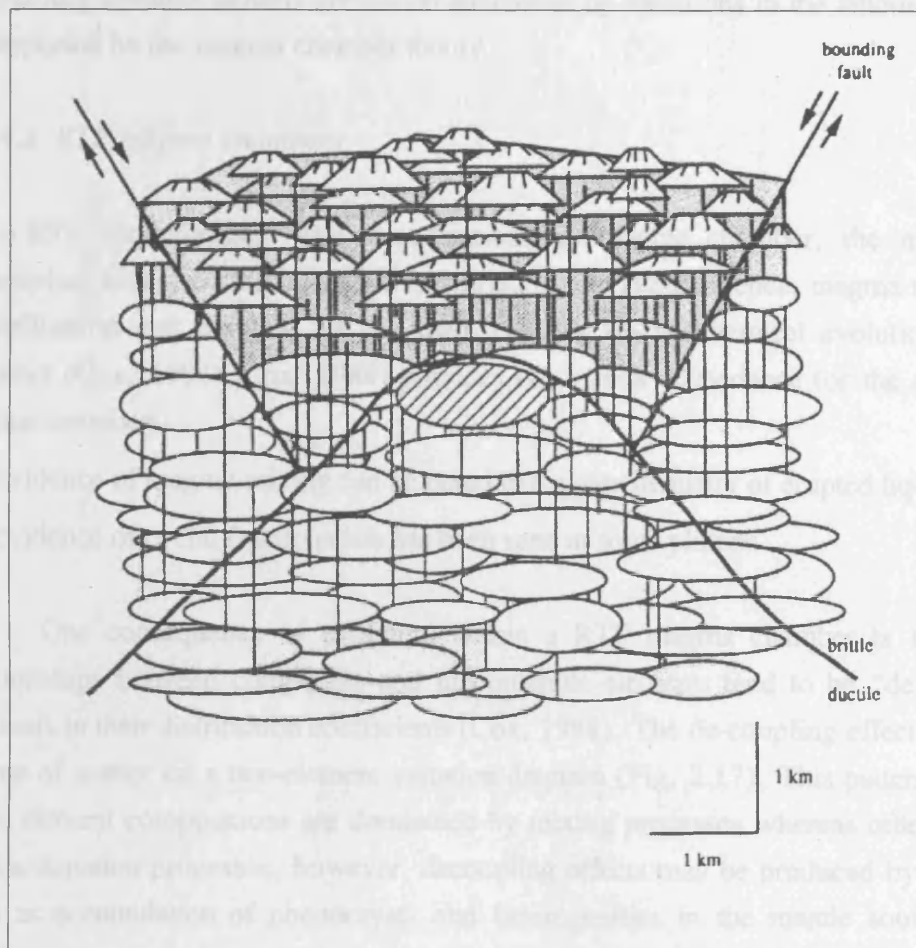


**Figure 2.16.** Model in which the crust is constructed of seamounts and fissure-fed flows. Each seamount is fed from a separate magma body. The current body feeding the ridge is striped (from Smith and Cann, 1984).

The dependence of magma chamber development on spreading rate is further supported by isotope evidence. Basalts from the slow-spreading Mid-Atlantic Ridge have a greater diversity of Pb, Sr and Nd isotopes than basalts from the fast-spreading East Pacific Rise (Batiza, 1984). Batiza (1984) suggests two main reasons for this observation:

- (a) the mantle source beneath a fast-spreading ridge may be more homogeneous than beneath a slow-spreading ridge. However, there is no substantial evidence to support this
- (b) varying amounts of homogenisation are caused by variations in the amount of mixing. This is supported by the magma chamber theory.

#### **2.5.4.2. RTF magma chambers**

In a RTF (replenished - tapped - fractionated) magma chamber, the magma supply is replenished before all the liquid has solidified (Cox, 1988). Hence, magma mixing, fractional crystallisation and eruption are the main controls on geochemical evolution in the magma chamber (Cox, 1988). Cox (1988) provides two pieces of evidence for the existence of RTF magma chambers:

- evidence of magma mixing can be noted in the geochemistry of erupted liquids,
- evidence of cyclic fractionation has been seen in some plutons.

One consequence of evolution within a RTF magma chamber is that inter-element relationships between compatible and incompatible elements tend to be “de-coupled” due to contrasts in their distribution coefficients (Cox, 1988). The de-coupling effect produces a large degree of scatter on a two-element variation diagram (Fig. 2.17). This pattern occurs because some element compositions are dominated by mixing processes whereas others are dominated by fractionation processes, however, decoupling effects may be produced by other processes, such as accumulation of phenocrysts and heterogeneities in the mantle source region (Cox, 1988).

#### **2.5.5. Seamount Geochemistry**

The study of seamounts at mid-ocean ridges is useful for investigating the melting conditions and the nature of the mantle source of mid-ocean ridge basalts. (Batiza *et al.*, 1989). Lava chemistry in seamounts is rather different than axis rocks, dredge samples from the Baja Seamount Province, close to the East Pacific Rise, were described by Engel and Engel (1964a) as being predominantly alkali basalts. Similar lithologies were also recovered from seamounts close to the Mid-Atlantic Ridge (Engel and Engel, 1964b).

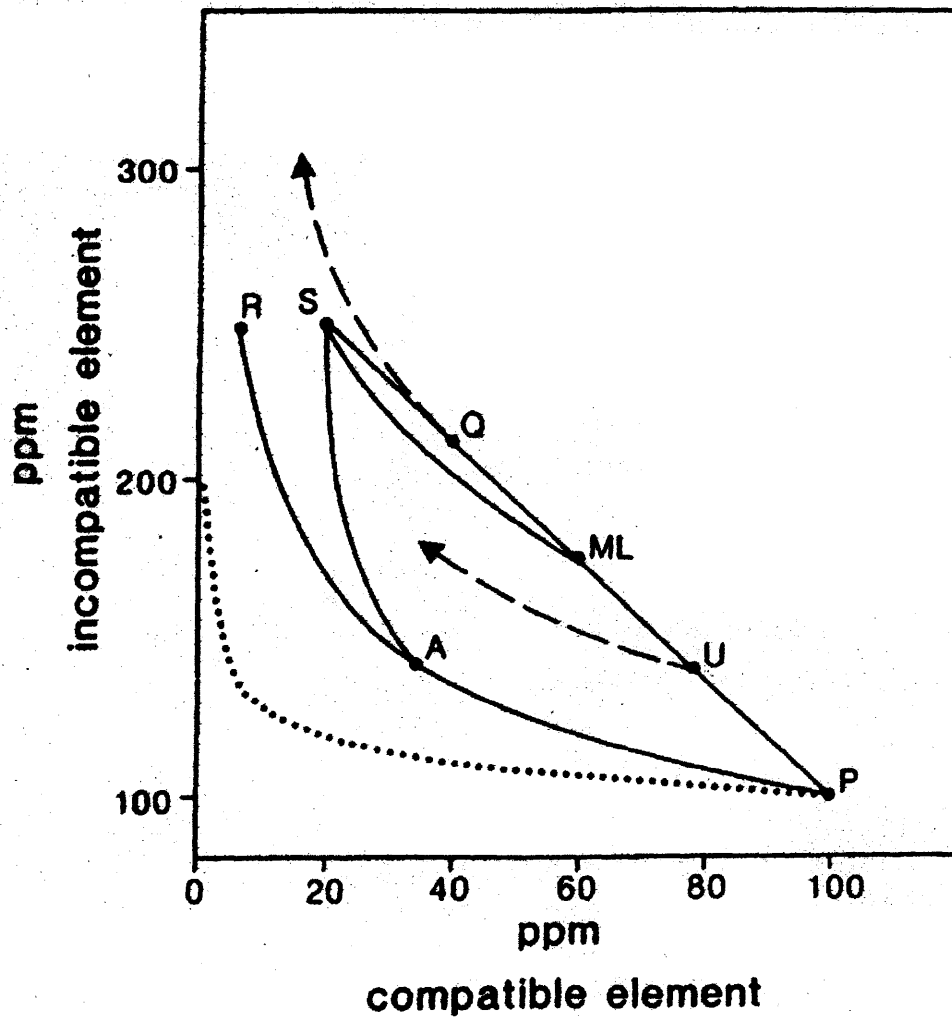


**Figure 2.17.** Two element variation diagram showing the decoupling effect of evolution in a RTF magma chamber, from Cox (1988). P = parent magma S = steady-state liquid. The 1st cycle of fractionation gives AR. The contrast between AR and AS is due to the decoupling effect. In ideal conditions, S mixes with P to produce mixed liquid ML. In random conditions, mixed liquids Q or U may be formed, these would fractionate along the curves shown.

Fornari *et al.* (1988) studied the Lamont seamount chain, situated approximately 8 km from the axis of the East Pacific Rise. They described the recovered lavas as having mafic compositions, representing relatively primitive lavas. All the lavas were light rare-earth element (LREE) depleted tholeiitic basalts with simple olivine and plagioclase mineral assemblages. The simple mineralogy and depleted chemistry of seamount basalts implies that the melts forming them underwent a simple and rapid ascent compared to most MORB generated at mid-ocean ridges (Fornari *et al.*, 1988).

Most seamounts appear to be fed by small batches of melt which ascend from the mantle without undergoing significant modification (Batiza *et al.*, 1989). Axis lavas tend to be more evolved than seamount lavas. Batiza *et al.* 1989 suggest that this is probably due to cooling in subaxial magma chambers. If these cooling effects are removed, it can be shown that axial lavas are the result of deeper initial melting accompanied by larger extents of melting (Batiza *et al.*, 1989). Lavas collected from seamounts tend to have higher MgO contents and are usually considerably more compositionally diverse than lavas from the ridge axis suggesting that not all off-axis seamounts are supplied by an axial magma chamber (Allan *et al.*, 1989).

Engel and Engel (1964a) note a relationship between the height and morphology of off-axis volcanic edifices and the composition of their constituent basalts. Alkali basalts tend to be concentrated on the upper flanks and summit regions of seamounts with tholeiites only occurring at heights of less than 2500m above sea-floor. Engel and Engel (1964a) conclude that the alkali basalts were derived from tholeiitic basalts by differentiation in magma chambers below the seamount.

Batiza (1981) observed that lava compositions appear to also vary with lithospheric age. Tholeiitic basalts tend to be erupted on seamounts formed on younger crust (1 to 3 m.y. old) whereas alkali basalts tend to occur at greater distances from the ridge crest. Batiza (1981) attribute this pattern to lower extents of partial melting at increasing distance from the ridge crest. This relies on two main assumptions: (a) that the mantle is heterogeneous and (b) that depleted mantle has a lower melting point than undepleted mantle.

K / TiO<sub>2</sub> ratios are very similar for both seamount and axial lavas, therefore, the magma sources for both are not significantly different (Batiza *et al.*, 1989). This suggests the presence of a broad upwelling zone which produces axial magmas from the hot centre of the upwelling and seamounts from the cooler upwelling margins (Batiza *et al.*, 1989).

## **2.6. Summary**

The simplest model for the architecture of the ocean crust generated at mid-ocean ridges is a three layer structure based on the evidence from ophiolites and seismic surveys. Seismically the crust can be divided into three main layers, these are largely analogous to those observed within ophiolite complexes. Seismic velocities increase in each successively deeper layer. The ocean crust rests along a seismic discontinuity, known as the Mohorovic discontinuity or MOHO, on a mantle composed of peridotites.

A variety of flow morphologies are produced at mid-ocean ridges, including pillow lavas, sheet flows and breccias. The main controls on flow morphology are thought to be effusion rate and viscosity and temperature of the erupting lava.

Mid-ocean ridges vary widely in their spreading rates with half-rates of between  $<1$  to  $>8$  cm/yr. and consequently also have variable morphology. Slow-spreading ridges tend to have a rugged morphology with a pronounced broad axial valley whereas fast-spreading ridges tend to have a much less rugged topography, often with a small axial summit graben. Intermediate spreading ridges have very simple morphologies, similar to slow-spreading ridges but with an axial rise rather than an rift valley.

Mid-ocean ridge basalts are generally uniform in composition. The main controls on their composition are source heterogeneities, shallow-level fractional crystallisation and magma mixing in a sub-axial magma chamber. Models for subaxial magma chambers vary widely however the old dome-shaped chamber models have been superseded by recent lens-type models.

## **2.6. Summary**

The simplest model for the architecture of the ocean crust generated at mid-ocean ridges is a three layer structure based on the evidence from ophiolites and seismic surveys. Seismically the crust can be divided into three main layers, these are largely analogous to those observed within ophiolite complexes. Seismic velocities increase in each successively deeper layer. The ocean crust rests along a seismic discontinuity, known as the Mohorovic discontinuity or MOHO, on a mantle composed of peridotites.

A variety of flow morphologies are produced at mid-ocean ridges, including pillow lavas, sheet flows and breccias. The main controls on flow morphology are thought to be effusion rate and viscosity and temperature of the erupting lava.

Mid-ocean ridges vary widely in their spreading rates with half-rates of between  $<1$  to  $>8$  cm/yr. and consequently also have variable morphology. Slow-spreading ridges tend to have a rugged morphology with a pronounced broad axial valley whereas fast-spreading ridges tend to have a much less rugged topography, often with a small axial summit graben. Intermediate spreading ridges have very simple morphologies, similar to slow-spreading ridges but with an axial rise rather than an rift valley.

Mid-ocean ridge basalts are generally uniform in composition. The main controls on their composition are source heterogeneities, shallow-level fractional crystallisation and magma mixing in a sub-axial magma chamber. Models for subaxial magma chambers vary widely however the old dome-shaped chamber models have been superseded by recent lens-type models.

## CHAPTER 3

---

### ***Reconstructing the upper oceanic crust using core and log data. Case Study 1: ODP Hole 896A***

#### **3.1. Introduction**

Chapter 3 comprises a case study of a basement borehole in the equatorial East Pacific, ODP Hole 896A. The hole has poor core recovery, only 26.9 %, but good quality logging data (Alt, Kinoshita *et al.*, 1993), hence, it is possible to reconstruct the lithostratigraphy of the crust in this area through integration of core and log data. This is supplemented by mineralogical and geochemical data in an attempt to constrain the processes responsible for the lithological variability within the core. The chapter can be divided into three main sections. Section 3.2 discusses the geological background of Site 896A. Sections 3.3 to 3.6 are concerned with the core and log data available for Hole 896A and the lithological variability present within the Hole 896A core. Finally, Sections 3.7 to 3.9 present a summary of the mineralogy and geochemistry of the Hole 896A core, discussing the processes responsible for these variations and their relationship to the lithostratigraphy.

ODP Hole 896A is located approximately 200 km south of the Costa Rica Rift in the equatorial East Pacific (Fig. 3.1). The site was drilled during ODP Leg 148, between the 21st January and the 10th March, 1993. The hole was initially drilled due to problems encountered whilst drilling the nearby ODP Hole 504B (Alt *et al.*, 1996). There were three main scientific objectives for drilling Hole 896A (Alt, Kinoshita *et al.*, 1993):

- examination of the heterogeneity of basement alteration in a ridge flank convection cell, Hole 896A represents an upwelling area whereas, in Hole 504B basement fluids are moving horizontally
- investigation into variations in the lithostratigraphy and geochemistry of the upper ocean crust
- investigation of the changes across a fault, Hole 504B is situated on the inferred hanging wall whereas Hole 896A is situated on the inferred footwall

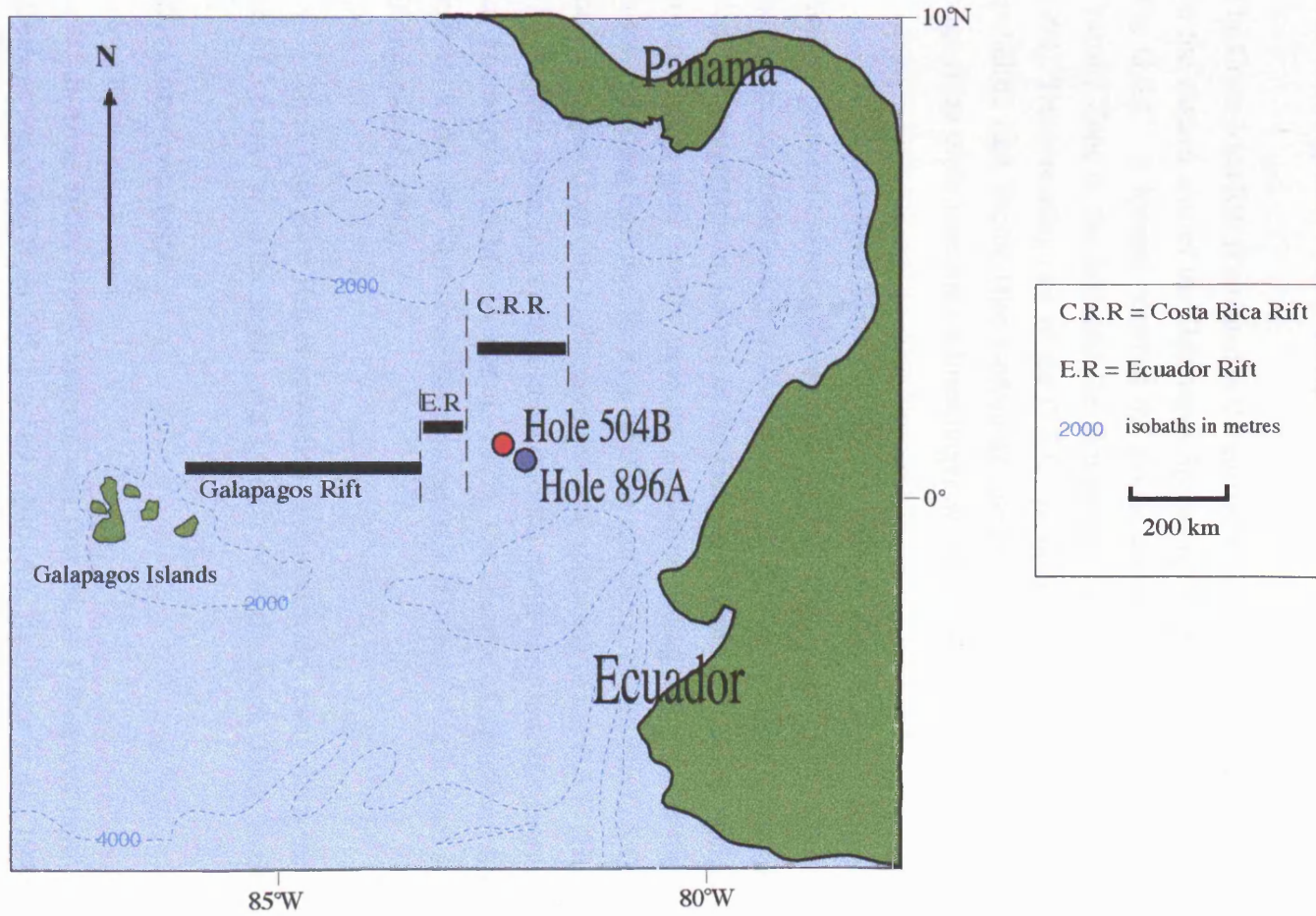


Figure 3.1. Location of ODP Holes 896A and 504B (adapted from Laverne *et al.*, 1996)

Site 896A is situated on a bathymetric high in a water depth of approximately 3450m (Alt, Kinoshita *et al.*, 1993). The site is close to Site 678, drilled on Leg 111 (Alt, Kinoshita *et al.*, 1993). The age of the crust in this area was determined by palaeontological evidence from sediments recovered from Hole 678 at between 5.8 and 6.4 Ma (Alt, Kinoshita *et al.*, 1993). reversal.

### 3.2. Geological background

The Costa Rica Rift is situated in the east-west segment of the Cocos - Nazca Spreading Centre, on the eastern arm of the Galapagos Spreading Centre (G.S.C) (Alt, Kinoshita *et al.*, 1993). The G.S.C. is located between the Cocos and Carnegie Ridges, and bound by the Panama Fracture Zone in the east and the Ecuador Fracture Zone to the west (Dick, Erzinger *et al.*, 1992). The spreading rate of the G.S.C. is variable from 5.7 to 7.2 cm / yr.; it joins the fast-spreading East Pacific Rise (spreading rate of approximately 14.2 cm / yr.) at a stable ridge-ridge-ridge triple junction (Allmendinger and Riis, 1979).

The Galapagos Spreading Centre was produced at approximately 25 Ma, when the Farallon plate split along a pre-existing fracture zone, forming the Cocos and Nazca plates and the Galapagos triple junction (Hey *et al.*, 1977). This resulted in the formation of a triangular wedge of rough terrain, known as the Galapagos Gore (Dick, Erzinger *et al.*, 1992). The high ground in the gore results from the slower-spreading rates inside the gore compared to the faster-spreading East Pacific Rise (Holden and Dietz, 1972). The G.S.C asymmetrically bisects the Galapagos Gore due to the asymmetrical spreading of the G.S.C (Holden and Dietz, 1972). The original spreading system trended to the north-east, but was reorganised into the present-day geometry by 23 Ma (Hey *et al.*, 1977). The absence of significant fracture zones within the segment in the last 10 million years suggests a relatively simple plate spreading history (Dick, Erzinger *et al.*, 1992).

The Costa Rica Rift is spreading asymmetrically away from the ridge axis with a half-rate of 3.6 cm / yr. to the north, and 3.0 cm / yr. to the south (Dick, Erzinger *et al.*, 1992).

### 3.3. Core recovery

In Hole 896A rubbly material was first felt at 179 metres below sea-floor (mbsf) and basement was cored from 195.1 to 569 mbsf (Alt, Kinoshita *et al.*, 1993). The upper 15 m of basement was not cored because it was too rubbly and unstable to set the casing. The total depth drilled was 469 mbsf, comprising 290 m of basement rocks, but only 73.68m of actual core was recovered, giving an average core recovery for the hole of 26.9 % (Alt, Kinoshita *et al.*, 1993).

As on all ODP legs, each cored interval is approximately 9.5 m in length and each recovered interval is numbered in sequence from the top of the drilled section to the base (Alt, Kinoshita *et al.*, 1993). Where recovery is < 100 %, core pieces are moved to the top of the core barrel, allowing the total core recovery to be calculated. This movement of core pieces produces a systematic bias into any estimation of depth of core pieces, for example in a 9.5 m long cored interval with only 5 % recovery, an individual core piece may be as much as 9 m from its true position within the core. The core recovery for Hole 896A is shown in Table 3.1., recovery varies greatly between cored intervals, ranging from as low as 1.3 % in core 13R up to 72.4 % in core 18R.

Core	Metres cored	Metres recovered	% Recovery	Core	Metres cored	Metres recovered	% Recovery
1R	5.8	0.78	13.4	16R	9.6	3.99	41.5
2R	9	0.89	9.9	17R	9.6	5.23	54.5
3R	9	1.38	15.3	18R	2.9	2.1	72.4
4R	9.5	1.06	11.1	19R	7.5	1.6	21.3
5R	9.5	4.5	47.3	20R	9.5	1.21	12.7
6R	9.5	3.59	37.8	21R	9.6	2.66	27.7
7R	9.7	1.21	12.5	22R	9.5	4.62	48.6
8R	9.6	1.14	11.9	23R	9.7	3.25	33.5
9R	9.7	1.96	20.2	24R	9.5	6.09	64.1
10R	9.6	1.38	14.4	25R	9.7	3.15	32.5
11R	9.6	3.49	36.3	26R	9.5	3.06	32.2
12R	9.5	1.83	19.2	27R	9.5	2.89	30.4
13R	9.5	0.12	1.3	28R	9.7	1.75	18.0
14R	9.7	3.55	36.6	29R	9.6	1.59	16.5
15R	9.6	2.29	23.8	30R	9.7	1.32	13.6

**Table 3.1.** Core Recovery for ODP Hole 896A, data from Alt, Kinoshita *et al.* (1993).

### 3.4. Lithologies recovered from Hole 896A

Three main lithological units were recovered from Hole 896A (Alt, Kinoshita *et al.*, 1993) : Massive Units, Pillow Lavas and Breccias. These were distinguished between on the basis of the gross structure and texture of the recovered rocks, summarised in Table 3.2. Two dyke margins were also recovered from Hole 896A and comprise < 1 % of the recovered material (Alt, Kinoshita *et al.*, 1993). This lithology is not discussed here, as this study is primarily concerned with the extrusive, rather than intrusive, units in ODP Hole 896A.

During ODP legs, the recovered core is logged in shifts by a number of specialist scientists, this may result in inconsistently recorded core data, as each individual's interpretation of the criteria may be different. On Leg 148, the Hole 896A core was logged in a different manner, with each individual scientist being responsible for logging a particular feature of the core, however, there was still a great deal of debate over the identification of individual lithological units (T.S. Brewer, pers. comm.). It was decided to relog the Hole 896A core for this study so that any lithological descriptions made were the work of only one individual, hopefully eradicating any inconsistencies due to individual interpretation of the core data.

During a visit to the ODP core repository in Texas, the core was relogged in great detail. The shape and size of each core piece was noted, along with any interesting features such as veins or alteration. The rocks present within the core were divided into the three main lithological units using the criteria specified by Alt, Kinoshita *et al.* (1993) as a guideline. The identification criteria for each unit are listed in Table 3.2.

Pillow lavas in the core are rarely observed whole or with more than one preserved glassy margin. An example of a small, intact, pillow lava is shown in Plate 3.1. In the majority of apparently pillowed core pieces the presence of a small, curved glass rim somewhere on the piece was sufficient to classify the piece as a pillow lava. However, in a number of examples, other features such as particularly high core recovery and / or a regular fracture pattern were deemed more representative, therefore the piece was classified as a massive unit (Plate 3.2). The igneous textures observed in thin-section are also diagnostic of the lithological unit, massive units tend to have intergranular textures whereas pillow lavas exhibit more porphyritic textures. The mineralogy of Hole 896A basalts is discussed in greater detail in § 3.7. The massive units in the Hole 896A core probably represent thick extrusive sheet flows rather than large intrusions. The main evidence for this assumption is the presence of glassy margins at the top or bottom of some core pieces. These glassy margins suggest rapid chilling, probably by quenching by seawater.



**Plate 3.1.** Small pillow lava from ODP Hole 896A (Sample 148-896A-11R-1 #1). Scale is indicated on the photograph.

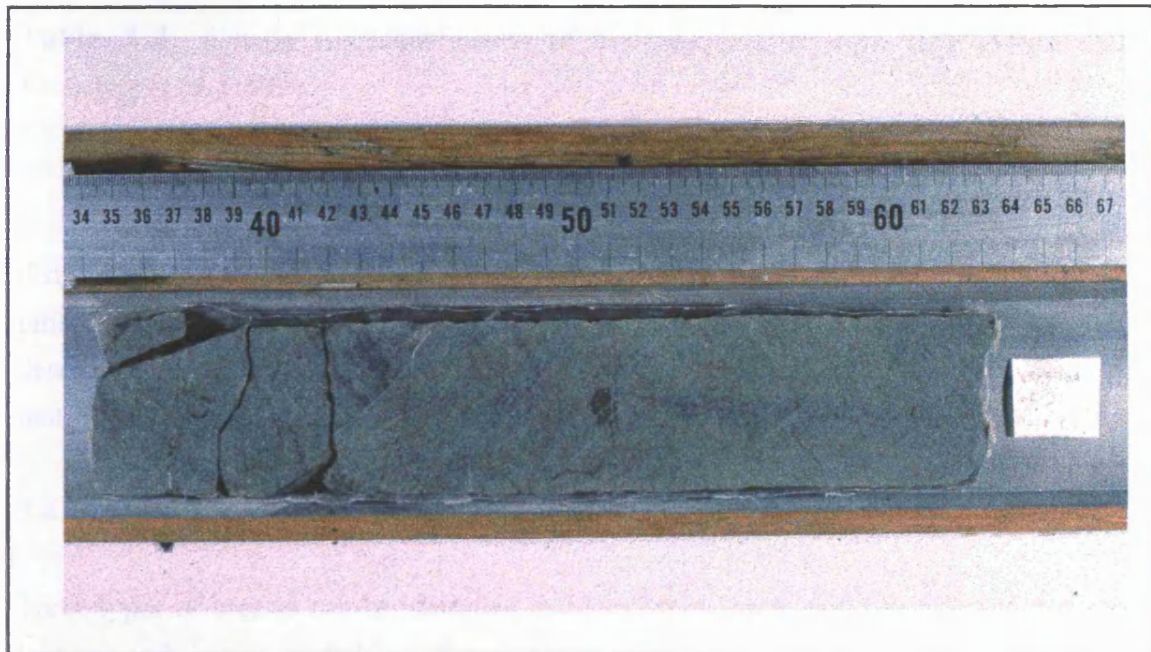


**Plate 3.2.** Massive unit from Hole 896A (Sample 148-896A-16R-2 #1). Scale is as shown on the photograph.

<u>Lithology</u>	<u>Identification Criteria</u>
<b>Massive units</b>	<ul style="list-style-type: none"> <li>- lack of curved glassy or chilled margins</li> <li>- presence of well developed oxidative alteration</li> <li>- higher recovery and longer sections than pillow lavas</li> <li>- more regular pattern of fractures than pillow lavas</li> </ul>
<b>Pillow lavas</b>	<ul style="list-style-type: none"> <li>- curved chilled or glassy margins</li> <li>- interior variolitic zone</li> <li>- poorly-developed oxidative alteration</li> <li>- abundant fracturing and veining</li> </ul>
<b>Breccias</b>	<p><b>Hyaloclastic:</b></p> <ul style="list-style-type: none"> <li>- angular clasts of subvariolitic basalt</li> <li>- blocky glass shards</li> <li>- cement is dark green / black clay or carbonate</li> <li>- many clasts are altered to clay</li> </ul> <p><b>Matrix-supported:</b></p> <ul style="list-style-type: none"> <li>- angular / subangular fragments of basalt</li> <li>- cemented by secondary clay minerals</li> <li>- found predominantly at depths &gt; 350 mbsf</li> </ul>

**Table 3.2.** Criteria for identification of lithological units from Hole 896A. After Alt, Kinoshita *et al.* (1993).

In the core descriptions made by Alt, Kinoshita *et al.* (1993), two types of breccia were distinguished between. However, on relogging the core, it was decided to divide the brecciated units present into three main groups, this represents a similar division of lithologies to that described by Dilek *et al.* (1996), comprising hyaloclastite breccias, poorly-sorted, polymict matrix-supported breccias and “jigsaw-puzzle” breccias.

#### 3.4.1. Brecciated units in Hole 896A

Three types of breccia can be identified in Hole 896A, each with very different macroscopic features and, hence, probably different modes of formation. In this study the brecciated units within the core have been divided into three main groups, A, B and C, which are discussed below.

#### 3.4.1.1. Breccia Type A

These comprise “hyaloclastite” breccias composed of altered basalt, dark green / grey clays and white crystalline carbonate (Plate 3.3). All basalt present has undergone extensive alteration and is largely replaced by clay minerals. Many of the basalt fragments are sub-angular to angular in shape.

**Occurrence:-** Large pieces of this breccia type are extremely rare. Samples are usually small fragments approximately 1 cm in diameter. Type A breccias mainly occur in the upper part of the hole (< 320 mbsf ) and are closely associated with pillow lava units. The brecciated material is very friable and breaks easily; probably due to the high degree of alteration of this breccia type and the fragile nature of the cementation. The scarcity of this rock type in the lower section of the core may be attributable to a larger degree of alteration, making recovery of this unit very difficult.

**Formation:-** This breccia type has all the characteristics of a typical hyaloclastite breccia comprising aggregates of glass and basalt fragments in a clay / carbonate matrix (Furnes and Freidleifsson, 1979). Two possible theories have been suggested for the formation of this rock type:

(1) MacDonald (1967) suggests that hyaloclastites are produced as the advancing front of a pillow lava is rapidly chilled to glass. The front is then granulated to form the brecciated material.

(2) Honnorez and Kirst (1975) and Bonatti (1970) claim that hyaloclastite breccias may form which are completely unrelated to pillow lavas. These result from direct granulation of the erupting magma. The rapid decrease in temperature and instantaneous vitrification creates stresses in highly viscous lava flows, hence the lava shatters forming a hyaloclastite breccia.

The close association of this breccia unit with pillow lavas suggests that the two have a common origin. This supports the theory that these represent granulated pillow fronts, hence, were formed contemporaneously with the pillow lavas. The angular shape of many of the basalt clasts suggests that the brecciated material has experienced only a small amount of transportation prior to deposition.

#### 3.4.1.2. Breccia Type B

These have been described as “jigsaw-puzzle” breccias by Harper and Tartarotti (1996). In this breccia the clasts are all basalt contained in a predominantly clay matrix. Most of the basalt clasts are angular to subangular in shape. Clast size varies considerably and appears to be largely dependant on the intricacy of the surrounding vein / fracture network. Individual clasts



**Plate 3.3.** Hyaloclastite breccia (Type A) from Hole 896A (Sample 148-896A-14R-1 #5). Scale is indicated on the photograph.

range in size from < 1 mm up to 50 mm. The clasts appear to have remained in place after brecciation and therefore can be fitted back together like a jigsaw puzzle (Plate 3.4).

**Occurrence:-** This type of breccia occurs throughout the core but is considerably more abundant at depths > 350 mbsf. It is more commonly associated with pillow lava units than massive units, however, some examples of this type of brecciation do occur within massive units. In many cases, pillow and massive units grade into this type of breccia and, in a number of pieces, the breccia is entirely enclosed by unbrecciated pillows or massive units.

**Formation:-** The angular nature of the clasts and the fact that they all comprise the same material, accompanied by the “jigsaw-puzzle” nature of the breccia, implies that Type B breccias formed *in situ*. Harper and Tartarotti (1996) discount formation as talus breccias due to the angular shape of the clasts and the lack of evident rotation or transportation. They suggest instead a tectonic origin by the process of hydrofracturing which is also associated with hydrothermal ore deposits. They claim that the steep breccia margins support a tectonic rather than sedimentary origin for this breccia type.

#### 3.4.1.3. Breccia Type C

Type C comprises polymict matrix-supported breccias. These consist of microcrystalline and fine-grained basalt clasts in a matrix of clay and carbonate (Plate 3.5). The basalt clasts are sub-angular to sub-rounded. Clast size is very variable, ranging from < 1 mm up to 50 mm in diameter. Some of the basalt clasts have been altered to clay whereas in other examples red oxidative alteration haloes can be seen within the clasts. Occasionally the basalt clasts contain small clay veins, these do not extend into the matrix and, hence are presumed to pre-date brecciation.

**Occurrence:-** This type of brecciated unit is more common towards the base of the core, at depths > 350 mbsf (Alt, Kinoshita *et al.*, 1993). It is particularly abundant at depths in excess of 430 mbsf and is found associated with both pillow and massive units.

**Formation:-** The angular nature of many of the basalt clasts in this breccia type suggests the brecciated material was rapidly transported and deposited. Alt, Kinoshita *et al.* (1993) suggest that this type of breccia was formed by mass wasting of massive units and represents talus breccia. Similar poorly-sorted, matrix-supported breccias have been described from dredge hauls of the Clipperton Fracture Zone (Barany and Karson, 1989). These were interpreted as being debris flow deposits, deposited at the base of talus slopes in debris fans. Alternatively this breccia type may represent cemented debris which fell into cracks on the



**Plate 3.4.** "Jigsaw-puzzle" breccia (Type B) from Hole 896A (Sample 148-896A-18R-2 #3). Scale is indicated on the photograph.

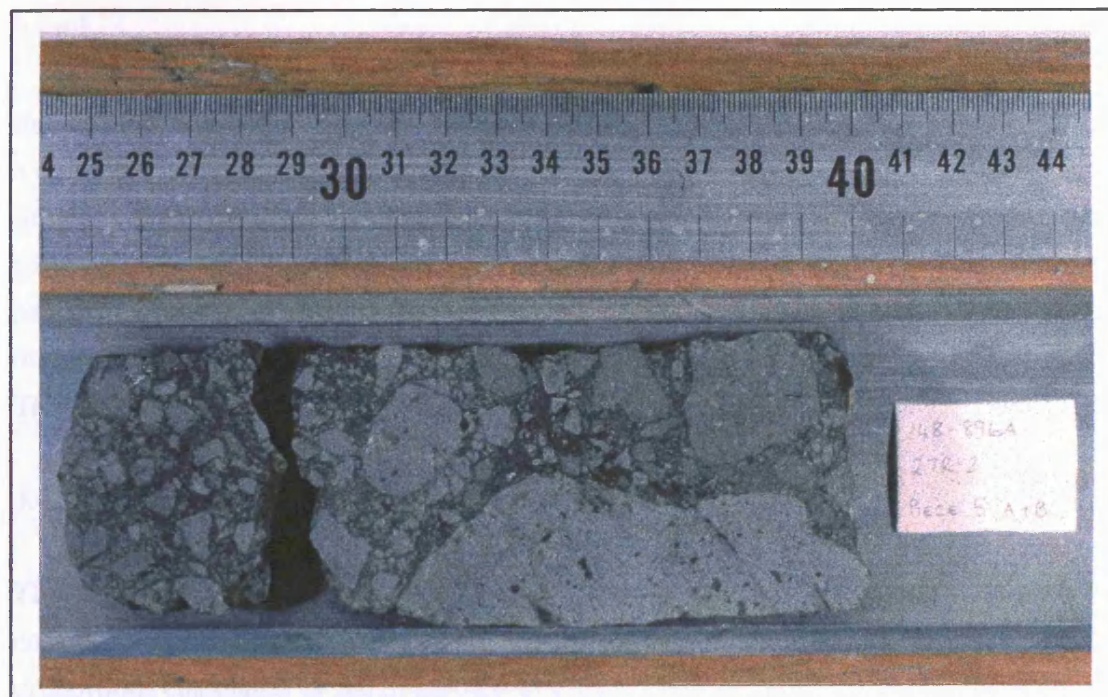


**Plate 3.5.** Polymict, matrix-supported breccia (Type C) from Hole 896A (Sample 148-896A-27R-2 #5). Scale is indicated on the photograph.

surface of a lava flow, known as fissure fills (Alt, Kinoshita *et al.*, 1993). Either of these processes may account for the variety of clast type observed in this breccia unit.

Harper and Tartarotti (1996) suggest that these breccias have a tectonic origin and propose dilational faulting as the most likely mode of formation. They claim that the evidence for this mode of formation is provided by the fact that some of the clast margins show microfracturing and, hence, appear to grade into the clay matrix. Breccias formed by this process are likely to show an increase in pore volumes and lack of evidence for frictional wear therefore they texturally resemble sedimentary breccias (Harper and Tartarotti, 1996).

### 3.4.2. Stratigraphical log of Hole 896A from core descriptions

From the new visual core descriptions, a log of the lithostratigraphy of Hole 896A has been constructed (Figure 3.2). In this new stratigraphical log, all three breccia types, A, B and C are included as one unit. An important point to note is that all recovered core pieces are moved to the top of each core barrel on curation according to ODP policy (Alt, Kinoshita *et al.*, 1993). This complicates interpretation of the lithostratigraphy considerably because the majority of the core pieces may not be *in situ*. In Figure 3.2, A is the log produced by using the recovered samples only, hence, where there is no recovery a gap of corresponding size has been left, whereas B shows an extrapolated version of A. Extrapolation of the core throughout the hole was achieved using the method described by Adamson (1985); in sections with low core recovery, the thickness of any recovered material is scaled to fill the remainder of the core barrel.

As can be seen from Figure 3.2, the lithostratigraphy of Hole 896A consists of intercalated massive units, pillow lavas and brecciated units. The various lithological units form a complex sequence throughout the core with no obvious relationships between the different lithologies. Thick pillow lava units are generally more abundant in the upper section of the core, particularly between 220 and 275 mbsf, whereas massive units are more dominant in the lower half of the core, with particularly thick units between 370 and 405 mbsf. Brecciated units are distributed throughout the core and occur associated with both pillow lavas and massive units. Thicker brecciated units occur in the lower two-thirds of the core.

#### 3.4.2.1. Comparison with shipboard core descriptions

The relative proportions of each lithology within the core were calculated from both the visual core descriptions and the stratigraphical log after extrapolation. These are compared with the proportions calculated by the Shipboard Scientific Party in Table 3.3. As can be seen, there is a large variation between the shipboard visual core descriptions and the new core descriptions

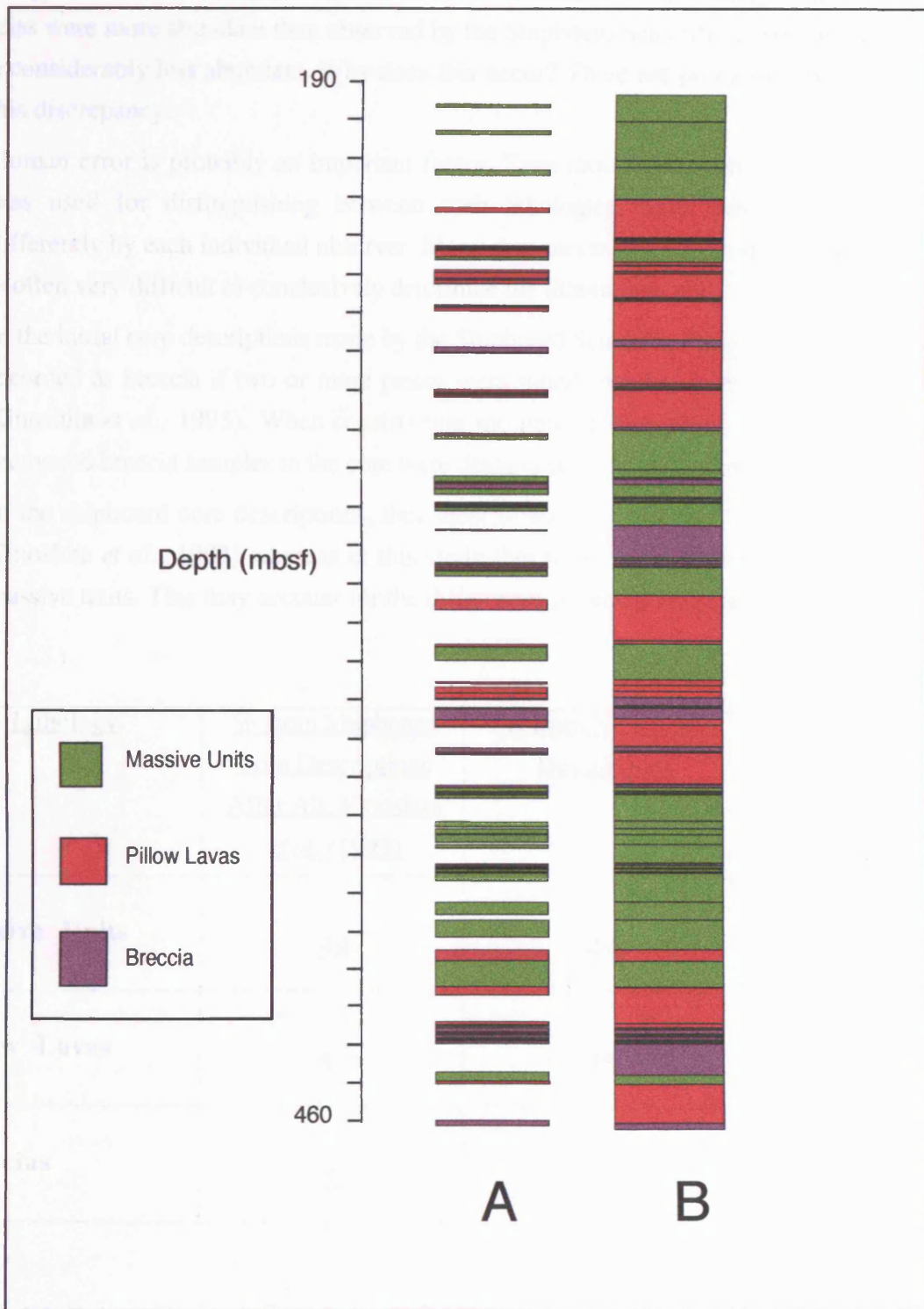


**Figure 3.2.** Lithostratigraphical log of Hole 896A derived from core descriptions.  
A) Log using recovered samples only.  
B) Extrapolation of core using the core interpretation policy of Adamson (1985)

made by the author. In the visual core descriptions made for this study, massive units and breccias were more abundant than observed by the Shipboard Scientific Party, and pillow lavas were considerably less abundant. Why does this occur? There are probably three main reasons for this discrepancy.

- Human error is probably an important factor. Even though the same identification criteria was used for distinguishing between each lithological unit, this may be interpreted differently by each individual observer. Many core pieces are very fragmentary, therefore it is often very difficult to conclusively determine the lithological unit.
- In the initial core descriptions made by the Shipboard Scientific Party, a unit would only be recorded as breccia if two or more pieces were found together in the recovered core (Alt, Kinoshita *et al.*, 1993). When constructing the new stratigraphical log for this study, all recovered breccia samples in the core were designated as brecciated units.
- In the shipboard core descriptions, thin sheet flows were included with pillow lavas (Alt, Kinoshita *et al.*, 1993) whereas in this study thin flows were preferentially included with massive units. This may account for the differences in pillow lavas and massive units.

<u>Lithology</u>	<u>% from Shipboard Core Descriptions After Alt, Kinoshita <i>et al.</i> (1993)</u>	<u>% from New Core Descriptions</u>	<u>% from Extrapolated Log</u>
<b>Massive Units</b>	38	49	52
<b>Pillow Lavas</b>	57	35	38
<b>Breccias</b>	5	16	10

**Table 3.3.** Relative proportions of lithological units on ODP Hole 896A, calculated from the Shipboard core descriptions and the new core descriptions made for this study

### 3.5. Logging tools deployed on Hole 896A

Downhole logging tools are used to investigate the physical, chemical and structural properties of the lithological units surrounding the borehole (Dick, Natland, Miller *et al.*, in press; Brewer *et al.*, 1998). The data logs produced are especially important for those holes with poor core recovery.

Two phases of downhole logging were conducted in Hole 896A during Leg 148 (Alt, Kinoshita *et al.*, 1993). The first phase of logging deployed a combination of a temperature logging tool (TLT) and a geochemical logging tool string (GLT). These tools logged from 120.73 to 347 mbsf hence, some of the data was recorded in the borehole casing and was subsequently removed during post-cruise processing (Alt, Kinoshita *et al.*, 1993). Two passes of the GLT were required, the second collecting excellent quality data. (An explanation of logging tool acronyms is provided in Appendix A).

After further drilling four more tool strings were deployed (Alt, Kinoshita *et al.*, 1993):

- Dual Laterolog (DLL) - Digital Sonic Tool (SDT) - Natural Gamma-ray Spectroscopy Tool (NGT). This logging suite was run successfully from 117.28 to 423 mbsf. Unfortunately an obstruction was felt at 423 mbsf therefore 46m of the hole was unavailable for logging. The DLL and SDT both collected excellent quality data.
- packer experiment
- magnetometer - run from 117.28 to 325 mbsf
- FMS -2 successful passes were run from 190 to 423 mbsf.

#### 3.5.1. Construction of a stratigraphical log for Hole 896A using log data

Formation Microscanner (FMS) data for Hole 896A is very high quality. For high resolution data to be obtained, good contact with the borehole walls is essential (Dick, Natland, Miller *et al.*, in press). Borehole ellipticity is calculated by subtracting the values from the two FMS calipers (Alt, Kinoshita *et al.*, 1993). In Hole 896A, very few sections had differences in the two calipers > 0.5 inches. These enlarged sections, or breakouts mainly occur in the upper parts of the borehole (Alt, Kinoshita *et al.*, 1993). FMS images for Hole 896A were used in conjunction with the downhole resistivity logs to produce a stratigraphical log of the lithologies present within the borehole (Fig. 3.3). The criteria used for identification of the various lithological units present are shown in Table 3.4.

The downhole resistivity data for Hole 896A is shown in Fig 3.4. The plot shows both the deep laterolog (LLD) and shallow laterolog curves (LLS) named due to their respective

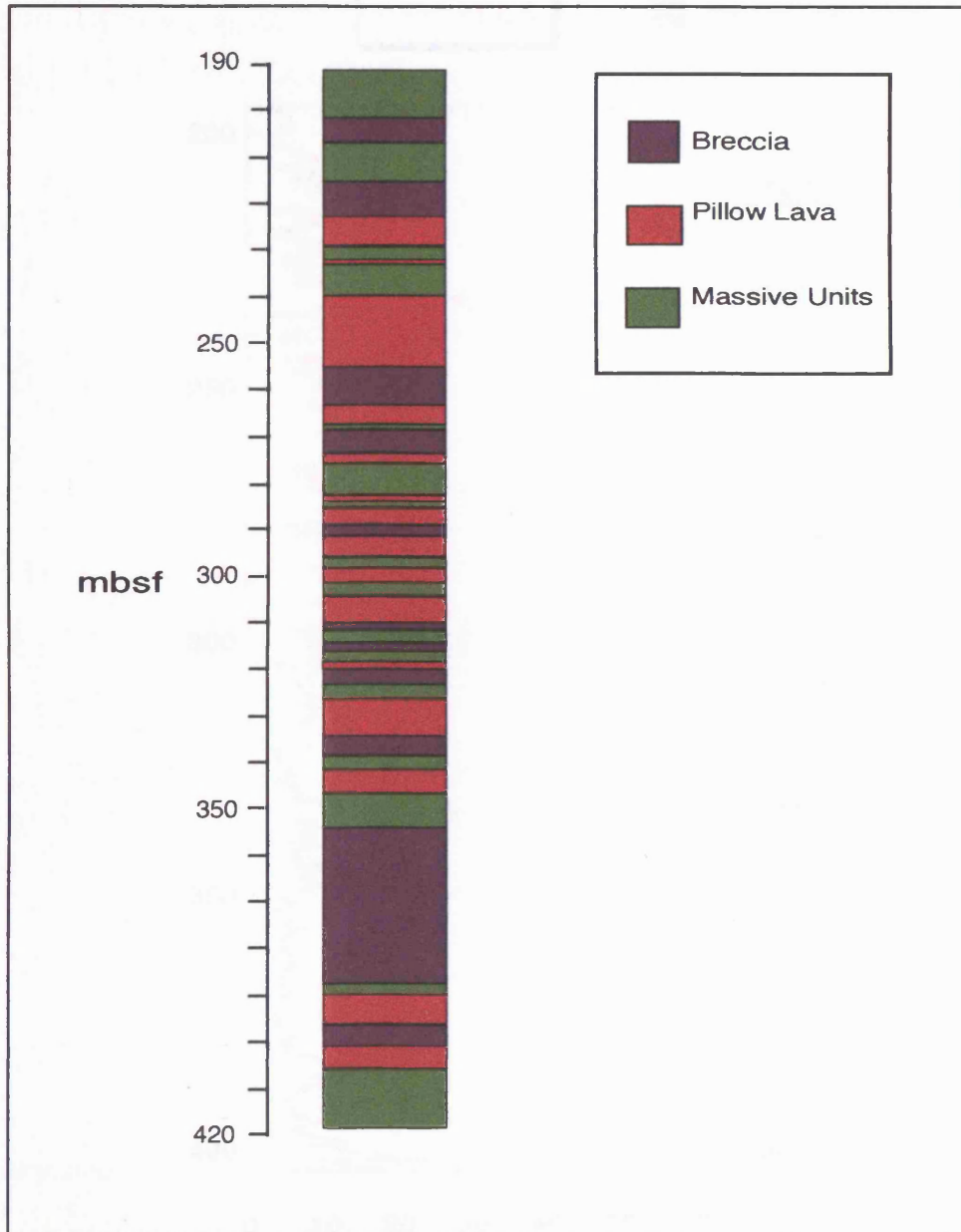


**Figure 3.3.** Lithostratigraphical log of Hole 896A derived from FMS Data



horizontal penetration into the formation (Pezard, 1990). The difference between the two measurements is related to rock anisotropy, the deep measurement is primarily related to the horizontal resistivity of the formation and is not greatly affected by vertical conductive features, whereas the shallow resistivity measurement is affected by both the horizontal and vertical resistivity of the formation (Pezard, 1990). The top of massive units is marked by a rapid increase in resistivity due to the presence of chilled margins (Pezard, 1990). The slight resistivity decrease in the centre of each massive unit has been attributed to an increase in grain-size towards the centre of the unit (Pezard, 1990).

<u>Lithology</u>	<u>Identification Criteria</u>
<b>Massive Units</b>	<ul style="list-style-type: none"> <li>- relatively uniform high resistivity throughout the unit</li> <li>- appear on FMS images as extensive areas with a uniform colour</li> <li>- fractures tend to be straight</li> </ul>
<b>Pillow Lavas</b>	<ul style="list-style-type: none"> <li>- variable resistivity within a small area</li> <li>- less variation than breccias</li> <li>- individual pillows often distinguished due to curved nature of the pillow boundaries</li> </ul>
<b>Breccias</b>	<ul style="list-style-type: none"> <li>- highly variable resistivity within a small area</li> <li>- presence of small clast like features with high resistivity</li> <li>- clasts are usually angular to sub-angular in shape</li> <li>- matrix of low resistivity material</li> </ul>

**Table 3.4.** Criteria for identification of lithological units using FMS images

The resistivity profile for Hole 896A, shows significant peaks at 213 mbsf, 233 mbsf, 295 mbsf, 310 mbsf, 319 mbsf, 333 mbsf, 387 mbsf and 402 mbsf (Figure 3.4). A number of these depths correspond closely with regions of uniform conductivity on the FMS log, hence can be designated as massive units (Figure 3.5.1), their high resistivity results from the low permeability and poor conductivity of massive basalt (Brewer *et al.*, 1998). In many cases these areas of uniform low conductivity (high resistivity) are cut by networks of conductive fractures which tend to be less curved and less dense than those observed in the pillow lava units. It is often very difficult to constrain the boundaries of very flow units which occur between pillow lava stacks. In these cases the dominant lithology is used to define the lithological unit.

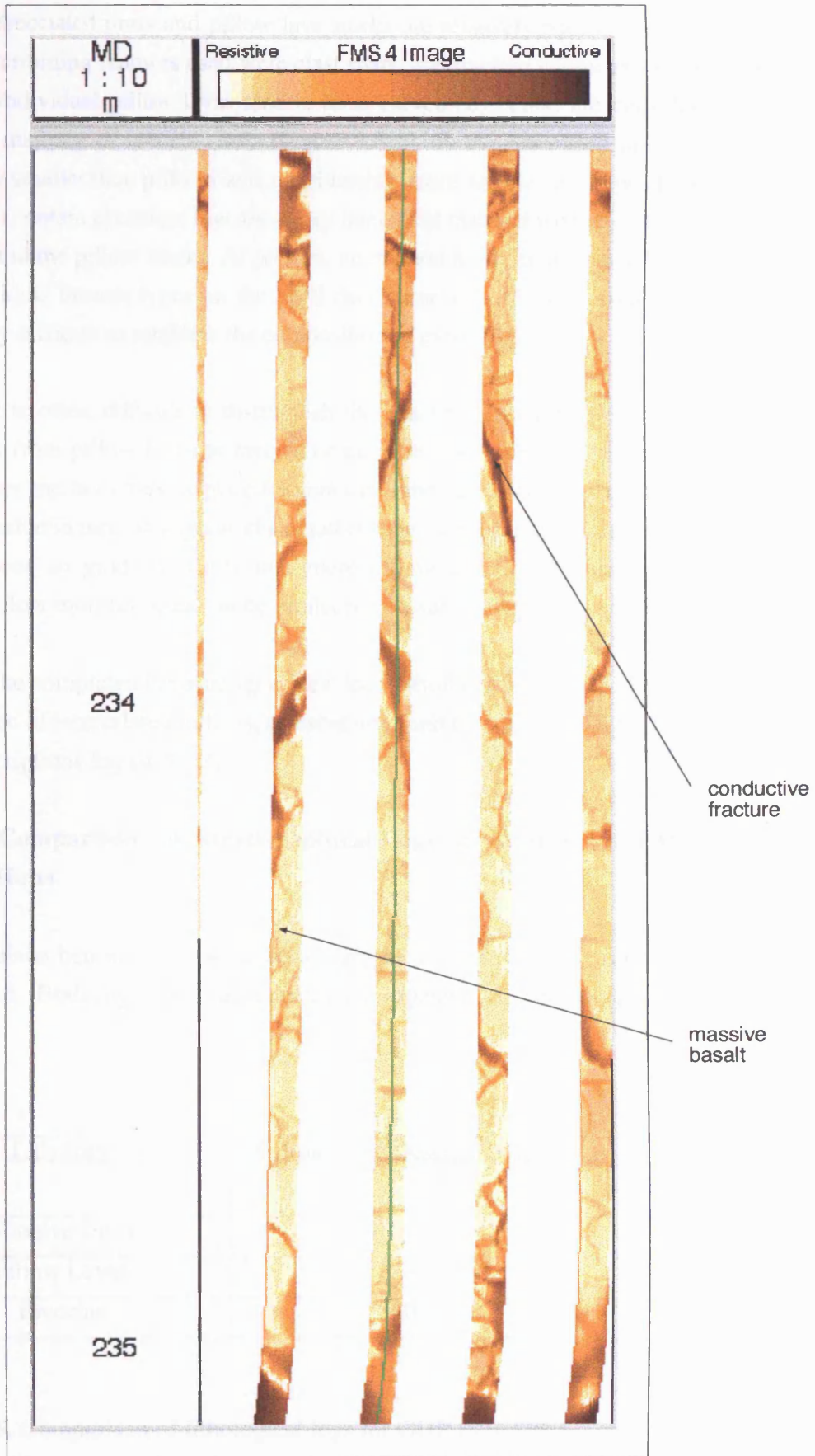


Figure 3.5.1. FMS image showing massive units in Hole 896A

Brecciated units and pillow lava stacks are relatively hard to distinguish between. The main determining features used were clast shape and fracture geometry as observed on the FMS profile. Individual pillow lavas tend to have curved edges and are considerably larger in size than the majority of breccia clasts (Figure 3.5.2). In the brecciated units individual clasts are generally smaller than pillows and considerably more angular in shape (Figure 3.5.3). Breccia units also contain abundant low resistivity interstitial material whereas interstitial material is less abundant in the pillow stacks. At present, no method has been developed to distinguish between the individual breccia types on the FMS data because at the scale used on the FMS logs it is extremely difficult to establish the composition of individual clasts.

It is often difficult to distinguish the exact boundary between individual units as the transition from pillow lavas to breccia or massive units to pillow lavas can be gradational. In these cases the boundary is placed where one lithology appears to be dominant over the other e.g. a predominance of angular clasts rather than more rounded features. Some massive units can be seen to grade upwards into more pillowed flows (Figure 3.5.4.), suggesting that different flow morphologies can be produced in a single eruptive event.

The completed lithostratigraphical log is shown in Figure 3.3. The log shows a complex association of intercalated pillows, massive units and breccias similar to that described from the core descriptions log (§ 3.4.2).

### 3.5.2. Comparison of stratigraphical logs derived from FMS data and core descriptions

A comparison between the two lithostratigraphical logs produced for this study is shown in Figure 3.6. Both logs show an intercalated sequence of breccias, pillow lavas and massive units.

<u>Lithology</u>	<u>% from Core Description Log</u>	<u>% from FMS log</u>
Massive Units	52	35
Pillow Lavas	38	33
Breccias	10	32

**Table 3.5.** Comparison of lithological logs for ODP Hole 896A

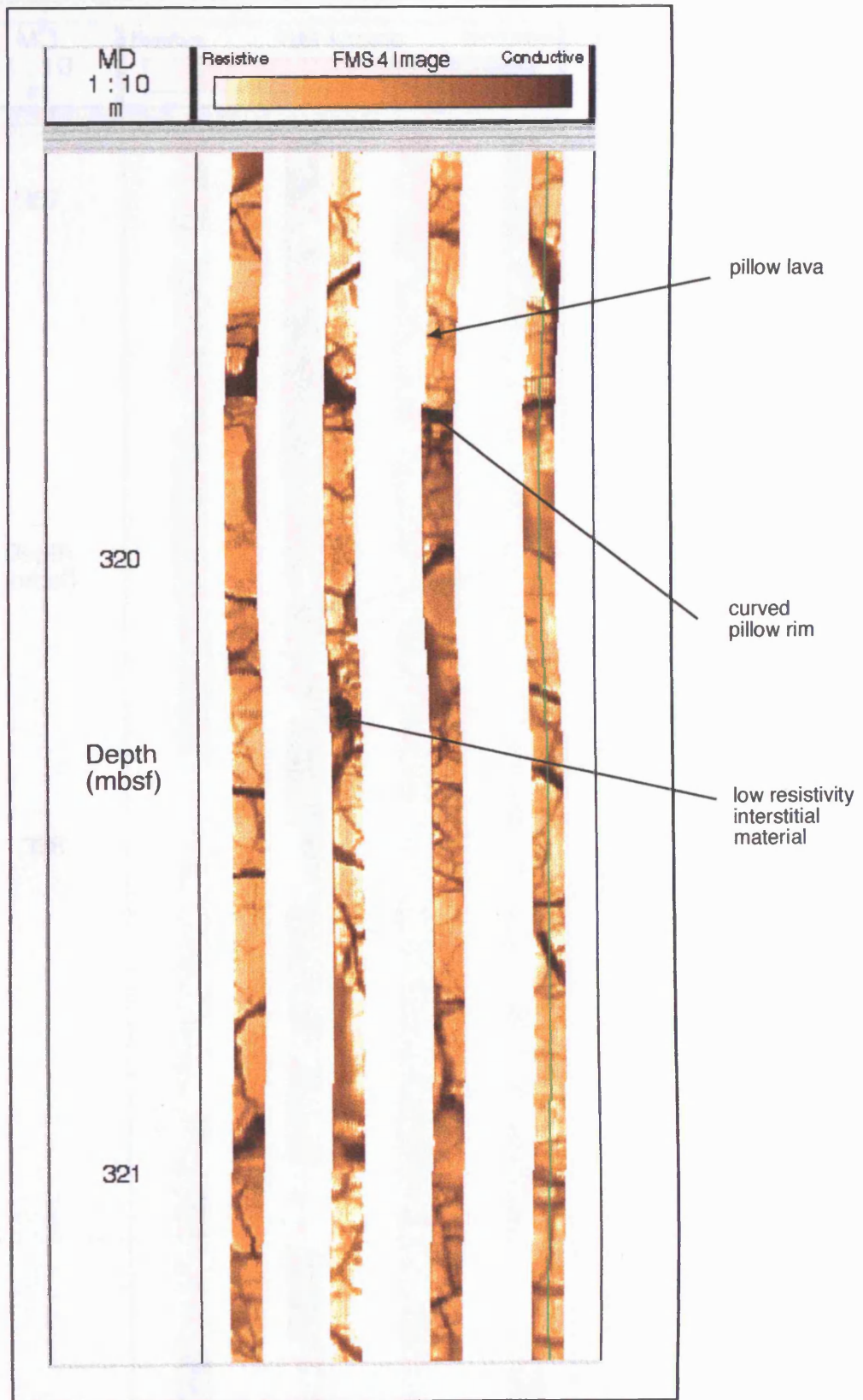
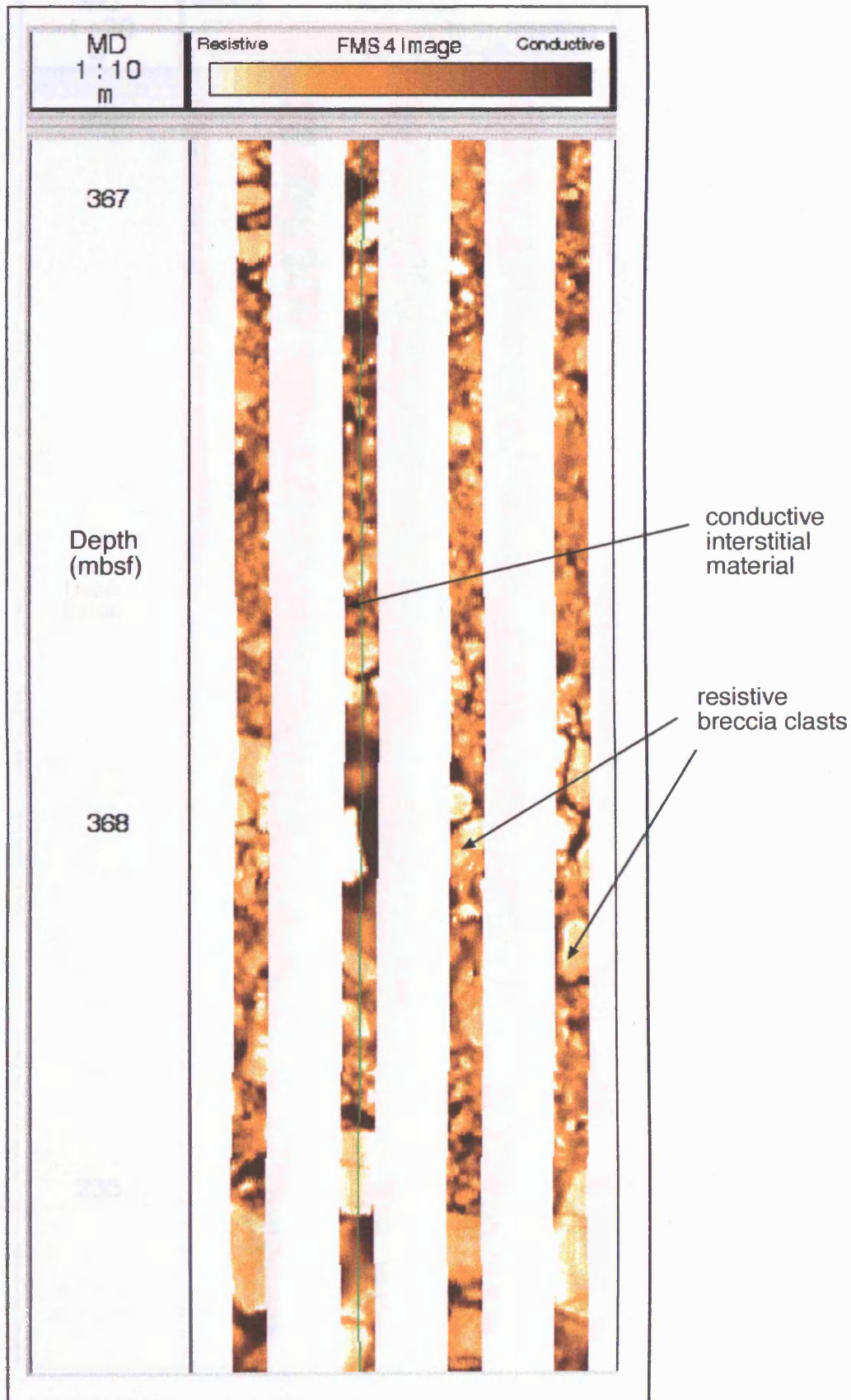
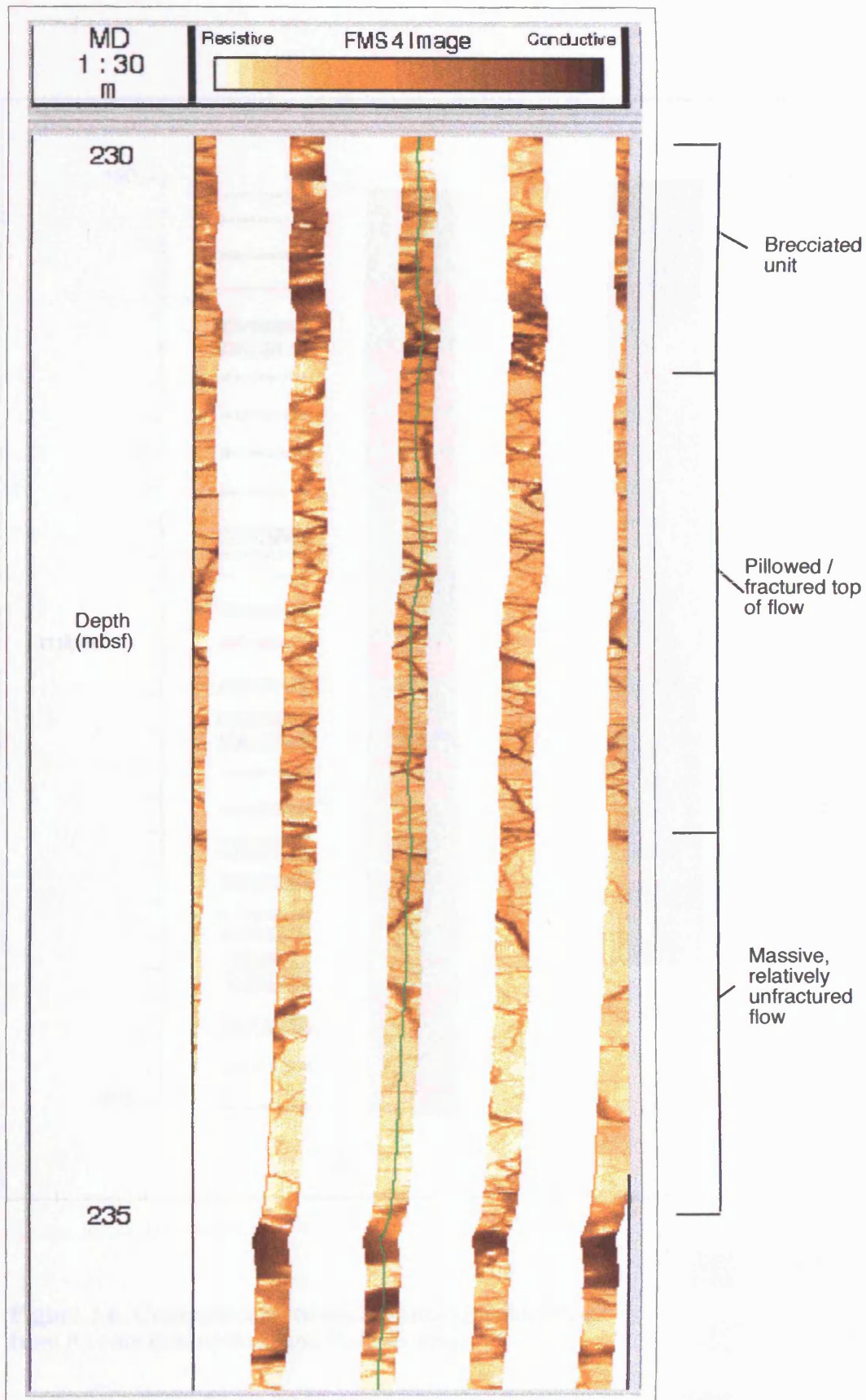


Figure 3.5.2. FMS image showing pillow lavas in Hole 896A



**Figure 3.5.3.** FMS image showing brecciated units in Hole 896A



**Figure 3.5.4.** FMS image of a basalt flow. The base of the flow is massive and relatively unfractured whereas the top of the flow is pillowed and much more heavily fractured. The unit is overlain by a breccia (after Brewer *et al.*, 1998)

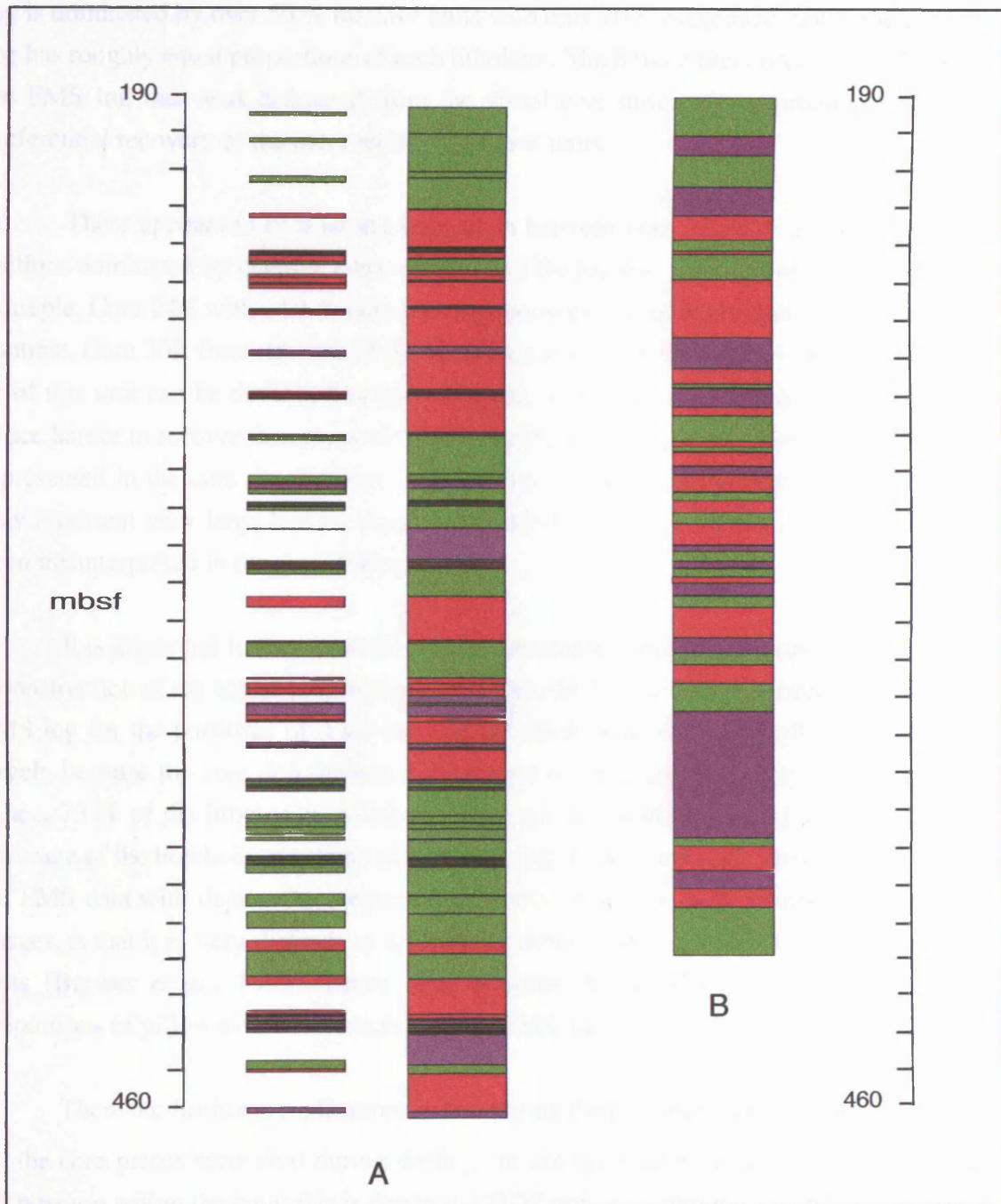


**Figure 3.6.** Comparison between lithostratigraphical logs from A) core descriptions and B) FMS data



Table 3.5 shows a comparison between the relative proportions of each lithological unit as calculated from the two lithostratigraphical logs produced by this study. The core description log is dominated by over 50 % massive units with only 10 % brecciated units whereas the FMS log has roughly equal proportions of each lithology. Much more brecciated material is present in the FMS log than was estimated from the visual core descriptions, probably largely due to preferential recovery of the more resistive massive units.

There appears to be a strong correlation between core recovery and lithology, the core sections dominated by massive units usually have the highest recovery (refer to Table 3.1). For example, Core 24R with 64.1 % core recovery consists almost exclusively of massive units. In contrast, Core 30R from the base of the hole has a total core recovery of only 13.6 %, over 50 % of this unit can be described as breccia. Breccia units are much more fractured, friable and hence harder to recover than massive units and pillow lavas and are, therefore, probably under-represented in the core descriptions. Alternatively, some of the massive core pieces recovered may represent very large breccia clasts or the interiors of large pillow lavas and have, hence, been misinterpreted in the core descriptions.

It is important to decide which of the lithostratigraphical logs provides a more accurate reconstruction of the actual lithostratigraphy within the borehole. It has been decided to use the FMS log for the purposes of discussion of the lithological variability within the core. This is largely because the core descriptions log is based on only approximately 27 % core recovery, hence, 73 % of the lithologies within the hole are not available. The FMS log provides full coverage of the borehole to a depth of 420 mbsf and there is minimal variation in the quality of the FMS data with depth. One important difficulty, however, with interpretation of the FMS images, is that it is very difficult to distinguish between unconsolidated pillows and brecciated units (Brewer *et al.*, 1995), hence there is some degree of uncertainty as to the relative proportions of pillow lavas and breccias in the FMS log.

There are further complications in comparing the two stratigraphical logs because:

- the core pieces recovered during drilling are not necessarily in their correct stratigraphical position within the core; this is due to the ODP policy of moving any recovered core to the top of each core barrel on curation,
- poor core recovery means there is no way of determining exactly which lithology is in the intervals with no recovered core, however with the FMS data full coverage of the borehole is possible,
- the available FMS data does not extend to the base of the hole.

### 3.6. Lithological variability in ODP Hole 896A

The first question to be addressed is that of the lithological diversity within the core. Why is there more than one form of basalt present? Variations in surface morphology of submarine basalts have been attributed to a number of factors including viscosity, temperature, effusion rate (discussed in § 2.3.4). There are two main approaches to this problem, one emphasising that the primary control is the viscosity of the magma (Bonatti and Harrison, 1988) and the other concluding that effusion rate is the main controlling factor on lava flow morphology (Ballard *et al.*, 1979). The two models are in many respects complementary, however Ballard *et al.* (1979) emphasise the flow mechanics of the lava rather than the intrinsic properties of the erupting lavas (Bonatti and Harrison, 1988). Either of these models could produce the layered stratigraphy observed in Hole 896A.

- Bonatti and Harrison (1988) suggest that the variation in flow morphologies seen at mid-ocean ridges (MOR) is the result of variations in the temperature and / or viscosity of the erupted lava. They conclude that massive units or sheet flows are formed by voluminous, rapid eruptions of low viscosity, high temperature magmas whereas pillow lavas and hyaloclastites are the result of smaller, slower eruptions of higher viscosity, cooler magmas. Why then do we get a change in the type of magma erupted? These changes can possibly be explained by the presence of some form of fractionating magma chamber beneath the mid-ocean ridge axis (Bonatti and Harrison, 1988). Large rapid, initial eruptions from a magma chamber may be of hot, low viscosity, relatively primitive lavas, producing sheet flows / massive units. The remaining liquid in the chamber will continue to fractionate until it is forced out of the magma chamber perhaps by a new influx of magma. This new lava will be cooler, considerably more viscous and evolved than previously-erupted lavas, producing pillow lavas and / or hyaloclastite breccias. This cyclicity would also be apparent in the geochemical data from the core (discussed in § 3.8) with pillow lavas showing more differentiated compositions than sheet flows (massive units).
- The lithological variation in ODP Hole 896A may be the result of volcanic cyclicity along the spreading ridge axis resulting from changes in the effusion rate of the erupting lava. Ballard *et al.* (1979) suggested that the initial stages of an eruption will be at high effusion rates from open fissures producing predominantly sheet flows. As these build-up at the ridge axis, it is harder for new flows to break through to the surface resulting in a decrease in effusion rate and consequently the formation of pillow lavas. When the current phase of volcanic activity ceases, the preceding flows are broken up to form breccias. At the onset of a new phase of volcanic activity, effusion rates are high and sheet flows are formed, beginning the cycle again. This process would result in a layered stratigraphy with breccias

overlying pillow lavas which in turn rest on sheet flows (Ballard *et al.*, 1979). If the duration of individual eruptions vary, then the thickness of individual volcanic sequences would also vary, producing a complex intercalated stratigraphy with lithological units of variable thickness. The main contrast with the model of Bonatti and Harrison (1988) is that pillow lavas and breccias in this model will not necessarily have different chemical signatures to sheet flows. Small variations in chemistry may occur due to fractionation after eruption, this would be expected to be greatest in the high temperature, slow cooling sheet flows.

Both these models reflect lithological variability over relatively short time scales. However the lithological variations in Hole 896A may represent long term variations.

### **3.6.1. Variations in lithology with distance from the ridge axis**

Ballard *et al.* (1979) and Francheteau and Ballard (1983) note that on fast and intermediate - spreading ridges the ratio of sheet flows to pillow lavas decreases with increasing distance from the ridge axis (§ 2.3.4). Therefore, as a section of crust is moved away from the axis by sea-floor spreading, there should be an increase in the amount of pillow lava sections towards the top of the lithostratigraphy

Unfortunately it is difficult to determine whether the lithological units in the Hole 896A core were erupted on or off-axis, or how far away from the axis, as it is difficult to establish the volume of lava erupted in each phase of volcanism. Another significant problem with the Hole 896A core is that it does not necessarily represent the complete volcanic section, the contact with the transition zone has not been recovered. Hence, the available core may comprise only a small part of the complete volcanic sequence of this section of crust. Therefore the core may be representative of only a relatively short episode in the constructive history of this particular crustal section

The difference between off-axis and axis lavas may be reflected in the downhole geochemistry (§ 3.9). Systematic variations in geochemistry with increasing distance from the ridge axis have been noted from both slow (Bryan and Moore, 1977) and fast - spreading ridges (Reynolds *et al.*, 1992) with flank lavas tending to have more evolved compositions than those erupted at the axis.

### **3.6.2. Sedimentary, tectonic or volcanic breccias ?**

An important issue to be considered is whether the brecciated units present in the core are sedimentary, tectonic or hydrovolcanic in origin. If the brecciated units were formed by

sedimentary processes or tectonic processes, such as mass wasting or faulting, volcanism at the time of formation must have been relatively low. This may represent a period of quiescence or reduction in volcanic activity at the ridge axis. Such sedimentary or tectonic breccias will therefore form by mechanical breakdown of previously erupted and cooled lavas.

Alternatively, if the breccias are hydrovolcanic, forming by explosive activity or granulation of pillow lava rinds, this suggests formation when volcanic activity was continuous with no periods of quiescence required. In this case, the change in erupted lithology must be related to changes in the properties (temperature, viscosity, effusion rate) of the erupted lava.

The breccias in the lower part of ODP Hole 896A are predominantly Type C (§ 3.4.1.3), polymict matrix-supported breccias containing fragments of massive units and pillow lavas. These breccias are therefore likely to have had either a sedimentary or tectonic origin as they contain fragments of previously-erupted lava flows (§ 3.4.1.3) and were probably formed during a period of limited volcanism, allowing for the break-up and / or redeposition of older flows. The Type B “jigsaw-puzzle” breccias appear to have formed in-situ and are therefore unlikely to have been deposited as sedimentary breccias. Low temperature alteration in Hole 896A appears to be greater at depths > 340 mbsf (§ 3.8.3), Type B breccias are also more abundant at depths > 350 mbsf hence are probably connected to this alteration. What is difficult to establish is whether the fragmentary nature of this rock type facilitated low temperature alteration, or whether low temperature alteration resulted in the formation of this breccia unit.

Breccia Type A is exclusively found at depths < 320 mbsf and is closely associated with pillow lavas. This type of breccia is more likely to be hydrovolcanic in origin, therefore, probably reflects changes in effusion rate, temperature or viscosity of the erupting lava.

The large breccia section from 350 to 390 mbsf on the lithostratigraphical log from FMS data (Figure 3.3) probably consists entirely of breccia types B and C. These are thought to have had either a tectonic or sedimentary origin therefore were probably formed during a period of limited volcanism or quiescence. Brewer *et al.* (1998) suggest that this may represent the period of time where this section of crust moved off-axis, hence the lavas below this brecciated zone were erupted at the ridge axis whereas the lavas above were erupted off-axis.

#### 3.6.2.1. Possible presence of an active fault zone in Hole 896A

De Larouziere *et al.* (1996) note that the lowest resistivities in Hole 896A occur at 356.0 mbsf, which is closely associated with a maximum in intensity of fractures. The borehole is also relatively cylindrical below 356.0 mbsf with the upper parts of the hole being considerably more elliptical. De Larouziere *et al.* (1996) suggest that this represents a possible change in

stress field conditions and, combined with the low resistivities and maximum intensity of fractures, implies the presence of a presently active fault zone at 356.0 mbsf in Hole 896A. This may account for the presence of large thicknesses of brecciated material at this depth and would be consistent with a tectonic origin for breccia types B and C.

### 3.6.3. Variations in magnetic properties of the Hole 896A core

Investigations into the magnetic properties of the Hole 896A core by Allerton *et al.* (1996) found that the core could be divided into three depth sections:

- an upper section from 0 to 330 mbsf has relatively high intensity of magnetic remanence and low magnetic susceptibility,
- the middle section extends from 330 to 360 mbsf and has relatively high intensity of magnetic remanence and intermediate susceptibility,
- the lower section, from 360 mbsf to the base of the hole, has low intensity of remanence and high susceptibility.

Magnetic susceptibility is dependent on the composition, concentration and grain-size of magnetic minerals within the core (Allerton *et al.*, 1996).

Allerton *et al.* (1996) conclude that the upper part of Hole 896A has several magnetic features that suggest that the basalts present were extruded at a slow rate, some distance from the ridge axis. Their evidence to support this is as follows:

- the low magnetic susceptibility suggests very fine grain sizes of magnetic minerals,
- inclinations of the upper section of Hole 896A are very close to the stable reference inclination suggesting that the section has not been substantially tilted. The section below has apparently been tilted, suggesting that the two sections are separated by some form of unconformity,
- alteration is more extensive in the lower part of the hole; the upper section may have been extruded after the main phase of hydrothermal circulation had ceased.

The conclusions reached by Allerton *et al.* (1996) would be consistent with the suggestion that the upper and lower sections of Hole 896A are separated by a reduction in volcanism, represented by the brecciated material from 350 to 390 mbsf (§ 3.6.2). The lower lavas, at depths > 350 mbsf, were probably erupted at the ridge axis, then, after moving away from the main axial zones they were tilted and broken up. Volcanism was then resumed off-axis producing the untilted upper lava section (0 to 350 mbsf). The depths of each section, determined by Allerton *et al.* (1996), are rather different to those suggested by the

lithostratigraphy, this is probably largely due to core location error resulting from the low core recovery experienced in Hole 896A.

### 3.7. Mineralogy

To fully explain the lithological diversity within Hole 896A, it is necessary to investigate the mineralogical and geochemical variations within the core. If the lithostratigraphical variations observed are the result of changes in the nature of the erupted magma this may also be reflected in the chemistry and mineralogy of the basalts.

#### 3.7.1. Review of shipboard scientific party results

The mineralogy of Hole 896A basalts was initially described by the Leg 148 shipboard scientific party (Alt, Kinoshita *et al.*, 1993). Their results are summarised below:

Samples recovered from Hole 896A range from aphyric (with < 1 % phenocrysts) to highly phyric (approximately 33.4 % phenocrysts) basalts. Alt, Kinoshita *et al.* (1993) divided the rocks present into 50 lithological units, based on phenocryst assemblages and textures. Forty-eight units are plagioclase-olivine or olivine-plagioclase phyric basalts with the remaining two units being moderately olivine-phyric basalts. Plagioclase-olivine basalts predominate in the upper sections of the core, from 195.1 to 390.1 mbsf, with olivine-plagioclase basalts being more common in the lower core sections (390.1 to 469 mbsf).

Alt, Kinoshita *et al.* (1993) identified four phenocryst phases in the basalts; plagioclase, olivine, clinopyroxene and spinel. Plagioclase is the most abundant phenocryst phase in the majority of the basalt samples and comprises euhedral to anhedral grains ranging from 0.1 to > 5 mm in size. Some examples show chemical zonation or the presence of glass and spinel inclusions. Many plagioclase grains occur in glomerocrysts, sometimes with olivine and/or clinopyroxene. These consist of 5 to 50 grains with a wide variety of textures, crystal shapes and grain-sizes. Olivine occurs as euhedral grains, ranging in size from < 0.1 to 5 mm. These often contain spinel and glass inclusions and, occasionally, rare plagioclase inclusions suggesting that plagioclase developed prior to olivine (Alt, Kinoshita *et al.*, 1993). The majority of olivine in the core samples is replaced by secondary minerals, however some primary grains are preserved. Clinopyroxene phenocrysts are very rare in the Hole 896A core, occurring only at depths between 353 and 392 mbsf. They range in size from < 0.5 to 7 mm, and, usually occur as rounded grains which Alt, Kinoshita *et al.* (1993) interpret as the result of crystal reaction with the host magma prior to quenching. Spinel also occurs as a minor phenocryst phase. It occurs as euhedral to anhedral equant grains, ranging in size from 10 µm to 200 µm. Spinel does not occur in cores containing clinopyroxene which leads Alt, Kinoshita *et al.* (1993) to suggest that the two minerals may be incompatible.

Alt, Kinoshita *et al.* (1993) note a systematic variation of phenocryst abundance with depth. The concentration of plagioclase shows a decrease with depth to approximately 330 mbsf, from here a rapid decrease in concentration is seen down to a depth of approximately 390 mbsf. Below 390 mbsf a sudden drop in plagioclase phenocryst abundance occurs followed by a general increase to the base of Hole 896A. Olivine shows a similar downhole variation to plagioclase whereas clinopyroxene only occurs in Units 31 to 36 (353.1 to 392.1 mbsf; Alt, Kinoshita *et al.*, 1993).

### 3.7.2. Results from this study

Thirty thin-sections from Hole 896A were examined to investigate the mineralogical variations within the core. The sections can be loosely divided into two groups on the basis of their igneous textures:

- Porphyritic / Glomeroporphyritic
- Intergranular

The former are found predominantly in the pillow lavas, the latter being more representative of the massive units.

#### 3.7.2.1. Primary Mineralogy

In all the sections plagioclase feldspar is the most abundant phenocryst phase comprising, on average, 5 % of the section. Plagioclase either occurs as euhedral to subhedral phenocrysts in a microcrystalline matrix, or intergrown with olivine (Plate 3.6). Plagioclase phenocrysts are usually lath-shaped crystals, ranging from 0.5 to 1 mm in size. In a number of examples, they occur as glomerocrysts (Plate 3.7). Each glomerocryst is, on average, 4 mm in diameter and consists of clusters of between 5 and 30 phenocrysts, ranging in size from 0.1 to 2 mm. The glomerocrysts do not appear to have an ordered structure, the individual phenocrysts have random orientations. The majority of the glomerocrysts are composed exclusively of plagioclase phenocrysts, however, in a few sections, glomerocrysts containing both plagioclase and olivine occur.

In rare cases, compositional zoning can be seen within the plagioclase crystals. This suggests that conditions within the magma changed whilst the crystals were developing (Alt, Kinoshita *et al.*, 1993). Most of the plagioclase present seems to have undergone little or no alteration.

Olivine also occurs in the majority of the sections but is less abundant than plagioclase, comprising only 2 % of the phenocrysts. Olivine crystals are generally anhedral, ranging up to



**Plate 3.6.** Intergranular texture in a massive basalt from Hole 896A. The section contains plagioclase, clinopyroxene and olivine. XPL. Field of view is 7 mm.



**Plate 3.7.** Glomerocrysts of plagioclase in a pillow lava from Hole 896A. The microcrystalline matrix contains plagioclase and altered olivine. XPL. Field of view is 7 mm.

1 mm in size. In the majority of the sections, olivine is altered to secondary clay and opaque minerals, many of which have been oxidised to an amorphous red / brown material. This has been identified by Teagle *et al.* (1996) as a mixture of saponite and iron oxyhydroxides ( $\text{Fe}(\text{O},\text{OH})_x$ ).

Clinopyroxene is rare throughout the core. It only occurs in those samples from depths greater than 350 mbsf (Alt, Kinoshita *et al.*, 1993). In the sections where it is present, it occurs as rare phenocrysts, on average 2 mm in size, with a strongly developed cleavage. The clinopyroxene phenocrysts are often simply twinned.

In the porphyritic sections the microcrystalline groundmass consists of acicular crystals of plagioclase and extensively altered olivines.

### 3.7.2.2. Alteration

None of the examined thin-sections show any foliation or preferred orientation of crystals.

Plagioclase as phenocrysts and in the groundmass seems to have undergone little or no alteration. This is in contrast to olivine which is almost always replaced by secondary clay and opaque minerals, many of which have been further altered and oxidised to an amorphous red / brown material, identified as a mixture of saponite and iron oxyhydroxides ( $\text{Fe}(\text{O},\text{OH})_x$ ; Teagle *et al.*, 1996). In some of the porphyritic samples the groundmass is extensively replaced by the same red / brown material. Some small opaque mineral grains can be found in a number of sections.

Small veins were observed in three of the sections. In sample 896-33 the vein is approximately 0.1 mm thick, and filled with green amphibole. In samples 896-21 and 896-27, similar sized veins are filled with red / brown iron oxyhydroxides ( $\text{Fe}(\text{O},\text{OH})_x$ ).

### 3.7.3. Variation in mineralogy with lithology

If the various lithological units in Hole 896A were formed at different effusion rates or from lavas with different viscosities or temperatures, then this may be reflected in the mineralogy of the erupted lavas. Unfortunately brecciated units cannot be included in this discussion as only one breccia thin-section was studied (HAG 896-6) and this represents a section through a clast therefore the nature of any interstitial material cannot be determined. The texture and composition of this section is purely a reflection of the original lithological units prior to brecciation. No examples of hyaloclastite breccias were sectioned, the material is too fragile for effective sampling.

Both pillow lavas and massive units within the Hole 896A core are very similar in composition, containing plagioclase and olivine, sometimes with rare clinopyroxenes. The main differences between the two lithologies are in terms of texture and grain-size. The majority of the massive units examined have intergranular textures comprising intergrowths of plagioclase and olivine. In contrast, the pillow lavas have porphyritic or glomeroporphyritic textures with sparse phenocrysts of plagioclase and olivine in a microcrystalline groundmass.

The fine-grained groundmass of the pillow lavas suggests rapid cooling, whereas the coarser-grained massive units probably cooled much more slowly. This is consistent with the premise that different eruption rates are responsible for different lava flow morphologies (§ 2.3.4). Pillow lavas are expected to form from cooler lavas erupted at low effusion rates, these would be cooled rapidly on contact with seawater. The phenocryst phases were probably crystallised from the melt before or during the lavas transport to the surface. Sheet flows (massive units) are thought to form at higher effusion rates from higher temperature lavas (Ballard *et al.*, 1979), these would cool at a much slower rate allowing a coarser-grained groundmass to develop.

### 3.8. Geochemistry

Geochemical data from Hole 896A was investigated to ascertain whether any relationships could be found between lithology and chemistry. Comparisons with global MORB values have been largely avoided as this study aims to investigate the lithological variations within this small section of the crust.

Both whole rock and glass data have been analysed for Hole 896A by the shipboard scientific party (Alt, Kinoshita *et al.*, 1993; Brewer *et al.*, 1996) and Fisk *et al.* (1996) respectively. The whole rock chemistry was analysed by X-ray fluorescence spectrometry (Brewer *et al.*, 1996) and the glass data by electron microprobe (Fisk *et al.*, 1996). Both these sets of data have been used in this study.

The whole rock chemistry does not provide an entirely accurate representation of the downhole geochemistry as it is affected by both alteration and mineralogical effects. Cores of pillow lavas tend to be preferentially altered rather than the glassy rims (Laverne *et al.*, 1996). The fresh glass at the pillow edges is considerably less porous than the pillow cores.

#### 3.8.1. Major element geochemistry

Each of the major oxides present in samples from Hole 896A were plotted versus depth downhole and % MgO.

For the whole rock data MgO ranges from 6.7 to 9.7 % with an average of 7.96 % and appears to show a slight increase in concentration with depth (Figure 3.7.a). For the glass data there is a much smaller range of MgO contents (8.15 to 9.84 %). In the upper part of Hole 896A there does not appear to be any systematic variation of MgO with depth for the whole rock chemistry until approximately 370 mbsf. In the lower part of the hole (370 mbsf to base) MgO shows a general decrease with increasing depth. The glass data shows a decrease in MgO with depth to approximately 330 mbsf where there is a sharp decrease in MgO. MgO then shows very little variation with depth until 420 mbsf where a sharp increase in MgO occurs. MgO then decreases to the base of the hole.

Fe<sub>2</sub>O<sub>3</sub> ranges from 7.99 to 10.32 % in the Hole 896 basalts with an average of 9.36. % and does not show any discernible trends with depth (Figure 3.7.b). Glass data for Fe<sub>2</sub>O<sub>3</sub> is unavailable for the Hole 896A core.

SiO<sub>2</sub> ranges from 47.67 to 50.51 % in the Hole 896A core with an average of 49.28 %. On the downhole profile for the whole rock chemistry, it decreases steadily downhole to approximately 320 mbsf. It then increases rapidly to approximately 380 mbsf, before decreasing again to the base of the hole (Figure 3.7.c). For the glass data, SiO<sub>2</sub> shows an overall increase with depth until 290 mbsf where an abrupt decrease occurs. At 340 mbsf a sharp increase in SiO<sub>2</sub> can be noted, values then remain relatively constant with depth until 420 mbsf where there is a rapid decrease in SiO<sub>2</sub>.

The glass data for Al<sub>2</sub>O<sub>3</sub> shows a decrease with depth for the first 320 m of the borehole (Figure 3.8.a). Between 320 and 390 mbsf there is a rapid decrease in Al<sub>2</sub>O<sub>3</sub>. Below 390 mbsf, values increase sharply, then decrease down to the base of the hole. Al<sub>2</sub>O<sub>3</sub> contents varies from 14.42 to 16.55 % with an average of 15.65 %. A similar variation with depth is shown by the whole rock chemistry, however, there is a greater degree of scatter probably due to the accumulation of phenocrysts, particularly plagioclase. This is confirmed by the mineralogy (§ 3.7) which confirms plagioclase was a fractionating phase in the Hole 896A basalts.

A plot of Al<sub>2</sub>O<sub>3</sub> versus MgO (Figure 3.8.b) for the Hole 896A glass data, shows two distinct clusters of points, one more depleted in both oxides than the other. On this basis the Hole 896A samples can be divided into two groups, both sample groups show a positive correlation between Al<sub>2</sub>O<sub>3</sub> and MgO. Fractionation of olivine increases Al<sub>2</sub>O<sub>3</sub> in the residual liquid and decreases MgO, however, the fractionation of plagioclase decreases Al<sub>2</sub>O<sub>3</sub> in the residual liquid and increases MgO. The combination of fractionation of olivine and plagioclase results in a positive correlation between Al<sub>2</sub>O<sub>3</sub> and MgO, i.e. Al<sub>2</sub>O<sub>3</sub> decreases as MgO decreases (Sun *et al.*, 1979). The mineralogy, discussed in § 3.7., confirms that these minerals were fractionating phases in Hole 896A basalts. In contrast to the glass data, the whole rock

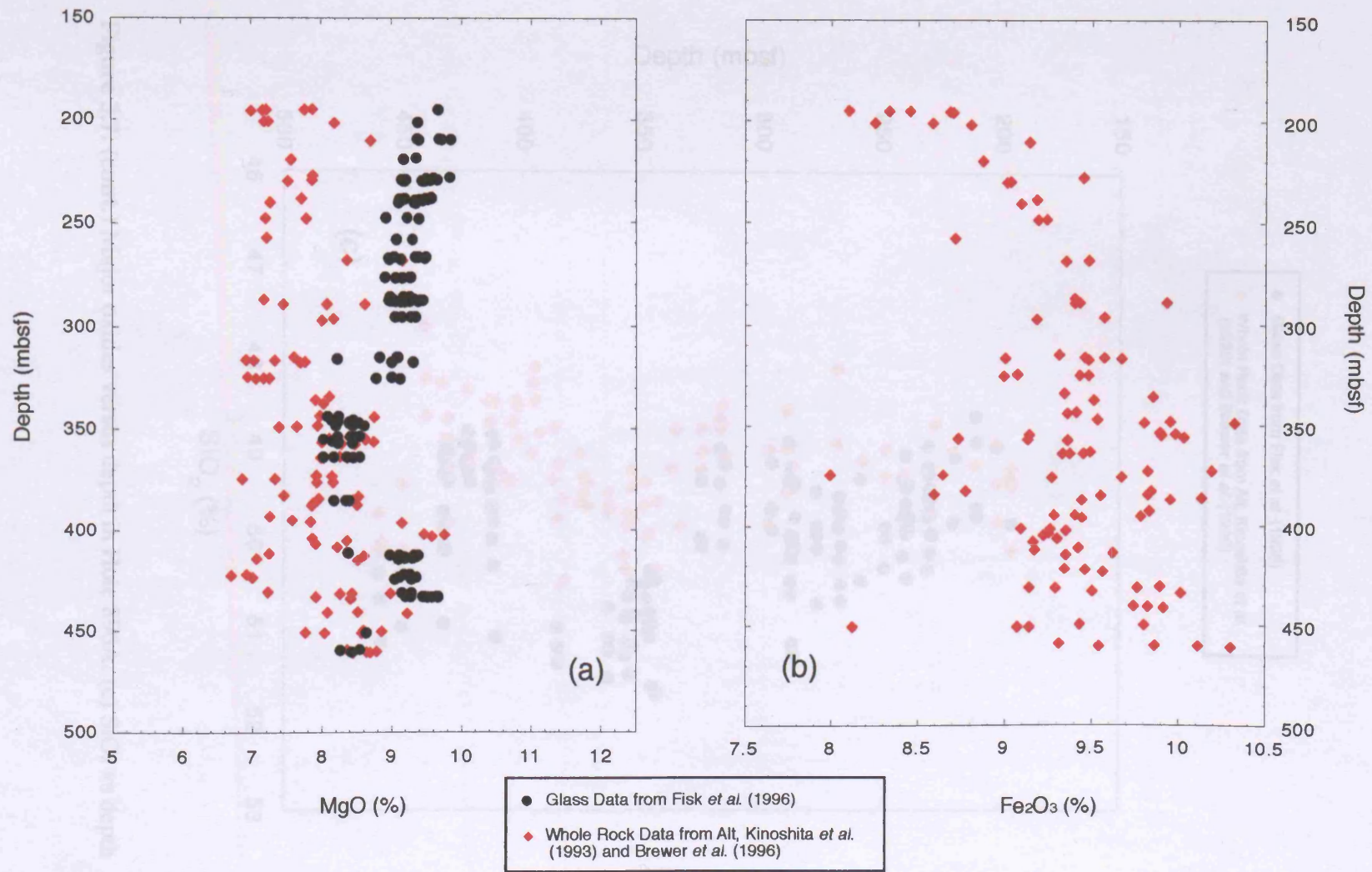


Figure 3.7. Variation of major oxides with depth in Hole 896A: (a) MgO vs depth, (b) Fe<sub>2</sub>O<sub>3</sub> vs depth

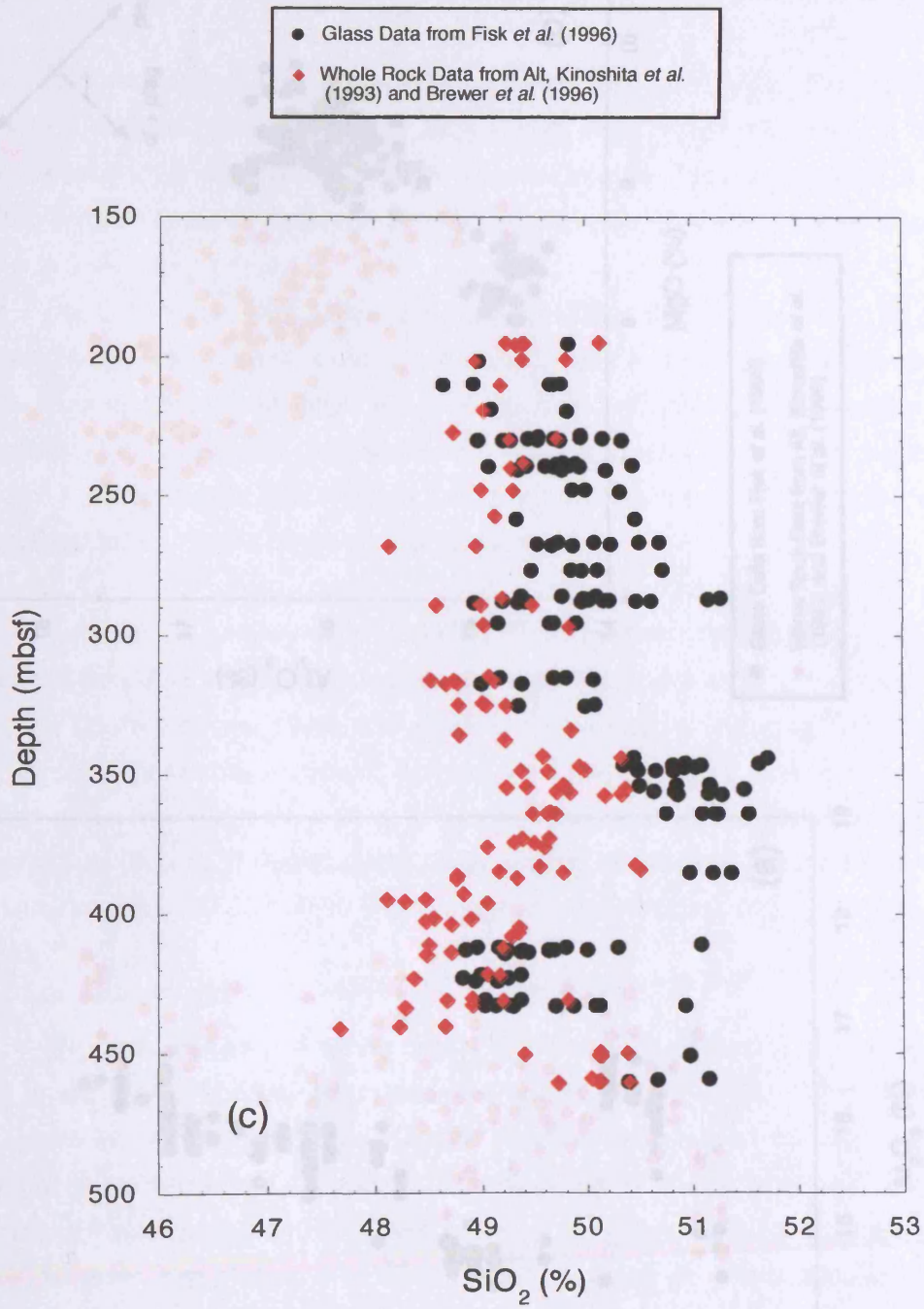
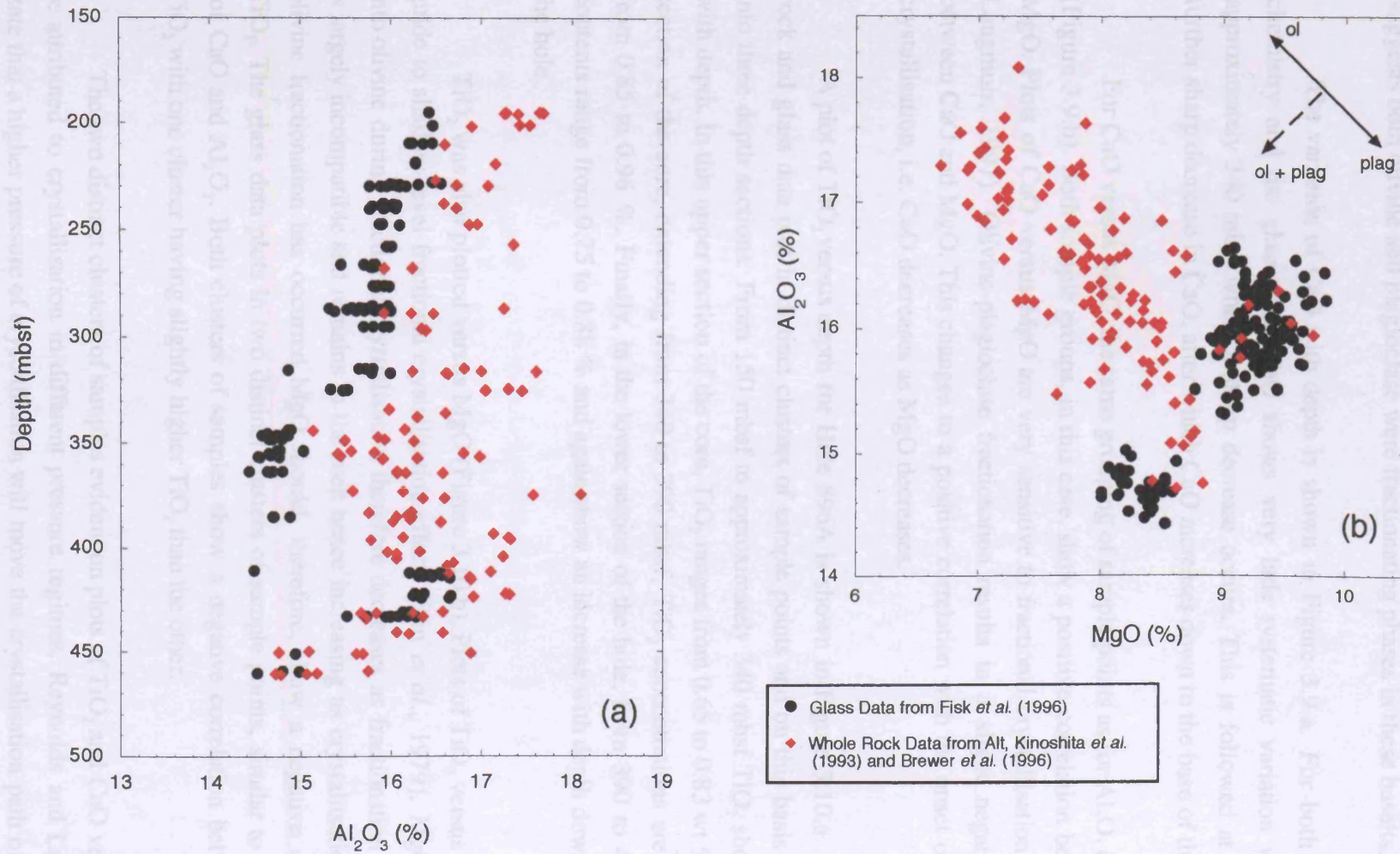


Figure 3.7. (cont.) Major oxides versus depth in Hole 896A: (c) SiO<sub>2</sub> vs depth



**Figure 3.8.** (a)  $\text{Al}_2\text{O}_3$  versus depth for Hole 896A, (b)  $\text{Al}_2\text{O}_3$  versus  $\text{MgO}$  for Hole 896A

geochemistry shows a negative correlation between  $\text{Al}_2\text{O}_3$  and  $\text{MgO}$ . This is likely to be the result of the accumulation of phenocrysts in the basalts, particularly olivine and plagioclase. The trend is unlikely to be the result of fractionation of only one mineral phase, as the mineralogy suggests both olivine and plagioclase were fractionating phases in these basalts.

The variation of  $\text{CaO}$  with depth is shown in Figure 3.9.a. For both the whole rock chemistry and the glass data,  $\text{CaO}$  shows very little systematic variation with depth until approximately 340 mbsf where a sharp decrease occurs. This is followed at 390 mbsf by a further sharp decrease in  $\text{CaO}$ , after which  $\text{CaO}$  increases down to the base of the hole.

For  $\text{CaO}$  versus  $\text{MgO}$ , the same grouping of sample points as for  $\text{Al}_2\text{O}_3$  can be observed (Figure 3.9.b). Both sample groups, in this case, show a positive correlation between  $\text{CaO}$  and  $\text{MgO}$ . Plots of  $\text{CaO}$  versus  $\text{MgO}$  are very sensitive to fractional crystallisation (Reynolds and Langmuir, 1997). Olivine-plagioclase fractionation results in a slight negative relationship between  $\text{CaO}$  and  $\text{MgO}$ . This changes to a positive correlation with the onset of clinopyroxene crystallisation, i.e.  $\text{CaO}$  decreases as  $\text{MgO}$  decreases.

A plot of  $\text{TiO}_2$  versus depth for Hole 896A is shown in Figure 3.10.a. Both the whole rock and glass data plot in distinct clusters of sample points and on this basis can be divided into three depth sections. From 150 mbsf to approximately 340 mbsf  $\text{TiO}_2$  shows an increase with depth. In this upper section of the core,  $\text{TiO}_2$  ranges from 0.65 to 0.83 wt %. In the central section of the core, extending from 340 to 390 mbsf,  $\text{TiO}_2$  concentrations are higher ranging from 0.85 to 0.96 %. Finally, in the lower section of the hole, from 390 to 470 mbsf,  $\text{TiO}_2$  contents range from 0.75 to 0.88 % and again show an increase with depth down to the base of the hole.

$\text{TiO}_2$  was also plotted versus  $\text{MgO}$  (Figure 3.10.b). Plots of  $\text{TiO}_2$  versus  $\text{MgO}$  provide a guide to shallow-level fractional crystallisation effects (Sun *et al.*, 1979).  $\text{MgO}$  is partitioned into olivine during fractional crystallisation therefore decreases as fractionation proceeds.  $\text{TiO}_2$  is largely incompatible and remains in the melt hence increasing as crystallisation continues. If olivine fractionation has occurred  $\text{MgO}$  should, therefore, show a negative correlation with  $\text{TiO}_2$ . The glass data plots in two distinct clusters of sample points, similar to those observed for  $\text{CaO}$  and  $\text{Al}_2\text{O}_3$ . Both clusters of samples show a negative correlation between  $\text{MgO}$  and  $\text{TiO}_2$  with one cluster having slightly higher  $\text{TiO}_2$  than the other.

The two distinct clusters of samples evident on plots of  $\text{TiO}_2$  and  $\text{CaO}$  versus  $\text{MgO}$  may be attributed to crystallisation in different pressure regimes. Reynolds and Langmuir (1997) state that a higher pressure of crystallisation will move the crystallisation path of clinopyroxene to higher  $\text{MgO}$ . The clusters of samples are also depth related with the sample group with lower

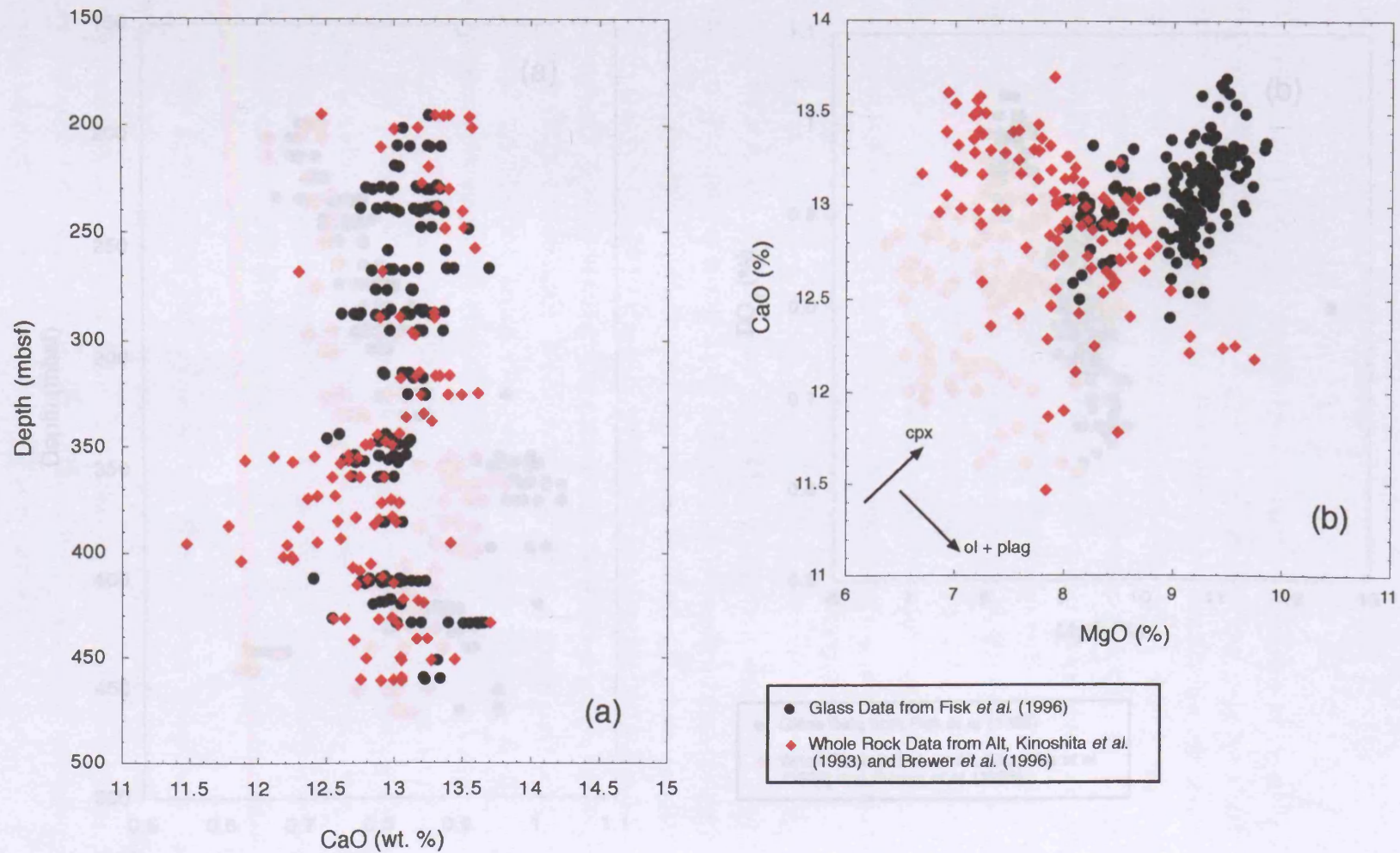


Figure 3.9. (a) CaO versus depth for Hole 896A, (b) CaO versus MgO for Hole 896A.

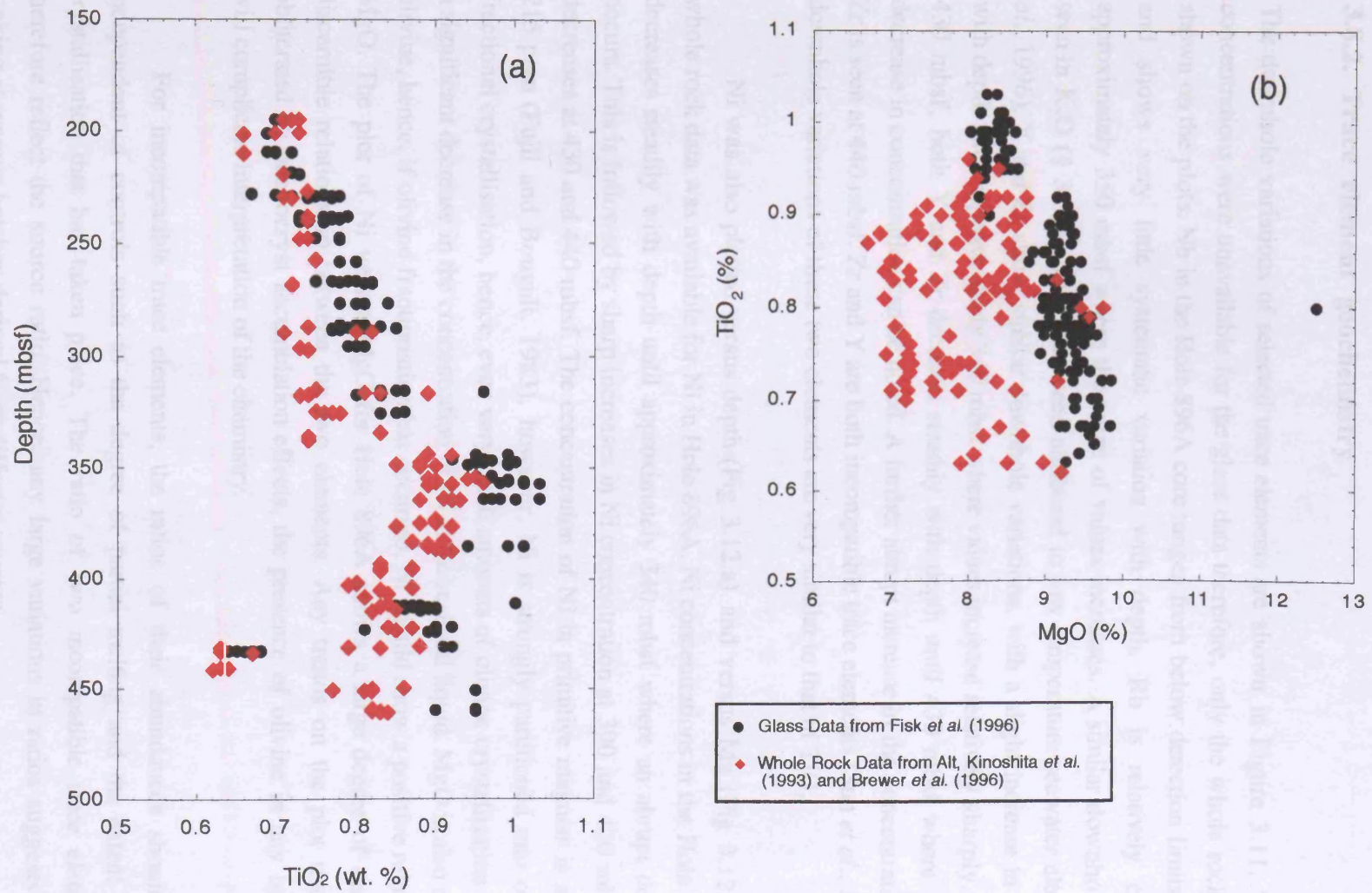


Figure 3.10. (a) TiO<sub>2</sub> versus depth for Hole 896A, (b) TiO<sub>2</sub> versus MgO for Hole 896A.

MgO corresponding to the section from 340 to 385 mbsf. This may suggest that the lavas from this section crystallised in a higher pressure regime than those above and below it.

### 3.8.2. Trace element geochemistry

The downhole variations of selected trace elements are shown in Figure 3.11. Trace element concentrations were unavailable for the glass data therefore, only the whole rock chemistry is shown on the plots. Nb in the Hole 896A core ranges from below detection limits to 1.12 ppm and shows very little systematic variation with depth. Rb is relatively constant until approximately 350 mbsf where the range of values increases. A similar downhole variation is seen in K<sub>2</sub>O (§ 3.8.3) which has been attributed to low temperature seawater alteration (Alt *et al.*, 1996). Y and Zr show similar downhole variations, with a slight increase in concentration with depth until approximately 340 mbsf where values increase relatively sharply. From 340 to 430 mbsf, both Y and Zr decrease steadily with depth until 430 mbsf where a very sharp decrease in concentration can be noted. A further abrupt increase in the concentrations of Y and Zr is seen at 440 mbsf. Zr and Y are both incompatible trace elements (Sun *et al.*, 1979) and the downhole variations of these two elements are very similar to that of TiO<sub>2</sub>.

Ni was also plotted versus depth (Fig 3.12.a) and versus Mg (Fig 3.12.b), only the whole rock data was available for Ni in Hole 896A. Ni concentrations in the Hole 896A basalts decreases steadily with depth until approximately 340 mbsf where an abrupt decrease in Ni occurs. This is followed by sharp increases in Ni concentration at 390 and 420 mbsf and sharp decreases at 430 and 440 mbsf. The concentration of Ni in primitive magmas is approximately 215 ppm (Fujii and Bougalt, 1983), however, Ni is strongly partitioned into olivine during fractional crystallisation, hence, even very small amounts of olivine crystallisation will result in a significant decrease in the concentration of Ni in the residual liquid. MgO is also compatible in olivine, hence, if olivine fractionation has occurred, Ni should show a positive relationship with MgO. The plot of Ni versus MgO for Hole 896A shows a large degree of scatter with no discernible relationship between the two elements. Any trends on the plot may have been obliterated by phenocryst accumulation effects, the presence of olivine in any basalt samples will complicate interpretation of the chemistry.

For incompatible trace elements, the ratios of their abundances should be largely independent of controls such as the degree of partial melting and the extent of fractional crystallisation that has taken place. The ratio of two incompatible trace elements should therefore reflect the source ratio. Hence, any large variations in ratios suggests that we are looking at magma batches derived from different sources.

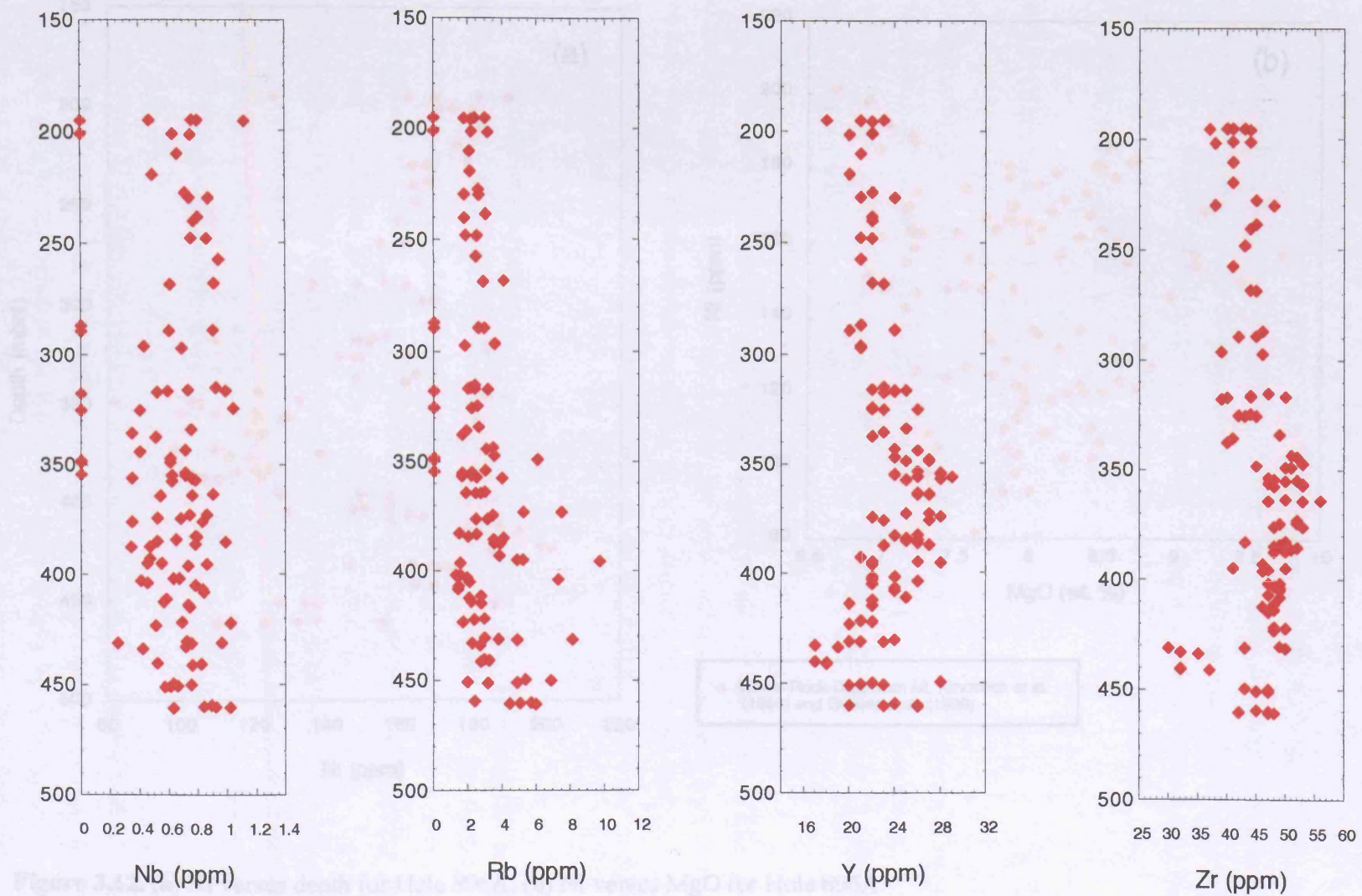
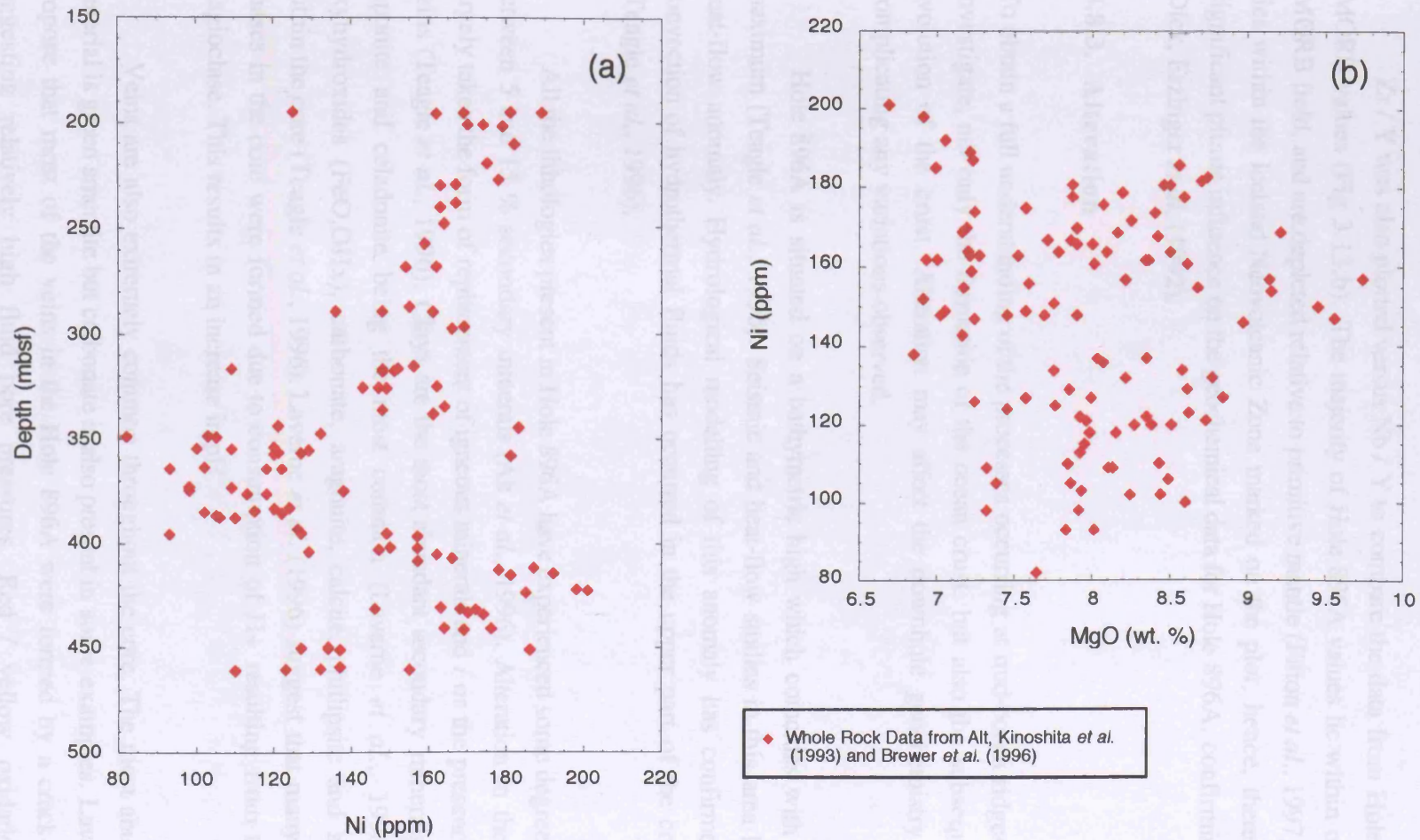


Figure 3.11. Variation in selected trace elements with depth downhole



**Figure 3.12.** (a) Ni versus depth for Hole 896A, (b) Ni versus MgO for Hole 896A.

Nb / Zr ranges from below the detection limit to 0.026 in the Hole 896A samples. A plot of Nb / Zr versus depth for 896A shows very little variation downhole (Figure 3.13.a), suggesting that the basalts present in Hole 896A were all derived from a similar source.

Zr / Y was also plotted versus Nb / Y to compare the data from Hole 896A with global MORB values (Fig 3.13.b). The majority of Hole 896A values lie within or below the global MORB field, and are depleted relative to primitive mantle (Fitton *et al.*, 1997). None of the data lies within the Iceland Neovolcanic Zone marked on the plot, hence, there appears to be no significant plume influence on the geochemical data for Hole 896A, confirming the assertion of Dick, Erzinger *et al.* (1992).

### 3.8.3. Alteration

To obtain a full understanding of the processes occurring at mid-ocean ridges it is necessary to investigate, not only the formation of the ocean crust, but also the subsequent alteration and evolution of the crust. Alteration may affect the downhole geochemistry of the borehole, complicating any variations observed.

Hole 896A is situated on a bathymetric high which coincides with a local heat flow maximum (Teagle *et al.*, 1996). Seismic and heat-flow studies in this area have discovered a heat-flow anomaly. Hydrological modelling of this anomaly has confirmed that significant convection of hydrothermal fluids has occurred in the upper part of the crust at Hole 896A (Teagle *et al.*, 1996).

All the lithologies present in Hole 896A have experienced some degree of alteration with between 5 and 15 % secondary minerals (Alt *et al.*, 1996). Alteration in the Hole 896A core largely takes the form of replacement of igneous minerals and / or the presence of cross-cutting veins (Teagle *et al.*, 1996). Clays are the most abundant secondary minerals within the core, saponite and celadonite being the most common (Laverne *et al.*, 1996). Chlorite, Fe-oxyhydroxides (FeO,OHx), carbonate, aragonite, calcite, phillipsite and zeolite also occur within the core (Teagle *et al.*, 1996). Laverne *et al.* (1996) suggest that many of the secondary phases in the core were formed due to consumption of H<sup>+</sup> resulting from the breakdown of plagioclase. This results in an increase in pH.

Veins are also extremely common throughout the core. The most abundant vein-filling material is green smectite but carbonate is also present in some examples. Laverne *et al.* (1996) propose that most of the veins in the Hole 896A were formed by a crack-seal mechanism, suggesting relatively high fluid pore pressures. Red / yellow oxidation haloes occur

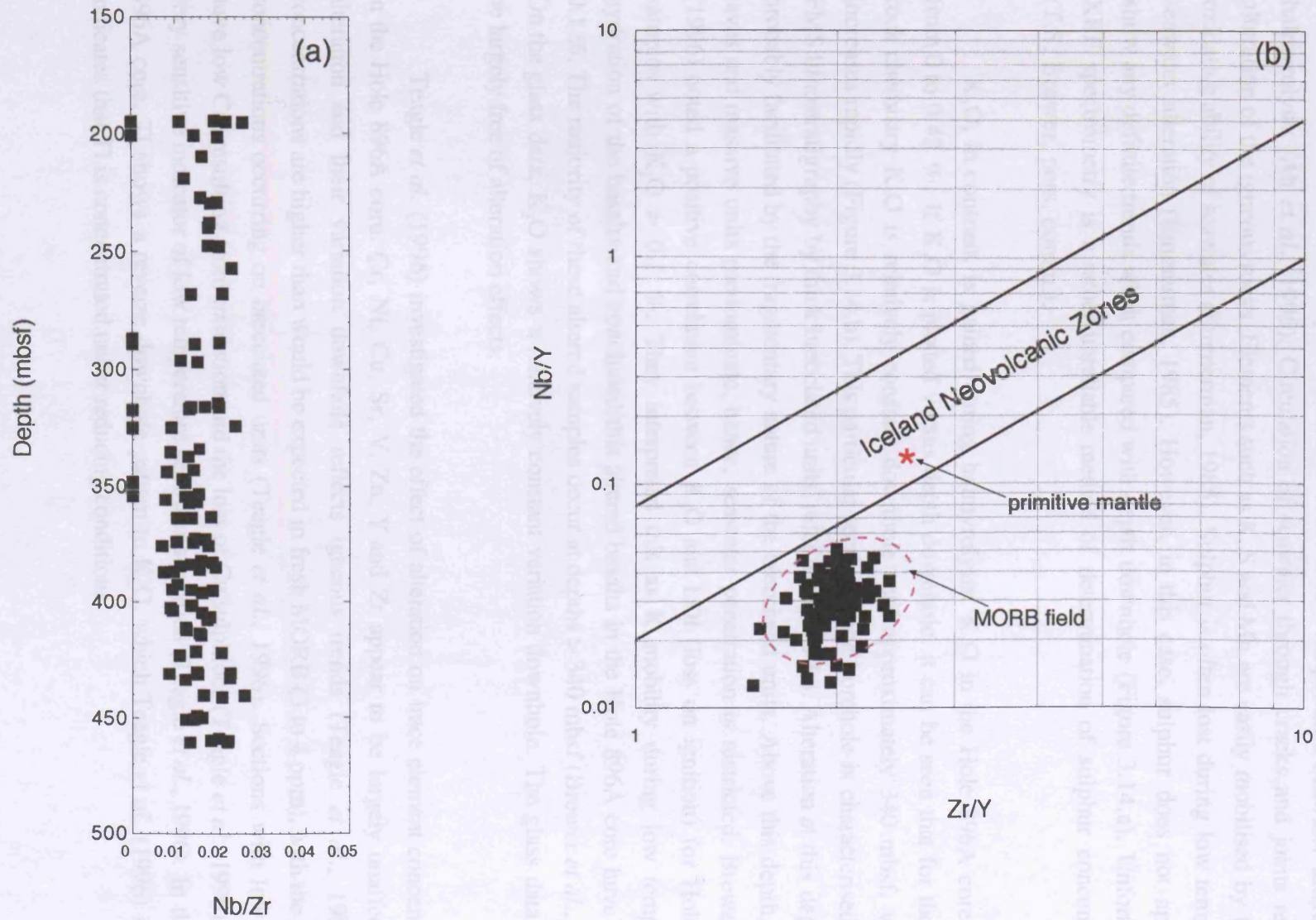


**Figure 3.13.** (a) Nb/Zr for Hole 896A samples, (b) Nb/Y versus Zr/Y For Hole 896A samples. The field of “normal” MORB and the position of primitive mantle are indicated, (after Fitton *et al.* (1997)). Data is from Alt, Kinoshita *et al.* (1993).

surrounding some fractures and veins. These are predominantly found in the massive units, but some rare examples do occur in the pillow lava sections.

Most of the alteration present in Hole 896A is low-temperature seawater alteration, or halmyrolysis (Alt *et al.*, 1996). Circulation of seawater through cracks and joints results in alteration of the igneous rocks. Elements such as K, S and Mn are easily mobilised by the high oxidative ability of seawater (Emmerman, 1985). Sulphur is often lost during low temperature seawater alteration (Emmerman, 1985). However, in this case, sulphur does not appear to show any definite trends when compared with depth downhole (Figure 3.14.a). Unfortunately XRF spectrometry is a rather unreliable method of determination of sulphur concentrations (T.S. Brewer, pers. comm.).

$K_2O$ , in contrast, is gained during halmyrolysis.  $K_2O$  in the Hole 896A core ranges from 0 to 0.42 %. If  $K_2O$  is plotted versus depth downhole, it can be seen that for the whole rock chemistry  $K_2O$  is relatively constant downhole until approximately 340 mbsf, where it increases rapidly (Figure 3.14.b). This particular section of the borehole is characterised on the FMS lithostratigraphy by thick brecciated units, refer to Figure 3.3. Alteration at this depth was probably facilitated by the fragmentary nature of the brecciated units. Above this depth, pillow lavas and massive units predominate, hence, seawater penetration is restricted. Brewer *et al.* (1996) noted a positive correlation between  $K_2O$  and LOI (loss on ignition) for Hole 896A samples with  $K_2O > 0.1$  %. They interpreted this as K mobility during low temperature hydration of the basalts and concluded that altered basalts in the Hole 896A core have  $K_2O > 0.1$  %. The majority of these altered samples occur at depths  $> 340$  mbsf (Brewer *et al.*, 1996). On the glass data,  $K_2O$  shows a relatively constant variation downhole. The glass data should be largely free of alteration effects.

Teagle *et al.* (1996) investigated the effect of alteration on trace element concentrations in the Hole 896A core. Cr, Ni, Cu, Sr, V, Zn, Y and Zr appear to be largely unaffected by alteration and their variation downhole reflects igneous trends (Teagle *et al.*, 1996). Li concentrations are higher than would be expected in fresh MORB (3 to 4 ppm), with the highest concentrations occurring on brecciated units (Teagle *et al.*, 1996). Sections with low S also have low Cu, resulting from oxidation and the loss of Cu sulphides (Teagle *et al.*, 1996). Tl is a very sensitive indicator of low temperature seawater alteration (Teagle *et al.*, 1996). In the Hole 896A core, Tl shows a reverse downhole pattern to  $K_2O$ , which Teagle *et al.* (1996) suggest indicates that Tl is concentrated under reducing conditions.

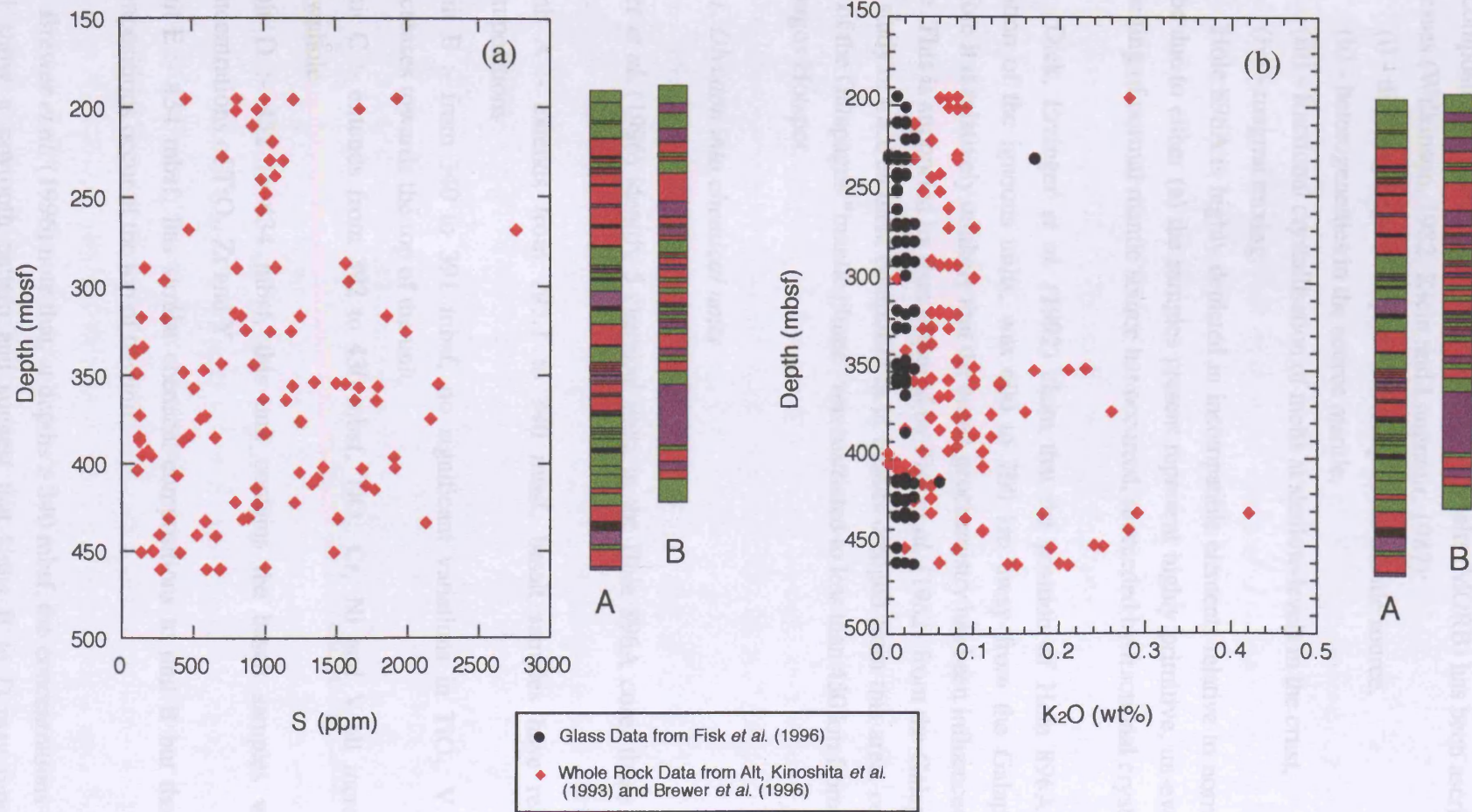


Figure 3.14. Variation in (a) S and (b) K<sub>2</sub>O with depth in Hole 896A

### 3.8.4. Discussion

The compositional diversity of mid-ocean ridge basalts (MORB) has been ascribed to four main processes (Wilkinson, 1982; Klein and Langmuir, 1987):

- (i) - differing degrees of partial melting of the mantle source,
- (ii) - heterogeneities in the source mantle,
- (iii) - fractional crystallisation of melts at shallow-levels in the crust,
- (iv) - magma mixing.

Hole 896A is highly depleted in incompatible elements relative to normal MORB. This may be due to either (a) the samples present represent highly primitive, un-evolved basalts, or (b) melting of normal mantle source has occurred, succeeded by fractional crystallisation.

Dick, Erzinger *et al.* (1992) claim that the position of Hole 896A, at the time of formation of the igneous units, was 600 to 700 km away from the Galapagos Hot Spot, therefore it is relatively unlikely that the basalt geochemistry has been influenced by the hot spot plume. This is supported by data acquired by Fisk *et al.* (1982) from the Galapagos Rift Zone. Their study of trace element compositions in basalts dredged from this area, concluded that the effect of the Galapagos “mantle plume” was restricted to less than 450 km from the centre of the Galapagos Hotspot.

#### 3.8.4.1. Division into chemical units

Brewer *et al.* (1996) identify 5 chemical units in the Hole 896A core, these are summarised below:

- Unit A :- extends from 195.1 to 340 mbsf, basalt samples have relatively uniform compositions
- Unit B :- from 340 to 391 mbsf, no significant variations in TiO<sub>2</sub>, V and Ni but Cr decreases towards the top of the unit.
- Unit C :- extends from 392 to 430 mbsf, TiO<sub>2</sub>, Cr, Ni and V all increase with depth downhole
- Unit D :- 432 to 434 mbsf, this unit contains the basalt samples with the lowest concentrations of TiO<sub>2</sub>, Zr and Y.
- Unit E :- 434 mbsf, has similar chemical compositions to unit B but the most primitive compositions occur at the top of the unit.

Brewer *et al.* (1996) note that, at depths > 340 mbsf, the concentrations of TiO<sub>2</sub>, V, Cr and Ni show a sawtooth pattern and suggest that Units B to D may represent fractional crystallisation of separate magma batches interspersed with magma chamber replenishment. In

Unit E, the most primitive magmas occur at the top of the unit, suggesting that magma-mixing is the dominant shallow-level process (Brewer *et al.*, 1996).

#### 3.8.4.2. Comparison of geochemical and lithological variations

Can the variations in geochemistry within Hole 896A be correlated with the observed lithological variations? In the majority of the Hole 896A core there appears to be very little correlation between lithology and geochemistry. No chemical distinctions can be made between pillow lavas, massive units and Type A and B breccias. However, one particular section of the borehole from 340 mbsf to 385 mbsf has higher  $\text{TiO}_2$  (0.88 to 1.4 %), and lower Ni than the lavas above and below it. If  $\text{TiO}_2$  versus depth is compared with the lithological log produced from FMS data (Fig 3.15.a), the section with higher  $\text{TiO}_2$  (%) correlates well with the large breccia zone between 350 and 390 mbsf. This section is bordered above and below by samples with lower  $\text{TiO}_2$  contents.  $\text{TiO}_2$  is expected to be largely incompatible and remains in the residual liquid during fractional crystallisation. Hence, as fractionation proceeds  $\text{TiO}_2$  increases in the residual liquid. This perhaps suggests that glass samples with higher  $\text{TiO}_2$  (%) have experienced a higher degree of fractional crystallisation. If this downhole variation is compared with that of a highly compatible element then the reverse pattern should be shown. Ni is preferentially partitioned into olivine during fractional crystallisation, therefore as fractionation proceeds Ni will become increasingly depleted in the residual liquid (Elthon, 1984).

The plot of Ni versus depth (Fig 3.15.b) shows that the section of the borehole with high  $\text{TiO}_2$  has correspondingly low Ni, confirming that this section of basalt has probably undergone greater amounts of fractionation of olivine  $\pm$  plagioclase  $\pm$  clinopyroxene.

How are these geochemical patterns reflected in the lithostratigraphical variation? This particular section of core has a large proportion of brecciated units (Type C), most of which appear to be sedimentary or tectonic in origin. These were interpreted in § 3.6.2. as representing a period of reduced volcanic activity. This decrease in activity may be related to a reduced influx of material into a RTF sub-axial magma chamber (§ 2.5.4.2 and 3.8.4.3), allowing more extensive fractional crystallisation to occur, any small amounts of lava that are erupted in this period will have undergone greater amounts of fractionation. A new influx of magma will mix this fractionated material with more primitive melts reducing  $\text{TiO}_2$  and increasing Ni in the magma chamber. Renewed volcanic activity ensures that more primitive lavas are erupted forming pillow lavas and massive units. Similar volcanic cycles are suggested by Stakes *et al.* (1984) for the Mid-Atlantic Ridge. They suggest that an eruptive cycle on at the ridge axis begins with rapidly extruded sheet flows with predominantly primitive compositions. As the cycle nears its conclusion, eruption rates decrease, forming more pillowed flows, with more evolved compositions due to fractional crystallisation in shallow lava conduits. A model

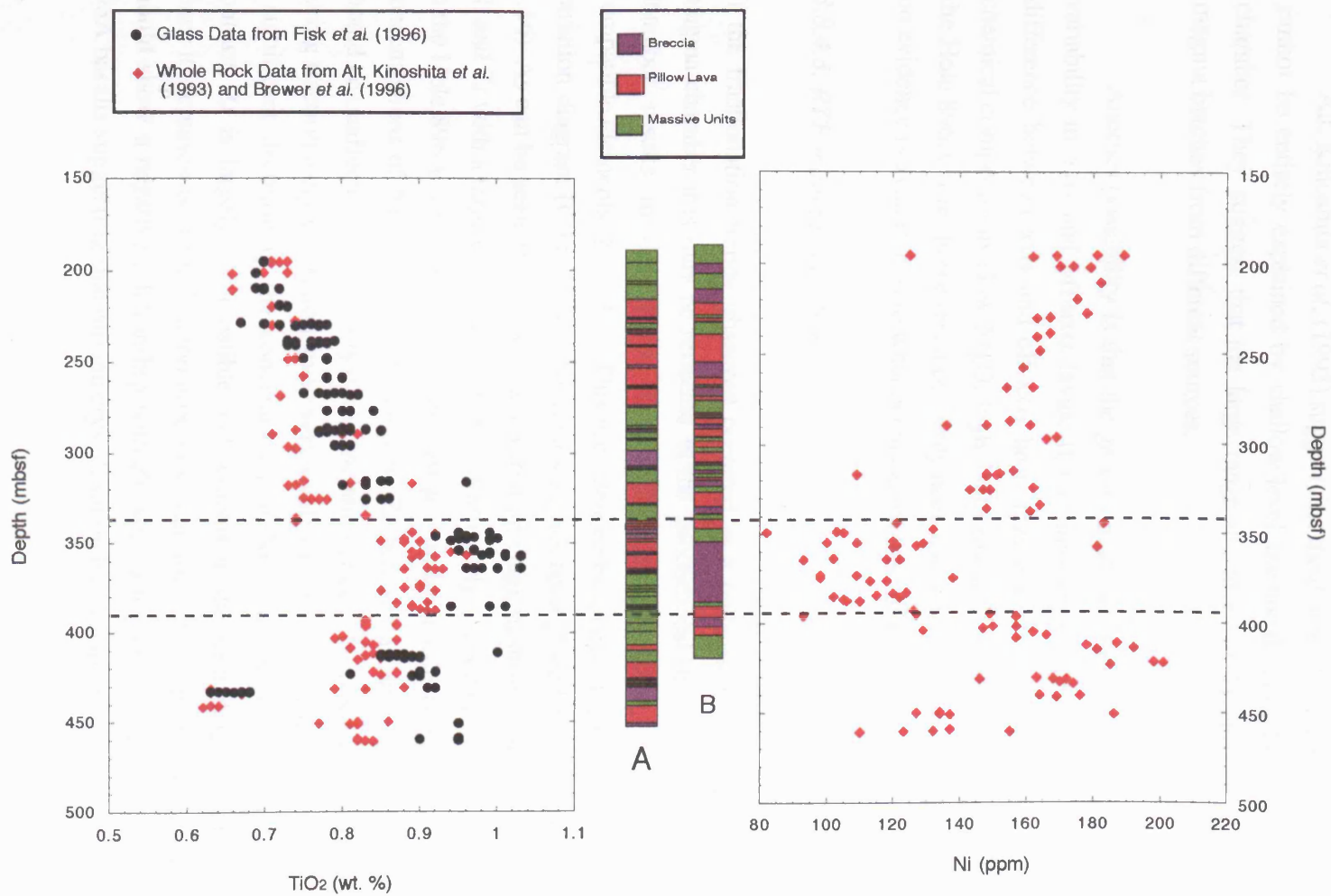


**Figure 3.15.** Comparison of downhole variations in (a) TiO<sub>2</sub> and (b) Ni with lithology in Hole 896A, A is the log derived from visual core descriptions and B is the log derived using FMS data.

of this type explains both the geochemical and lithological variability in upper ocean crust sections.

Alt, Kinoshita *et al.* (1993) suggest that the downhole variation in incompatible elements cannot be entirely explained by shallow-level fractional crystallisation in a sub-axial magma chamber. They suggest that the large range in values of Ti and Zr suggests production of magma batches from different sources.

Another possibility is that the geochemical and lithological variations are the result of variability in axis and off-axis lavas. If the lithological variability in Hole 896A reflects the difference between axis and off-axis lavas may expect to see an increase in more evolved chemical compositions (low MgO, high TiO<sub>2</sub>) towards the top of the core. This is not seen in the Hole 896A core, however, it probably does not represent the complete volcanic section and no evidence is available as to what occurs at the base of the section.

#### 3.8.4.3. RTF magma chambers

If the fractionation trends observed occurred in a replenished - tapped - fractionated (RTF) magma chamber this may be reflected in the geochemical data. Evolution in an RTF magma chamber results in decoupling of inter-element relationships between incompatible and compatible elements (§ 2.5.1.1). This is evidenced by a large degree of scatter on a two-element variation diagram (Cox, 1988). Ni versus Zr has been plotted for the Hole 896A basalts (Fig 3.16). As can be seen, the two-element variation diagram shows a negative correlation between Ni and Zr with a large degree of scatter. Unfortunately, glass data is not available for Ni and Zr in the Hole 896A core, therefore phenocryst accumulation effects may have an influence on the concentrations of Ni in the basalt samples. Zr behaves as an incompatible element therefore should be unaffected by phenocryst accumulation effects. Ni is strongly partitioned into olivine during fractional crystallisation, even very small amounts of olivine crystallisation will result in a significant decrease in the concentration of Ni in the residual liquid (Elthon, 1984). In contrast, Zr is largely incompatible and remains in the melt during fractional crystallisation hence it increases as crystallisation proceeds, therefore, if olivine fractionation has occurred Ni should show a negative relationship with Zr. such a negative correlation is seen in the Hole 896A basalts suggesting that olivine crystallisation has occurred.

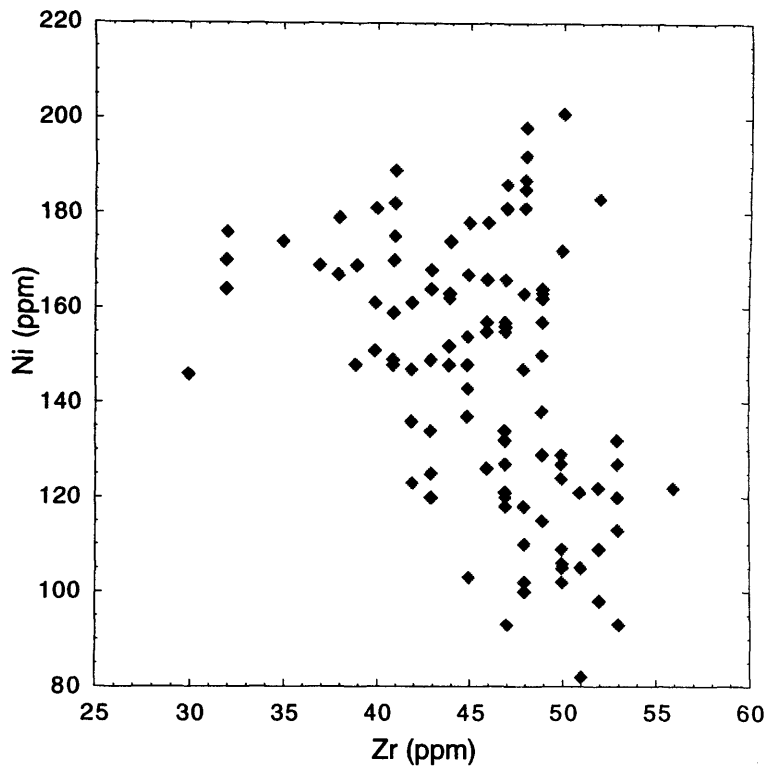


**Figure 3.16.** Zr versus Ni for Hole 896A basalts

#### 3.8.4.4. The clinopyroxene “paradox”

The geochemical data for Hole 896A suggests that clinopyroxene is a fractionating phase, however, as stated in § 3.7.1, clinopyroxene only occurs at depths below 340 mbsf. How is this possible? This clinopyroxene “paradox” has been discussed by Grove *et al.* (1992) who model a magma saturated with clinopyroxene at high pressure. If the magma cools at that pressure then olivine + plagioclase + clinopyroxene will crystallise, but if the magma is extracted and moved to lower pressure prior to the onset of fractional crystallisation, it will no longer reside on the olivine + plagioclase + clinopyroxene saturation boundary. The magma will now lie on the olivine + plagioclase saturation boundary, therefore, it will crystallise only olivine and plagioclase on eruption. This means that even though clinopyroxene has occurred, no clinopyroxene is present in erupted samples.

Grove *et al.* (1992) further suggest that the clinopyroxene paradox may also be explained by (a) magma mixing or (b) *in situ* crystallisation i.e. mixing of cooler clinopyroxene saturated magmas at the sides of a magma chamber with hotter, less evolved magmas from the magma chamber interior.

For Hole 896A, the absence of clinopyroxene in the majority of the core may suggest that a subaxial magma chamber beneath the Costa Rica Rift is not located at a fixed depth within the crust / mantle (Brewer *et al.*, 1996).

### **3.9. Development of Hole 896A crustal section**

The lithological and geochemical variations in the Hole 896A core lead to the following model for development of the crustal section. The lavas below approximately 340 mbsf were probably erupted at the axis of the Costa Rica Rift from a sub-axial magma chamber. Olivine  $\pm$  plagioclase  $\pm$  clinopyroxene fractionation occurred in the magma chamber probably accompanied by magma mixing of any new influxes of magma. As the section of crust began to move away from the axis, the supply to the magma chamber was diminished, therefore, the number of eruptions decreased allowing for brecciation of previously erupted lava flows. Any small eruptions during this time were of more fractionated lavas. Further off-axis, lavas supply was renewed, allowing for the eruption of new lava flows, the dominant shallow level process being magma mixing. The lava morphology erupted during any volcanic events was largely dependant on the viscosity and / or temperature of the erupting lava and was not significantly affected by its chemical composition.

#### **3.9.1. Variations in depth of magma chamber**

The magma chamber beneath the crustal section of Hole 896A must vary in its position within the crust. This would account for the distribution of clinopyroxene in the Hole 896A core and the two clusters of samples evident on plots of major element oxides versus MgO. When the section from 340 to 390 mbsf was being formed, the sub-axial magma chamber must have been in a higher pressure regime than for the lavas above and below it, allowing for the fractionation of clinopyroxene and the presence of the higher MgO group of samples.

### **3.10. Summary**

Three main types of lithology were recovered from ODP Hole 896A; pillow lavas, massive units and breccias. The brecciated units present in the core can be divided into three main groups, two of which were formed by sedimentary or tectonic processes, the third by hydrovolcanic processes. A lithostratigraphical log of the Hole 896A produced from core descriptions shows that each lithological unit is highly variable in thickness throughout the core and there appears to be no systematic variation of lithology with depth. A similar lithostratigraphical log constructed using wireline log data shows a similar complex stratigraphy, however, this new log contains considerably more brecciated units than suggested by the visual core descriptions. A large breccia section is indicated between 350 and 390 mbsf.

The individual lithological units have similar compositions but different textures in thin-section, massive units are characterised by intergranular textures, whereas the pillow lavas have porphyritic textures. This is thought to be a consequence of different effusion rates of lavas, with pillow lavas formed from cooler lavas erupted at low effusion rates and massive units formed at higher effusion rates.

The Hole 896A core can be divided into at least three chemical units. From 0 to 340 mbsf there is a decrease in the extent of fractionation with depth, therefore the dominant shallow-level process is probably magma mixing. The central section from 340 to 390 mbsf has more evolved compositions and corresponds with the large breccia section from 350 to 390 mbsf. This section of the crust has been interpreted as representing a period of limited volcanism during formation of this crustal section, probably related to a reduction in magma supply to a subaxial magma chamber beneath the Costa Rica Rift. This may have occurred as the section was moved off-axis.

## CHAPTER 4

---

# *Reconstructing the upper oceanic crust using core and log data. Case Study 2: ODP Hole 504B*

### 4.1 Introduction

This chapter provides an overview of some of the data obtained from ODP Hole 504B in an attempt to compare the lithostratigraphy and geochemistry of the hole with Hole 896A. At present, Hole 504B is the deepest oceanic crust borehole, with a total depth of 2111 mbsf, penetrating 274.5 m of sediments and 1836.5 m of basement rocks (Alt, Kinoshita *et al.*, 1993); this is the only borehole to have penetrated the sheeted dyke complex *in situ*, (Alt, Kinoshita *et al.*, 1993). Hole 504B is located approximately 1 km to the north-west of Hole 896A, (Alt, Kinoshita *et al.*, 1993), refer to Fig 3.1., § 3.1., and the material recovered from Hole 504B is approximately 28,000 years younger than at Hole 896A (Laverne *et al.*, 1996). Comparisons of Holes 896A and 504B, which are in close proximity to one another, may provide an insight into the small-scale spatial and temporal variations operating at the Costa Rica Rift, helping to explain some of the lithological and geochemical variations in the ocean crust in this area.

Hole 504B has been extensively studied by numerous workers (e.g. Cann, Langseth *et al.*, 1983; Anderson, Honnorez *et al.*, 1985; Becker, Sakai *et al.*, 1988; Becker, Foss *et al.*, 1992; Dick, Erzinger *et al.*, 1992; Alt, Kinoshita *et al.*, 1993), however, for this study, only a brief discussion of the data from Hole 504B is provided, since the main purpose of the chapter is to provide a lithological and geochemical comparison between Holes 504B and 896A.

### 4.2. Previous Legs

Hole 504B has been drilled by seven DSDP / ODP legs to a total depth of 2111 mbsf, comprising over 1800 m of basement rocks, (Dick, Erzinger *et al.*, 1992; Alt, Kinoshita *et al.*, 1993). Average core recovery for the whole hole is 22.9 %, with 29.8% for the volcanic units, 25.3% for the transition zone and 13.7% for the sheeted dyke complex (Alt, Kinoshita *et al.*, 1993). The drilling history and lithostratigraphy of Hole 504B are summarised in Figure 4.1. and Table 4.1.

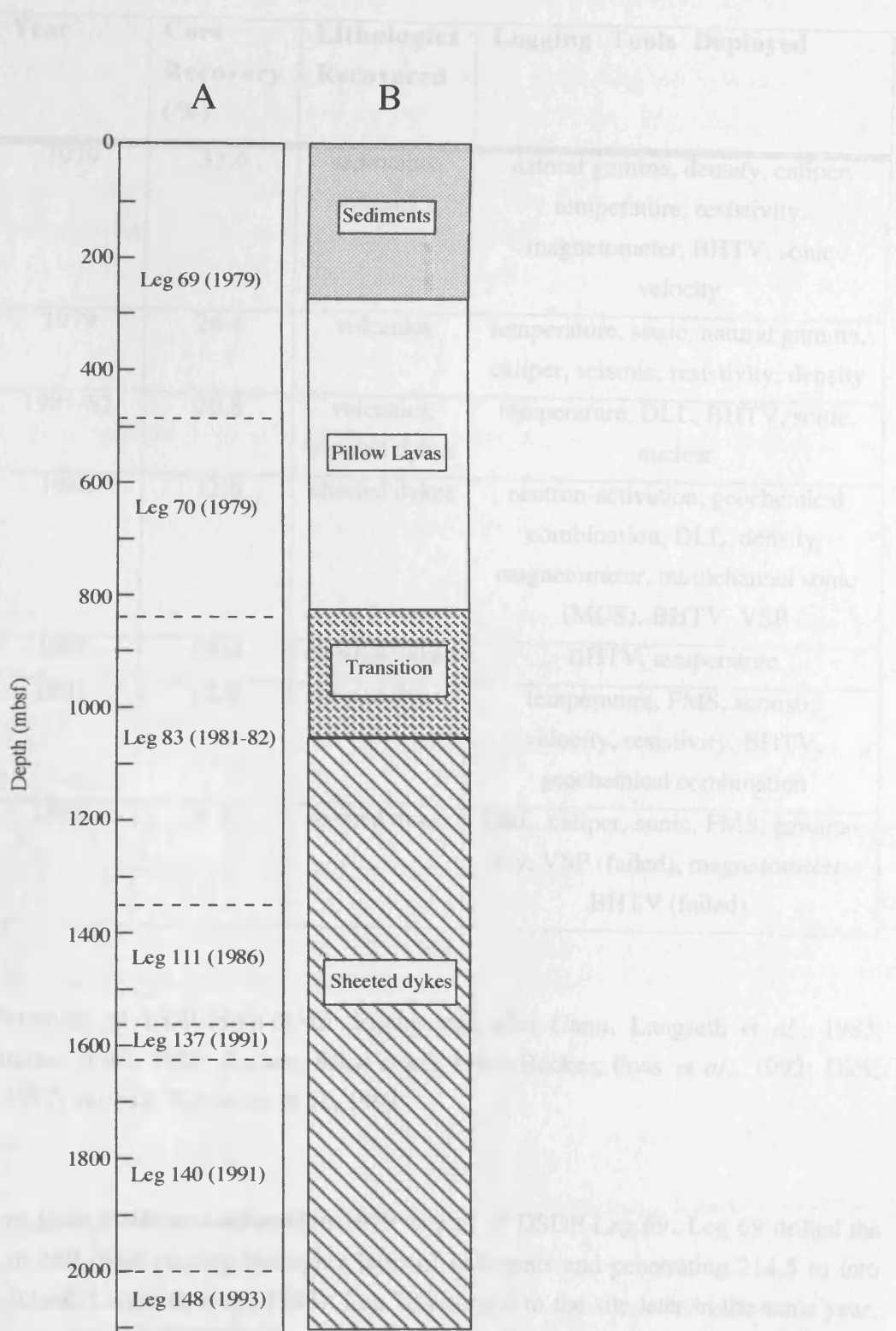


**Figure 4.1. Drilling history (A) and lithostratigraphy (B) of ODP Hole 504B. Adapted from Alt, Kinoshita *et al.* (1993)**

ODP / DSDP Leg	Year	Core Recovery (%)	Lithologies Recovered	Logging Tools Deployed
69	1979	33.6	sediments, volcanics	natural gamma, density, caliper, temperature, resistivity, magnetometer, BHTV, sonic velocity
70	1979	26.4	volcanics	temperature, sonic, natural gamma, caliper, seismic, resistivity, density
83	1981-82	20.8	volcanics, sheeted dykes	temperature, DLL, BHTV, sonic, nuclear
111	1986	12.6	sheeted dykes	neutron-activation, geochemical combination, DLL, density, magnetometer, multichannel sonic (MCS), BHTV, VSP
137	1991	18.0	sheeted dykes	BHTV, temperature
140	1991	12.6	sheeted dykes	temperature, FMS, acoustic velocity, resistivity, BHTV, geochemical combination
148	1993	8.7	sheeted dykes	DLL, caliper, sonic, FMS, gamma-ray, VSP (failed), magnetometer, BHTV (failed).

**Table 4.1.** Summary of ODP Hole 504B drilling legs after Cann, Langseth *et al.*, 1983; Anderson, Honnorez *et al.*, 1985; Becker, Sakai *et al.*, 1988; Becker, Foss *et al.*, 1992; Dick, Erzinger *et al.*, 1992; and Alt, Kinoshita *et al.*, 1993.

Drilling of Hole 504B was initiated in 1979 as part of DSDP Leg 69. Leg 69 drilled the hole to a depth of 489 mbsf passing through a layer of sediments and penetrating 214.5 m into basement rocks (Cann, Langseth *et al.*, 1983). Leg 70 returned to the site later in the same year, deepening the hole to 836 mbsf. This leg recovered predominantly pillow basalts and reached the top of the transition zone (Cann, Langseth *et al.*, 1993). At the end of 1981, Leg 83 penetrated the sheeted dyke complex to a depth of 1350 mbsf, recovering 106.9 m of core with a total core recovery of 20.8 % (Anderson, Honnorez *et al.*, 1985). Three subsequent ODP legs, 111 (1986), 137 (1991) and 140 (1991) drilled further into the sheeted dyke complex. Leg 111 in 1986

deepened Hole 504B by a further 213 m, giving a total depth of 1562.3 mbsf (Becker, Sakai *et al.*, 1988). This leg had particularly low core recovery, only 12.6 %, due to difficulties in drilling the sheeted dyke complex. In 1991, Leg 140, succeeded in deepening the hole to over 2 km below seafloor, coring 378.9 m but recovering only 47.69 m (Dick, Erzinger *et al.*, 1992). Finally, Leg 148 in 1993 deepened Hole 504B to its present depth of 2111 mbsf (Alt, Kinoshita *et al.*, 1993). At this depth, the drill string became stuck in a fault zone in the sheeted dyke complex, preventing further crustal penetration (Alt *et al.*, 1996).

### 4.3. Lithological Units

Hole 504B consists of 571 m of extrusive rocks, predominantly pillow lavas, and 200 m of transition zone rocks, with the remainder of the hole comprising sheeted dykes, (Detrick *et al.*, 1994). Adamson (1985) divides the rocks present in the Hole 504B core into three zones:

- Upper Zone (274.5 to 846 mbsf) - consists of intercalated pillow lavas, flows, breccias and massive units,
- Transition Zone (846 to 1055 mbsf) - with pillows, thin flows, massive units and dykes. The dykes were identified due to the intrusive nature of their contacts in thin-section. The last pillow lava was recorded at 1055 mbsf,
- Lower Zone (1055 to base) - comprises predominantly sheeted dykes, some of which are intensely brecciated.

This study is concerned with the volcanics from 274.5 mbsf to 846 mbsf. This represents the section of the borehole designated by the Shipboard Scientific Party as pillow lava, above 274.5 mbsf are sediments and below 846 mbsf is the transition zone and sheeted dyke complex (Cann, Langseth *et al.*, 1983; Alt, Kinoshita *et al.*, 1993), comprising the section drilled during Legs 69 and 70. Only the pillow lava stack from Hole 504B is being used for this study, so that the section may be more easily compared with the data available for Hole 896A, the core and log data available for Hole 896A does not include sedimentary or transition zone layers.

### 4.4. Log Data

Various geochemical and geophysical logs have been deployed in Hole 504B throughout its long drilling history. These are summarised in Table 4.1. Temperature, resistivity, natural gamma and density logs were collected from Legs 69, 70, 83, 111, 140 and 148. The Borehole Televiwer was run on all the legs with the exception of Leg 70, however, no data was obtained on Leg 148 due to failure of the tool (Alt, Kinoshita *et al.*, 1993). Formation Microscanner (FMS) images were obtained from Legs 140 and 148 (Dick, Erzinger *et al.*, 1992; Alt, Kinoshita *et al.*, 1993).

#### 4.4.1. Construction of a lithostratigraphical log for Hole 504B

The FMS data for Hole 504B is of a much poorer quality than for Hole 896A (Figure 4.2; Alt, Kinoshita *et al.*, 1993). At many depths only two of the four pads appear to be collecting interpretable data and one pad is not registering any data at all. On the other faulty pad some of the buttons are not responding. Outlines of individual features are very blurred on much of the data therefore it is very difficult to distinguish individual pillow lavas or clasts. Interpretation of the data is further complicated because the FMS log is not continuous, two passes, 7a and 7b, imaged from 655 to 979 mbsf and 289 to 579 mbsf respectively, leaving a section of 76 m with no available FMS data. In order to supplement the FMS data for Hole 504B, the core descriptions made by the Shipboard Scientific Party and the resistivity data from Leg 111 were used to aid the reconstruction of the lithostratigraphy of the hole. To identify the different lithological units within the hole, the same criteria as for Hole 896A were used (Table 3.4, § 3.5.1.).

Interpretable data begins at approximately 295 mbsf. At lower depths the borehole was too large for the FMS pads to have close contact with the borehole walls, hence, no data could be recovered (T.S. Brewer, pers. comm.). Above 295 mbsf the shipboard core descriptions describe massive aphyric basalt from 278 to 280 mbsf and moderately phyric basalt pillows from 280 to 295 mbsf (Cann, Langseth *et al.*, 1983).

At a number of depths within the FMS log, apparently brecciated units occur. An example occurs at a depth of approximately 480 mbsf, only one breccia piece at this depth was noted in the core descriptions (Piece 504B-28R-4 #1546), however, the thin-section descriptions for piece 1541 state “the sample is more or less a breccia” (Cann, Langseth *et al.*, 1983). Similarly, a number of pieces in Core 28R-2 are described as being heavily fragmented and altered in the shipboard core descriptions, some of the larger pieces recovered in this section may represent the interiors of large pillows or massive clasts.

The downhole resistivity data for Hole 504B is shown in Fig 4.3. The plot shows both the deep laterolog (LLD) and shallow laterolog curves (LLS). On the resistivity data (Figure 4.3), lava flows occur as discrete areas with relatively high, uniform resistivity. Three main positive peaks occur in the data, at depths of 522, 580 and 665 mbsf. These areas of high resistivity probably correspond to massive units within the core. Pillow lavas and brecciated units are represented by more variable resistivity profiles due to the presence of low resistivity interstitial material between more resistive pillows and breccia clasts.

The completed lithostratigraphical log for Hole 504B is shown in Figure 4.4. As can be seen from the reconstructed lithostratigraphy, the upper part of Hole 504B is dominated by pillow lavas with a few thin massive units. At depths greater than approximately 500 mbsf the proportion

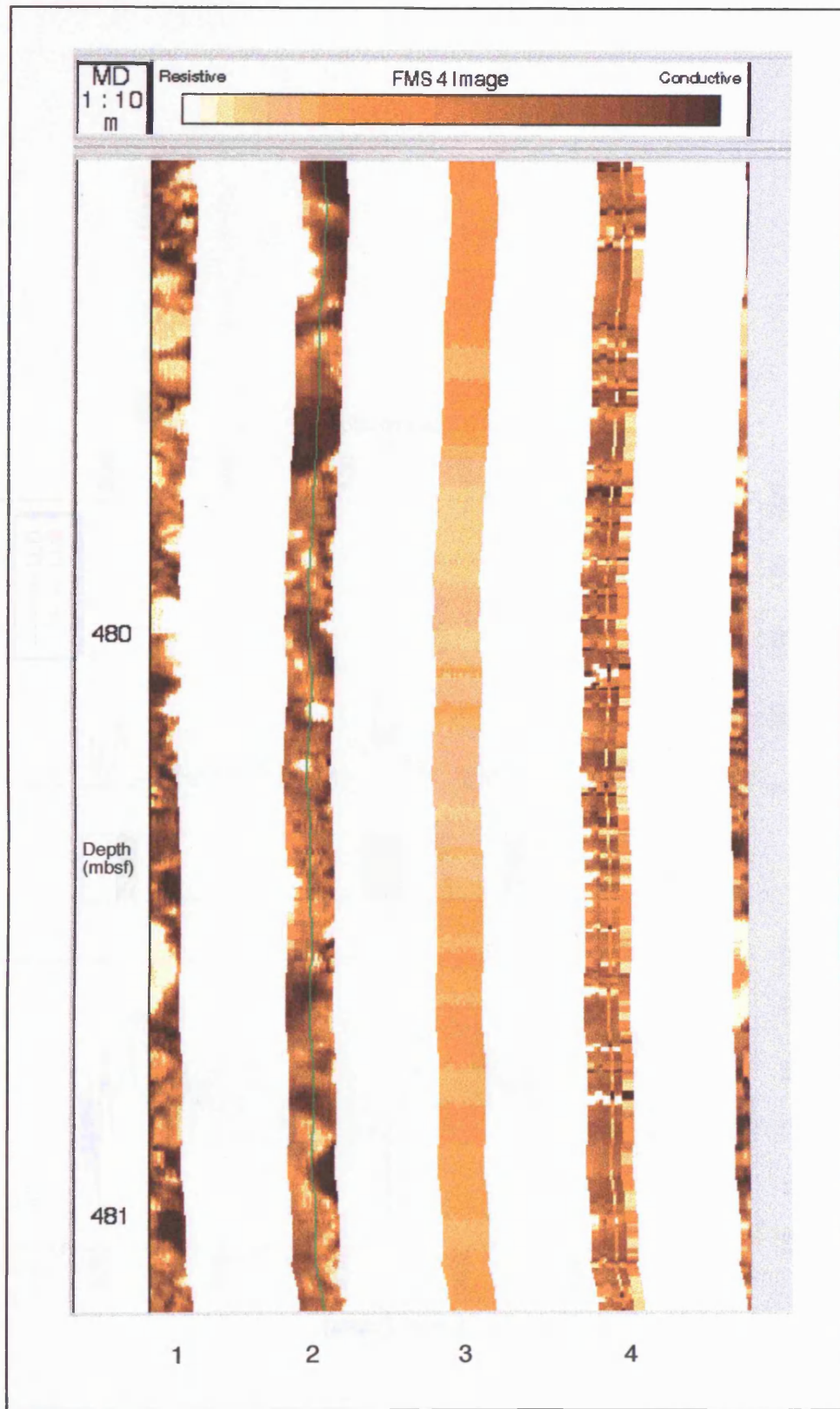


**Figure 4.2.** Example of FMS data from Hole 504B (Leg 140) showing the relatively poor quality of the data obtained. Pad 3 is not collecting any data and many of the buttons on Pad 4 are not operating.

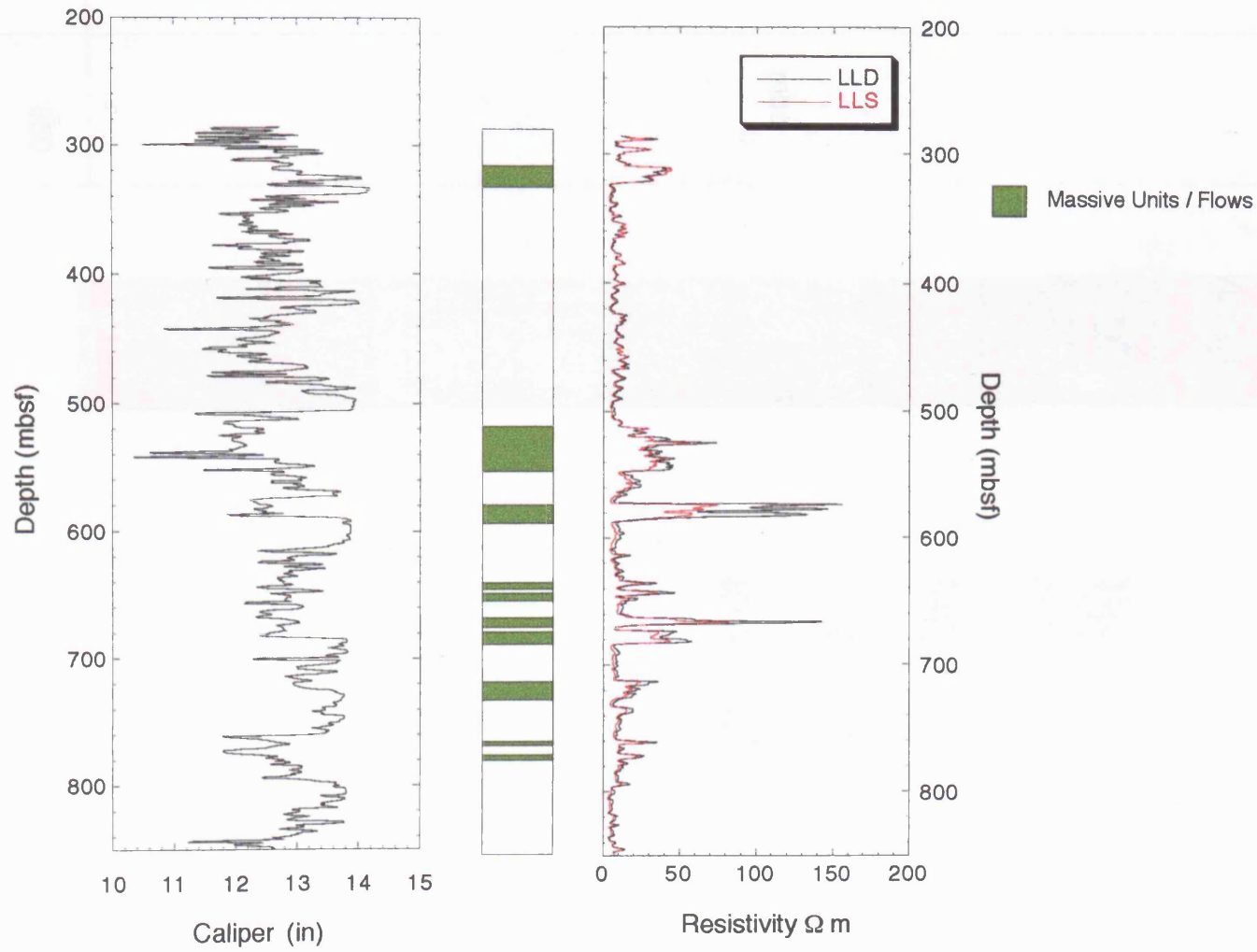


**Figure 4.3.** Caliper and resistivity downhole logs for Hole 504B. The inferred positions of massive units / flows within the core are shown. Data is from ODP Leg 111 (Becker, Sakai *et al.*, 1988).

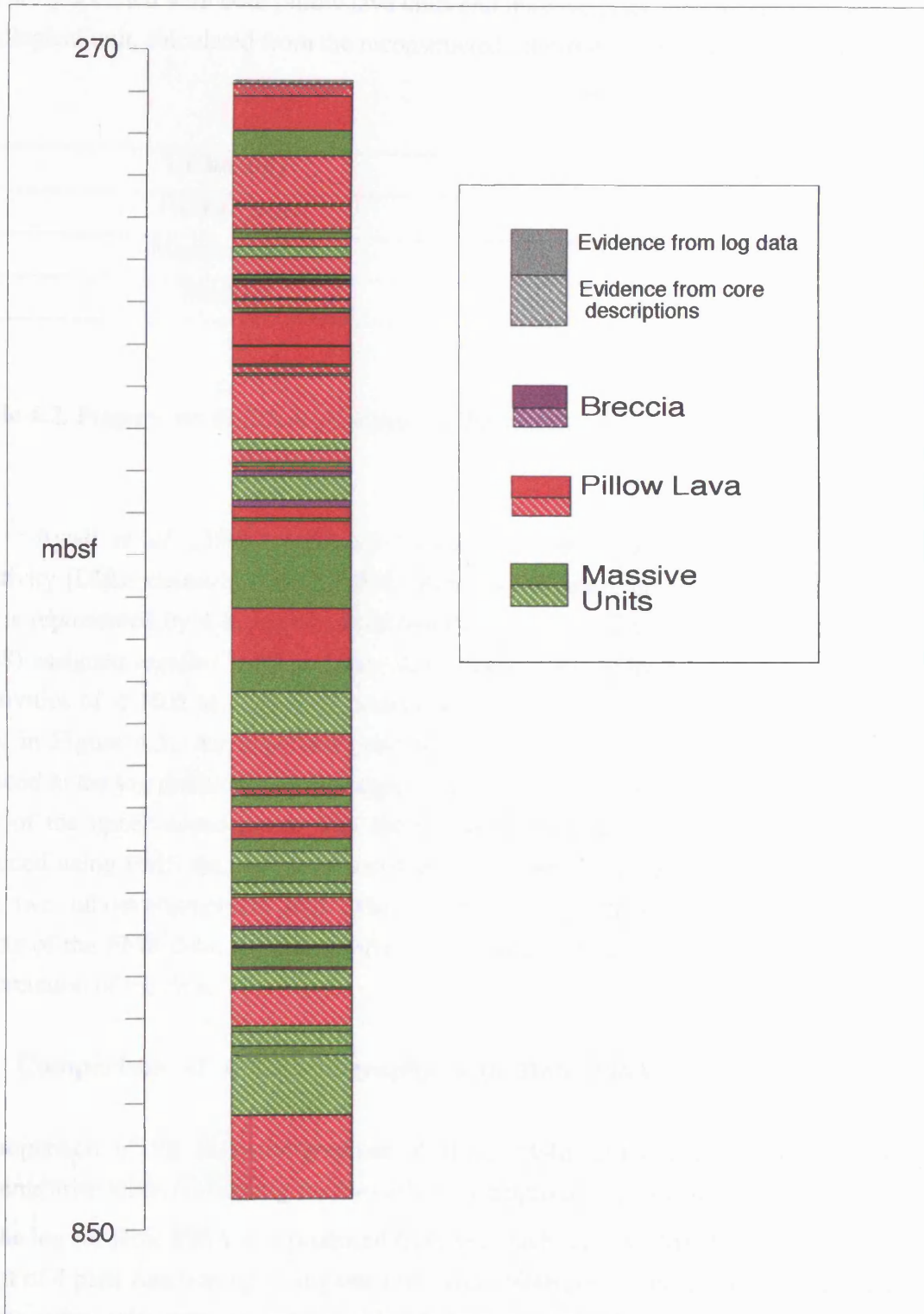


**Figure 4.4.** Lithostratigraphical log of Hole 504B using log data and shipboard core descriptions

of massive units in the core increases with pillow lavas becoming less common. Brecciated units are rare throughout the core only occurring in thin units at depths of 480, 495, 656 and 705 mbsf and are associated with both pillow lava units and massive units. The relative proportions of each lithological unit, calculated from the reconstructed lithostratigraphy are shown in Table 4.2.

Lithology	%
Pillow Lavas	55.2
Massive Units	42.1
Breccias	2.7

**Table 4.2.** Proportions of lithological units in the volcanic section of ODP Hole 504B

Ayadi *et al.* (1998) produced two lithostratigraphical logs derived from downhole resistivity (DLL) measurements and FMS data prior to image processing, at this stage the FMS data is represented by a series of microconductance curves. For the resistivity log, Ayadi *et al.* (1998) assigned massive units and thin sheet flows a resistivity  $> 10.0$  m and pillow lavas to resistivities of  $< 10.0$  m. These are compared with the lithostratigraphical log produced for this study in Figure 4.5. An important point to note is that dykes and intrusive bodies were not included in the log produced for this study as this work is primarily concerned with the extrusive units of the upper ocean crust. The most directly comparable lithostratigraphies are the two produced using FMS data and it is possible to correlate a number of lithological units between these two lithostratigraphical logs. The two lithostratigraphies were produced from different aspects of the FMS data, the main differences between them may be largely due to individual interpretation of the data.

#### 4.4.1 Comparison of lithostratigraphy with Hole 896A

A comparison of the lithostratigraphies of Holes 504B and 896A is shown in Figure 4.6. Problems arise when comparing the two lithostratigraphical logs because of two main points:

- The log for Hole 896A was produced from very high quality FMS data, with usually at least 3 out of 4 pads functioning at any one time. Hole 504B, in contrast, has very poor quality FMS data, often with only one pad working to its full potential. In order to fully reconstruct the lithostratigraphy of the volcanic section of Hole 504B, it was therefore necessary to use the visual core descriptions and resistivity logs to supplement the FMS data. This introduces a

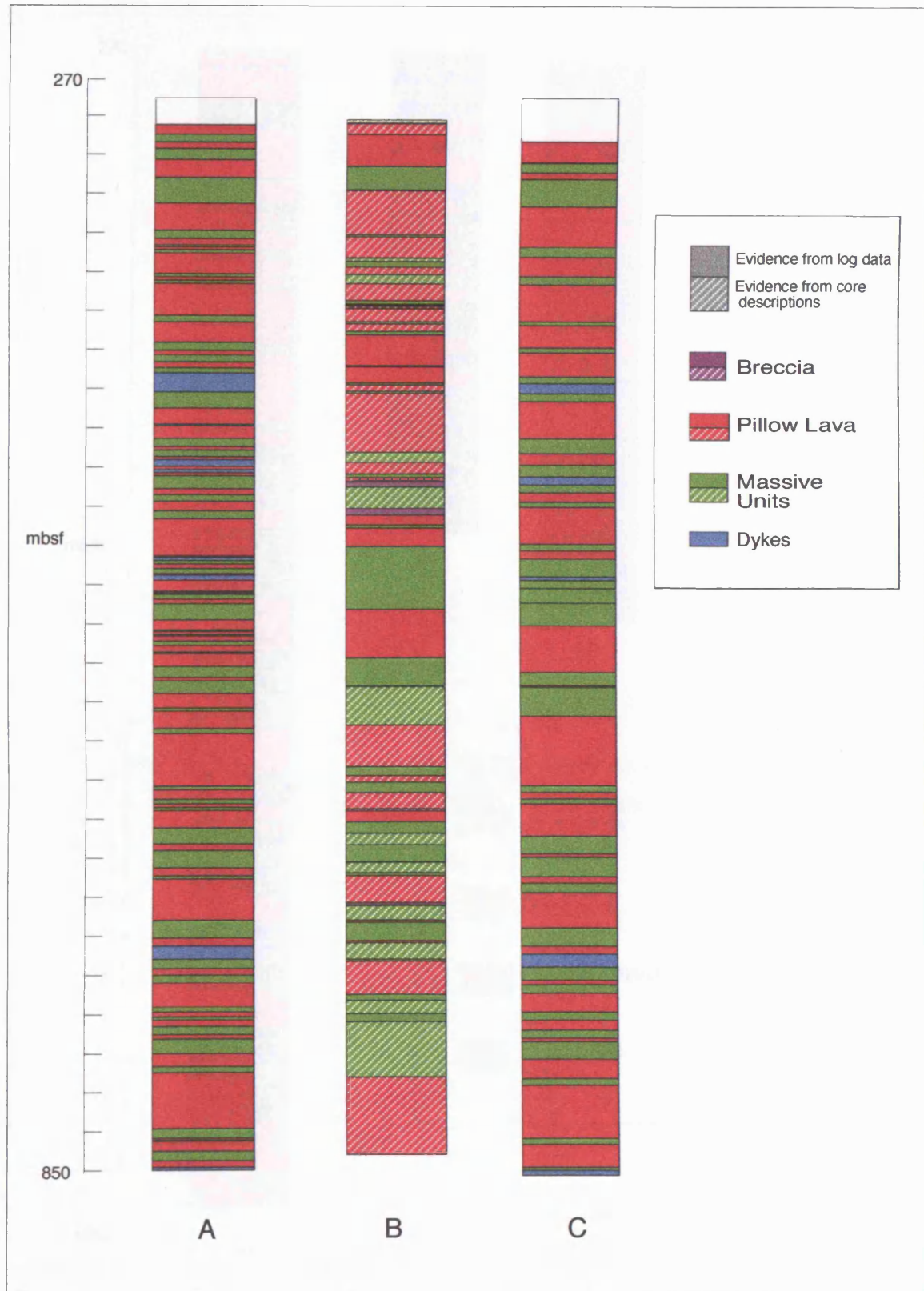


**Figure 4.5.** Comparison of lithostratigraphical logs produced for this study and by Ayadi *et al.* (1998). (A) Log produced by Ayadi *et al.* (1998) from analysis of DLL data. (B) Log produced by this study incorporating FMS image data and shipboard core descriptions. (C) Log produced by Ayadi *et al.* (1998) from analysis of FMS microconductance curves.

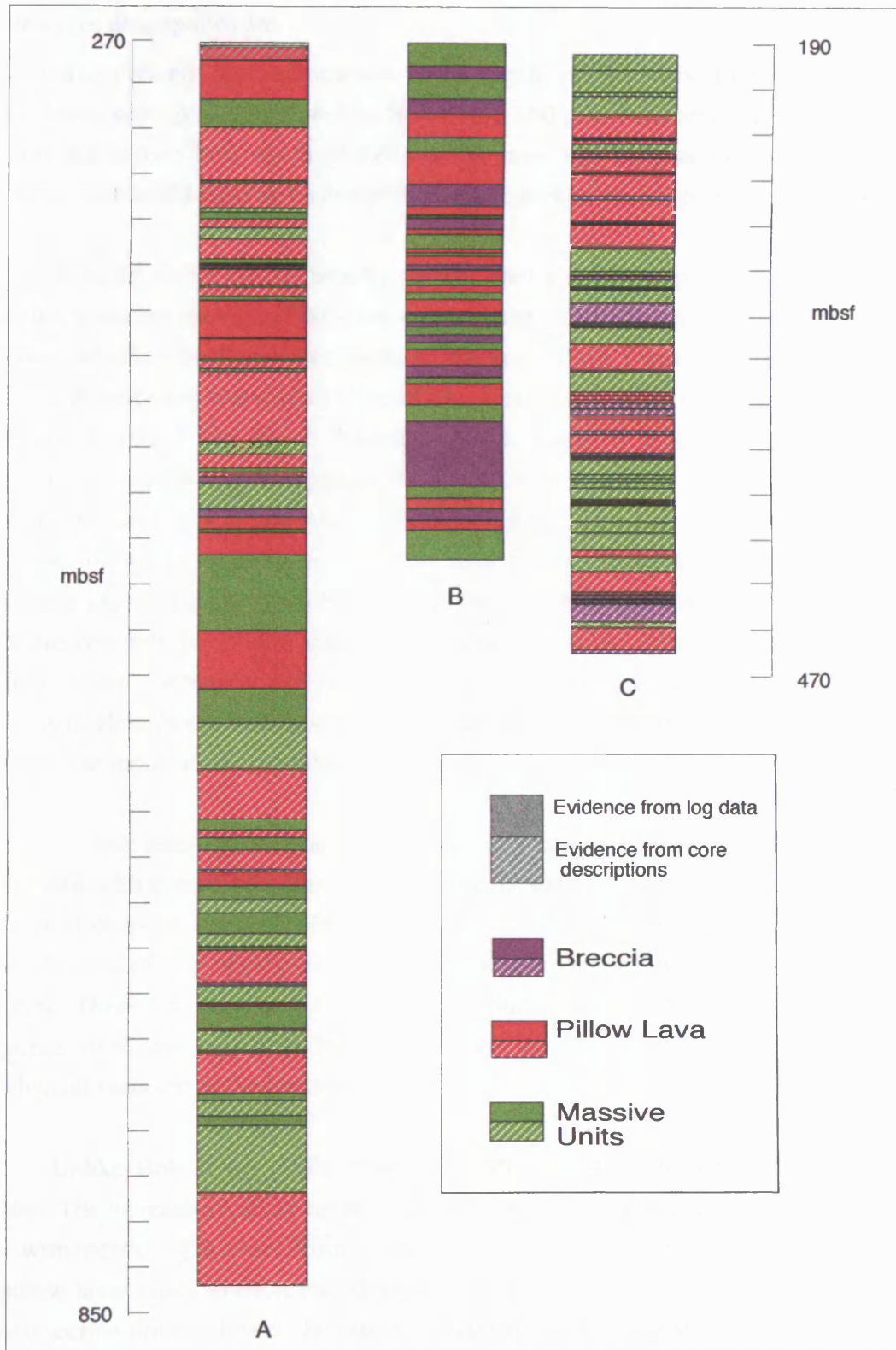


**Figure 4.6.** Comparison of lithostratigraphical logs from ODP Holes 504B and 896A: (A) Log of Hole 504B, (B) Log of Hole 896A using FMS data and (C) Log of Hole 896A using visual core descriptions.

measure of uncertainty into any interpretation as it is not known how reliable and consistent the core descriptions are.

- Another problem with comparison is the depths of the holes. In Hole 504B the complete volcanic section is represented. In Hole 896A, 290 m of basement material was recovered and it is not known how much further into the crust this material extends. Therefore the Hole 896A core could represent a complete volcanic section or only part of the complete Layer 2.

Both boreholes contain broadly similar lithological units, pillow lavas, massive units and breccias, however, the Hole 504B core was not examined by the author, therefore, it is difficult to ascertain whether the units have identical features in both cores. The brecciated units in Hole 896A were described and studied in detail, this is not the case for the Hole 504B brecciated units therefore it is very difficult to determine which types of breccia are present. In terms of relationships with other lithological units, the brecciated units in the Hole 504B core are more closely associated with pillow lavas than massive units. This may suggest that these are volcanic breccias, formed by granulation of pillow lava fronts, rather than sedimentary breccias. The absence of significant amounts of sedimentary brecciated material in Hole 504B would imply that there are very few periods of quiescence represented in the core, therefore, there were limited periods where substantial brecciation of previous lava flows could occur. However, as the breccias in Hole 504B were not studied by the author, it is very difficult to establish with any certainty the mode of origin of these brecciated units.

In Hole 896A there appears to be a much greater variation of lithology with depth than Hole 504B with thinner lithological units. There appears to be very little systematic variation with depth in Hole 896A whereas in Hole 504B the core can be divided into two distinct sections, with pillow lavas at the top of the core and an increasing amount of massive units towards the base of the core. However, we are not comparing identical sections, the lower parts of the volcanic sequence were not drilled in Hole 896A therefore it is difficult to establish the complete lithological variation in the upper crustal section.

Unlike Hole 896A, Hole 504B represents samples obtained from a complete volcanic section. The increase in pillow lavas towards the top of the hole may reflect a change in eruption type with increasing distance from the ridge axis. As discussed in § 2.3.4, the ratio of sheet flows to pillow lavas tends to decrease off-axis (Francheteau and Ballard, 1983), hence, a theoretical crustal section drilled close to the axis would be expected to consist predominantly of sheet flows. These would be overlain by increasing thicknesses of pillow lavas as the crust is moved away from the axis by sea-floor spreading. The complete volcanic section of Hole 504B probably includes both axis and off-axis lava flows, with the lower section (~ 500 mbsf to base) being erupted near to or at the axis and the upper section (0 to ~ 500 mbsf), with more pillow lavas,

representing flows erupted further away from the axis. The Hole 896A core contains considerably more breccias and pillow lavas than may be expected from eruption entirely at the ridge axis. It is possible that the lavas recovered from Hole 896A were predominantly erupted off-axis and that the lava sections erupted at the ridge axis have not been fully penetrated at this site

There appears to be very limited correlation between lithological units in the two cores, Alt *et al.* (1996) suggest that this may be due to the lateral extent of individual lava flows. Flows erupted at the ridge axis tend to be channelled along the strike of the ridge with limited flow perpendicular to the axis (Ballard *et al.*, 1979), hence, the two crustal sections, represented in Holes 504B and 896A, were probably produced by separate eruptive events. The neovolcanic zone at intermediate-spreading ridges is usually approximately 2 km wide (Brewer *et al.*, 1996) hence the drilled section of Hole 896A would be near to the margin of this zone when the lower parts of the Hole 504B section were formed. It is therefore very difficult to compare even the upper sections of the two cores, as they are separated by a time gap which may be sufficient for conditions, in a sub-axial magma chamber beneath the Costa Rica Rift, to change significantly.

#### 4.5. Mineralogy

The Leg 69 and 70 Shipboard Scientific Party divided the recovered basalts from Hole 504B into five groups on the basis of their phenocryst assemblages present in thin-section (Cann, Langseth *et al.*, 1983). These five groups are summarised below:

**Type 1 - Moderately plagioclase - olivine - Cr spinel phyric :-** In contrast to the other four groups, this basalt group contains no clinopyroxene (augite). Plagioclase occurs as glomerocrysts, individual phenocrysts and in the groundmass constituting 5 to 10% of the rock. Plagioclase phenocrysts are generally euhedral to subhedral with an average size of 0.4 to 0.8 mm, some examples showing simple zoning. The glomerocrysts have an average size of 0.6 to 1.2 mm and are composed of subhedral to euhedral plagioclase crystals with some zoned examples. Olivine constitutes 2 to 3 % of the rock and occurs as euhedral to subhedral grains. Both larger (1.2 - 1.5 mm) and smaller (0.1 - 1.4 mm) olivine crystals occur. Olivine has been extensively pseudomorphed by clays. Clinopyroxene occurs only in the groundmass with no phenocrysts. Cr -spinel phenocrysts comprise less than 5 % of the rock. They are generally < 3 mm in size and often poikilolitically enclosed in olivine or plagioclase phenocrysts.

**Type 2 - Moderately plagioclase - augite phyric :-** This group is dominated by ophitic and sub-ophitic textures with a glassy to intergranular groundmass. Plagioclase phenocrysts are generally euhedral with blocky or lath morphologies. The phenocrysts are sometimes zoned. Examples of Carlsbad, albite and pericline twinning have been observed. Clinopyroxene (augite)

occurs as subhedral to anhedral grains with rare twins. Clinopyroxene usually occurs as aggregates of two or more crystals.

**Type 3 - Moderately plagioclase - olivine - clinopyroxene phyric :-** This group has a higher phenocryst content than the other groups (15 - 20%). Plagioclase occurs as both glomerocrysts and phenocrysts and comprises 20 - 25% of the rock. The plagioclase phenocrysts are 0.2 to 3.5 mm in size, most are euhedral. The glomerocrysts contain 5 to 30 phenocrysts of variable size which are chaotically arranged. Plagioclase phenocrysts show complex twinning and are occasionally oscillatory zoned. Olivine comprises 3 to 8% of the rock and usually occurs as euhedral to subhedral phenocrysts. These range in size from 0.1 to 1.6 mm with an average size of 0.3 to 0.5 mm. Olivine is extensively replaced by coloured clays both as phenocrysts and in the groundmass. Clinopyroxene occurs as large individual phenocrysts and as aggregates. The phenocrysts are euhedral or anhedral with a large size range (0.05 to 4.2 mm). Larger phenocrysts sometimes show simple twinning.

**Type 4 - Moderately plagioclase - olivine - clinopyroxene phyric :-** Plagioclase occurs as phenocrysts and glomerocrysts of variable size (average 1.5 to 2.0 mm). These are often zoned. Olivine occurs as euhedral to subhedral phenocrysts, ranging from 1.0 to 2.5 mm in size, and glomerocrysts. Olivine in the groundmass is completely replaced by blue and green smectite, olivine phenocrysts are only partially replaced. Clinopyroxene occurs as rare phenocrysts, ranging in size from 1.0 to 4.0 mm, which are anhedral and twinned.

**Type 5 - Plagioclase - olivine - augite phyric :-** Plagioclase comprises 10 to 15% of the rock and occurs as phenocrysts and glomerocrysts. Phenocrysts are usually euhedral and zoned. Rare glomerocrysts of plagioclase occur, comprising 5 to 10 subhedral / euhedral crystals 0.2 to 0.4 mm in size. Olivine occurs as euhedral phenocrysts, on average 0.2 to 0.3 mm, usually completely replaced by clays and Fe-oxyhydroxide minerals. Clinopyroxene occurs both as single crystals and as aggregates. Individual grains are euhedral to subhedral and range in size from 0.05 to 0.3 mm. The aggregates consist of a mass of anhedral augite grains.

#### 4.6. Geochemistry

Both whole rock geochemistry (Cann, Langseth *et al.*, 1983) and electron microprobe glass data (Natland *et al.*, 1983) are available for the Hole 504B basalts, both sets of data have been used in this study. For the whole rock chemistry, any geochemical variations observed in the data are potentially affected by alteration and phenocryst accumulation effects.

#### 4.6.1. Basalt types

Autio and Rhodes (1983) and Kempton *et al.* (1985) divide the basalts present in hole 504B into three main chemical groups designated D, M, and T (Table 4.3). Group D basalts are highly depleted in magmophile (incompatible) elements relative to average Mid-Ocean Ridge Basalt (MORB) and are saturated in olivine and plagioclase and are close to clinopyroxene saturation (Kempton *et al.*, 1985). These constitute the majority of 504B basalts.

Group M basalts are rare throughout the core. They have low abundances of MgO, FeO and CaO and appear to have undergone substantial fractionation (Kempton *et al.*, 1985). Group T basalts also have low abundances of moderately incompatible elements but are enriched in La, Nb and other highly incompatible elements. The high MgO content suggests that these are not primitive basalts. Group T basalts are saturated in olivine and plagioclase and possibly clinopyroxene (Kempton *et al.*, 1985).

Basalt Type	MgO (wt. %)	TiO <sub>2</sub> (wt. %)	Ni (ppm)	Zr (ppm)	Nb (ppm)
D	7.3 - 9.0	0.75 - 1.2	75 - 165	34 - 60	0.5 - 1.2
M	7.9 - 8.5	1.3 - 1.4	94 - 99	103 - 104	2 - 3
T	8.6 - 8.8	1.08 - 1.1	105 - 108	66.6 - 68.2	3.8 - 4.2

**Table 4.3.** Chemical composition of Hole 504B basalts, D, M and T. After Autio and Rhodes (1983) and Kempton *et al.* (1985).

The division of Hole 504B basalts as described by Autio and Rhodes (1983) and Kempton *et al.* (1985) can be seen most markedly on plots of Zr versus Nb (Fig 4.7) and Zr versus depth, (Fig 4.8). The M and T basalts lie in discrete horizons at depths of approximately 400 mbsf and 700 mbsf. Both M and T basalts have a higher Zr content than the D type basalts.

#### 4.6.2. Major element variations

Variations with depth were plotted for Fe<sub>2</sub>O<sub>3</sub>, MgO, Al<sub>2</sub>O<sub>3</sub>, SiO<sub>2</sub> and CaO. For all the plots in this section the Type M and T basalts have been plotted together, as this study is primarily concerned with the Type D basalts, which are most geochemically similar to the basalts recovered from Hole 896A (§ 4.6.5.3.).

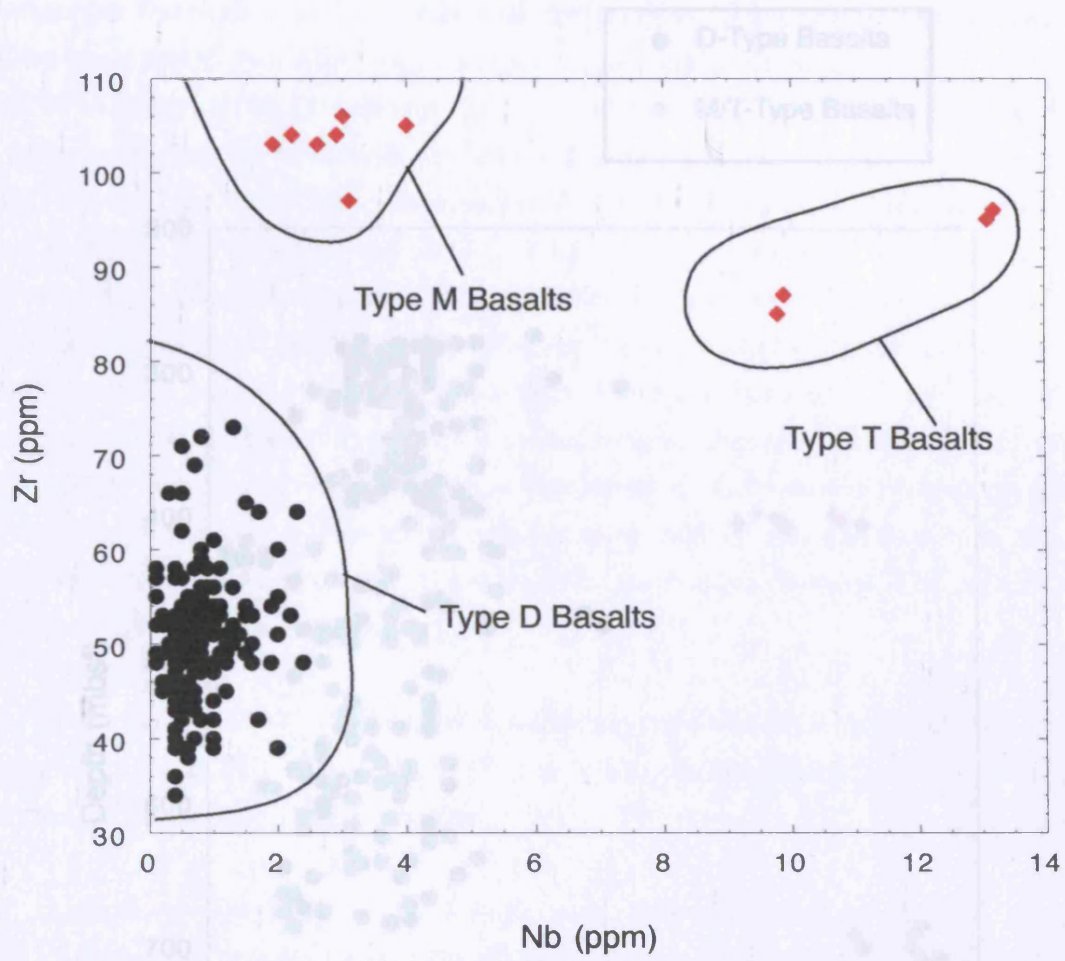


**Figure 4.7.** Zr vs Nb for Hole 504B basalts. The plot shows the classification of basalts discussed by Aulio and Rhodes (1983) and Kempton *et al.* (1985)

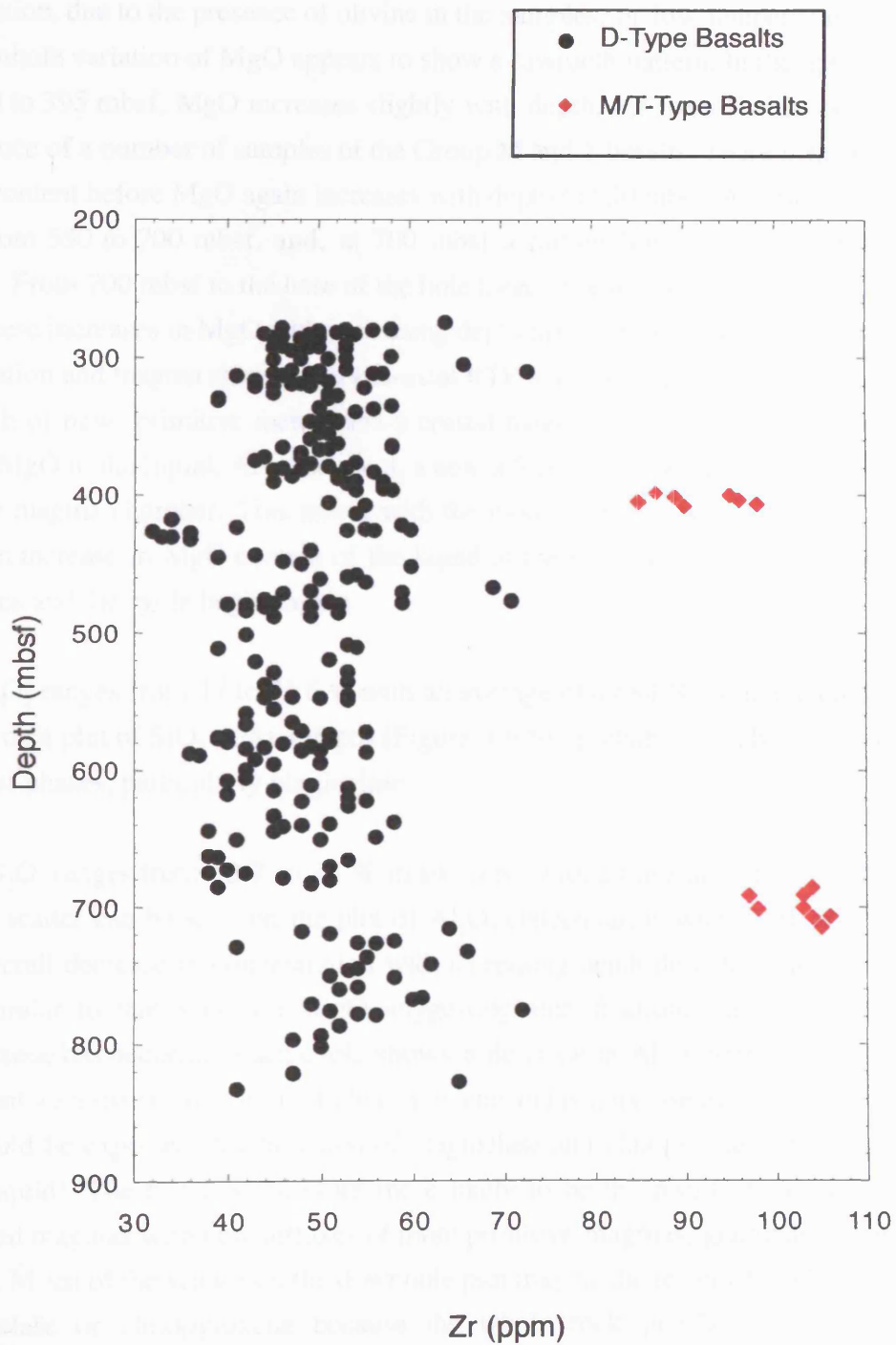


**Figure 4.8.** Variation of Zr with depth for ODP Hole 504B. Classification of basalt types is after Autio and Rhodes (1983).

MgO ranges from 6.39 to 10.94 % with an average of 8.33 %. On a plot of variation with depth, there is a large degree of scatter (Fig 4.9.a.). This may be the result of phenocryst accumulation, due to the presence of olivine in the samples, or low temperature alteration effects. The downhole variation of MgO appears to show a sawtooth pattern. In the upper part of the core, from 280 to 395 mbsf, MgO increases slightly with depth, the base of this section is marked by the presence of a number of samples of the Group M and T basalts. There is then a sharp decrease in MgO content before MgO again increases with depth to 550 mbsf. A similar pattern with depth occurs from 550 to 700 mbsf, and, at 700 mbsf a further horizon of M and T basalts can be observed. From 700 mbsf to the base of the hole there appears to be no systematic variation with depth. These increases in MgO with increasing depth may represent separate periods of fractional crystallisation and magma mixing in a sub-axial RTF magma chamber (§ 2.5.4.3 and § 3.8.4.3). As a batch of new, primitive melt enters a crustal magma chamber, fractionation of olivine will decrease MgO in the liquid. At some point, a new influx of melt with more primitive compositions enters the magma chamber. This mixes with the more evolved material already in the chamber, causing an increase in MgO content of the liquid in the magma chamber. This new mixed liquid fractionates and the cycle begins again.

SiO<sub>2</sub> ranges from 47 to 51.6 % with an average of 49.84 %. Again, there is a large degree of scatter on a plot of SiO<sub>2</sub> versus depth (Figure 4.9.b), probably largely due to accumulation of phenocryst phases, particularly plagioclase.

Al<sub>2</sub>O<sub>3</sub> ranges from 12.7 to 18 % in the core, with an average of 15.54 %. Again a large degree of scatter can be seen on the plot of Al<sub>2</sub>O<sub>3</sub> concentration with depth (Fig 4.10.a.). Al<sub>2</sub>O<sub>3</sub> has an overall decrease in concentration with increasing depth downhole and shows a sawtooth pattern similar to that seen for MgO suggesting that fractionation of plagioclase and / or clinopyroxene has occurred. Each cycle shows a decrease in Al<sub>2</sub>O<sub>3</sub> with increasing depth, this is inconsistent with the fractionation of clinopyroxene and plagioclase as an increase with increasing depth would be expected (fractionation of plagioclase and clinopyroxene decreases Al<sub>2</sub>O<sub>3</sub> in the residual liquid). The trend is therefore more likely to be the result of magma mixing of more fractionated magmas with new influxes of more primitive magmas, gradually decreasing Al<sub>2</sub>O<sub>3</sub> in the liquid. Much of the scatter on the downhole plot may be the result of phenocryst accumulation of plagioclase or clinopyroxene because the whole rock geochemistry does not eliminate phenocryst effects. No distinction can be made between the Al<sub>2</sub>O<sub>3</sub> concentrations of the D and M / T basalts. A plot of Al<sub>2</sub>O<sub>3</sub> versus MgO (Fig 4.11.a) shows no discernible relationship between the two major oxides, this may again be the result of phenocryst accumulation, particularly of plagioclase and olivine, which contain Al<sub>2</sub>O<sub>3</sub> and MgO respectively. This is consistent with the mineralogy (§ 4.5) which suggests that both these minerals are fractionating phases. The outlying points with lower Al<sub>2</sub>O<sub>3</sub> and MgO contents may be samples which are relatively phenocryst-free or represent samples with low analytical precision.

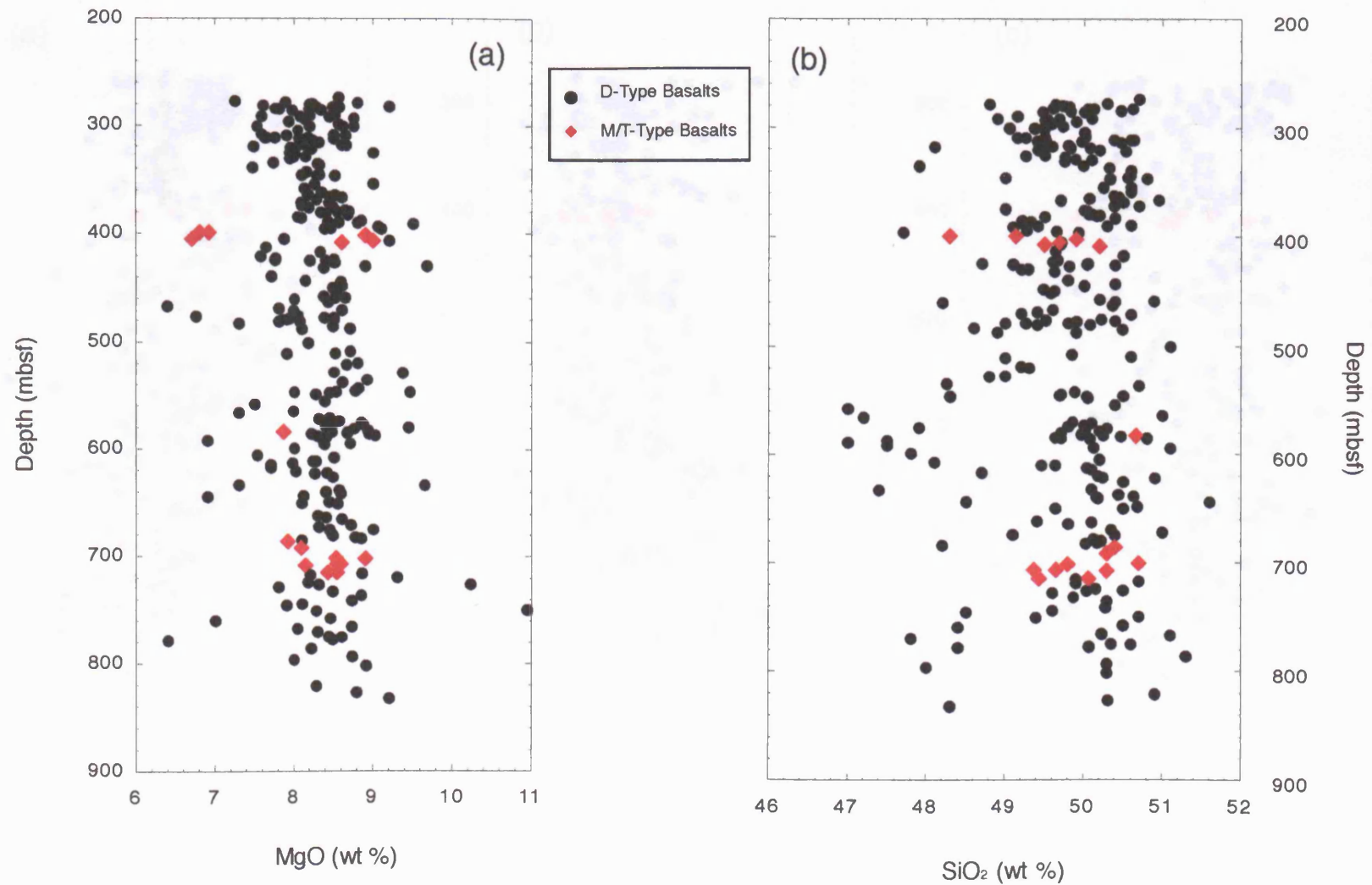


**Figure 4.9.** Major elements versus depth downhole for Hole 504B : (a) MgO versus depth, (b) SiO<sub>2</sub> versus depth. Division of basalt types is after Autio and Rhodes (1983) and Kempton *et al.* (1985).

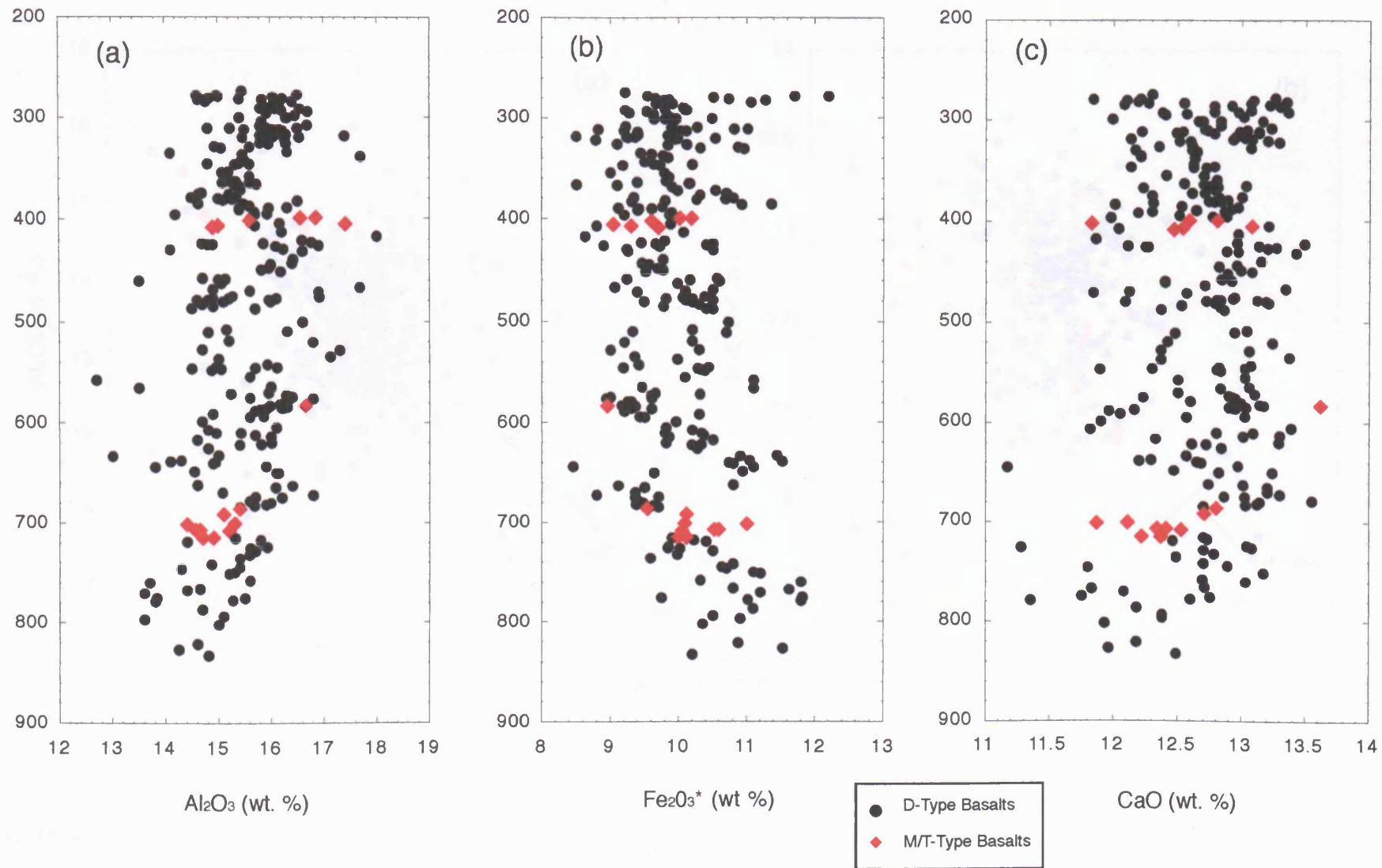


**Figure 4.10.** Major oxides versus depth downhole for Hole 504B: (a) Al<sub>2</sub>O<sub>3</sub> versus depth, (b) Fe<sub>2</sub>O<sub>3</sub> versus depth, (c) CaO versus depth. Classification of basalts is after Autoio and Rhodes (1983).

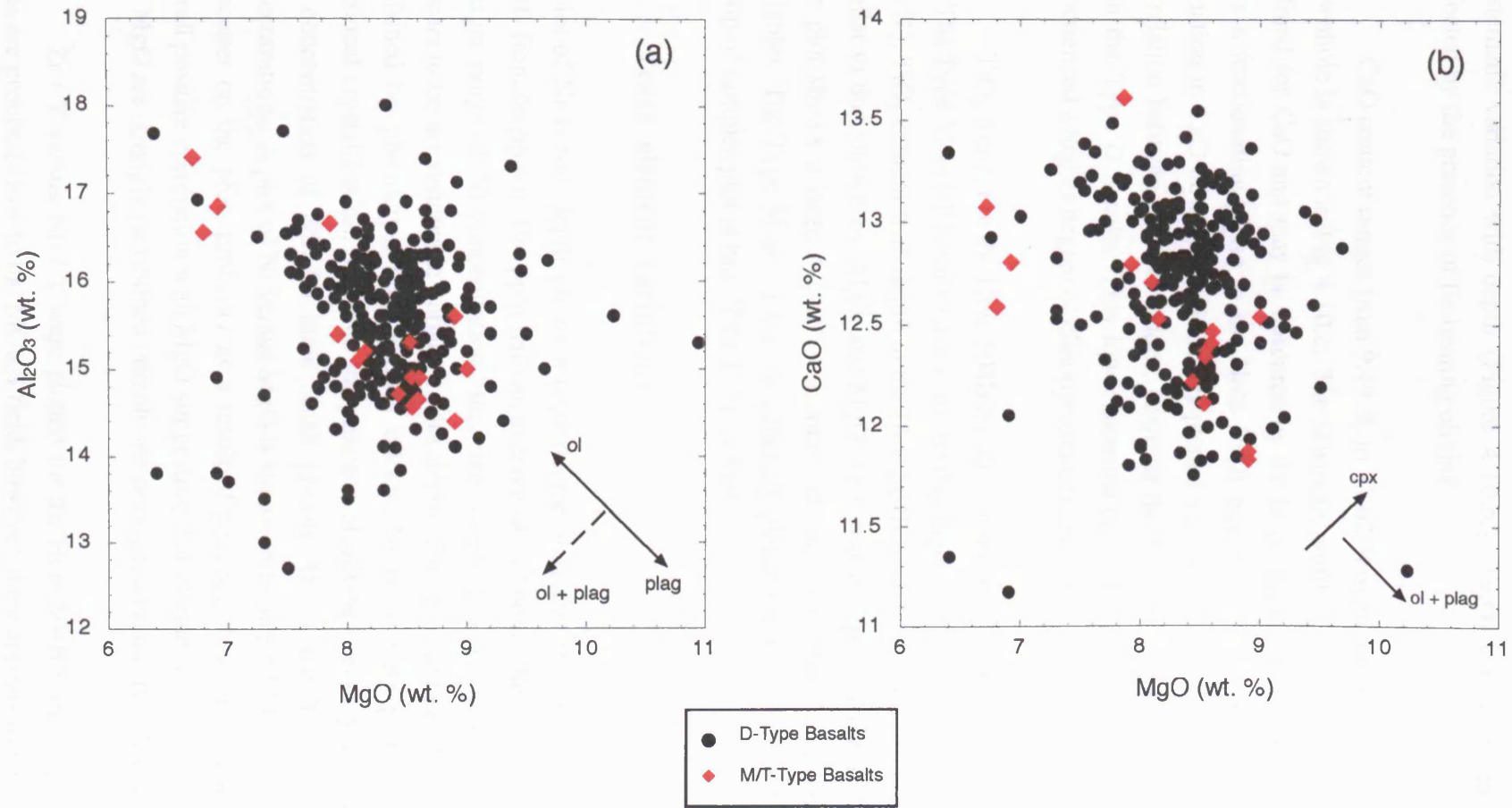


**Figure 4.11.** Major oxides versus MgO for Hole 504B: (a) Al<sub>2</sub>O<sub>3</sub> versus MgO, (b) CaO versus MgO. Classification of basalts is after Autio and Rhodes (1983).

$\text{Fe}_2\text{O}_3$  content in the Hole 504B basalts ranges from 8.46 to 12.2 %, with an average of 9.99 %. The plot of  $\text{Fe}_2\text{O}_3$  variation with depth shows a large degree of scatter with no apparent systematic variation with depth (Figure 4.10.b.),  $\text{Fe}_2\text{O}_3$  content in the core samples will be affected by the presence of Fe-bearing olivine.

CaO content ranges from 9.49 % to 13.62 % with an average of 12.65 %. The variation downhole is shown in Fig 4.10.c. The sawtooth profile shown for  $\text{Al}_2\text{O}_3$  and MgO is less well-defined for CaO and may be obscured by the large degree of scatter on the plot. Clinopyroxene was a fractionating phase in the Hole 504B basalts (§ 4.5.) and may be contributing to the variation in CaO downhole. If CaO is plotted versus MgO (Fig 4.11.b.) there appears to be no correlation between the two oxides, however the Type M and T basalts have much lower CaO than the Type D basalts. This low concentration of CaO may suggest that these basalts have experienced a higher degree of clinopyroxene fractionation, reducing CaO in the residual liquid.

$\text{TiO}_2$  content in the Hole 504B basalts ranges from 0.7 to 1.41 %, with an average of 0.93 %. The Type M and T basalts have considerably higher  $\text{TiO}_2$  than the Type D basalts (average 1.4 wt. %).  $\text{TiO}_2$  content with depth in the Hole 504B basalts (Fig 4.12.a.) shows a sawtooth pattern similar to that shown by  $\text{Al}_2\text{O}_3$  and MgO.  $\text{TiO}_2$  was also plotted versus MgO (Figure 4.12.b.). The plot shows a large degree of scatter with no well-defined relationship between the two variables. The Type M and T basalts generally plot at similar values of MgO, however, a small group of samples plot at high  $\text{TiO}_2$  but low MgO.

#### 4.6.3. Trace element variations

A plot of Ni versus depth shows a large degree of scatter (Figure 4.13.a.). Ni ranges in Hole 504B from 66 ppm to 191 ppm with an average of 117 ppm. The upper 400 m of Hole 504B has a larger range of Ni concentrations than the lower sections of the borehole, however, there appears to be no systematic variation with depth. The large degree of scatter on the plot may be explained by phenocryst accumulation effects, Ni is strongly partitioned into olivine during fractional crystallisation, therefore the presence of olivine phenocrysts in a sample will increase the concentration of Ni. All three basalt groups, D, M and T, have similar ranges of Ni concentrations. A plot of Ni versus MgO is shown in Figure 4.13.b. Again there is a large degree of scatter on the plot, probably as a result of phenocryst accumulation effects. Ni shows an overall positive correlation with MgO suggesting that olivine fractionation has occurred. Both Ni and MgO are strongly partitioned into olivine during fractional crystallisation.

Zr / Y versus Nb / Y were plotted for the Hole 504B lavas (Figure 4.14). The Type D lavas are grouped close to the MORB field, however, there appears to be a much larger degree of scatter than for Hole 896A. Nb / Y has a larger range of values than Zr / Y. The Type M and T

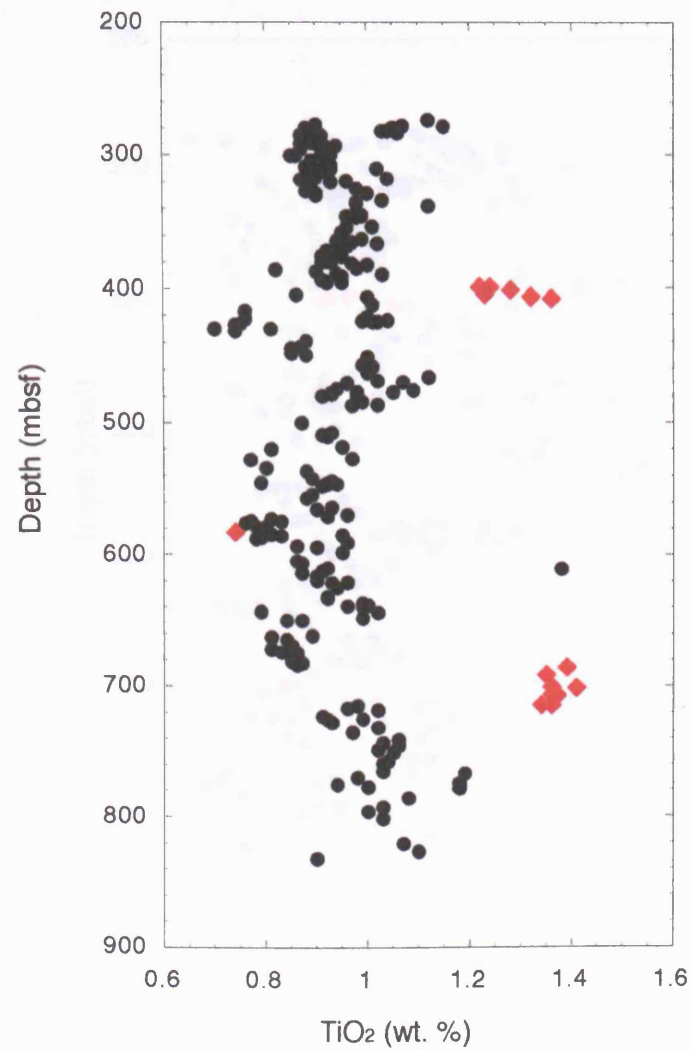


**Figure 4.12.a.** TiO<sub>2</sub> versus depth downhole for Hole 504B. Classification of basalts is after Autio and Rhodes (1983).

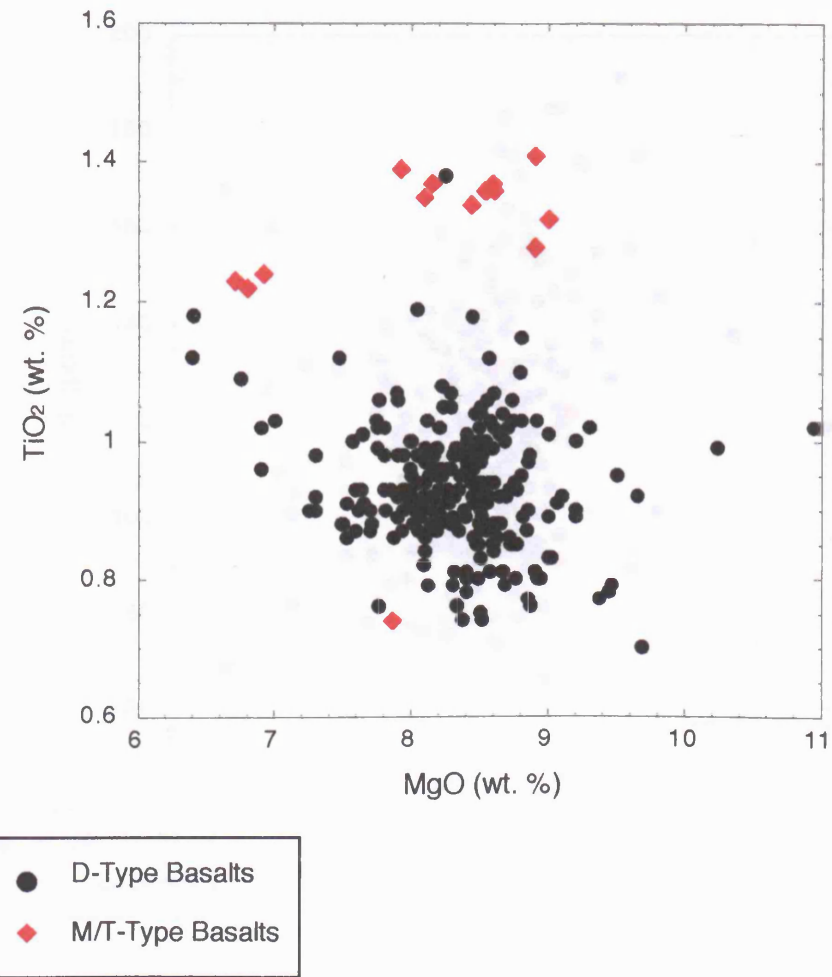


**Figure 4.12.b.** TiO<sub>2</sub> versus MgO for Hole 504B. Classification of basalts is after Autio and Rhodes (1983).

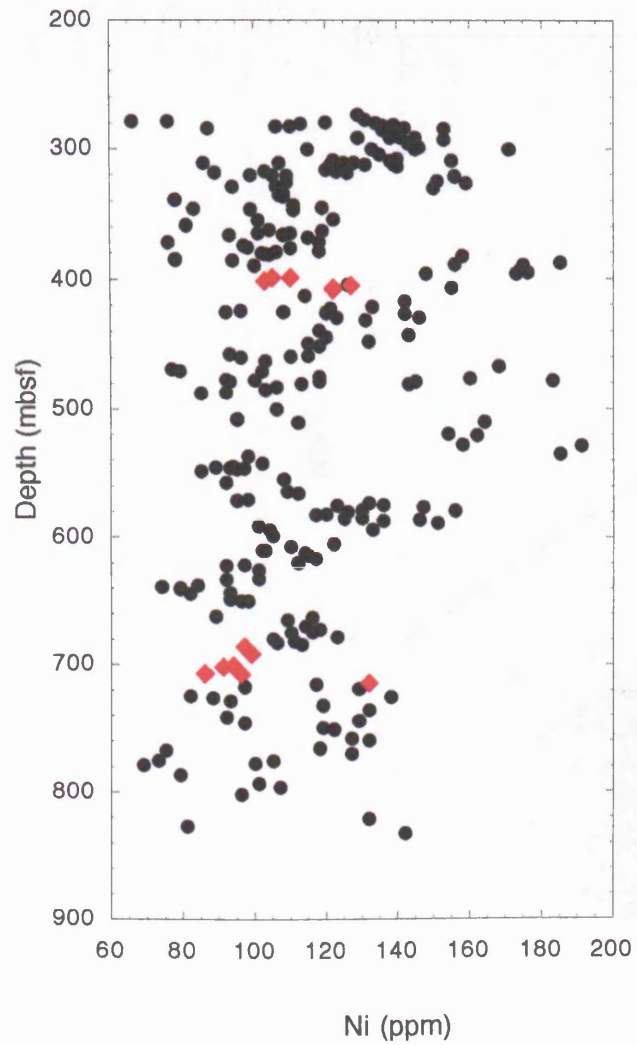


**Figure 4.13.a.** Ni versus depth downhole for Hole 504B. Classification of basalts is after Autio and Rhodes (1983).

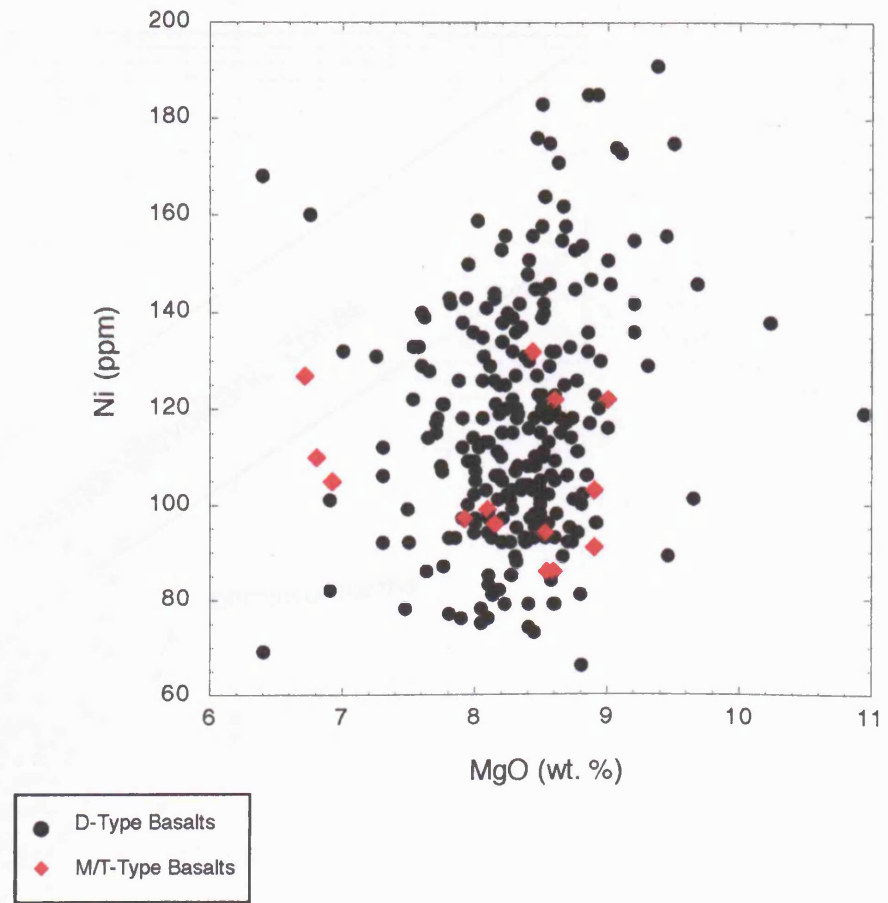


**Figure 4.13.b.** Ni versus MgO for Hole 504B. Classification of basalts is after Autio and Rhodes (1983).

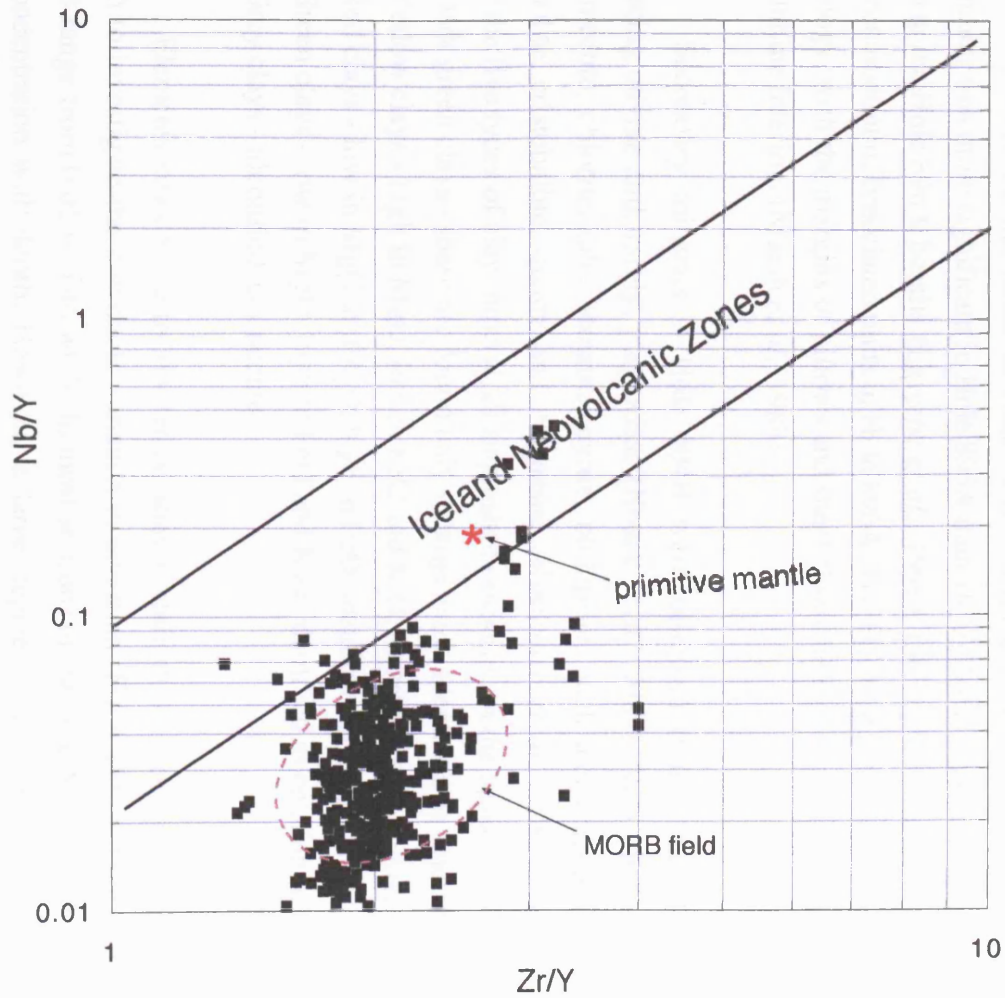


**Figure 4.14.** Nb/Y versus Zr/Y For Hole 504B samples. The field of “normal” MORB and the position of primitive mantle are indicated, (after Fitton *et al.* (1997)). Data is from Cann, Langseth *et al.* (1983).

lavas have both higher Nb / Y and Zr / Y than the Type D lavas with a number of samples plotting within the field of the Iceland neovolcanic zone. This may suggest that some of the Hole 504B lavas have a different, more enriched, source than the majority of the basalts in the core.

#### 4.6.4. Alteration

In general terms the alteration of the upper portion of Hole 504B can be regarded as very similar to that observed in Hole 896A, however Hole 504B contains considerably less abundant and smaller hydrothermal veins (Dilek *et al.*, 1996). The red / yellow oxidation haloes observed in the Hole 896A core do not occur in Hole 504B (Laverne *et al.*, 1996), suggesting that oxidative alteration was more significant in Hole 896A than Hole 504B. This implies a higher water / rock ratio in the Hole 896A basalts (Laverne *et al.*, 1996), this higher permeability may be due to the greater amount of brecciated units in Hole 896A. The extent of alteration varies within a particular lithology, with the margins of pillows and sheet flows being considerably more altered than their crystalline interiors (Marsh *et al.*, 1989).

Secondary minerals in Hole 504B were observed filling fractures and vesicles and replacing olivine and, rarely, plagioclase (Noack *et al.*, 1983). Vein minerals include saponite, Fe-smectite, chlorite, talc, hematite, pyrite, phillipsite, analcime, aragonite, calcite, anhydrite, actinolite, cristoballite, quartz and magnesite (Kurnosov *et al.*, 1983). Noack *et al.*, (1983) describe five types of clay mineral, distinguished primarily on the basis of colour:

- (1) Dark green clays - these are found only in large veins, identified as smectite,
- (2) Yellow clays - high in MgO, low in FeO and K<sub>2</sub>O, identified as saponite.
- (3) Red clays - low in MgO and K<sub>2</sub>O, high in FeO, identified as iddingsite,
- (4) Green clays - low in MgO, high in FeO and K<sub>2</sub>O, identified as celadonite,
- (5) Grey clays - identified as smectite.

Elements susceptible to low-temperature mobilisation, such as K<sub>2</sub>O, were plotted versus depth to investigate the downhole variation in alteration (Fig 4.15). K<sub>2</sub>O concentrations in Hole 504B range from 0.01 to 0.46 wt %. In most sections of the core K<sub>2</sub>O shows an overall decrease in concentration with depth. However, a large degree of scattering of sample points can be observed. The range of values of K<sub>2</sub>O is considerably higher between 250 and 400 mbsf, therefore it can probably be assumed that halmyrolysis was more pronounced in the uppermost sections of the lava stack. Hubberten *et al.* (1983) use previous investigations of oceanic basalts to define the limits for fresh basalt, and suggest that a K<sub>2</sub>O content of < 0.25 % is the limit for unaltered basalts. If this is applied to the Hole 504B data, "altered" basalts are restricted to the upper 500 m of the core, with more "fresh" basalts in the lower volcanic section. Interestingly, this change in alteration at 500 mbsf corresponds with the depth at which the proportion of

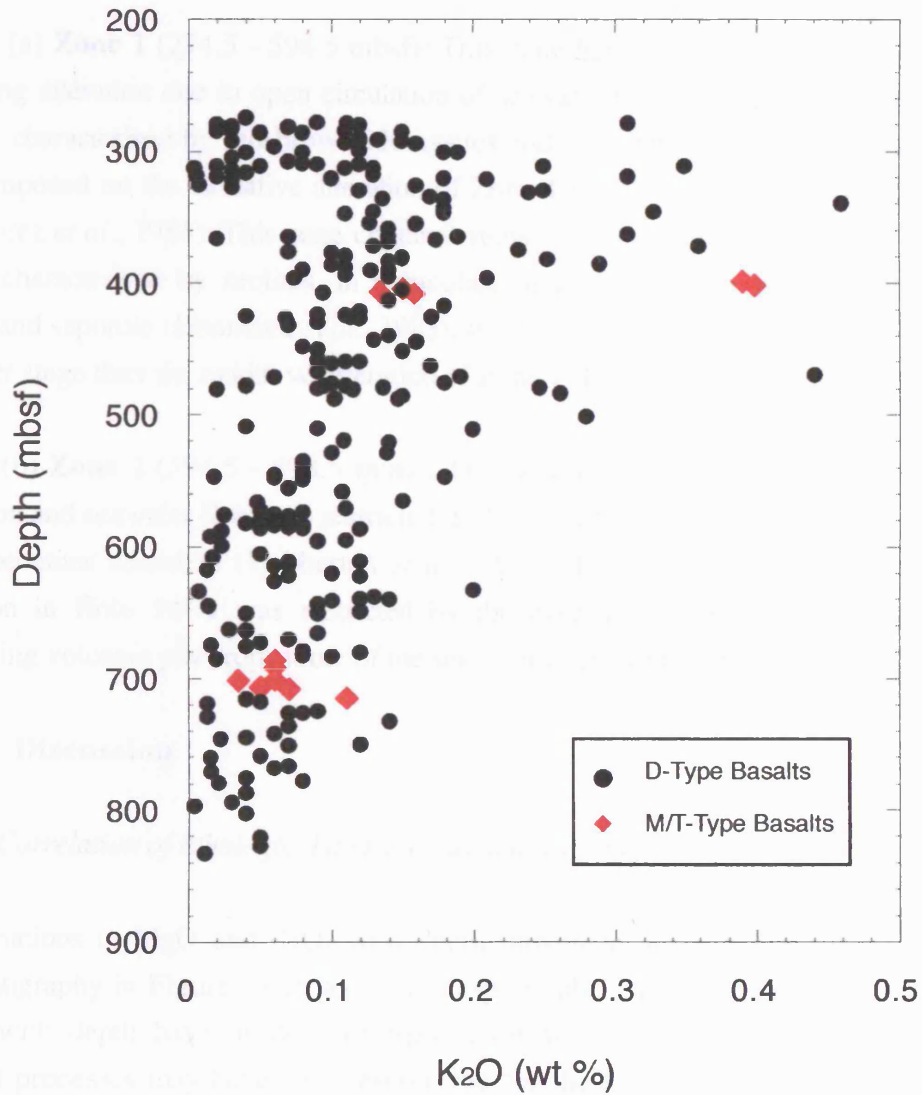


**Figure 4.15.** Variation of K<sub>2</sub>O with depth for ODP Hole 504B. Classification of basalts is after Autoio and Rhodes (1983).

massive units starts to increase (§ 4.4.1), and has been interpreted as representing the transition between off-axis and axis lava flows.

Alt, Kinoshita *et al.* (1996) divide the volcanic section of Hole 504B into two alteration zones:

(a) **Zone 1** (274.5 - 594.5 mbsf): This zone has experienced low temperature (< 100°C) oxidising alteration due to open circulation of seawater through relatively permeable rocks. The zone is characterised by red-brown iddingsites and Fe-oxyhydroxides (Hubberten *et al.*, 1983). Superimposed on the oxidative alteration of Zone 1 is a “zeolite zone” from 528.5 to 563 mbsf (Honnorez *et al.*, 1983). This zone contains veins with minerals not found elsewhere in the core and is characterised by zeolites, in particular, analcime, natrolite and thomsonite, with minor calcite and saponite (Honnorez *et al.*, 1983). It is believed that this zone of alteration was formed at a later stage than the oxidative alteration of Zone 1 (Honnorez *et al.*, 1983).

(b) **Zone 2** (594.5 - 898.5 mbsf): This section has undergone low temperature reducing alteration and seawater flow was restricted. Below 594.5 mbsf oxidative alteration disappears and pyrite becomes abundant (Hubberten *et al.*, 1983). Emmerman (1985) suggests that extensive alteration in Hole 504B was restricted by the overlying sedimentary blanket, protecting the underlying volcanic pile from some of the seawater circulation and from convective heat loss.

#### 4.6.5. Discussion

##### 4.6.5.2 Correlation of lithological and geochemical variations

The variations in MgO and TiO<sub>2</sub> with depth downhole are compared with the reconstructed lithostratigraphy in Figures 4.16 and 4.17 respectively. The cyclic sawtooth variations in these oxides with depth have limited correspondence with the lithological cycles suggesting that different processes may have been responsible for the lithological variations and the downhole geochemistry. This supports the assertion that lava morphology is primarily a function of cooling rate / temperature and viscosity of the lava, and is not necessarily affected by variations in chemistry of the lavas (§ 2.3.5). The geochemical variations downhole are the result of fractional crystallisation and magma mixing in some form of magma chamber beneath the ridge axis (Natland *et al.*, 1983).

##### 4.6.5.3. Comparison of geochemistry and mineralogy with Hole 896A

A point to consider when comparing Holes 896A and 504B is that the two cores do not necessarily represent equivalent sections. Whilst the lavas of Hole 504B were being erupted at the ridge axis, Hole 896A would be situated on the flanks of the ridge, at some distance from the

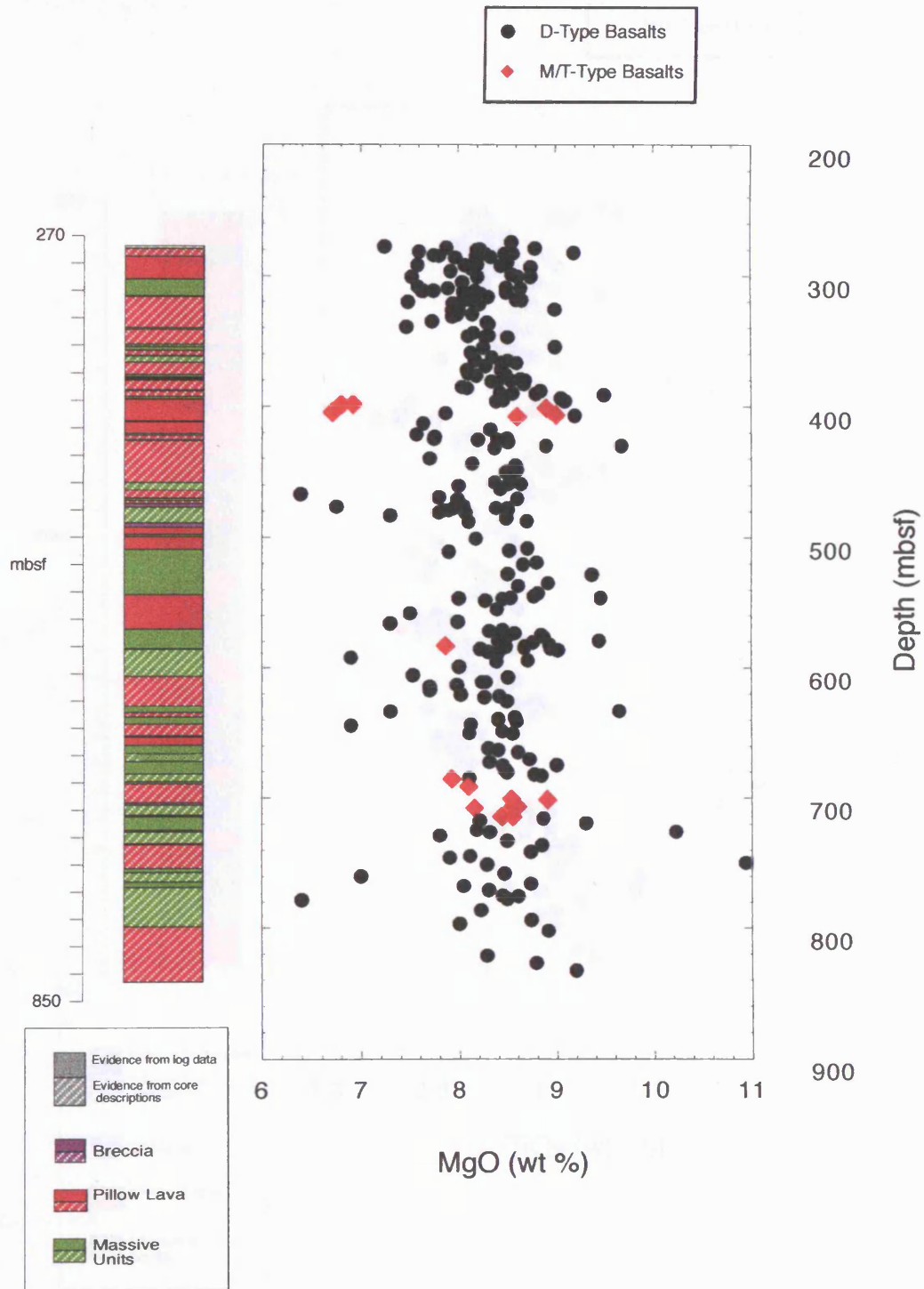


**Figure 4.16.** Comparison of lithostratigraphy with variation in MgO for Hole 504B. Classification of basalts is after Autio and Rhodes (1983).

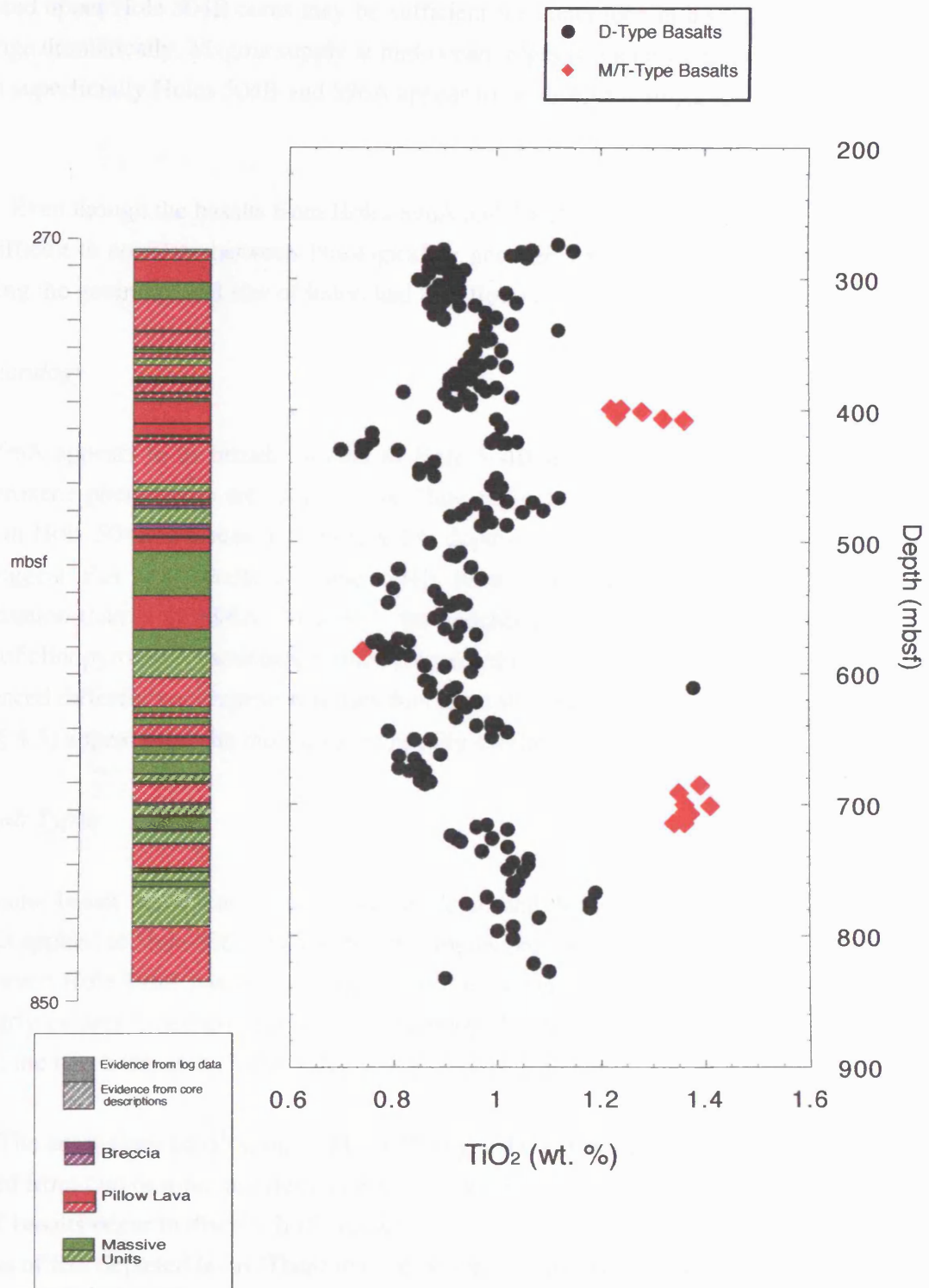


**Figure 4.17.** Comparison of lithostratigraphy with variation in TiO<sub>2</sub> for Hole 504B. Classification of basalts is after Autio and Rhodes (1983).

main axial extrusion zone, Lavas erupted off-axis often have slightly different chemical characteristics to axis lavas (§ 2.5.3.). The period of time elapsed between eruption of the Hole 896A and upper Hole 504B cores may be sufficient for conditions in a subaxial magma chamber to change dramatically. Magma supply at mid-ocean ridges is not necessarily constant, hence even though superficially Holes 504B and 896A appear to be directly comparable, this may not be the case.

Even though the basalts from Holes 896A and 504B have broadly similar chemistries, it is very difficult to correlate between lithological or geochemical units in the two cores, probably reflecting the geometry and size of individual lava flows (Alt *et al.*, 1996).

#### (a) Mineralogy

Hole 896A appears to be broadly similar to Hole 504B in terms of mineralogy. However less clinopyroxene phenocrysts are found in the Hole 896A basalts. Clinopyroxene occurs at most depths in Hole 504B whereas it is restricted to depths > 340 mbsf in the Hole 896A core. This may suggest that the basalts of Hole 504B have undergone greater degrees of fractional crystallisation than Hole 896A. However, the geochemistry of Hole 896A suggests that some degree of clinopyroxene fractionation has occurred, therefore, the lavas of Hole 504B may have experienced different pre eruptive histories than lavas in Hole 896A. The Type D basalts in Hole 504B (§ 4.5) appear to be the most mineralogically similar to Hole 896A basalts.

#### (b) Basalt Types

If the same basalt classification described by Autio and Rhodes (1983) and Kempton *et al.*, (1985) is applied to Hole 896A, all the basalt samples present can be assigned to chemical group D. However, Hole 896A has lower concentrations incompatible elements than Hole 504B. This is particularly evident when comparisons of magmophile elements, such as Ti and Zr, are made between the two boreholes (Table 4.4.).

The anomalous basalt groups, M and T, suggest that the rocks present in Hole 504B were generated from two or more different magma sources (Emmerman, 1986). The fact that the Type M and T basalts occur in discrete horizons within the lava stack implies that they represent isolated eruptions of less depleted lavas. There may be two main reasons for this (Emmerman, 1985) :

- the presence of chemical heterogeneities in the mantle source
- the majority of the basalts were derived from a depleted source with periodic eruptions from pockets of less depleted mantle (or metasomatically altered mantle).

	MgO (wt. %)	TiO <sub>2</sub> (wt. %)	Ni (ppm)	Zr (ppm)	Nb (ppm)
Hole 504B					
Range :	6.39 - 10.94	0.7 - 1.41	66 - 191	32 - 106	0.1 - 3.2
Average :	8.30	0.96	116.66	52.84	1.26
Hole 896A					
Range :	6.7 - 9.7	0.62 - 0.96	82 - 201	30 - 56	0 - 1.12
Average :	7.96	0.81	145.73	45.67	0.62

**Table 4.4.** Comparison of Holes 504B and 896A

The less depleted Type M and T basalts do not occur in the Hole 896A core suggesting two possible theories:

- the recovered section of Hole 896A does not penetrate through these less depleted horizons, either they were not recovered or they occur at a greater depth than was penetrated,
- they simply do not occur in the crustal section penetrated by Hole 896A.

If these less depleted basalts do not occur in the Hole 896A crustal section it suggests that any chemical heterogeneities or pockets of less depleted mantle have a small lateral or temporal extent.

*(c) Geochemistry*

The thickness of the overlying sediments is different in each borehole, to compensate for this, the Hole 504B samples were depth shifted upwards by 80 m so that the top of the volcanic section corresponds with the top of the Hole 896A volcanic section. Comparative plots of MgO, Al<sub>2</sub>O<sub>3</sub>, CaO and TiO<sub>2</sub> are shown in Figure 4.18.

In the upper 120 m of Hole 896A has higher MgO and lower TiO<sub>2</sub> than the corresponding section of Hole 504B. This may suggest that the Hole 504B basalts have experienced a greater degree of fractional crystallisation than the Hole 896A basalts. MgO would be expected to incorporate into olivine during fractionation whereas TiO<sub>2</sub> remains in the residual liquid. The base of the Hole 896A section, from 400 to 420 metres below sediment interface (mbsi), also has more primitive compositions of MgO and TiO<sub>2</sub>, whereas the central section, from 300 to 400 mbsi, has similar concentrations to Hole 504B. This is consistent with the results discussed in § 3.8.4.2, where it was concluded that this central section of the Hole 896A core had undergone greater amounts of fractionation than the lavas above and below it.

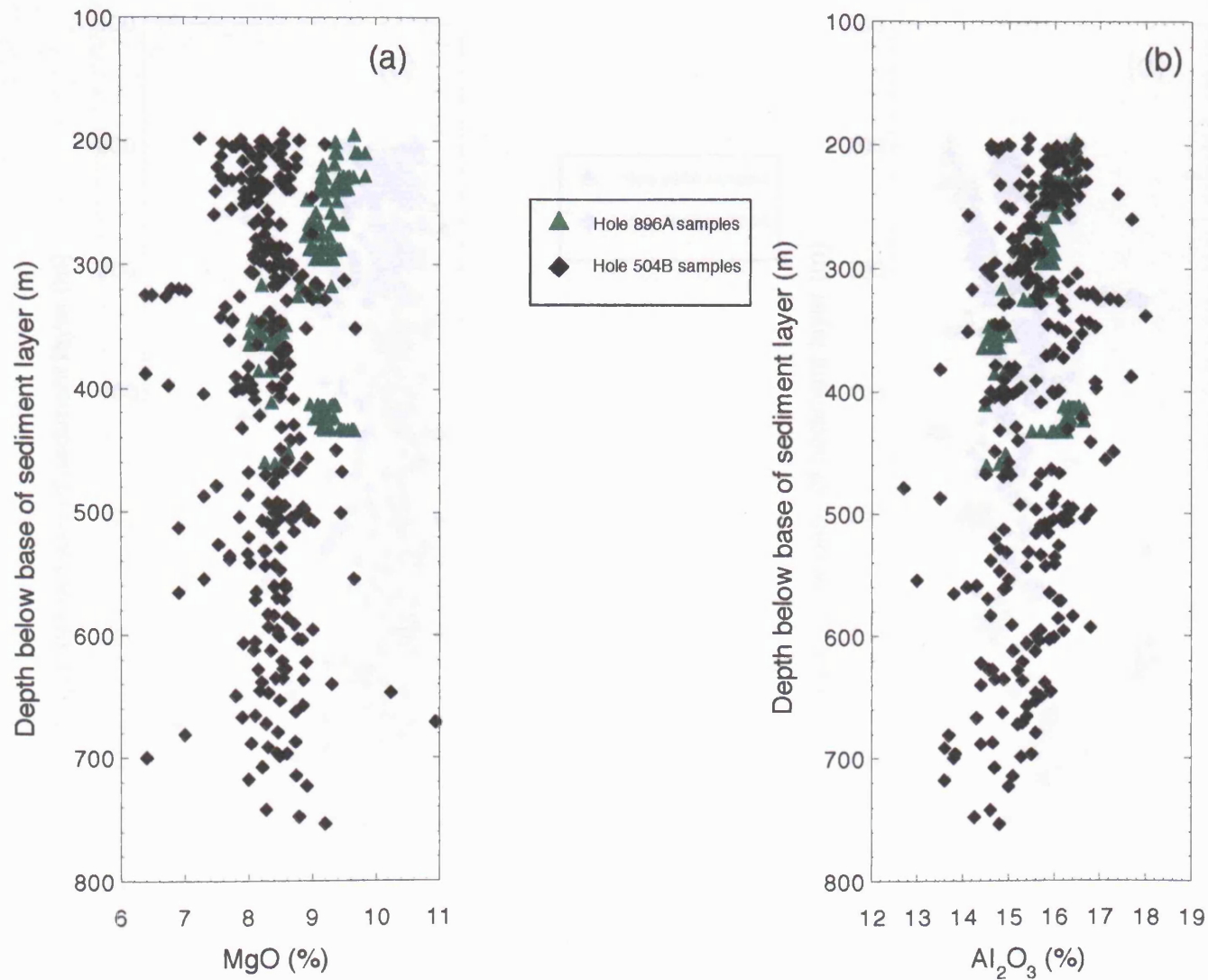


**Figure 4.18.** Comparison of downhole geochemistry of Holes 504B and 896A, (a) MgO versus depth, (b) Al<sub>2</sub>O<sub>3</sub> versus depth.

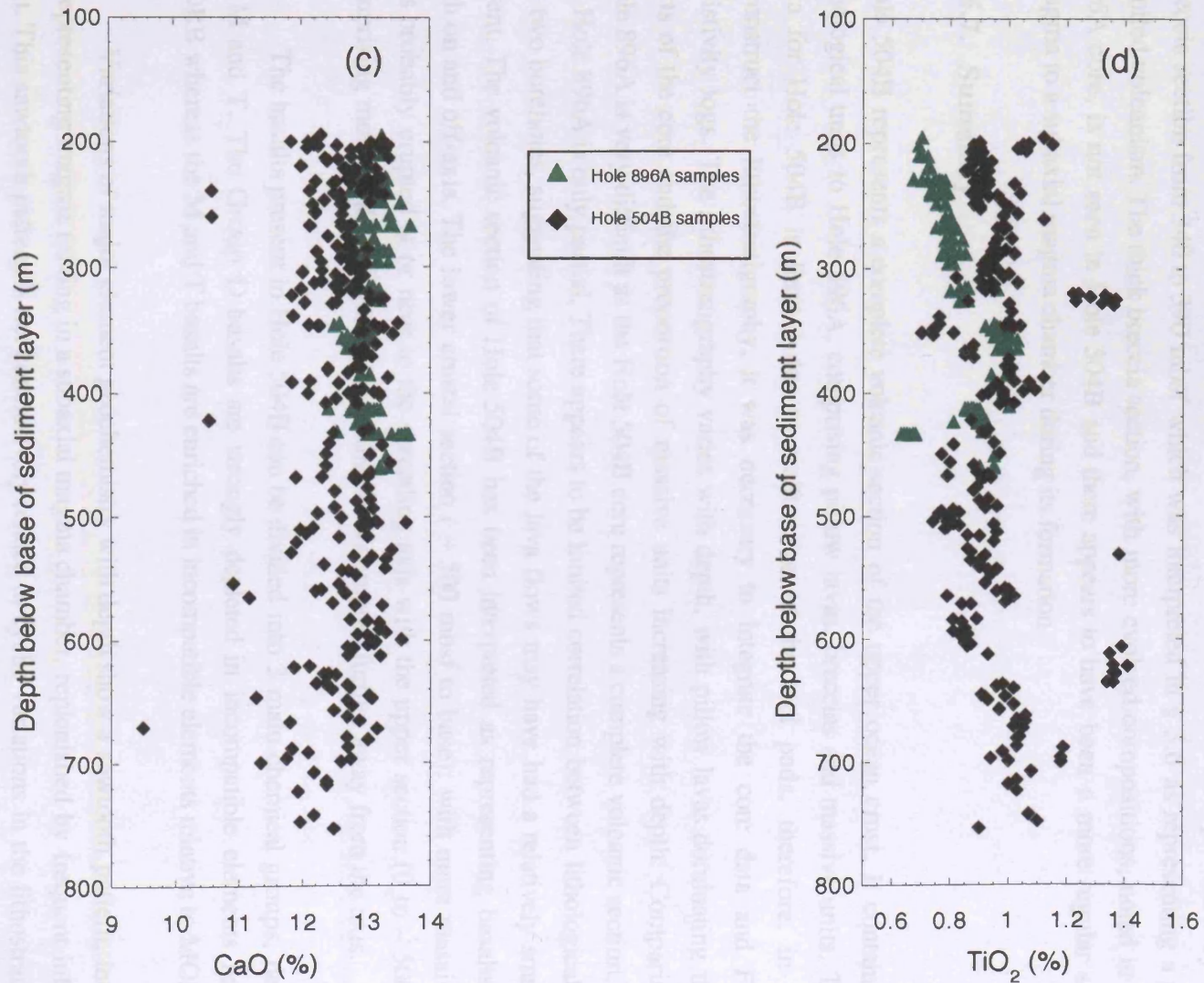


**Figure 4.18.(continued)** Comparison of downhole geochemistry of Holes 504B and 896A, (c) CaO versus depth, (d) TiO<sub>2</sub> versus depth.

The cyclic or “sawtooth” variations in the Hole 504B geochemistry are not well-defined in Hole 896A. Brewer *et al.* (1996) suggest that the sawtooth profiles in Hole 504B represent magma mixing in a subaxial magma chamber, frequently replenished by new influxes of melt. The lack of such a sawtooth profile in Hole 896A implies that replenishment of the magma chamber occurred over longer time scales in this section (Brewer *et al.*, 1996). Evidence for a more intermittent lava supply during formation of Hole 896A, is also provided by the large breccia section from 340 to 390 mbsf which was interpreted in § 3.6 as representing a period of limited volcanism. The thick breccia section, with more evolved compositions, noted in the Hole 896A core, is not seen in Hole 504B and there appears to have been a more regular supply of magma to a subaxial magma chamber during its formation

#### 4.6.7. Summary

Hole 504B represents a complete volcanic section of the upper ocean crust. It contains similar lithological units to Hole 896A, comprising pillow lavas, breccias and massive units. The FMS data for Hole 504B is limited due to malfunction of the tool pads, therefore, in order to reconstruct the lithostratigraphy, it was necessary to integrate the core data and FMS and resistivity logs. The lithostratigraphy varies with depth, with pillow lavas dominating the upper parts of the core and the proportion of massive units increasing with depth. Comparison with Hole 896A is very difficult as the Hole 504B core represents a complete volcanic section, whereas the Hole 896A is only partial. There appears to be limited correlation between lithological units in the two boreholes, suggesting that some of the lava flows may have had a relatively small lateral extent. The volcanic section of Hole 504B has been interpreted as representing basalts erupted both on and off-axis. The lower crustal section ( ~ 500 mbsf to base), with more massive units, was probably erupted at or near to the spreading axis with the upper section (0 to ~ 500 mbsf), comprising mostly pillow lavas, representing flows erupted further away from the axis.

The basalts present in Hole 504B can be divided into 3 main chemical groups, designated D, M and T. The Group D basalts are strongly depleted in incompatible elements relative to MORB whereas the M and T basalts are enriched in incompatible elements relative to MORB.

Variations of major element geochemistry with depth show a sawtooth pattern, interpreted as representing magma mixing in a subaxial magma chamber, replenished by frequent influxes of melt. This sawtooth pattern is not conclusively related to cyclic variations in the lithostratigraphy, suggesting that flow morphology may sometimes be independent of lava geochemistry. These regular cyclic variations are not well-defined in Hole 896A suggesting that replenishment of the magma chamber over longer time scales occurred during construction of this crustal section.

## CHAPTER 5

---

### *Applications of downhole logs in basement cores with high core recovery. Case Study 3: ODP Hole 735B*

#### 5.1. Introduction

Factors such as spreading rate have a large influence on the lithostratigraphy of the ocean crust. To fully constrain the processes responsible for the accretion of the crust it is essential to fully investigate the nature of the lower oceanic crust.

On very rare occasions, basement boreholes have high core recovery, ODP Hole 735B, drilled into lower ocean crust formed at an ultra-slow spreading centre, has a core recovery of 86.5 %, hence, a different core-log integration approach was used. The hole has particularly high core recovery so it is largely unnecessary to use the downhole logs to reconstruct the lithological architecture of the hole. Instead the high core recovery and reasonably high quality log data could be used to determine the nature of any missing material and reorientate and accurately locate a number of core pieces within the core. The cores retrieved on all ODP drilling legs are unorientated therefore the strikes of structural features such as veins, fractures and foliations are not known. The ability to reorientate ODP cores allows for the more accurate determination of tectonic settings. As this chapter is concerned with work still in progress, only a few isolated core pieces have been placed in their correct orientation at the time of writing. If core and log data can be integrated in boreholes with high core recovery, the results can hopefully be translated into those boreholes with poor core recovery.

ODP Hole 735B was first visited in 1987 on ODP Leg 118, and subsequently revisited October - December, 1997 during ODP Leg 176 (Robinson, Von Herzen, Adamson *et al.*, 1989; Dick, Natland, Miller *et al.*, in press). This borehole provides perhaps the first representative section through the lower ocean crust generated at a slow-spreading ridge, providing us with valuable insights into its composition and structure. The site is located in the rift mountains of the Southwest Indian Ridge (SWIR) and situated in a water depth of 719.9 m, the position of the site

in the magnetic anomaly pattern suggests the age of the crust in this area is approximately 12 Ma (Robinson, Von Herzen, Adamson *et al.*, 1989).

Unfortunately, even though the total penetration of Hole 735B is > 1500 mbsf, approximately 1400 m of drill-pipe broke off in the borehole after coring on leg 176 (Dick, Natland, Miller *et al.*, in press). Five hundred metres of this broken pipe was recovered by fishing operations, leaving 600 m of hole available for downhole logging (Dick, Natland, Miller *et al.*, in press).

This chapter comprises a discussion of the results obtained from ODP Legs 118 and 176. The logging data and core image data from Leg 176 is discussed in greater detail, as is the method proposed for reorientation of individual core pieces. A brief overview of the downhole geochemistry is also provided, in order to investigate whether the chemical stratigraphy present in Hole 735B is also reflected in the downhole logging data.

## 5.2. Geological Background

The spreading rate along the SWIR is approximately 0.8 cm / yr. and therefore classified as ultra-slow (Fisher and Sclater, 1983). The SWIR was created in the Mesozoic at the break-up of Gondwanaland (Dick *et al.* 1991b). Prior to 80 Ma the axis of the ridge moved southwards, changed direction, and separation of Madagascar and India began. The SWIR forms a ridge-ridge-ridge triple junction with the Central Indian Ridge and the Southeast Indian Ridge (Dick *et al.* 1991b). This triple junction has migrated to the north-east, resulting in the extension of the SWIR, creating fracture zones such as the Atlantis II Fracture Zone (Dick *et al.* 1991b).

Hole 735B is situated 93 km south of the ridge axis, and 18 km east of the Atlantis II Fracture Zone. (Dick, Natland, Miller *et al.*, in press) (Figure 5.1). The Atlantis II Fracture Zone is a large-offset, left-lateral transform which cuts the Southwest Indian Ridge at 31°S 57°E (Dick *et al.*, 1991b). Hole 735B is located on a shallow platform, this is one in a series of uplifted blocks which comprise a ridge parallel to the transform fault (Dick *et al.*, 1991b). The Atlantis II Fracture Zone and surrounding crust is believed to be entirely of oceanic origin with no continental crust component.

Seismic refraction measurements in this area have estimated a crustal thickness of approximately 4 km, with the absence of extrusive basalts and gabbros (as seen at Site 735B), the crust-mantle transition should therefore be at approximately 2 km in this area. Thinner crustal sections are usually found at fracture zones which leads Robinson, Von Herzen, Adamson *et al.* (1989) to infer that this is due to cold zones separating spreading centre cells beneath ridge axes.

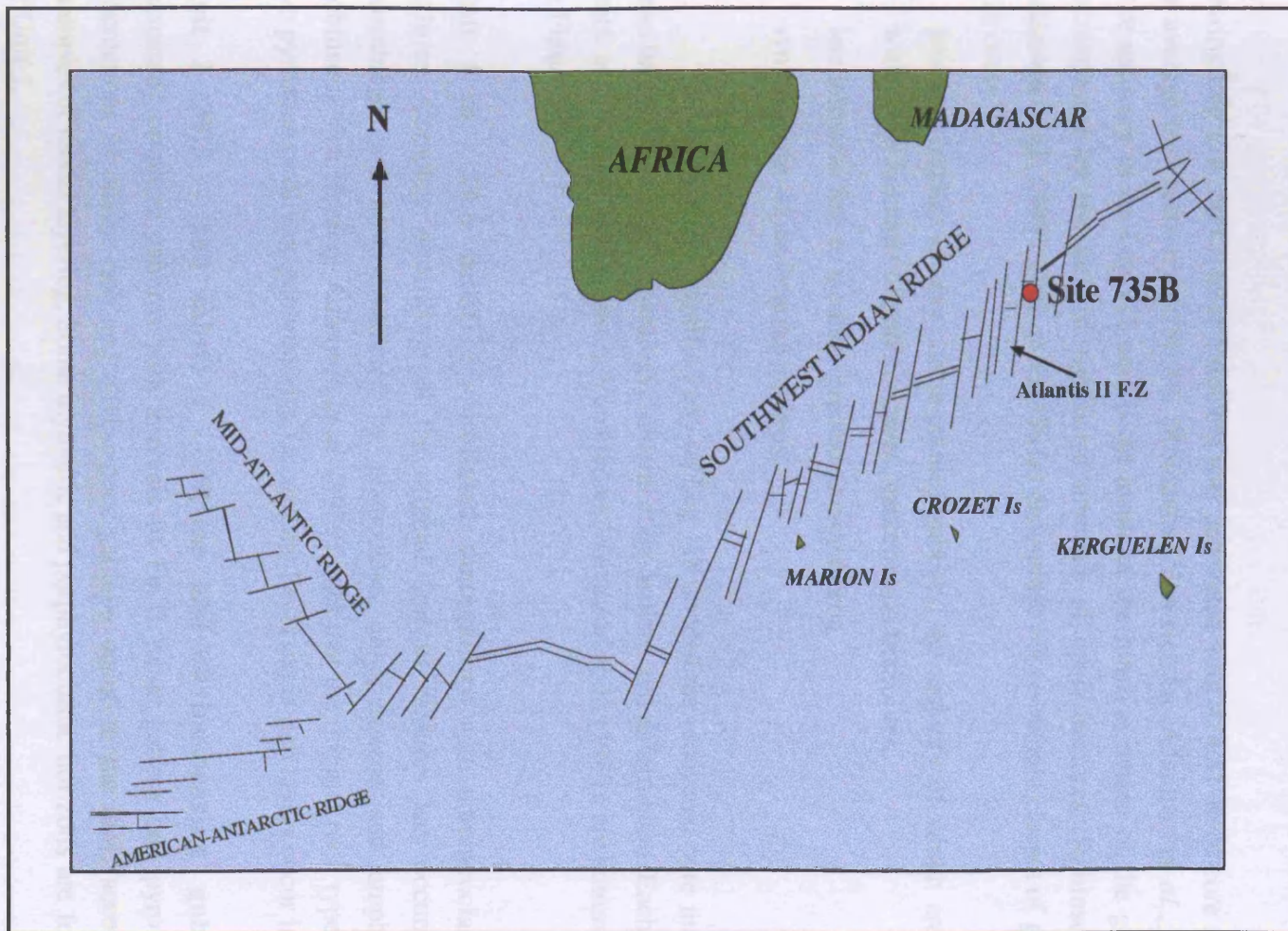


Figure 5.1. Location of Site 735B. Adapted from Dick *et al.* (1992).

Less magma is supplied to the edge of the cells than the centre, therefore, thinner crust is developed at the cell edges, hence in these areas mantle and lower crust may be exposed.

### 5.3. Summary of Leg 118 results

#### 5.3.1. Lithological units

During Leg 118, 500.7 m of basement was penetrated with 434.81 m of core recovered, giving an average core recovery of 86.8% (Robinson, Von Herzen, Adamson *et al.*, 1989). The high core recovery in the Leg 118 core is the result of the massive nature of the gabbros recovered accompanied by the lack of significant amounts of open fractures (Robinson, Von Herzen, Adamson *et al.*, 1989). Dick *et al.* (1991a) distinguish between three classes of gabbro in the Leg 118 core:

- primary medium to very coarse-grained gabbros, the majority of which are olivine gabbros with lesser amounts of gabbro-norites, gabbros and troctolites,
- late intrusive fine to medium-grained microgabbros,
- synkinematic oxide-bearing gabbros.

The Shipboard Scientific Party on Leg 118 divided the recovered core into six lithological units based on igneous mineralogy, mineral compositions and deformation. Each of the individual units, as described by Robinson, Von Herzen, Adamson *et al.* (1989), are summarised below and in Figure 5.2:

**Unit 1 (0 - 39.5 mbsf) :** - **Foliated metagabbro** with porphyroclastic to mylonitic textures. Complete destruction of the original igneous textures has occurred and mineral assemblages are now dominated by plagioclase, clinopyroxene and amphibole neoblasts. Robinson, Von Herzen, Adamson *et al.* (1989) infer that the original rock type was probably a two pyroxene or olivine gabbro-norite. Occasional Fe-Ti oxide rich layers occur in this unit.

**Unit 2 (39.5 - 180 mbsf) :** - **Olivine and olivine-bearing gabbro.** These are chemically primitive gabbros with intervals of Fe-Ti oxide gabbro and pyroxene-rich layers. Alternations of olivine-rich and olivine-poor gabbros occur in the unit, accompanied by rare examples of modal layering. Some mylonitic and porphyroclastic horizons are found near the top of Unit 2.

**Unit 3 (180 - 224 mbsf) :** - **Olivine gabbro** with intervals of Fe-Ti oxide gabbros. This is similar in hand specimen to Unit 2 but has more evolved compositions. The unit contains well-

developed igneous laminations, these are steep at the top of the unit and gradually flatten with depth. Mylonitic and foliated zones are common in Unit 3.

**Unit 4 (224 - 272 mbsf) :- Fe-Ti oxide-rich gabbro.** This unit has more abundant opaques ( $\geq 10\%$ ) and less olivine than Unit 3.  $\text{Fe}_2\text{O}_3$  content is approximately 30 wt. % and  $\text{TiO}_2$  is 9 wt. %. The lower contact with Unit 5 has a 3 m thick mylonitic layer. A felsic intrusion breccia with trondjemite veins occurs in two locations.

**Unit 5 (272 - 403.5 mbsf) :- Olivine gabbro** with scarce Fe-Ti oxide layers and rare low Ca pyroxene. Some of the gabbros show primary grain-size layering. This unit has similar mineralogy and chemistry to Unit 2 with troctolites and plagioclase-rich gabbros occurring in thin horizons. Unit 5 also contains a number of brecciated zones with felsic veins containing epidote and albite.

**Unit 6 (403.5 - 500.7 mbsf) :- Olivine-rich gabbro** with abundant troctolitic layers. This unit is similar to Unit 5 but has a greater abundance of olivine. The olivine gabbros are interlayered with troctolitic horizons which Robinson, Von Herzen, Adamson *et al.* (1989) interpret as intrusive layers. Coarse Fe-Ti oxide gabbros are found occasionally throughout the unit. Intervals of metagabbro also occur, these are characterised by mylonitic to porphyroclastic textures.

#### 5.3.1.1. Redefinition of Leg 118 unit boundaries

More detailed analysis of the core data by Dick *et al.* (1991a) resulted in redefinition of the unit boundaries, the unit names were also changed and a number of sub-units were added. A comparison of the new unit division with that of the original shipboard scientific party is shown in Figure 5.2. The new division of units, as described by Dick *et al.* (1991a) are reviewed below:

**Unit I (0 - 37.5 mbsf) :- Gabbronorite.** This unit has been divided into two sub-units IA and IB.

IA comprises **massive gabbronorite**. This sub-unit is 27.99 m thick and consists of thick gabbronorite layers alternated with much thinner olivine gabbro layers.

IB is **olivine gabbro and gabbronorite** consisting of olivine gabbro with thin gabbronorite intervals. This sub-unit is 9.5 m thick and represents a transition from Unit I to Unit II.

**Unit II (37.5 - 170.2 mbsf) :- Upper compound olivine gabbro.** Most of the lithological intervals in this unit are olivine gabbros with two metagabbros. The remainder of the unit contains intrusive microgabbros, oxide gabbro zones, diabase dykes and layers of oxide olivine gabbros.

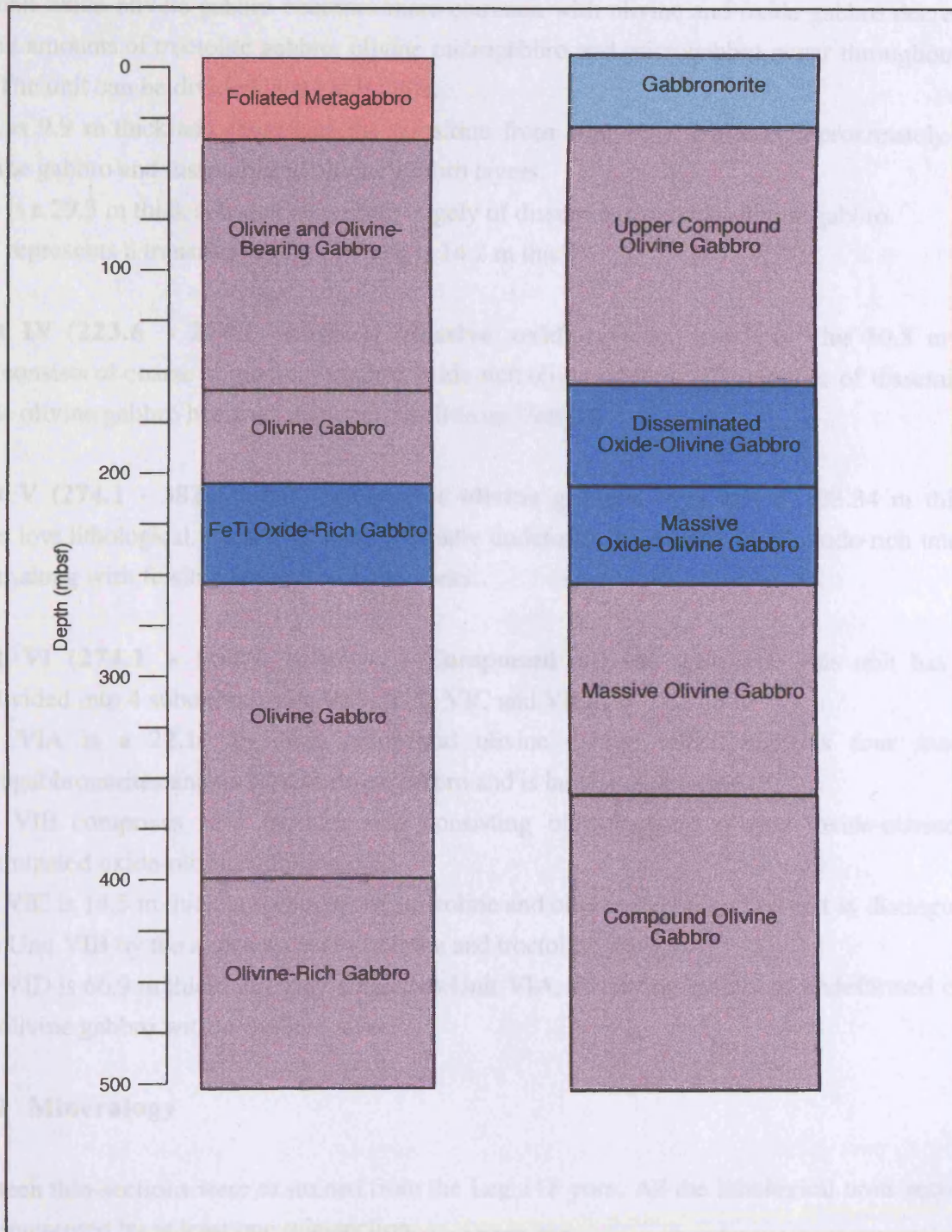


**Figure 5.2.** Lithostratigraphy of Hole 735B drilled on Leg 118 after (A) Robinson, Von Herzen, Adamson *et al.* (1989) and (B) Dick *et al.* (1991a).

**Unit III (170.2 - 223.6 mbsf) :- Disseminated oxide-olivine gabbro.** 66 % of Unit III is massive disseminated oxide-olivine gabbro with pigeonite and hypersthene. Lower down the unit oxide olivine gabbro becomes more common with olivine and oxide gabbro decreasing. Small amounts of troctolite gabbro, olivine microgabbro and microgabbro occur throughout Unit III. The unit can be divided into 3 sub-units.

IIIA is 9.9 m thick and represents the transition from Unit II. It contains approximately equal olivine gabbro and disseminated olivine gabbro layers.

IIIB is a 29.3 m thick sub-unit consisting largely of disseminated oxide-olivine gabbro.

IIIC represents a transition to Unit IV and is 14.2 m thick.

**Unit IV (223.6 - 274.1 mbsf) :- Massive oxide-olivine gabbro.** This 50.5 m thick unit consists of coarse to medium-grained oxide-rich olivine gabbro. The absence of disseminated oxide olivine gabbro horizons distinguishes it from Unit III.

**Unit V (274.1 - 382.4 mbsf) :- Massive olivine gabbro.** This unit is 108.34 m thick. It has a low lithological variability and is virtually undeformed. Locally, small oxide-rich intervals occur along with felsic veins and vein networks.

**Unit VI (274.1 - 500.7 mbsf) :- Compound olivine gabbro.** This unit has been subdivided into 4 subunits, Units VIA, VIB, VIC and VID.

Unit VIA is a 22.14 m thick compound olivine gabbro which contains four intrusive microgabbro and an olivine microgabbro and is largely undeformed.

Unit VIB comprises 15.3 m thick unit consisting of compound olivine, oxide-olivine and disseminated oxide-olivine gabbros.

Unit VIC is 14.5 m thick and consists of troctolitic and olivine gabbros. The unit is distinguished from Unit VIB by the appearance of troctolite and troctolitic gabbros.

Unit VID is 66.9 m thick and very similar to Unit VIA, consisting mainly of undeformed oxide-free olivine gabbro with some intrusives.

### 5.3.2 Mineralogy

Fourteen thin-sections were examined from the Leg 118 core. All the lithological units recovered are represented by at least one thin-section.

Eight of the examined sections comprise olivine gabbro or olivine-bearing gabbro. These have granular to sub-ophitic textures (Plate 5.1), most of the sections being medium to coarse-grained. Many of the sections show some foliation, this is usually due to the alignment of clinopyroxene grains. Plagioclase occurs as subhedral to anhedral grains, ranging in size from 0.5 to 3 mm. These are usually multiply twinned and most are relatively fresh and unaltered.

Clinopyroxene occurs as anhedral to subhedral grains, on average 1 mm in size. Clinopyroxene is usually altered at crystal edges to fibrous brown / green amphibole and, in some cases, biotite. Most grains have a strongly developed cleavage and some examples of simple twinning occur. Olivine occurs as rounded anhedral grains ranging from 1 to 2 mm in size. These are often replaced by opaque minerals along fractures and at the edges of grains. In some examples, replacement by talc and serpentine also occurs. This material is mildly pleochroic with anomalous birefringent colours and relatively high relief.

Troctolite occurs in two of the thin-sections, both of which are from Unit 6. The two sections are medium-grained with sub-ophitic textures. This lithology is dominated by subhedral to anhedral crystals of plagioclase, ranging from 2 to 3 mm in size, which are relatively fresh and unaltered. Olivine occurs as anhedral crystals, 2 to 3 mm in size. Olivine is often replaced by red / brown iddingsite, the strong colour of which masks the birefringent colours (Plate 5.2). Rare clinopyroxenes also occur, these are generally < 2 mm in size and anhedral in shape

Two of the examined sections comprise metagabbros, 735-1 is a porphyroclastic metagabbro and 735-3 is a massive metagabbro. The porphyroclastic metagabbro has experienced extensive replacement and alteration of the primary mineralogy. The massive metagabbro comprises altered and recrystallised plagioclase and clinopyroxene. Clinopyroxene has been extensively replaced by green amphibole, any remnant clinopyroxenes are anhedral and, on average, approximately 5 mm in size. The section is crossed by small veins, < 1 mm wide, most of which contain green amphibole.

One example of a Fe-Ti oxide gabbro (olivine-bearing) was studied (735-8 from Unit 4). This section is relatively coarse-grained and dominated by a large clinopyroxene crystal, > 20 mm in size. This large crystal contains inclusions of biotite, pale green amphibole and opaque minerals. Opaque minerals are common throughout the section, comprising approximately 5 % of the phenocryst phases. These are anhedral and range in size from 0.1 to 2 mm and have been identified in reflected light as ilmenite and sulphides (T.S. Brewer, pers. comm).

The final thin-section studied from the Leg 118 core comprises ilmenite-bearing gabbro. This is a coarse-grained section consisting primarily of plagioclase, clinopyroxene and ilmenite. Clinopyroxene is commonly replaced at the edges of grains by green amphibole and biotite. The ilmenite grains are anhedral and range in size up to approximately 5 mm. They occasionally occur rimmed with amphibole and biotite.



**Plate 5.1.** Thin-section photomicrograph in cross-polarised light of an olivine gabbro with ophitic texture (735-12). A number of plagioclase grains are enclosed by a large twinned clinopyroxene crystal. Field of view is 12 mm.

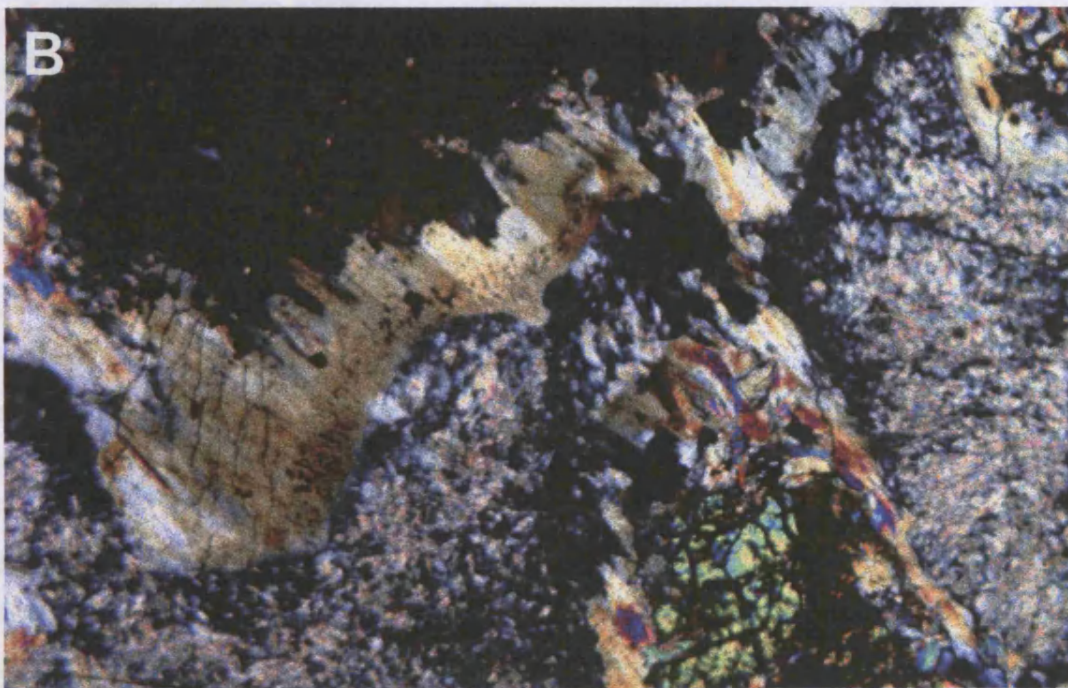


**Plate 5.2.** Thin-section photomicrograph in cross-polarised light of alteration and replacement by secondary minerals in a troctolite from ODP Hole 735B (735-13). Olivine has been extensively replaced by iddingsite, talc and serpentine. Field of view is 4 mm.

### 5.3.3. Geochemistry

The geochemistry of Leg 118 samples is discussed along with the data from Leg 176 in § 5.4.3.

### 5.3.4. Structural features and deformation in the Leg 118 core

The deformation in the Leg 118 core was extensively examined by the shipboard scientific party and is reviewed below (Robinson, Von Herzen, Adamson *et al.*, 1989):

The type and degree of deformation in the Leg 118 core varies considerably with depth downhole. Veins and fractures are most abundant at the top of the core, particularly at depths between 0 and 220 mbsf. The most abundant veins are monomineralic green amphibole veins which range widely in size from 0.1 to > 1 cm. Amphibole veins are distributed throughout the entire length of the Leg 118 core. Plagioclase + amphibole and smectite veins both appear at approximately 85 mbsf and then continue to the base of the hole. Most of the veins in the Leg 118 core can be seen to cross-cut the foliation implying that they occurred subsequent to deformation, however, they very rarely cross mylonitic zones indicating that they actually occurred before plastic deformation of the core.

Plastic deformation in the core ranges from poorly foliated through foliated and augen gneissic to mylonitic. The mylonitic zones consist of pyroxene augen and recrystallised olivine grains in a very fine-grained matrix, the foliation is often very difficult to see in these zones. Foliated sections are characterised by the alignment of pyroxenes in a plagioclase matrix. In some cases partial recrystallisation of plagioclase has occurred.

### 5.3.5. Logging Data

A total of 18 logging runs were conducted in Hole 735B during Leg 118 which are summarised below (Robinson, Von Herzen, Adamson *et al.*, 1989):

- the first logging run deployed a dual induction tool (DIT), sonic, natural gamma and caliper logs, good data was obtained from 500 to 269 mbsf from the sonic and natural gamma tools. Unfortunately, an electrical fault caused loss of data from the DIT and the caliper,
- the second logging run deployed a lithodensity tool (LDT) and a USGS three-component magnetometer probe, good data was obtained by both of these tools,
- The Schlumberger™ geochemical combination tool (GLT) and magnetometer were then deployed, two passes were made, both collecting good quality data,

- the fourth run comprised a repeat deployment of the failed tool from run 1, good data was obtained with resistivities in the core ranging from 2  $\Omega$  m to the tool maximum detection limit of 2,000  $\Omega$  m,
- run 5 deployed the dual laterolog (DLL), good quality data was collected with resistivities in the hole ranging from 2 to 40,000  $\Omega$  m,
- the USGS temperature tool was the next tool to be deployed, data from this run suggested that temperatures were slightly higher at the top of the hole than the bottom,
- run 7 deployed the borehole televiewer (BHTV), the tool unfortunately did not collect any data during this run,
- the eighth logging run deployed the multichannel sonic tool (MCS), good data was collected from the hole, with the exception of the first 100 m,
- runs 9 and 10 collected magnetometer and magnetic susceptibility data, the magnetometer data was of a good quality but the magnetic susceptibility data showed a large amount of noise,
- the next run was a repeat deployment of the magnetic susceptibility tool, good quality data was obtained from 49 to 490 mbsf,
- run 12 comprised a repeat of the MCS tool to obtain data from the upper 100 m of the borehole, good quality data was obtained from 127 mbsf to the seafloor,
- run 13 was a second deployment of the USGS temperature tool, results were consistent with those obtained from run 6,
- run 14 comprised the first of three runs of the vertical seismic profile (VSP), unfortunately the tool failed and no data was collected,
- next, the BHTV was redeployed, the full length of the borehole was logged with good quality data being obtained,
- run 16 comprised the second run of the VSP, again the tool failed,
- in run 17 a vertical component VSP was deployed, the data obtained was obscured by a large amount of downhole noise,
- finally, the third run of the VSP was attempted and good quality data was obtained.

More detailed descriptions of selected logging tools are included in Appendix C

### **5.3.6. Models for crustal structure at Site 735B**

Interpretation of the Leg 118 data led Dick *et al.* (1997) to propose three possible models for the crustal structure at the site of Hole 735B (Figure 5.3):

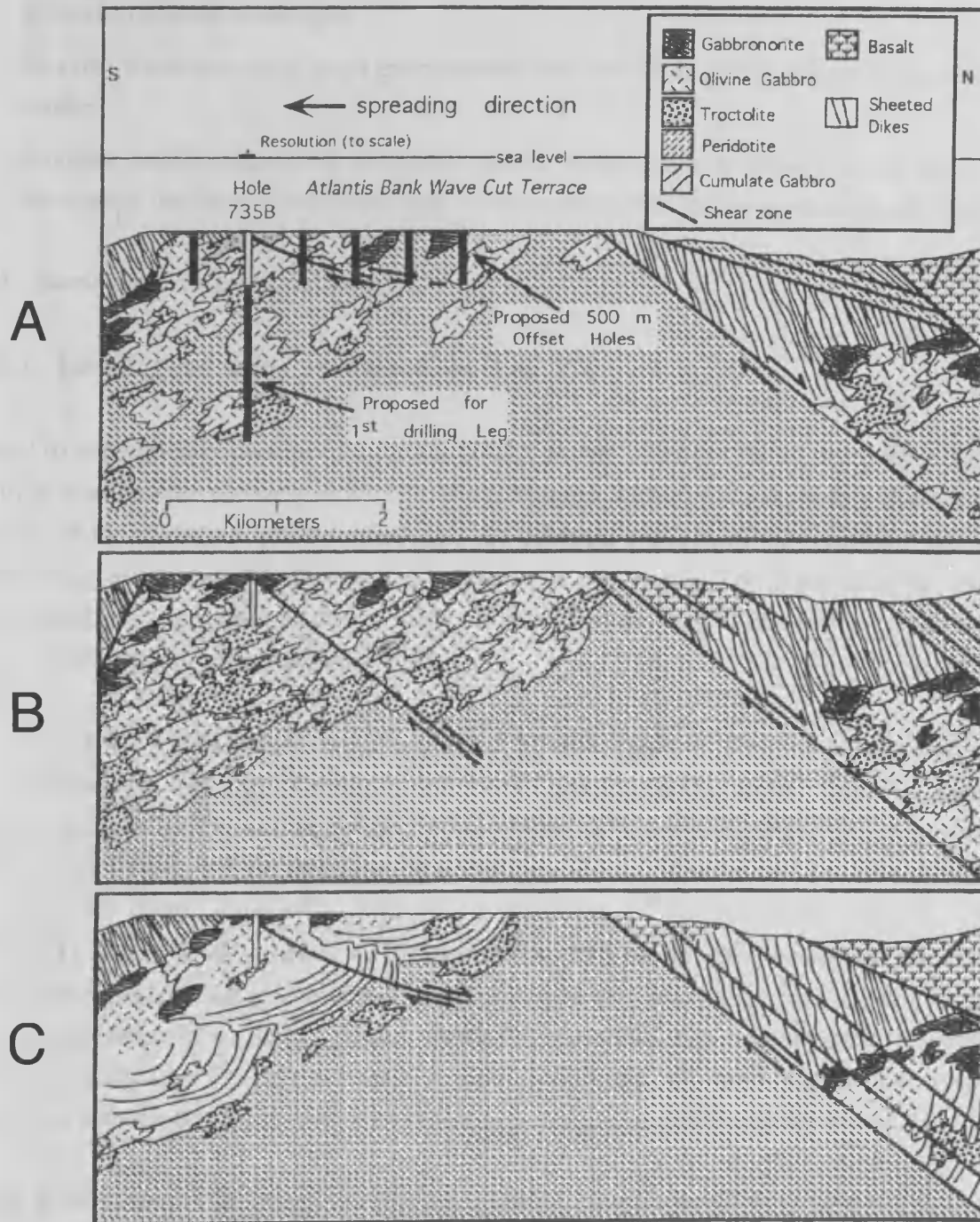


**Figure 5.3.** Models for crustal structure at Site 735B after Leg 118 (from Dick *et al.*, 1997). A) the crust is composed of cross-cutting gabbro bodies, decreasing in number with depth, B) the crust is composed of small gabbro bodies but there is an abrupt transition into the upper mantle, C) gabbro bodies are only present in the upper crust, these grade into layered intrusions which have a sharp contact with the peridotites of the upper mantle.

- the crust is constructed of relatively small gabbro bodies cross-cutting each other and the serpentinised upper mantle, the number of these magma bodies would be expected to gradually decrease with depth.
- the crust is constructed of small gabbro bodies but there is an abrupt transition into the upper mantle.
- ophiolite models suggest that discordant gabbro bodies are only present in the upper crust, these grade into layered intrusions with a sharp contact with the upper mantle peridotites.

#### 5.4. Summary of Leg 176 results

##### 5.4.1. Lithological units recovered on Leg 176

Leg 176 subsequently penetrated a further 1003.2 m into basement rocks, recovering 865.99 m with an average core recovery of 86.3 % (Dick, Natland, Miller *et al.*, in press). Greater than 99 vol. % of the recovered igneous lithologies are gabbroic rocks with the remaining 0.5 vol. % comprising felsic veins (Dick, Natland, Miller *et al.*, in press). The division of the core into lithological units is a continuation of the scheme devised by Dick *et al.* (1991a), these units are shown in Figure 5.4 and reviewed below:

**Unit VI (382 - 536 mbsf) :- Compound olivine gabbro.** This is a continuation of Unit VI recovered on Leg 118. The lower part of the unit, at depths greater than 504 mbsf, has abundant olivine gabbro and troctolitic gabbro intervals with some mixtures of the two. Unit VI is relatively primitive, with an abundance of troctolitic rocks.

**Unit VII (536 - 599 mbsf) :- Gabbronorite and oxide gabbronorite.** The transition from Unit VI to Unit VII is indicated by the occurrence of gabbronorite / oxide gabbronorite and the disappearance of troctolitic gabbro. Oxide-bearing rocks also become more abundant and grain-size decreases. The unit is subdivided into 2 sub-units VIIa and VIIb at 560 mbsf. This coincides with the occurrence of a major fault zone and the disappearance of olivine gabbro.

**Unit VIII (599 - 670 mbsf) :- Olivine gabbro.** The transition from Unit VII to Unit VIII is marked by an increase in grain size. This is accompanied by an increase in the abundance of olivine gabbro. Occasional gabbronorite intervals occur in this unit.

**Unit IX (670 - 714 mbsf) :- Gabbronorite and gabbro.** The transition from Unit VIII to IX is marked by a decrease in grain-size. The unit is dominated by gabbronorites but with fewer oxide gabbronorites than Units VII and VIII. This unit contains no microgabbro intervals.

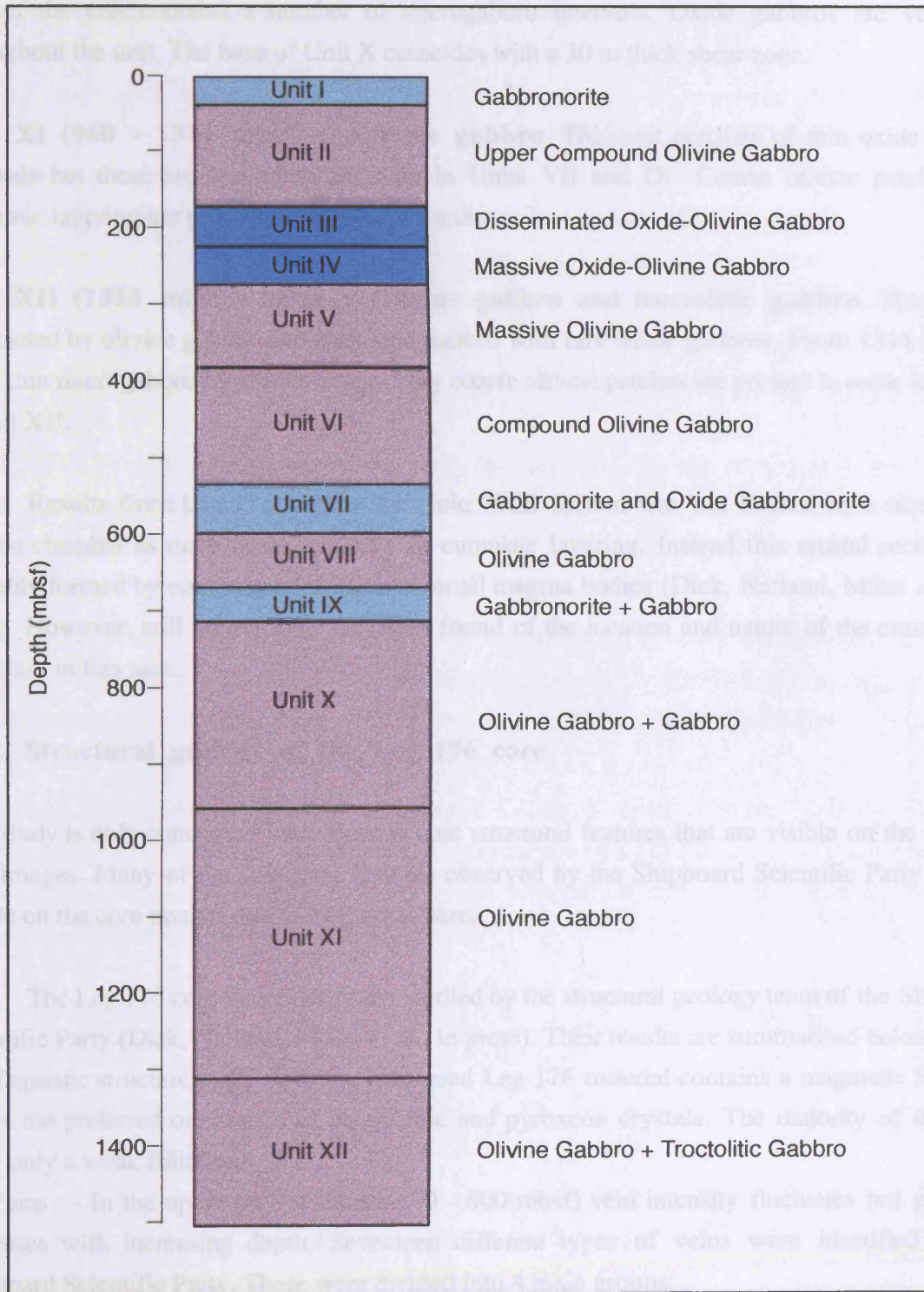


**Figure 5.4.** Lithostratigraphy of ODP Hole 735B after Dick *et al.* (1991a) and Dick, Natland, Miller *et al.* (in press).

**Unit X (714 - 960 mbsf) :- Olivine gabbro and gabbro.** The transition from Unit IX is marked by the disappearance of orthopyroxene and a corresponding increase in olivine. The upper part of the unit contains a number of microgabbro intervals. Oxide gabbros are very rare throughout the unit. The base of Unit X coincides with a 30 m thick shear zone.

**Unit XI (960 - 1314 mbsf) :- Olivine gabbro.** This unit consists of thin oxide gabbro intervals but these are less abundant than in Units VII and IX. Coarse olivine patches and rhythmic layering are present throughout the unit.

**Unit XII (1314 mbsf - base) :- Olivine gabbro and troctolitic gabbro.** This unit is dominated by olivine gabbro and troctolitic gabbro with rare oxide gabbros. From 1314 to 1390 mbsf thin microgabbro intrusions occur. Very coarse olivine patches are present in some locations in unit XII.

Results from Leg 176 suggest the Hole 735B section was not formed in a steady-state magma chamber as there is no evidence of cumulate layering. Instead this crustal section was probably formed by continuous intrusion of small magma bodies (Dick, Natland, Miller *et al.*, in press). However, still no evidence has been found of the location and nature of the crust-mantle boundary in this area.

#### **5.4.2. Structural geology of the Leg 176 core**

This study is only concerned with macroscopic structural features that are visible on the scanned core images. Many of the structural features observed by the Shipboard Scientific Party are not visible on the core images due to their small size.

The Leg 176 core was extensively studied by the structural geology team of the Shipboard Scientific Party (Dick, Natland, Miller *et al.*, in press). Their results are summarised below :

(a) Magmatic structures: - 22 % of the recovered Leg 176 material contains a magmatic foliation, due to the preferred orientation of plagioclase and pyroxene crystals. The majority of these show only a weak foliation.

(b) Veins : - In the upper part of the hole (0 - 800 mbsf) vein intensity fluctuates but generally decreases with increasing depth. Seventeen different types of veins were identified by the Shipboard Scientific Party. These were divided into 4 main groups:

(1) Magmatic veins - include compound felsic and plagioclase  $\pm$  clinopyroxene  $\pm$  amphibole veins. Felsic veins comprise only 4.08 % of the veins recorded in the Leg 176 core, however, they are volumetrically important due to their large widths and lengths (Dick, Natland, Miller *et al.*, in press). They are usually associated with plagioclase  $\pm$  amphibole veins. Both these vein types decrease in abundance downhole.

(2) Amphibole veins - These comprise 17 % of the total number of veins but most are very fine, generally < 0.5 mm in width. They often form complex vein networks. Most of the veins are subvertical and are associated with highly deformed areas. Again, their abundance decreases with depth.

(3) Carbonate veins - most of which consist of calcite. Carbonate veins comprise 9.1 % of the recorded veins, most of which are concentrated in the section between 500 and 600 mbsf. This area appears to have been affected by low temperature oxidative alteration.

(4) Smectite / zeolite veins - Smectite veins are the most abundant vein type in the Leg 176 core, comprising 47 % of the total number of veins. The concentration of smectite veins is highest in two sections, 573 to 833 mbsf and 1054 to 1500 mbsf.

### 5.4.3. Downhole logging on Leg 176

Hole 735B was logged before and after drilling on Leg 176. The hole was logged at the start of the leg to establish whether conditions in the borehole had changed substantially since Leg 118; two tool strings were deployed during this first logging run (Dick, Natland, Miller *et al.*, in press):

- Density (HLDS) - Porosity (APS) - Resistivity (DLL) - Spectral Gamma-Ray (HNGS) - Temperature (TLT). Good quality porosity, temperature, shallow resistivity and gamma-ray measurements were obtained, however, the deep resistivity measurements were poor as was the density data at depths > 385 mbsf.
- Natural Gamma-Ray (NGT) - Centraliser - Dipole Sonic Imager (DSI) - Formation Microscanner (FMS). Problems were encountered with the FMS data during this logging run, saturation of the data occurred resulting in very poor quality images and, in addition, telemetry was lost for the entire tool string at 275 mbsf.

The hole was also logged after drilling on Leg 176. Four tool strings were deployed during this second logging run (Dick, Natland, Miller *et al.*, in press):

- HNGS - Bowspring - APS - Caliper - HLDT. Good quality density, porosity and gamma-ray data were obtained from 50 (bottom of the BHA) to 595 mbsf.
- NGT - Centraliser - DSI - FMS. Good quality sonic data was obtained but similar problems occurred with the FMS, to those experienced in the first logging run.
- NGT - GPIT - DLL. Good shallow and deep resistivity measurements were acquired from 50 to 595 mbsf.
- VSP

(for an explanation of logging tool acronyms, refer to Appendix A)

### 5.4.3.1 Logging Results

A selection of the downhole logs obtained on Leg 176 are shown in Figures 5.5 and 5.6. This set of logs includes data for the section of the borehole drilled on Leg 118. Due to breakage of the drillpipe blocking the borehole, data is only available from 500 to 595 mbsf (Dick, Natland, Miller *et al.*, in press). Hence only a small proportion of the newly drilled section has available log data.

Resistivity in the hole varies from 0.1 to approximately 37,000  $\Omega\text{m}$ . Both the shallow (LLS) and deep (LLD) laterolog measurements show similar variations downhole (Dick, Natland, Miller *et al.*, in press). Particularly noticeable is the large decrease in resistivity seen in Unit 4, 230 to 280 mbsf, this unit is characterised by highly conductive Fe-Ti oxide gabbros.

The downhole variation in porosity is shown in Figure 5.5.b. Porosity in Hole 735B ranges from < 1 to 58 %. Porosity is relatively low for the majority of the borehole as the core contains predominantly massive olivine gabbro with relatively few fractures. However, a number of peaks can be seen in the data, the largest peak in porosity is as at approximately 565 mbsf, here, porosity is up to 58 %. This large peak in porosity is mirrored by a trough in the density data at the same depth. The downhole density effectively shows the reverse profile of the porosity log, where porosity is high, density is low, and vice versa. The porosity of the core is determined by lithology and the intensity of fracturing, most of the peaks in the porosity data represent more intensely fractured gabbro sections. Density is at its highest in the Fe-Ti oxide gabbros of Unit 4 (230 to 280 mbsf), the contact between Unit 4 and Unit 5 is marked by an abrupt decrease in density. Further troughs in the density data occur where fracturing or faulting is high

The logs for just the section drilled on Leg 176 are shown in Figure 5.6. The logs show clearly a section of the borehole, from 562.5 to 565 mbsf, with higher porosity and lower density and resistivity than the rest of the section. This has been interpreted by the structural geology team of the shipboard scientific party as an extensively faulted zone (Dick, Natland, Miller *et al.*, in press). A smaller peak in porosity is seen at 550 mbsf, corresponding with troughs in density and resistivity. This corresponds to an intensely fractured section of core (Dick, Natland, Miller *et al.*, in press).

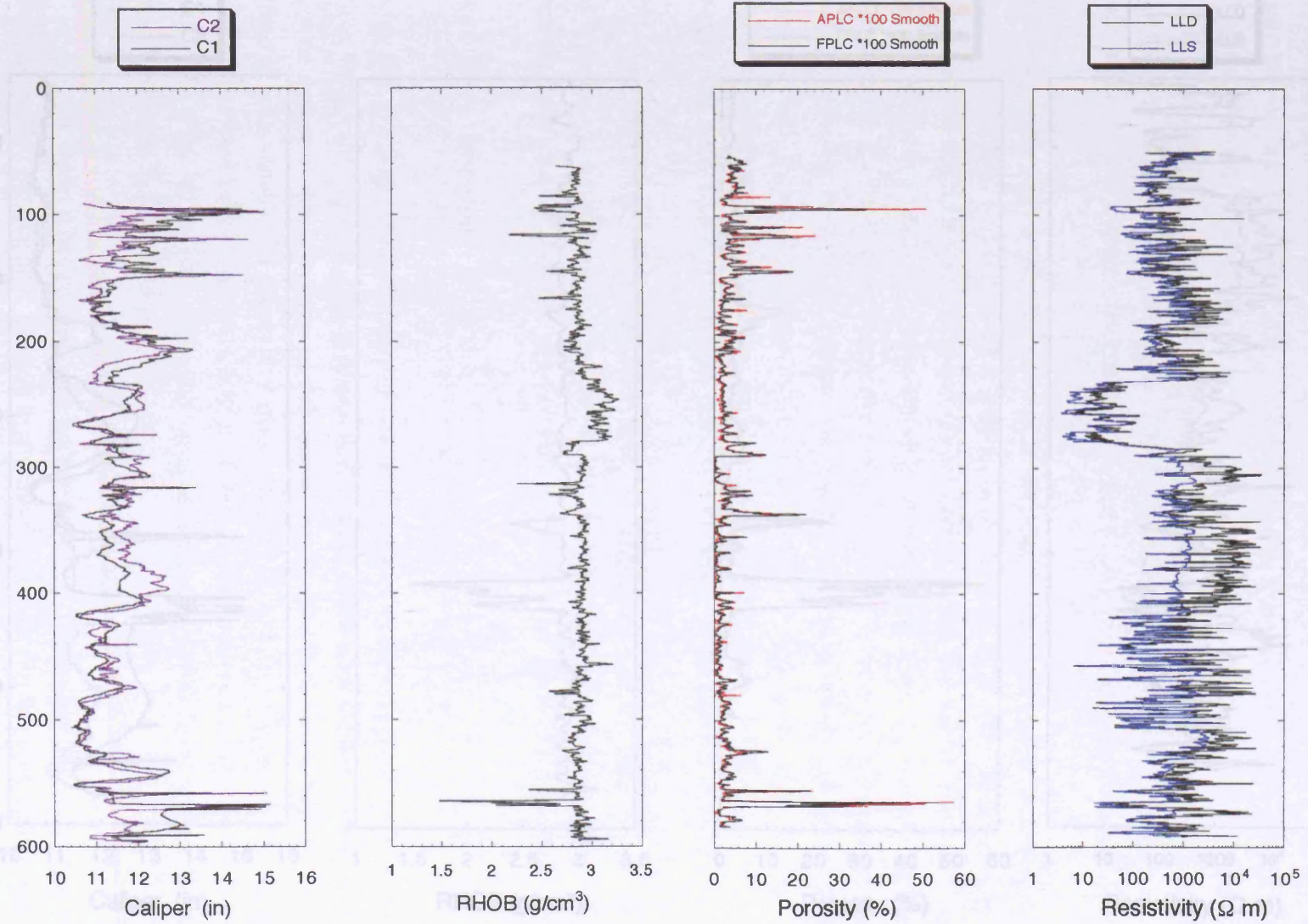


**Figure 5.5.** Downhole logs for Hole 735B. An explanation of logging tool acronyms is given in Appendix A.

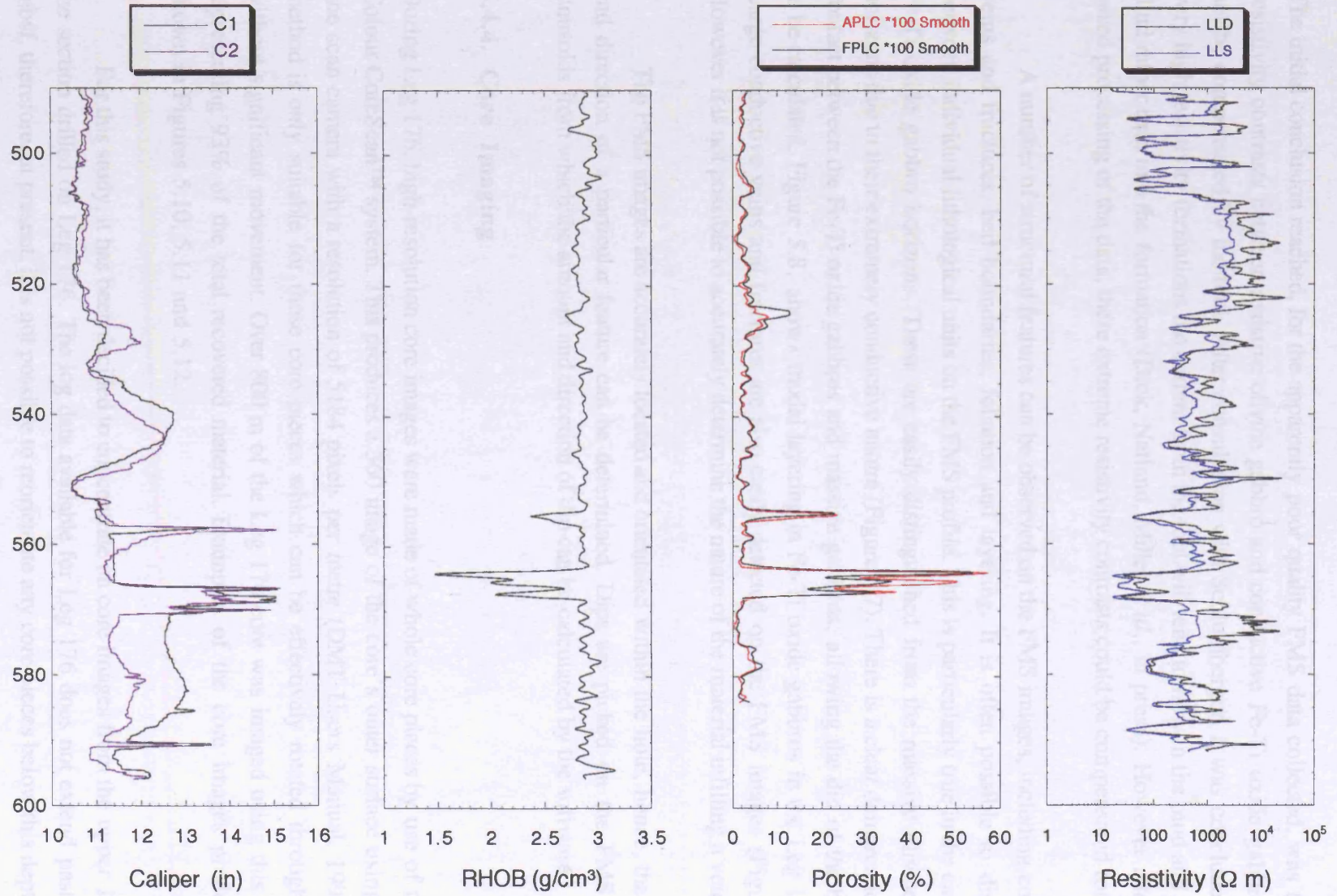


Figure 5.6. Downhole logs for borehole section drilled during Leg 176

#### 5.4.3.2 FMS Data

The initial conclusion reached, for the apparently poor quality FMS data collected, was that large resistivity contrasts between resistive olivine gabbro and conductive Fe-Ti oxide gabbros could not be compensated by the tool. After consultation with Schlumberger, it was concluded that in very high resistivity formations the current from the tool will tend to flow in the mud and borehole fluid rather than into the formation (Dick, Natland, Miller *et al.*, in press). However after shore-based processing of the data, these extreme resistivity contrasts could be compensated for.

A number of structural features can be observed on the FMS images, including conductive veins and fractures, bed boundaries, foliation and layering. It is often possible to distinguish between individual lithological units on the FMS profile. This is particularly true in the case of the Fe-Ti oxide gabbro horizons. These are easily distinguished from the massive olivine gabbro horizons due to their extremely conductive nature (Figure 5.7). There is a clear demarcation of the contact between the Fe-Ti oxide gabbros and massive gabbros, allowing the dip of the boundary to be calculated. Figure 5.8. shows modal layering in Fe-Ti oxide gabbros in the Leg 118 core. Large conductive veins and fractures are also easily detected on the FMS images (Figure 5.9). However it is not possible to accurately determine the nature of the material infilling a vein.

The FMS images are accurately located and orientated within the hole, hence, the true dip and direction of a particular feature can be determined. Dips are picked on the FMS data as sinusoids from which the amount and direction of dip can be calculated by the software.

#### 5.4.4. Core Imaging

During Leg 176, high-resolution core images were made of whole core pieces by use of the DMT Colour CoreScan™ system. This produces a 360 image of the core's outer surface using a CCD line scan camera with a resolution of 5184 pixels per metre (DMT Users Manual, 1996). This method is only suitable for those core pieces which can be effectively rotated throughout 360 without significant movement. Over 800 m of the Leg 176 core was imaged using this method, representing 93% of the total recovered material. Examples of the core images produced are shown in Figures 5.10, 5.11 and 5.12.

For this study, it has been decided to concentrate on core images from the upper 100 m of the section drilled on Leg 176. The log data available for Leg 176 does not extend past 595.88 mbsf, therefore, at present, it is not possible to reorientate any core pieces below this depth.

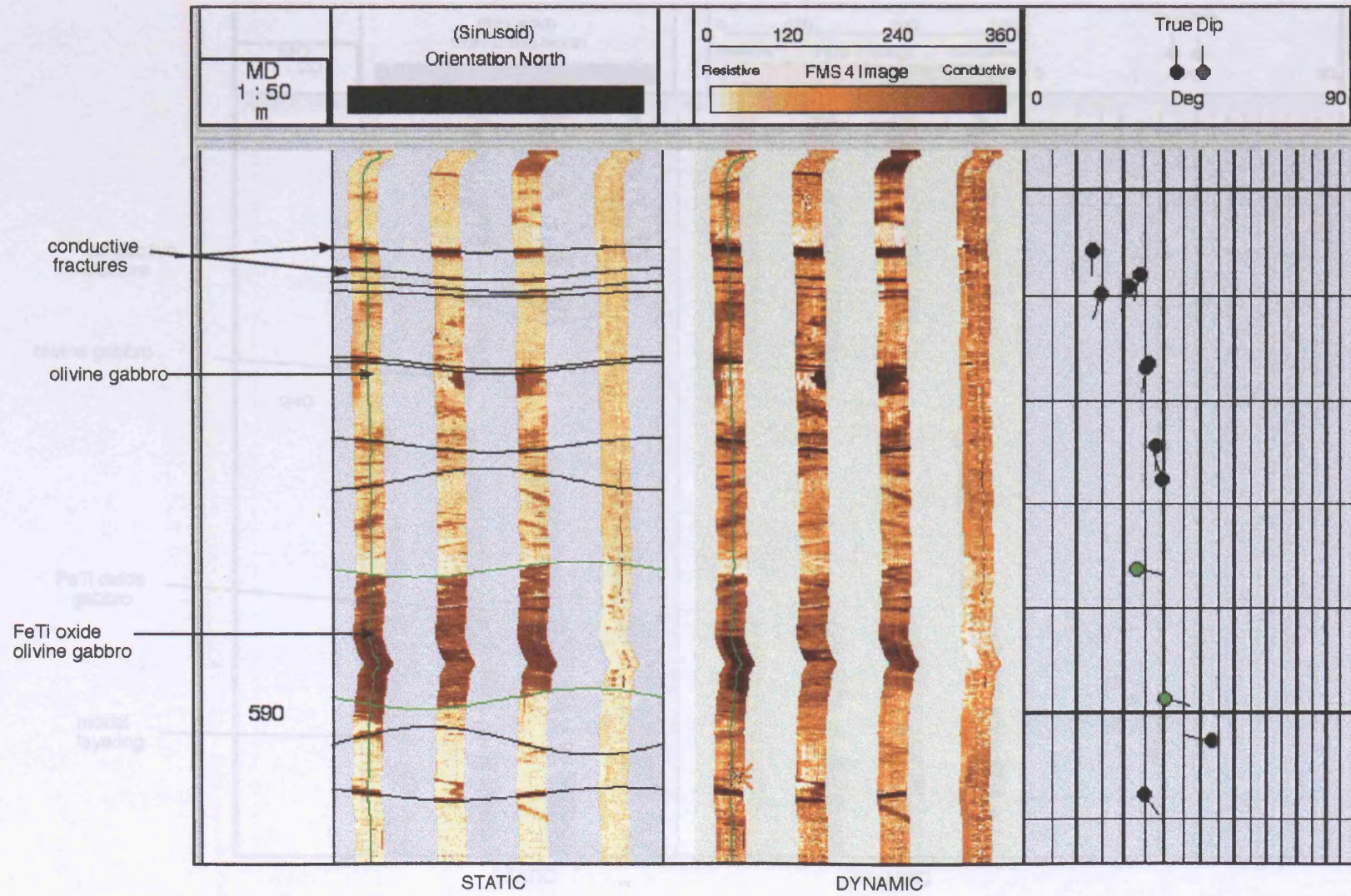


**Figure 5.7.** FMS image showing a FeTi oxide olivine gabbro layer within olivine gabbros. The olivine gabbro contains a number of fractures.

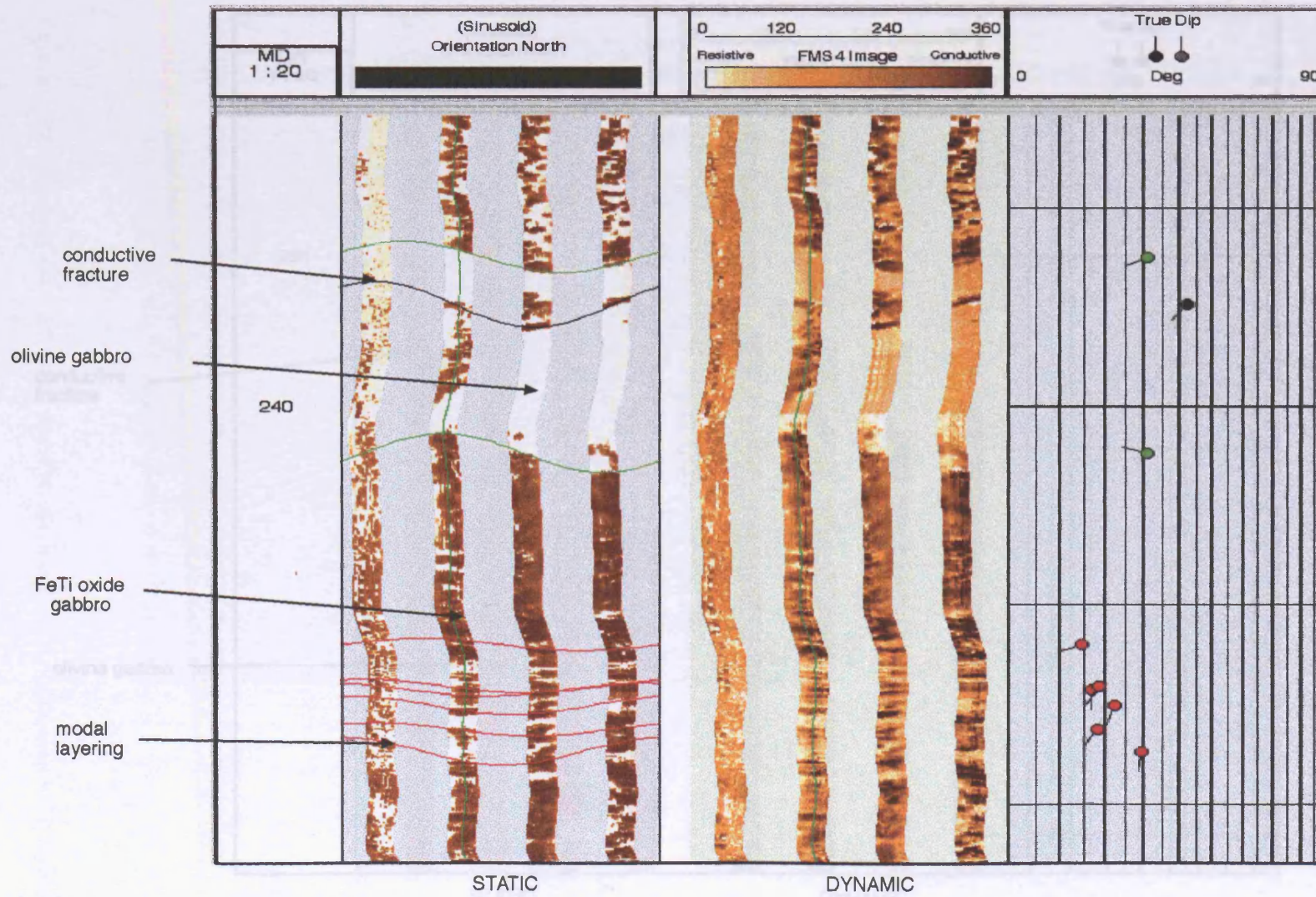


Figure 5.8. FMS image showing modal layering in FeTi oxide gabbros

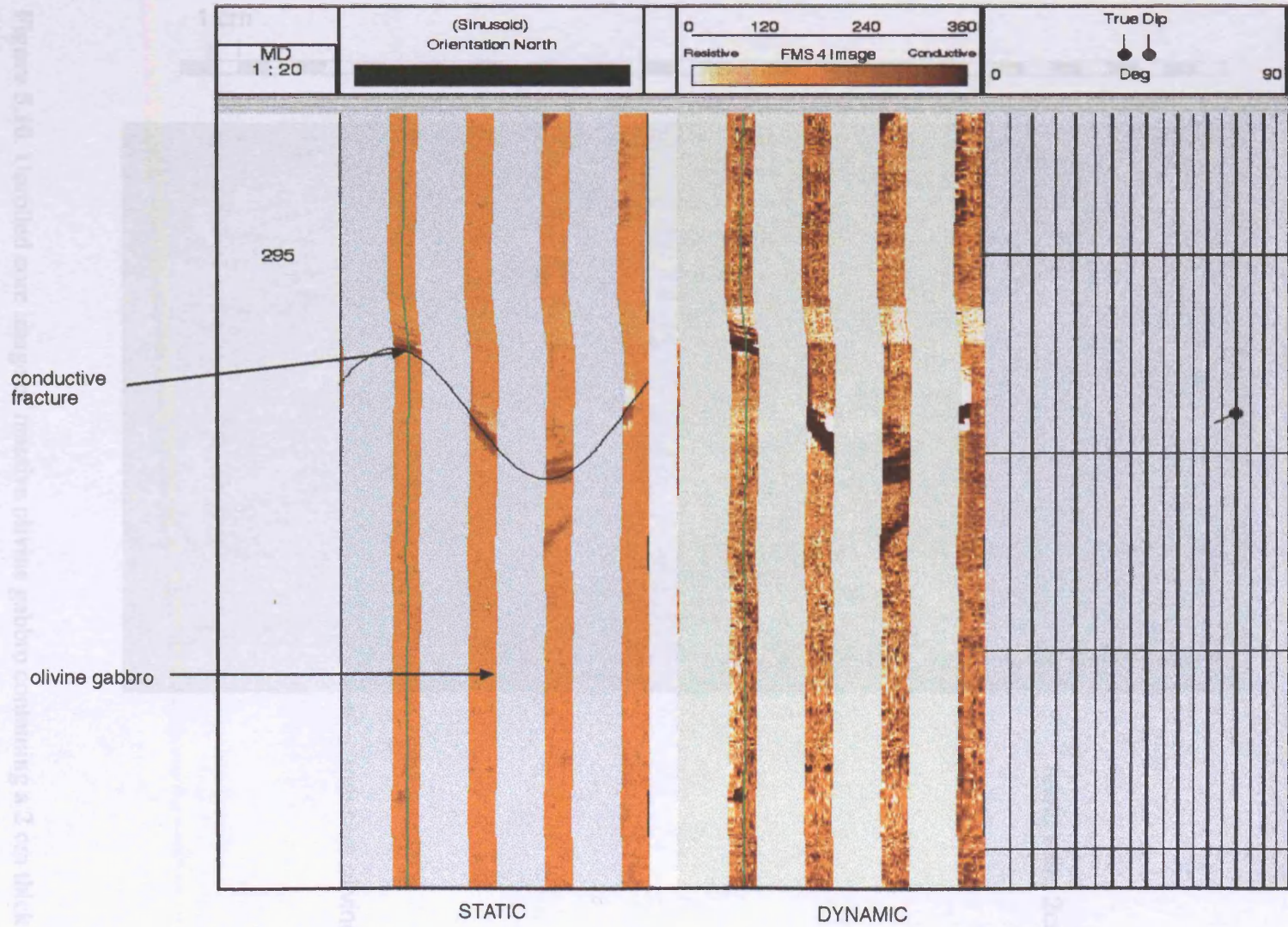
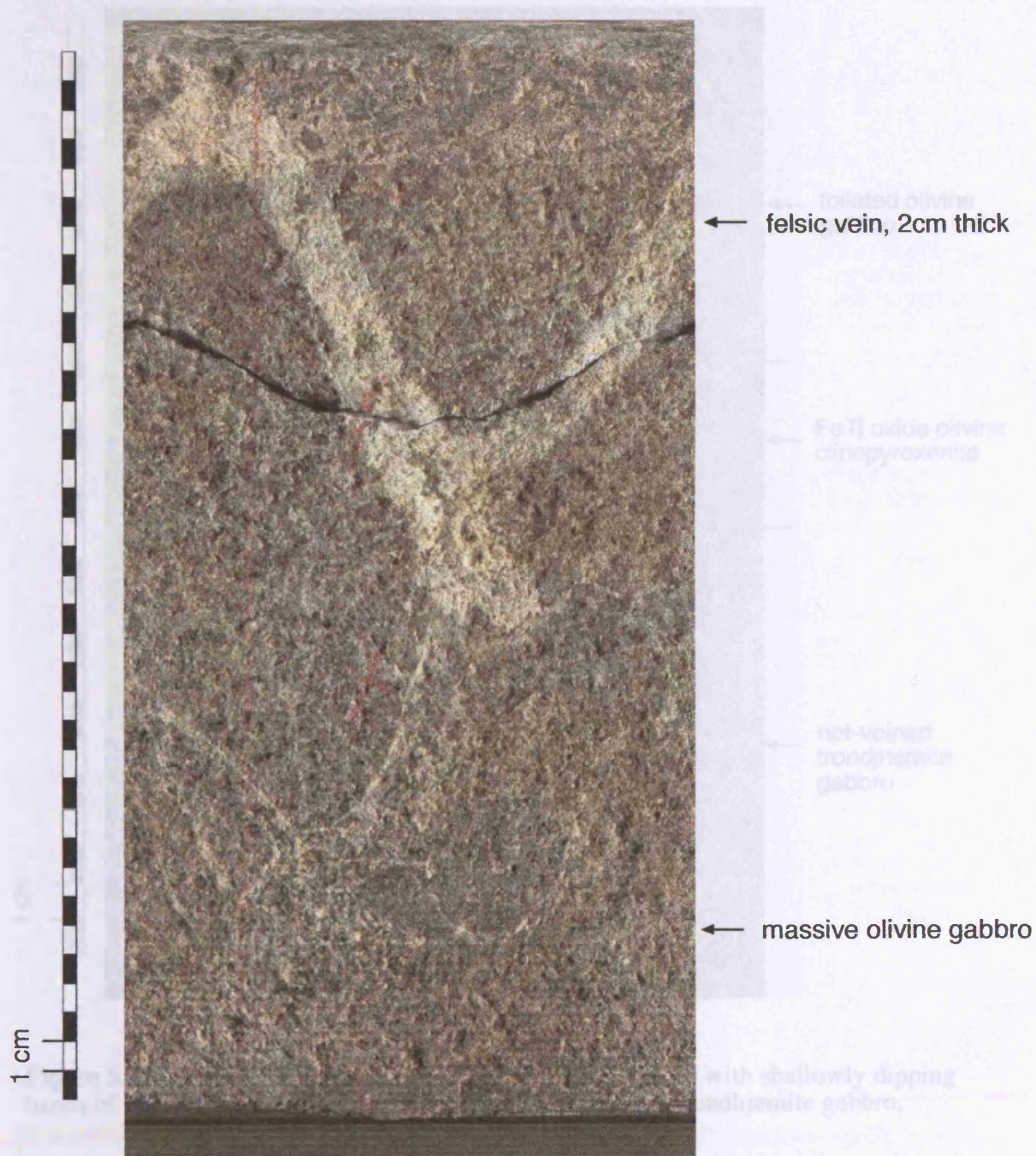


Figure 5.9. FMS image showing a conductive fracture in olivine gabbro

176-735B-109R-1 Piece 2A



**Figure 5.10.** Unrolled core image of massive olivine gabbro containing a 2 cm thick felsic vein.

176-735B-135R-1 Piece 2F

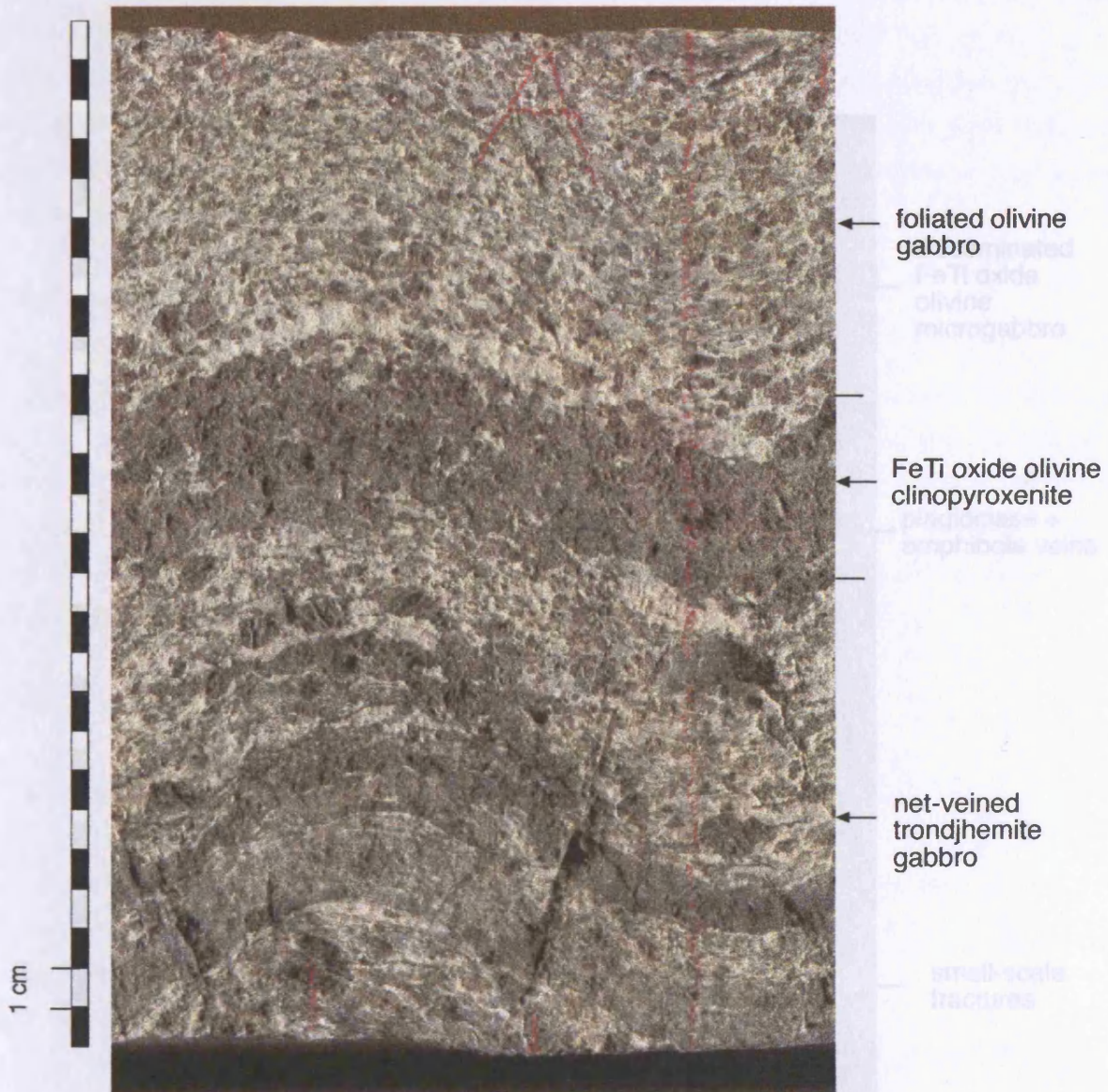


**Figure 5.11.** Unrolled core image of laminated olivine gabbro with shallowly dipping bands of FeTi oxide olivine clinopyroxenite and net-veined trondjemite gabbro.

Figure 5.12: Unrolled core image of laminated FeTi oxide olivine microgabbro containing 0.2-0.6 wt% pyroxene + amphibole veins and small-scale fractures

176-735B-142R-1 Piece 6A

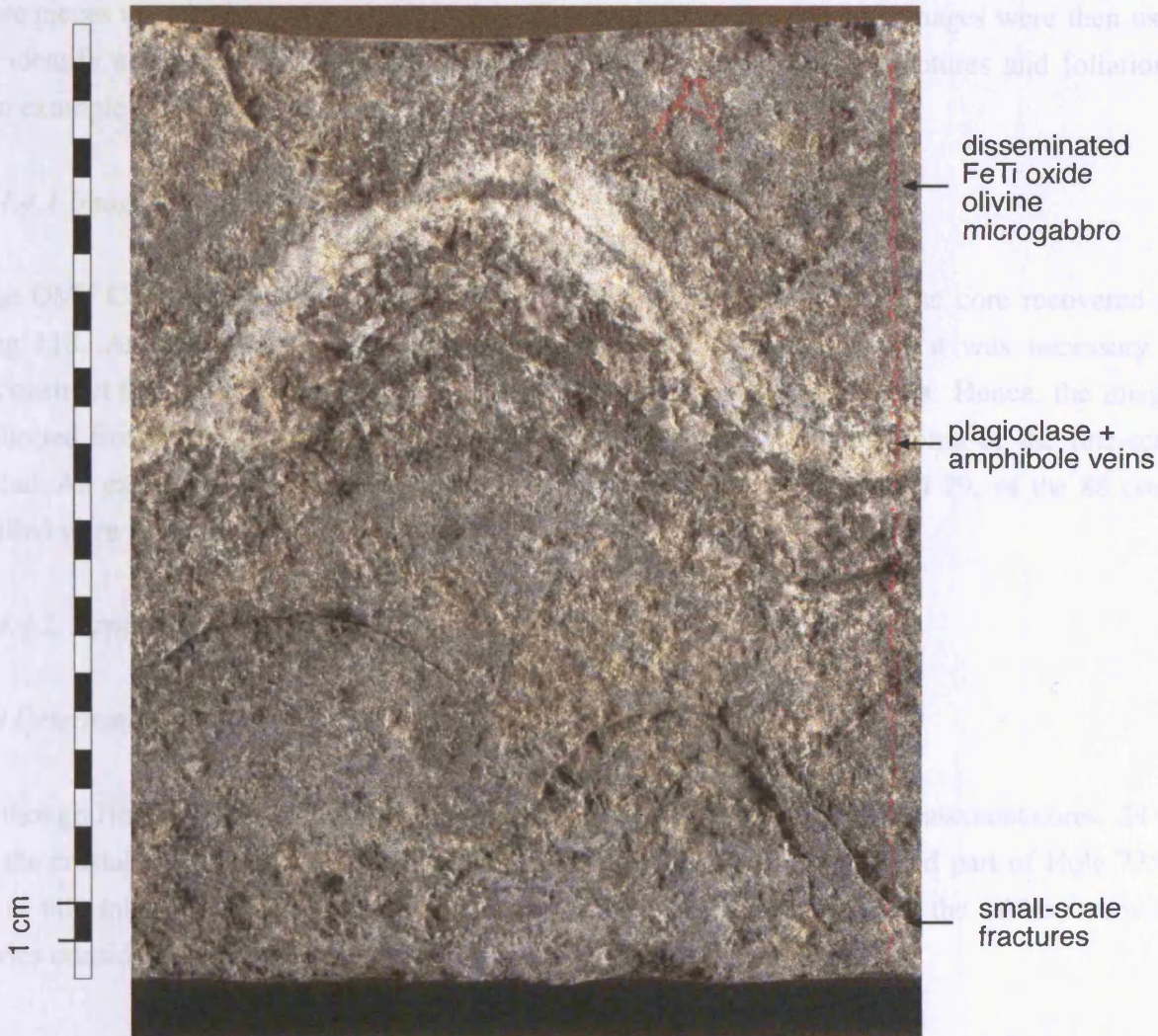


**Figure 5.12.** Unrolled core image of disseminated FeTi oxide olivine microgabbro containing a 0.2 - 0.6 mm thick plagioclase + amphibole veins and small-scale fractures

The images obtained by this method were then reconstructed into core barrel lengths using the software DMT Corelog™. Each image is loaded into the software separately. An example of the imported core images prior to integration into core barrel lengths is shown in Figure 5.13. The top and bottom of each piece was then selected as a sinusoid. This allows for the trimming of any superfluous material from the core image. Each piece was then fitted to the one preceding it. The software allows a gap to be left if a core image is absent. A red china marker line, marked on the core by the structural geology team prior to splitting, was used to rotate each image so that all the core pieces were in their curated orientation. The reconstructed core barrel images were then used to identify and measure structural features in the core, including veins, fractures and foliations. An example is shown in Figure 5.14.

#### *5.4.4.1 Imaging of Leg 118 core*

The DMT Colour CoreScan was also used to image selected pieces from the core recovered on Leg 118. As the Leg 118 core has been split and extensively sampled, it was necessary to reconstruct the whole core using foam spacers, shrink wrap and elastic bands. Hence, the images collected from the Leg 118 core are of a much poorer quality obscuring some of the fine-scale detail. An example of the images obtained is shown in Figure 5.15. In total 29, of the 88 cores drilled were imaged.

#### *5.4.4.2. Applications of the core image and log data*

##### *(a) Determination of missing core material*

Although Hole 735B has relatively high core recovery with respect to other basement cores, 24 % of the crustal section is still unaccounted for. The core recovery for the logged part of Hole 735B (0 to 600 mbsf) is shown in Tables 5.1.1 and 5.2.2. As can be seen from the tables, recovery varies considerably between individual cores.

Several cores in this upper section have core recoveries > 100 % because 9.5 m was cored but > 9.5 m was actually recovered. This can occur when the core barrel contains material cored earlier and left behind after previous coring runs.

For those cores with less than average core recovery, the FMS images were compared with the visual core descriptions and scanned core images in an attempt to determine what material was preferentially not being recovered. Cores 1D to 11D all have  $\leq 50$  % core recovery, as this uppermost section of core contains highly altered metagabbros and in addition, these cores were

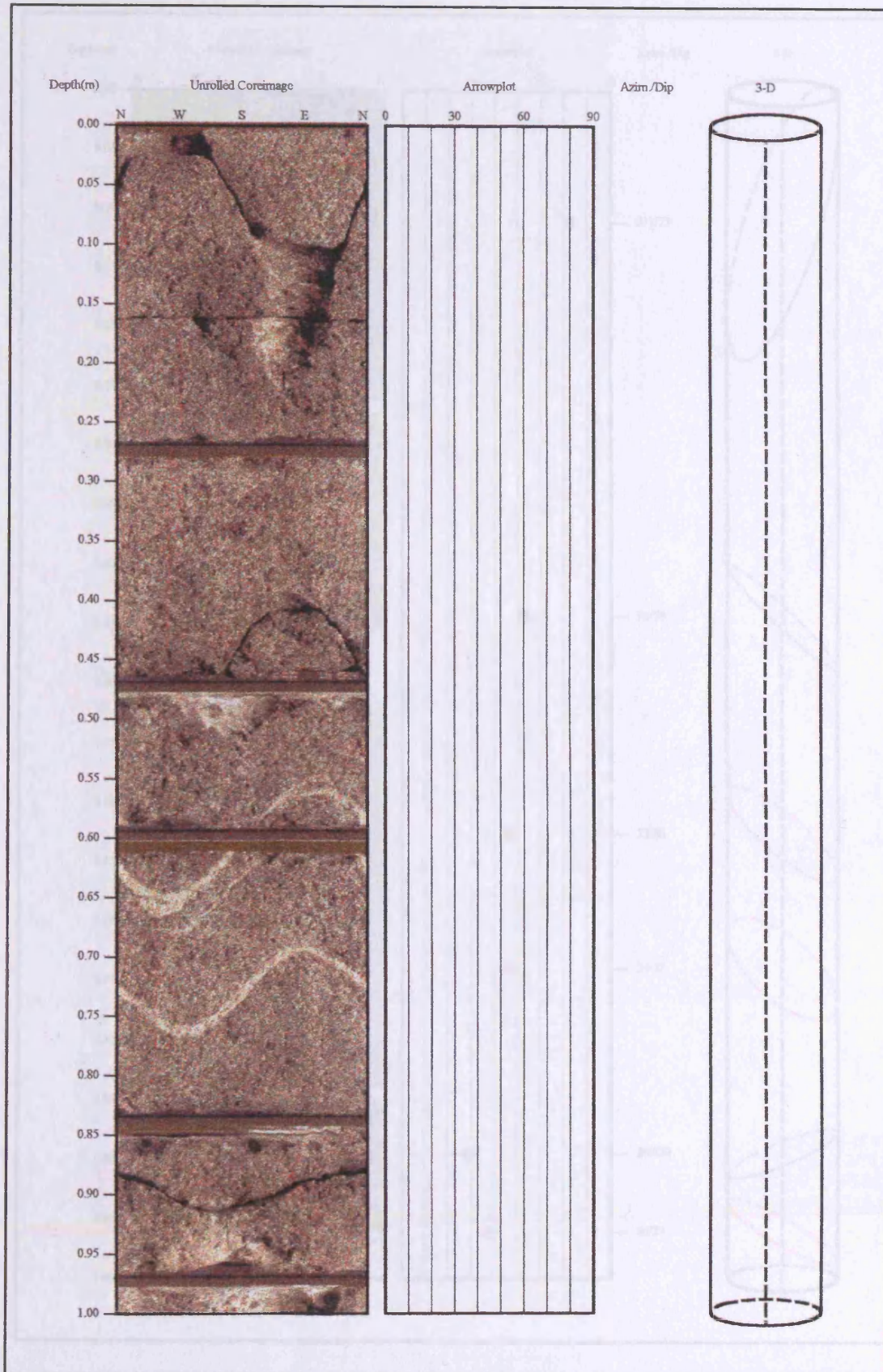
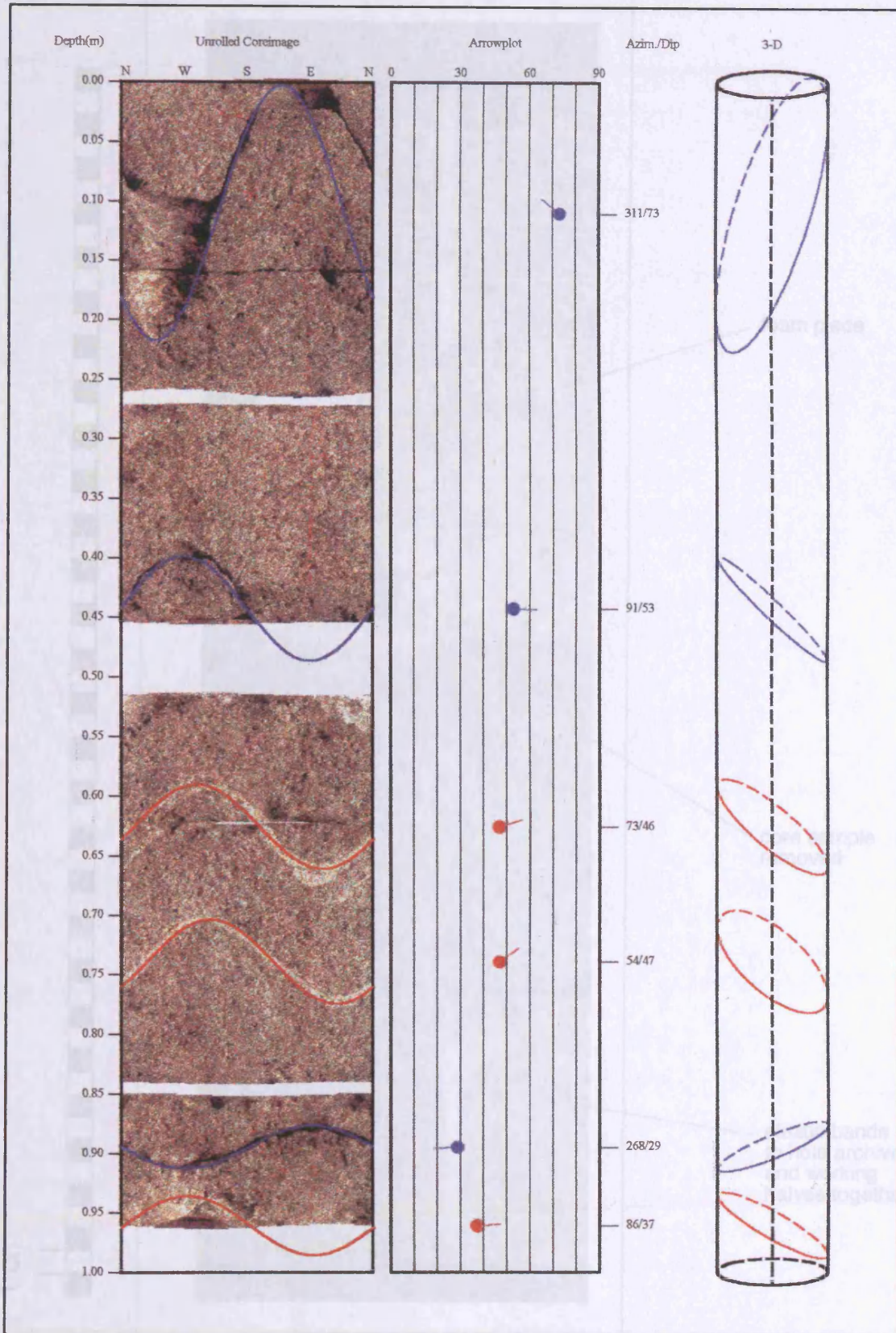
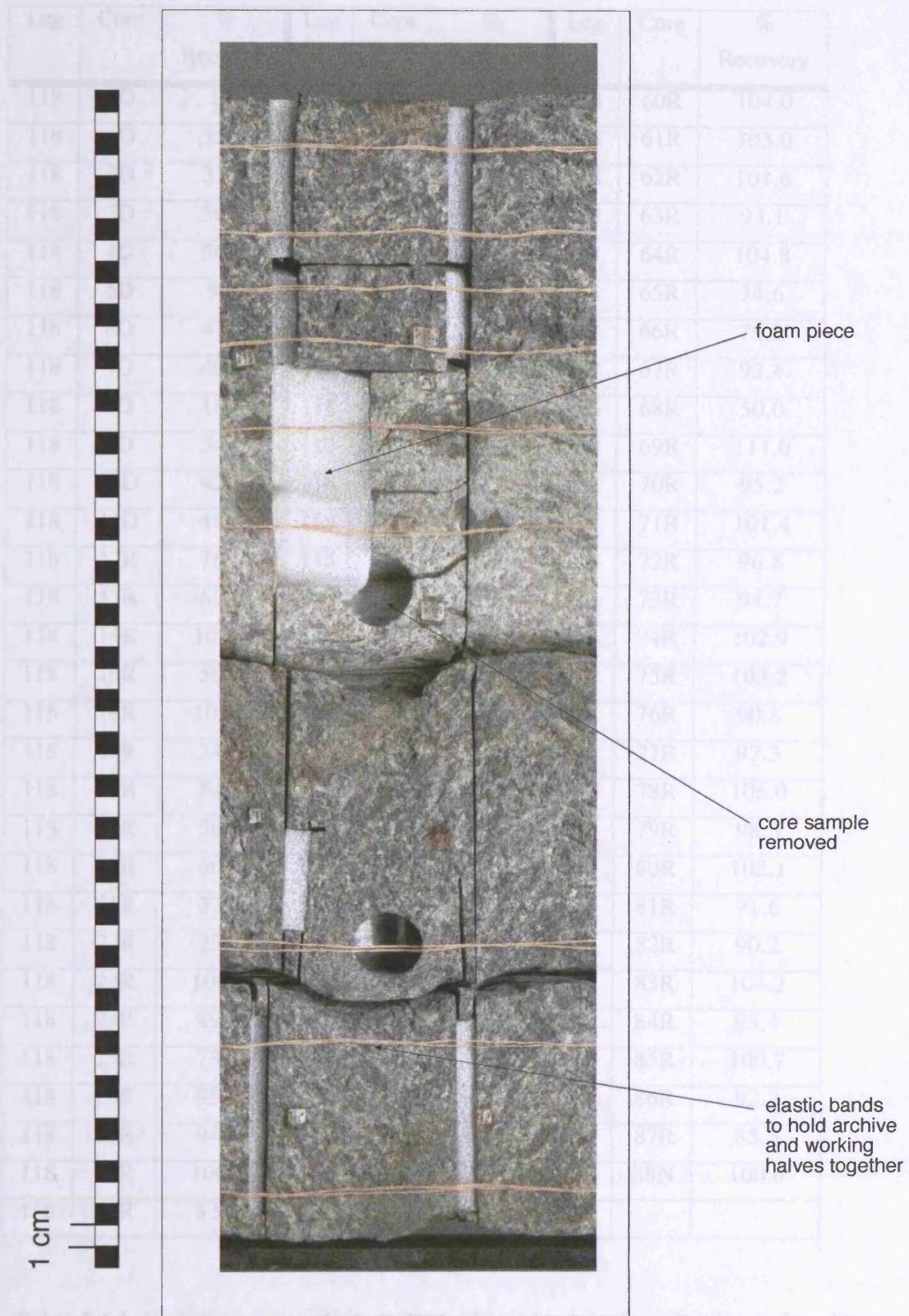


Figure 5.14. Reconstructed core barrel of core 99R-4 from ODP Hole 735B using the DMT CoreLog™. Software used is DMT CoreLog™.



**Figure 5.14.** Reconstructed core barrel of core 99R-4 from ODP Hole 735B using the DMT software CoreLog™. Dips of fractures (blue) and veins (red) are shown. The core pieces have been rotated so that the red marker line, marked on the core by the structural geology team is orientated to the east.



**Figure 5.15.** Example of a reconstructed core piece from the Hole 735B core drilled on Leg 118 (Sample 118-735B-28R-1 #7). Foam pieces fill the gaps where slabbed core samples have been removed and the archive and working halves are held together by elastic bands

Leg	Core	% Recovery	Leg	Core	% Recovery	Leg	Core	% Recovery
118	1D	1.4	118	30R	82.8	118	60R	104.0
118	1D	35.4	118	31R	103.2	118	61R	103.0
118	2D	37.5	118	32R	93.0	118	62R	101.6
118	3D	50.0	118	33R	100.0	118	63R	93.1
118	4D	50.0	118	34R	79.2	118	64R	104.8
118	5D	9.3	118	35R	106.3	118	65R	74.6
118	6D	47.0	118	36R	95.6	118	66R	79.0
118	7D	40.6	118	37R	77.6	118	67R	93.4
118	8D	18.6	118	38R	105.6	118	68R	50.0
118	9D	34.0	118	39R	84.8	118	69R	111.0
118	10D	42.0	118	40R	98.4	118	70R	95.2
118	11D	40.0	118	41R	83.6	118	71R	101.4
118	12R	78.6	118	42R	102.0	118	72R	96.8
118	13R	63.0	118	43R	93.6	118	73R	94.7
118	14R	101.6	118	44R	98.6	118	74R	102.9
118	15R	50.2	118	45R	103.8	118	75R	103.2
118	16R	101.2	118	46R	103.0	118	76R	90.8
118	17R	24.0	118	47R	97.4	118	77R	97.3
118	18R	54.8	118	48R	95.2	118	78R	106.0
118	19R	58.7	118	49R	126.0	118	79R	98.3
118	20R	60.0	118	50R	105.6	118	80R	102.1
118	21R	57.2	118	51R	89.2	118	81R	91.6
118	22R	73.2	118	52R	97.8	118	82R	90.2
118	23R	100.0	118	53R	104.6	118	83R	104.2
118	24R	89.4	118	54R	99.7	118	84R	93.4
118	25R	73.8	118	55R	93.4	118	85R	100.7
118	26R	95.7	118	56R	83.8	118	86R	92.2
118	27R	94.2	118	57R	93.0	118	87R	85.5
118	28R	100.6	118	58R	74.8	118	88N	100.0
118	29R	83.2	118	59R	98.0			

**Table 5.1.1.** Core Recovery in Hole 735B for Leg 118. Data from Robinson, Von Herzen, Adamson *et al.* (1989).

drilled with a diamond core bit rather than the usual rotary core bit. This type of drill bit had a low coring rate and low core recovery and was consequently only used to a depth of 39.4 mbsf (Robinson, Von Herzen, Adamson *et al.*, 1989).

Leg	Core	% Recovery	Leg	Core	% Recovery
176	89R	68.3	176	98R	46.5
176	90R	102.9	176	99R	78.0
176	91R	61.1	176	100R	31.3
176	92R	43.7	176	101R	80.4
176	93R	111.6	176	102R	72.0
176	94R	43.5	176	103R	61.2
176	95R	81.1			
176	96R	34.9			
176	97R	104.0			

**Table 5.1.2.** Core recovery in Hole 735B for Leg 176. Data from Dick, Natland, Miller *et al.* (in press).

The majority of the cores with less than average core recovery are represented on the FMS images as areas of highly variable resistivity, comprising foliated or intensely fractured sections. The highest recovery occurs in the massive olivine gabbros which contain lower densities of fractures and are generally undeformed. Recovery is therefore biased towards the massive olivine gabbro sections, with the foliated and fractured horizons being underrepresented in the core to some degree. This may be significant in any attempts to constrain the structural and tectonic history of the core as a number of the key deformation zones may be absent from the core data. The use of FMS data may be essential, in this case, as it allows the determination of the dip and orientation of unrecovered structural features. However, the overall core recovery is high so probably very few lithological units are missing from the core.

*(b) Orientation and location of core pieces*

Any recovered core is not orientated therefore any structural directions cannot be known. This causes problems in interpretation of the tectonic setting of the site. If individual core pieces can be orientated using log data, dip directions can be determined allowing the tectonic setting to be constrained. Orientation and location of individual core pieces can be achieved by cross-

correlation of structural features on the FMS logs and core images. This is done visually by attempting to locate by eye a structure (with calculated dip) picked on the core images with the FMS profile. This is a long and time-consuming process as it is often difficult to find an exact match. Once a potential match has been found, the structures above and below are also compared to confirm the correlation. An example of this process is shown in Figures 5.16 to 5.18. A large fracture was identified in Core 77R-2 (Figure 5.16) the dip of which was calculated by the CoreLog software as 70°. This fracture is also clearly imaged on the FMS log at a depth of 404.80 mbsf (Figure 5.17). The dip and strike of this fracture has been calculated by GeoFrame as 70° and 260° respectively. The core piece can then be moved to its correct position in the core and rotated to its true orientation (Figure 5.18).

The core from Hole 735B provides an unique opportunity to develop this method of core location because of three main points:

- Hole 735B has relatively high core recovery, 86.8 % for Leg 118 and 86.3 % for Leg 176, giving a total core recovery of 86.6 %. The average core recovery for DSDP / ODP legs is only ~ 30 % (Brewer *et al.*, 1998). Hence, in the majority of cases, core piece orientation and location would be very difficult as low core recovery increases the uncertainty of core piece location. The ODP policy of moving all recovered core pieces to the top of the core barrel on curation means that in cores with low recovery, each piece may be several metres away from its correct stratigraphic depth.
- Core images are available for a large proportion of the Hole 735B core. The Leg 176 core was imaged prior to splitting and sampling.
- FMS data is available for the upper 600 m of Hole 735B, allowing for correlation of structures on the log data and core images.

#### *Limitations of this method*

(1) Scale : - Very small-scale features can be detected on both the core images and FMS logs including veins < 1 mm in size. However these may be difficult to observe with the human eye. Similarly large-scale fractures on the FMS log may not be seen in the core due to low recovery of such features.

(2) Identification of features : - It is difficult to distinguish between different types of veins on the FMS logs. At present there is no method for determining the contents of veins and fractures on the FMS data. On the core images veins can be compared with the core barrel sheets and it is possible to see the colour and nature of any infill.

(3) ODP Policy : - Even though the Leg 176 core has high recovery, 24 % of the borehole material is unaccounted for. ODP policy is to move all recovered material in a particular core to the top of the core barrel on curation. Core recovery varies widely between cores therefore in those

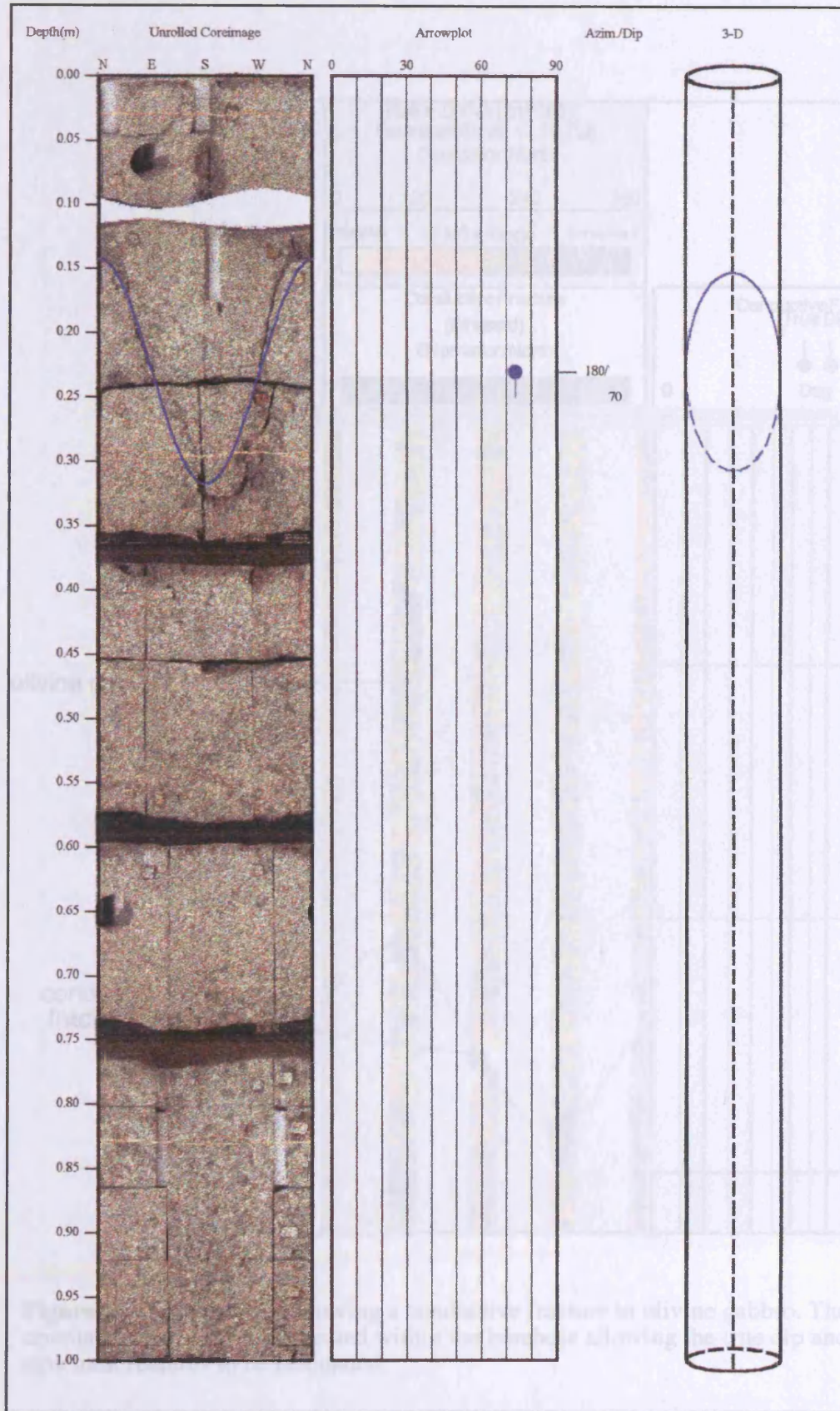


**Figure 5.16.** Core 77R-2 from ODP Hole 735B. A fracture dipping  $70^\circ$  has been picked using the DMT software CoreLog™. The true depth and strike of the fracture cannot be determined by core data alone.

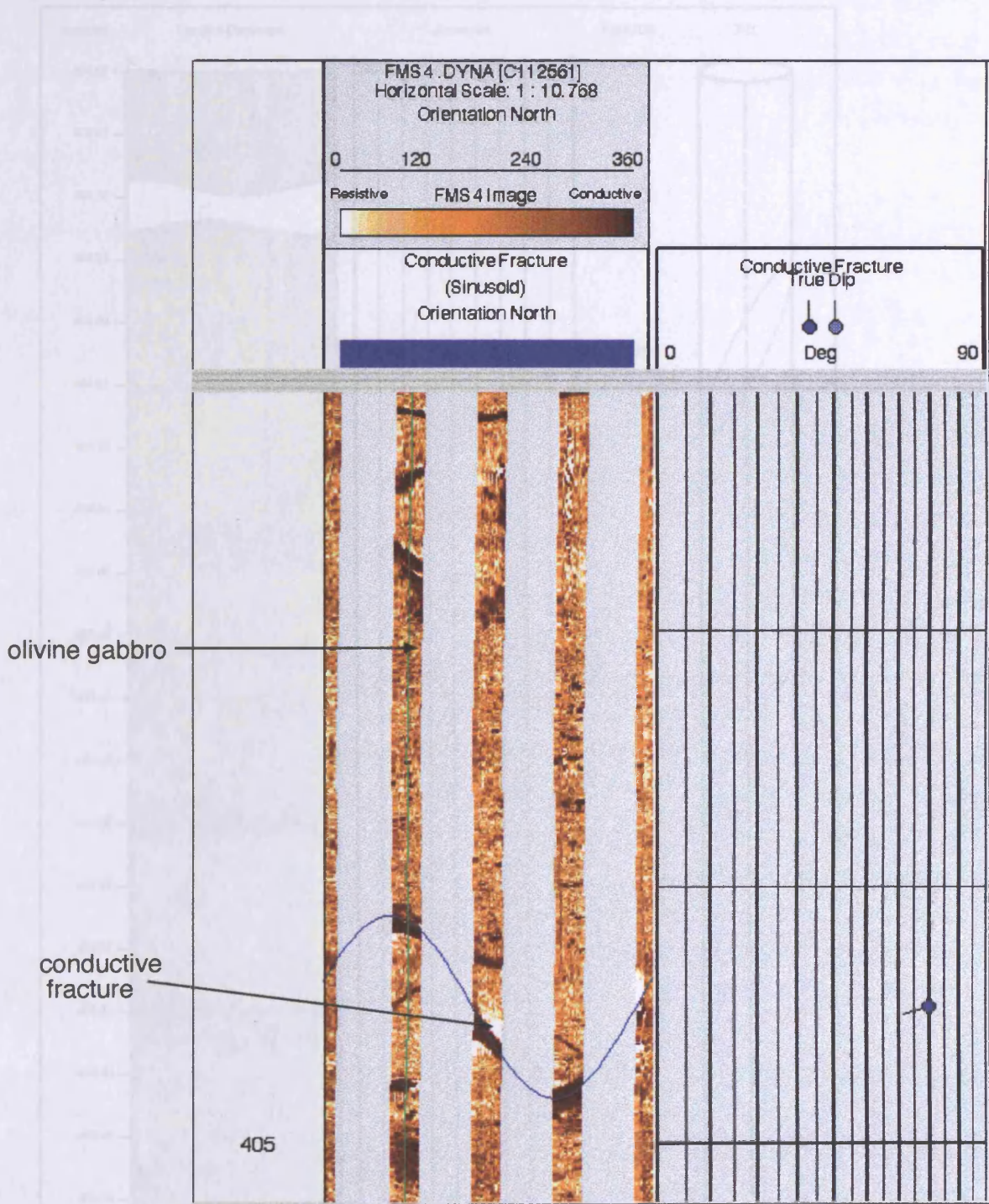


**Figure 5.17.** FMS image showing a conductive fracture in olivine gabbro. The FMS data is orientated and accurately located within the borehole allowing the true dip and strike of structural features to be calculated.

Figure 5.18. Orientation and location of the fractured piece in Core 77R-2 according to the information provided by the FMS data.

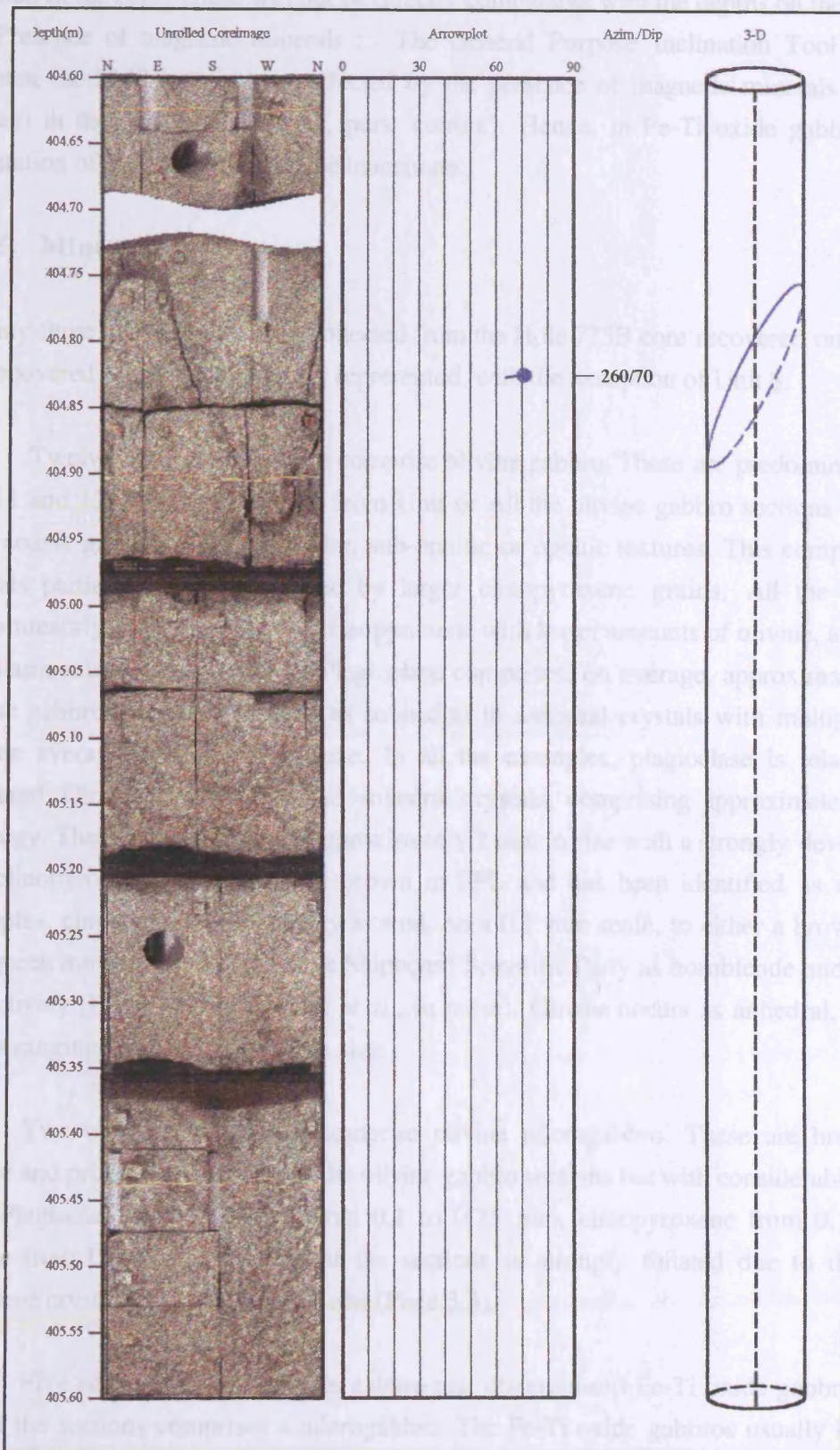


**Figure 5.18.** Orientation and location of the fractured piece in Core 77R-2 according to the information provided by the FMS data.

with low core recovery (some as low as 30 %) pieces may not be in their correct stratigraphic position in the core. These will not be directly comparable with the depths on the FMS logs.

(4) Presence of magnetic minerals : - The General Purpose Inclination Tool (GPIT) used to orientate the FMS logs may be affected by the presence of magnetic minerals (including Fe-Ti oxides) in the formation (Pezard, pers. comm.). Hence, in Fe-Ti oxide gabbro horizons, the orientation of the FMS logs may be inaccurate.

#### 5.4.5. Mineralogy

Twenty-three thin-sections were collected from the Hole 735B core recovered on Leg 176. All of the recovered lithological units are represented, with the exception of Unit 8.

Twelve of the thin-sections comprise olivine gabbro. These are predominantly from Units 10, 11 and 12, with one example from Unit 6. All the olivine gabbro sections have medium to very coarse grain-size with granular, sub-ophitic or ophitic textures. This comprises plagioclase crystals partially or fully enclosed by larger clinopyroxene grains. All the sections consist predominantly of plagioclase and clinopyroxene with lesser amounts of olivine, and in rare cases, small amounts of orthopyroxene. Plagioclase comprises, on average, approximately 50 % of the olivine gabbros. It occurs usually as subhedral to anhedral crystals with multiple twins. These are, on average, 1 to 2 mm in size. In all the examples, plagioclase is relatively fresh and unaltered. Clinopyroxene occurs as anhedral crystals, comprising approximately 40 % of the lithology. These are, on average, approximately 2 mm in size with a strongly developed cleavage. The clinopyroxene present is pale brown in PPL and has been identified as augite. In many examples, clinopyroxene is patchily altered, on a 0.1 mm scale, to either a brown material or a pale green mineral, identified by the Shipboard Scientific Party as hornblende and green actinolite respectively (Dick, Natland, Miller *et al.*, in press). Olivine occurs as anhedral, almost rounded grains ranging from 0.1 to 1 mm in size.

Two of the thin-sections comprise olivine microgabbro. These are broadly similar in texture and primary mineralogy to the olivine gabbro sections but with considerably smaller grain-size. Plagioclase ranges in size from 0.1 to 0.75 mm, clinopyroxene from 0.1 to 1 mm and olivine from 0.1 to 1 mm. One of the sections is strongly foliated due to the alignment of pyroxene crystals and plagioclase laths (Plate 5.3).

Five sections of Fe-Ti oxide gabbro and disseminated Fe-Ti oxide gabbro were studied, one of the sections comprises a microgabbro. The Fe-Ti oxide gabbros usually have granular to ophitic textures with highly variable grain-size, ranging from 0.1 to 7 mm. The primary mineralogy is broadly similar to the olivine gabbros, however, this lithology contains more orthopyroxene (up to 5 %) and Fe-Ti oxides (5 %). The Fe-Ti oxides occur as small, anhedral

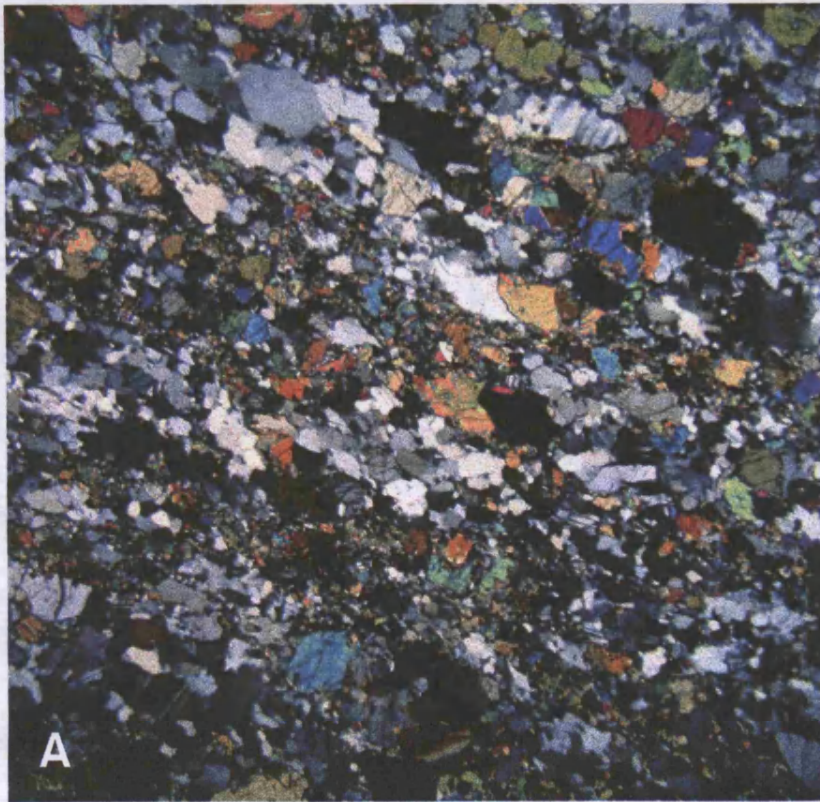


**Plate 5.3.** Thin-section photomicrograph in cross-polarised light of a foliated metagabbro (HAG-15). The foliation is due to the alignment of plagioclase and pyroxene grains. Field of view is 12 mm.

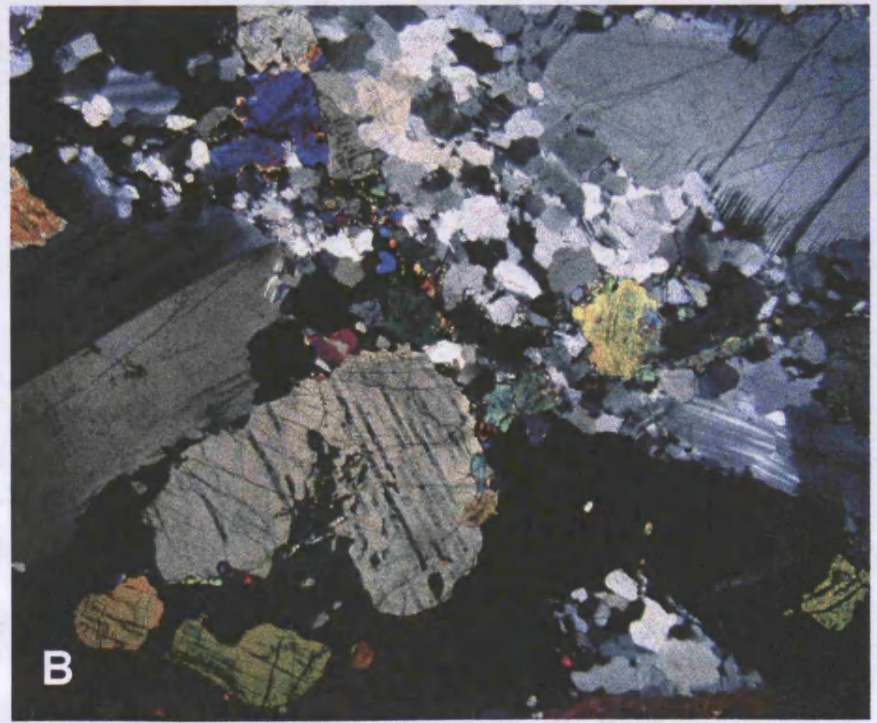


**Plate 5.4.** Thin-section photomicrograph in cross-polarised light of the contact between a Fe-Ti oxide gabbro and a less Fe-Ti oxide-rich olivine gabbro (HAG-10). Field of view is 12 mm.

grains and are usually found filling fractures and between mineral grains (Plate 5.4). The Fe-Ti oxide gabbros appear to have suffered a greater degree of alteration than the olivine gabbros, in one particular example, (HAG-5), large deformed crystals of plagioclase show undulose extinction.

Clinopyroxene and orthopyroxene are usually extensively replaced by green / brown amphibole. Olivine is altered at the edges of grains to pale green - brown amphibole and is also often replaced along fractures by opaques and red / brown iddingsite. In the heavily altered HAG-5 olivine crystals have been almost entirely replaced, with only the original core of the olivine crystal remaining. A number of Fe-Ti oxide gabbro sections are cut by small veins, 0.1 to 1 mm thick which are filled with either brown biotite or pale to deep green amphibole. Any mineral grains close to the veins have been altered. The disseminated Fe-Ti oxide olivine microgabbro section (HAG-9) has a similar mineralogy but is finer-grained (average grain-size is 0.25 to 0.75 mm). The section is weakly foliated due to the alignment of plagioclase laths.

Two sections comprise **gabbro**, these are similar to the olivine gabbros in texture and grain-size but contain considerably less olivine (0 to 2 %).

One example of **gabbronorite** was studied (HAG-4), this comprised a coarse-grained section with granular textures containing plagioclase, olivine, clinopyroxene and orthopyroxene with an average grain size of 2 to 3 mm. The olivine grains are heavily fractured and filled by opaque minerals. The pyroxene grains are also altered, grain edges are often replaced by brown biotite and amphibole, some examples show evidence of deformation, with undulose extinction.

HAG 1 comprises **troctolite**. This lithology contains mostly plagioclase (65 %) and olivine (35 %) with small amounts of clinopyroxene (< 5 %). The section also contains some opaque grains (< 1 %). Plagioclase occurs as anhedral to subhedral crystals some of which show undulose extinction. Olivine occurs as rounded anhedral grains. The rare clinopyroxene crystals are pale brown in PPL. Edges of clinopyroxene grains are often altered to a brown amphibole.

#### 5.4.6. Geochemistry

##### 5.4.6.1. Review of shipboard scientific party results

Natland, Dick *et al.* (1998) divide the gabbros in Hole 735B into 5 chemical units, 250 to 450 m thick. Each of these chemical units is interpreted as a plutonic mass which become more differentiated towards the top of the unit, with more primitive and Mg-rich rocks at the base. The units consist of a number of smaller magma bodies which probably represent intrusive masses, intruded into either cold rocks or crystal mushes (Natland, Dick *et al.*, 1998).

Dick, Natland, Miller *et al.* (in press) note low concentrations of Y in the majority of the core indicating that many of the Hole 735B gabbros have significantly lower rare earth element (REE) abundances than commonly found in mantle magmas. From this, they conclude that substantial amounts of REE have been lost from the gabbros or are concentrated in the minor lithological units, confirmed by the high Y content observed in some Fe-Ti oxide gabbro horizons and felsic veins.

#### 5.4.6.2. Results from this study

In order to provide an overview of the downhole geochemistry of Hole 735B, core samples were taken from both the Leg 118 and Leg 176 cores. Major element oxide and trace element abundances in the Hole 735B core samples were determined by X-ray fluorescence spectrometry (XRF). Only 37 core samples were available for analysis therefore the data set was supplemented with the data from the PhD thesis of Pelling (1992).

##### (a) Downhole variations

Figures 5.19 and 5.20 show the downhole variations in major element oxides and selected trace elements, the chemical units designated by Natland, Dick *et al.* (1998) are indicated on the plots. Geochemical variability within the core is greatest to approximately 500 mbsf. Below this depth, concentrations become much more uniform, particularly at depths > 950 mbsf. Below 950 mbsf, the core is dominated by relatively uniform massive olivine gabbros with considerably less Fe-Ti oxide gabbro horizons, foliated gabbros and metagabbros.

##### Major element variations

Fe-Ti oxide gabbro horizons are easily detected on the downhole geochemical profiles, characterised by peaks in  $\text{Fe}_2\text{O}_3$ ,  $\text{TiO}_2$  and  $\text{MnO}$  and troughs in  $\text{SiO}_2$ ,  $\text{MgO}$  and  $\text{Al}_2\text{O}_3$ . Samples with particularly high  $\text{Fe}_2\text{O}_3$  and  $\text{TiO}_2$  occur in Unit IV, 230 to 280 mbsf, characterised by Fe-Ti oxide gabbros. A smaller peak at approximately 825 mbsf corresponds to a thin Fe-Ti oxide layer in massive olivine gabbro (Dick, Natland, Miller *et al.*, in press). Many of the small Fe-Ti oxide gabbro layers in the core are not evident on the downhole geochemistry resulting from sampling bias due to the small amount of core samples available.

##### Trace element variations

Sr is strongly incorporated into plagioclase during fractional crystallisation (Dick, Natland, Miller *et al.*, in press). and consequently is at its lowest concentrations in the Fe-Ti oxide gabbro

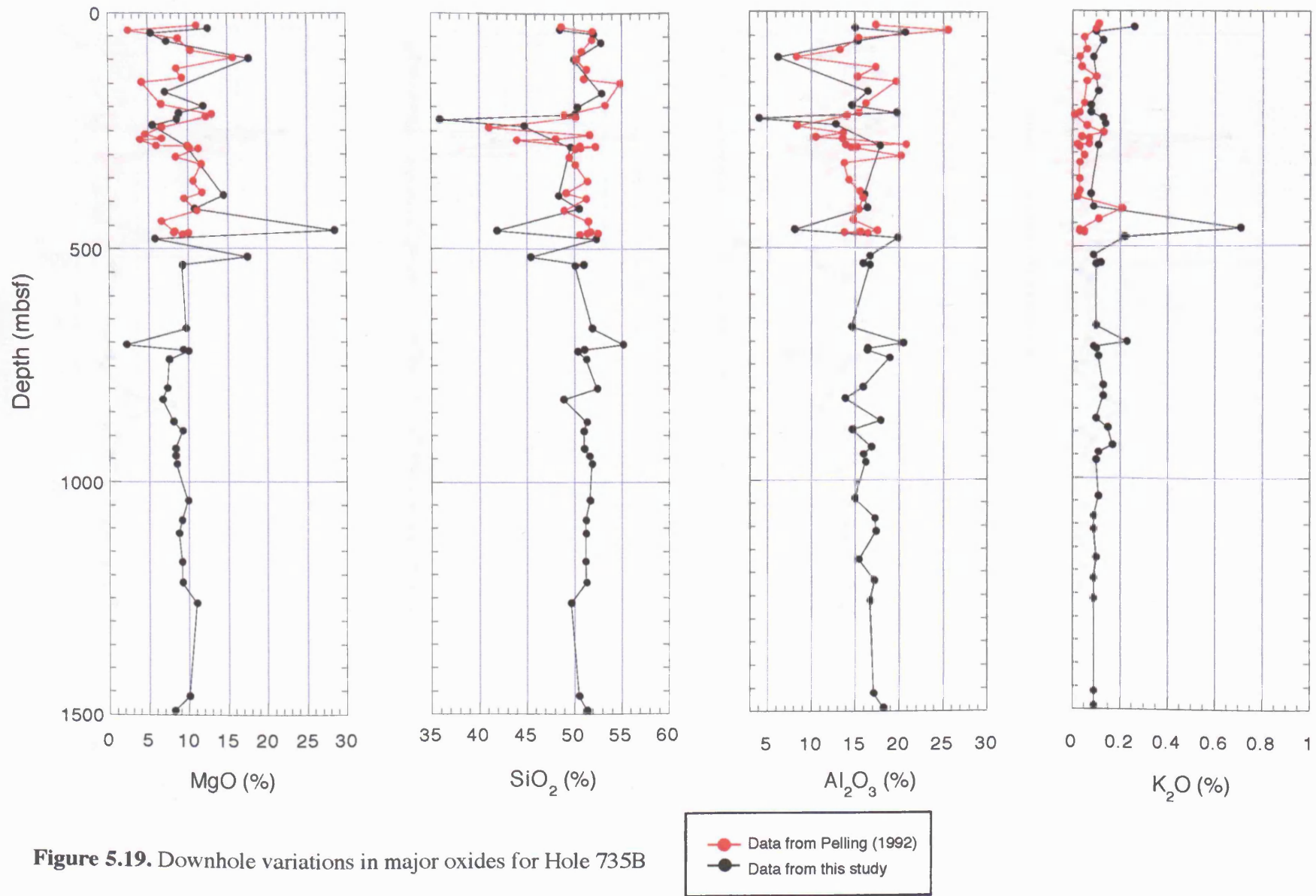


Figure 5.19. Downhole variations in major oxides for Hole 735B

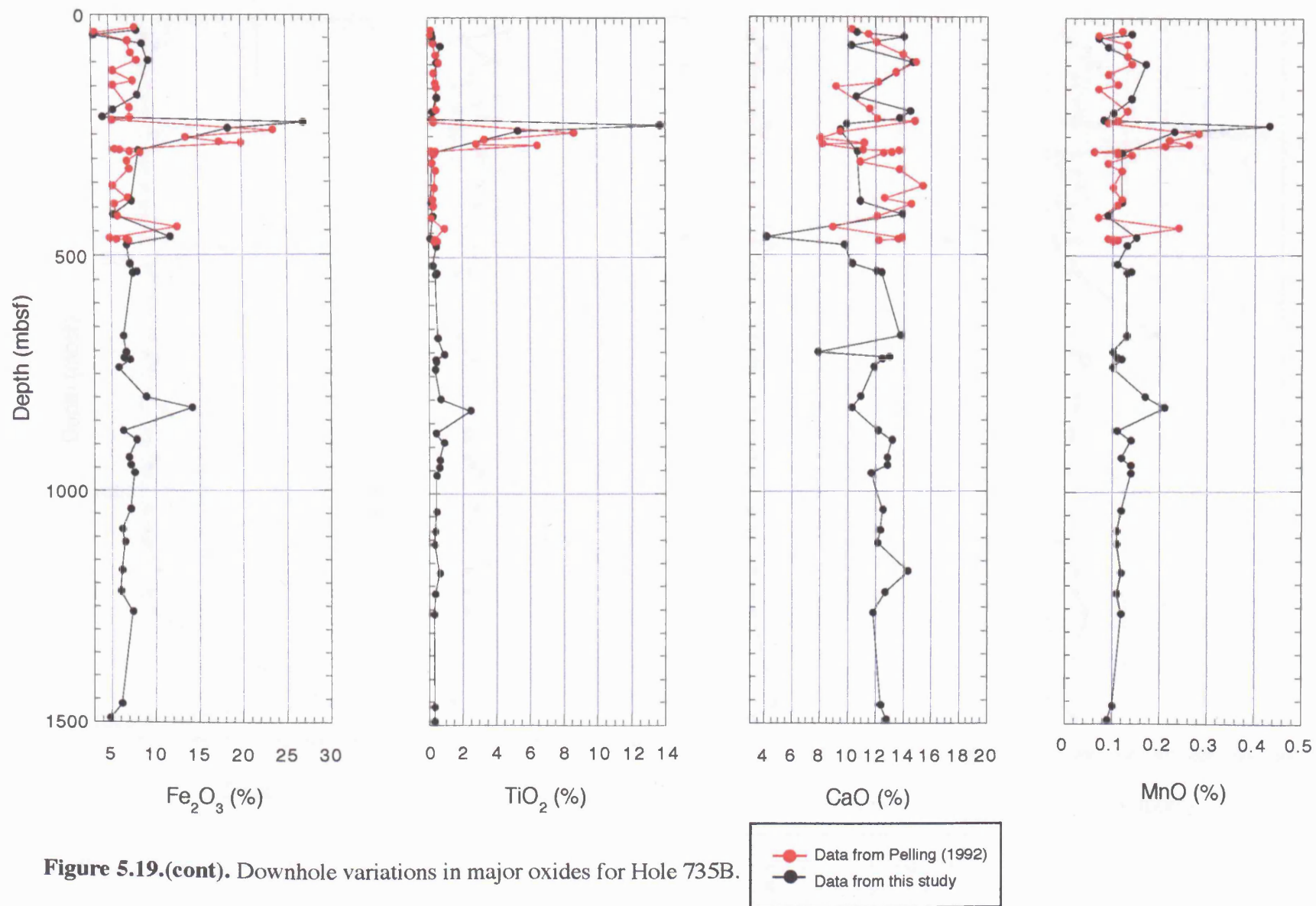


Figure 5.19.(cont). Downhole variations in major oxides for Hole 735B.

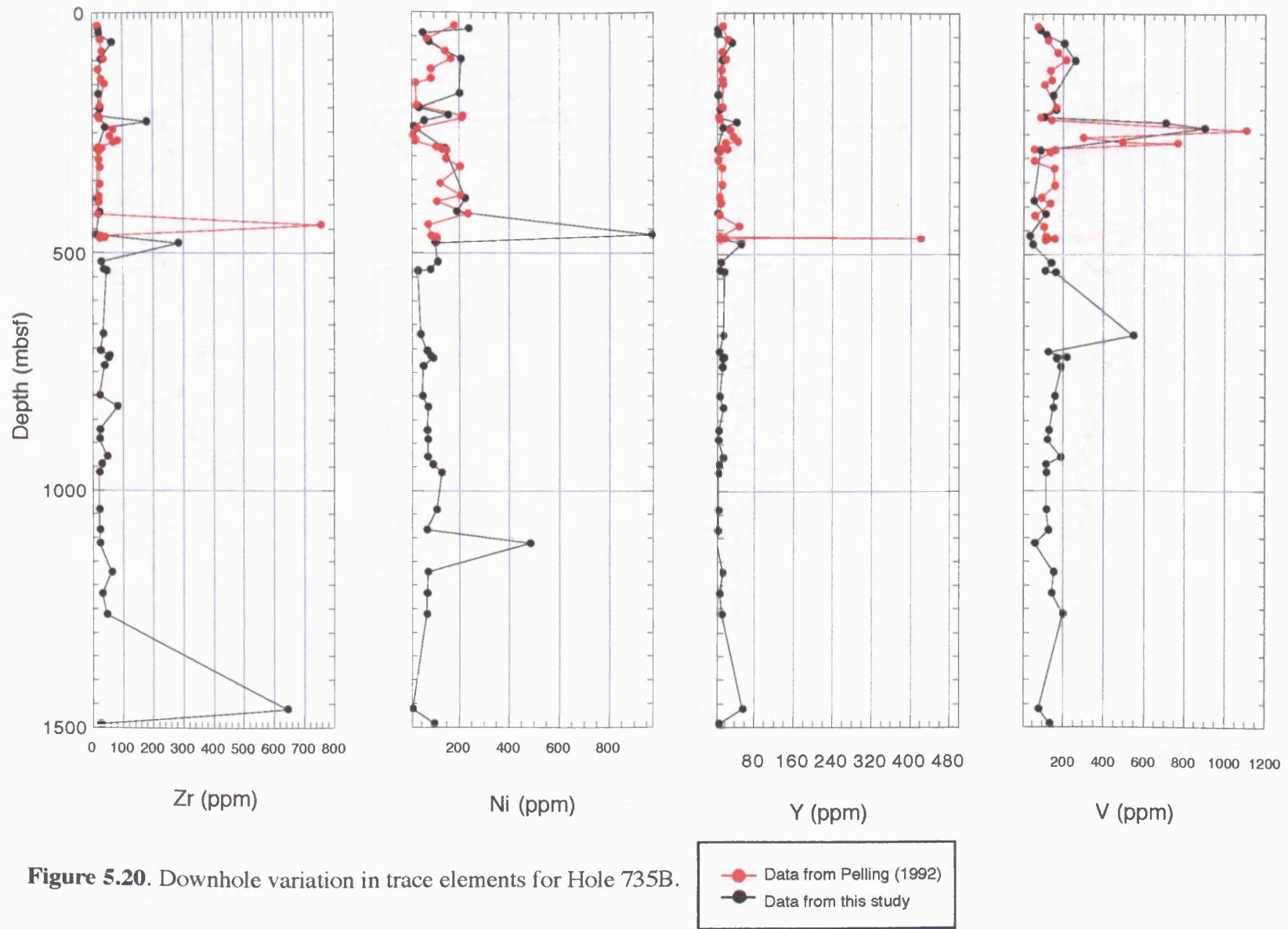


Figure 5.20. Downhole variation in trace elements for Hole 735B.

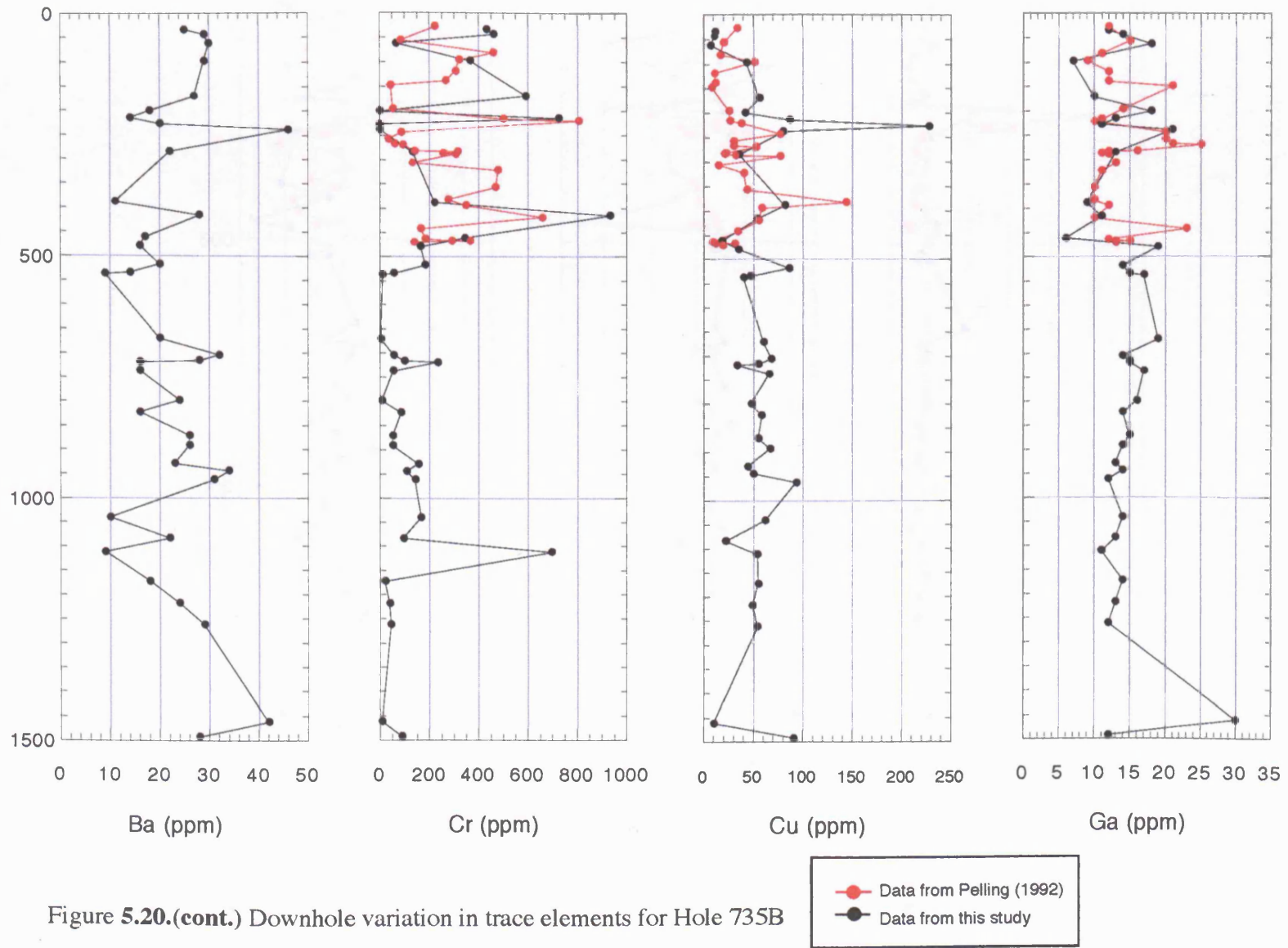


Figure 5.20.(cont.) Downhole variation in trace elements for Hole 735B

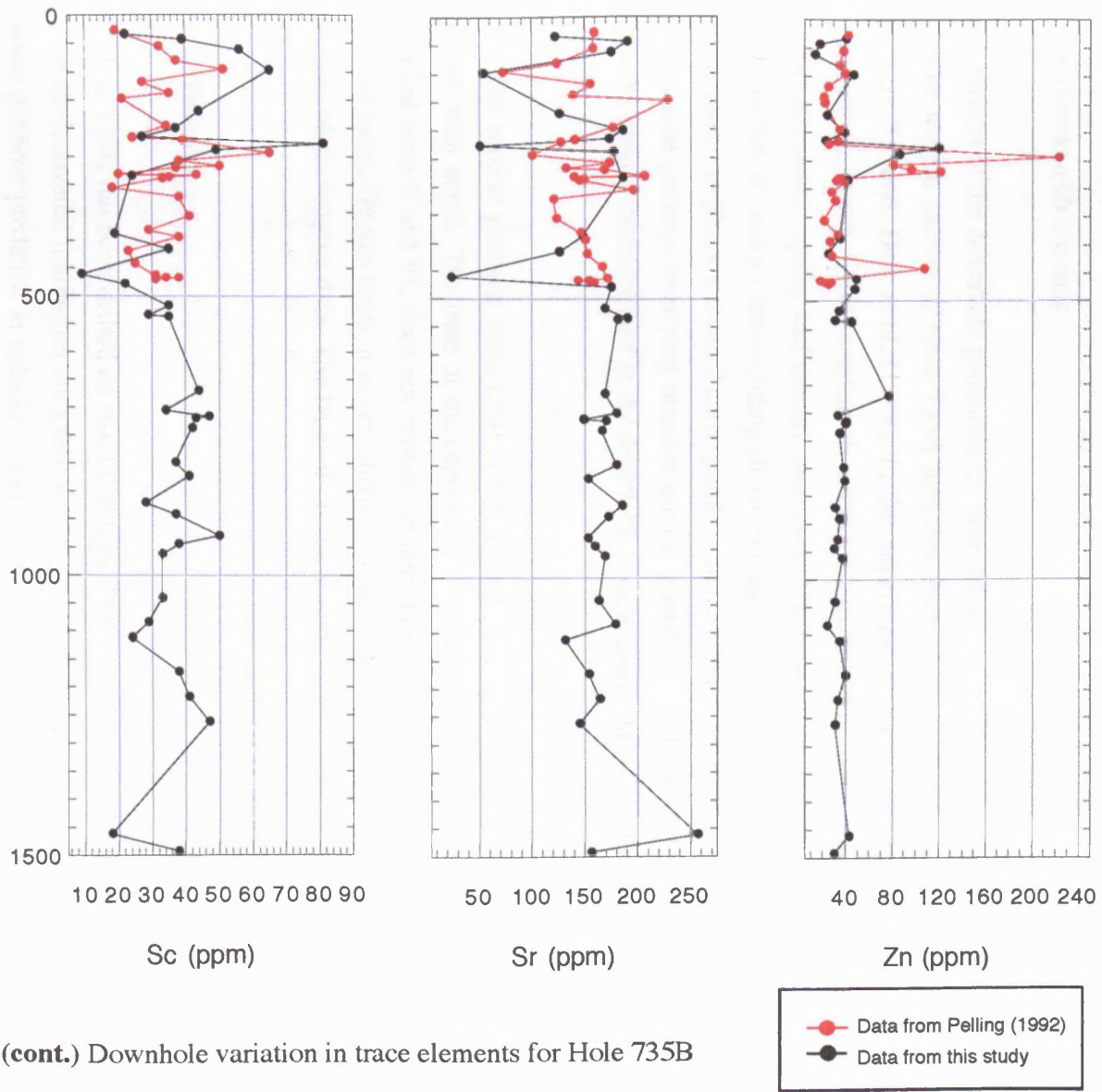


Figure 5.20.(cont.) Downhole variation in trace elements for Hole 735B

horizons. A large peak occurs in Sr in sample HAG-22, an olivine gabbro, this is a coarse-grained section and perhaps represents sampling of a large plagioclase grain enriched in Sr.

Cr and Cu both show complex patterns with depth, Cr substitutes into both clinopyroxene and oxides during fractionation and Cu is controlled by the presence of sulphides (Dick, Natland, Miller *et al.*, in press). Hence, the variations shown in their downhole chemistry probably reflect the abundances of these minerals within the core.

#### (b) Correlation with log data

A comparison of the downhole geochemistry with the downhole logging data is shown in Figure 5.21. The logged section of Hole 735B includes three of the plutonic masses / chemical units defined by Natland, Dick *et al.* (1998). In the uppermost of these units, from 0 to 280 mbsf, density and resistivity show a relatively constant variation with depth until 230 mbsf, where resistivity decreases rapidly and density increases. The base of the mass is marked by an abrupt decrease in density and a corresponding sharp increase in the resistivity data. The transition from plutonic mass 1 to plutonic mass 2 corresponds with the contact between lithological units IV and V, Fe-Ti oxide gabbros overlying massive olivine gabbros. The Fe-Ti oxide gabbros of Unit IV can also be clearly distinguished in the downhole geochemistry due to their high concentrations of  $\text{TiO}_2$ .

The second plutonic mass (280 to 536 mbsf) shows very little variation in density and resistivity with depth. The base of the chemical unit, which corresponds to the contact between lithological units V and VI, does not contain an abundance of Fe-Ti oxide gabbros similar to the uppermost mass. On this basis, it is very difficult to distinguish between plutonic masses 2 and 3 on the downhole logging data. The base of chemical unit 3 is not seen on the downhole logging data.

### 5.5. Summary

ODP Hole 735B has been drilled on two ODP legs, 118 and 176, to a total depth of 1503.9 mbsf. Most of the recovered lithologies are gabbroic rocks (~ 99 %) with minor felsic veins. The layered cumulate gabbros predicted in ophiolite models are not found in Hole 735B indicating that the lower crust at this location was formed by intrusion of small magma bodies. Hole 735B provides an unique opportunity to develop core-log integration techniques as it represents an *in situ* section of the lower ocean crust with high core recovery relative to other basement boreholes.

Downhole logging data for the borehole is only available to a depth of 600 mbsf due to blockage of the hole by a broken drillpipe. However, good quality data is available from 0 to 600

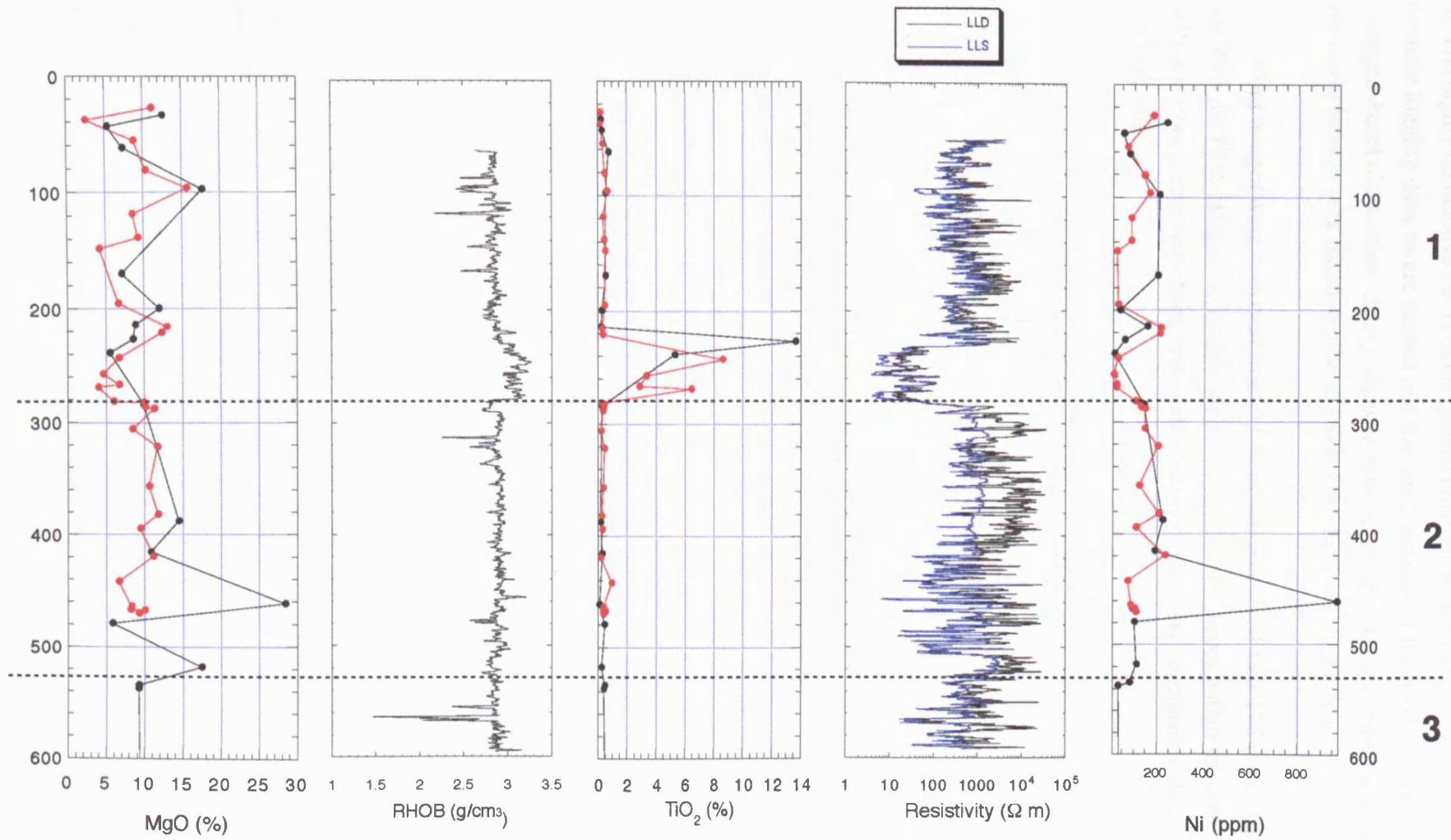


**Figure 5.21.** Comparison of downhole log data and geochemistry, the chemical units defined by Natland, Dick *et al.* (1998) are indicated.

mbsf, comprising the entire section drilled on leg 118 and 100 m of the section drilled during leg 176. The highly conductive Fe-Ti oxide gabbro horizons within the core are clearly evident on the downhole logging data, as are faulted and fractured sections of the borehole. The FMS images for the logged borehole section clearly show a number of structural features and bed boundaries, particularly between the massive olivine gabbro and Fe-Ti oxide gabbros.

Core images were collected from 93 % of the recovered Leg 176 core. These were used, along with the FMS images, to reorientate a number of core pieces within the core. Unfortunately, insufficient core pieces have been orientated to date to reach any conclusions about the Hole 735B crustal section.

## CHAPTER 6

---

# *Conclusions and suggestions for further work*

### 6.1. Summary and conclusions

#### 6.1.1. Lithological variability in the upper ocean crust

The reconstructed lithostratigraphical logs for Holes 896A and 504B show a complex layered stratigraphy with variable thicknesses of massive units, pillow lavas and breccias. Comparison of the log-derived lithostratigraphy for Hole 896A and the visual core description lithostratigraphy shows more brecciated units than previously estimated, with a particularly thick breccia section from approximately 350 to 390 mbsf. Three types of breccia are present in the Hole 896A core, one interpreted to be of hydrovolcanic origin, the other two to be of sedimentary or tectonic origin. The hyaloclastite breccias (Type A), found only at depths < 320 mbsf, were probably formed at the conclusion of an eruptive cycle, from lavas erupted at very low effusion rates. In contrast, breccias Type B and C probably comprise sedimentary or tectonic breccias, unrelated to volcanism. The presence of large amounts of sedimentary and / or tectonic breccias in the core indicates that magma supply to the ridge was not constant, as brecciation of older lava flows could occur. Little correlation is seen between lithology and geochemistry therefore the type of lava flow produced is largely unrelated to the lava chemistry. For the pillow lavas, massive units and hyaloclastite breccias, the flow morphology is largely a function of the cooling rate, temperature and viscosity of the erupting lava. Evidence for this is produced by the mineralogical data, different mineralogical textures are seen in the pillow lavas and massive units (porphyritic and intergranular respectively) but they have similar chemistries, these textural differences are therefore a reflection of different physical properties of the erupting lava.

The large breccia section from approximately 350 to 390 mbsf is interpreted as representing a period of reduced volcanism, allowing for brecciation of earlier flows. This large brecciated zone corresponds with a section of the core with more evolved chemical compositions. This has been interpreted as representing reduced magma supply to a subaxial

magma chamber allowing for more extensive fractional crystallisation with limited magma mixing. The pause in volcanism in this crustal section is supported by the magnetic susceptibility data which divides the core into 3 depth sections, the lower two sections are separated from the upper section by an unconformity.

The Hole 504B core includes a complete volcanic section, overlying the transition zone and sheeted dyke complex. In Hole 504B, reconstruction of the lithostratigraphy from log data is complicated by the fact that only 3 pads of FMS data are available, therefore the log data was supplemented by the shipboard visual core descriptions which may be inconsistent. However, the reconstructed lithostratigraphy shows that pillow lavas are dominant at the top of the core with increasing amounts of massive units towards the base. Holes 896A and 504B contain similar lithological units, however, individual flows cannot be correlated between the two cores. This indicates that the lateral extent of lava flows must be relatively small (< 1 km) therefore the two crustal sections were probably constructed from separate eruptive cycles. The Hole 504B volcanic section appears to contain flows erupted both on and off-axis. The flows from 0 to approximately 500 mbsf consist predominantly of pillow lavas probably erupted off-axis at relatively low effusion rates. Hot, rapid eruptions on the axis probably produced the flows from 500 mbsf to the base of the volcanic section, here more massive units occur. The Hole 896A core contains predominantly off-axis flows, hence the section contains large amounts of pillow lavas and breccias.

The Hole 504B geochemistry shows a cyclic variation downhole or 'saw-tooth' pattern, interpreted as separate periods of evolution in a subaxial magma chamber. The supply of magma to the magma chamber may have been more constant during formation of the Hole 504B section than the Hole 896A section, hence the lesser thicknesses of breccia and less well-defined cyclic variations in chemistry.

Three different chemical groups of basalt are found in the Hole 504B core (derived from different sources), two of these are more enriched in LREE than the remaining group which includes the majority of the Hole 504B basalt samples. The enriched basalt groups do not occur in the Hole 896A core, either they were not recovered / penetrated or they simply do not occur in this section of crust.

The conclusions reached from Chapters 3 and 4 can be summarised as follows:

- the different extrusive lithological units in the upper ocean crust are formed from lavas erupted at different temperatures or speeds, with massive units being formed from hot, rapid eruptions and pillow lavas / hyaloclastites being formed from slower cooler lava flows. This results in the units having similar chemistries but different mineralogical textures,

- the volume and duration of individual eruptive events is not constant, resulting in variable thicknesses of lithologies, producing a complex intercalated sequence. Individual eruptive events may produce the full sequence of massive units, pillow lavas and breccias or only one lithology,
- the eruptive cycles forming the crustal section drilled at Hole 896A were not continuous, with a substantial period where brecciation of older lava flows could occur,
- the percentage of sedimentary / tectonic brecciated units in the core appears to be closely related to the frequency of magma supply to a subaxial magma chamber,
- breccias are probably underrepresented in the majority of upper oceanic crust boreholes, the large breccia section indicated on the FMS image data for Hole 896A was not evident in the core data,
- the variation in downhole geochemistry for Hole 896A appears to be dominated by magma mixing processes, with an overall decrease in degree of fractionation with decreasing depth,
- the large breccia section in Hole 896A from 350 to 390 mbsf corresponds with a section of the core with more evolved compositions, suggesting that, during this period of reduced magma supply, more extensive fractional crystallisation could occur,
- from comparison with the complete volcanic section recovered from Hole 504B, it can be concluded that eruptive events off-axis produce less massive flow units than those occurring close to the axis. The amount of brecciated material increases off-axis, suggesting that the magma supply to off-axis crustal sections is reduced in comparison to the ridge axis.

### **6.1.2. Core-log techniques in basement holes with relatively high core recovery**

In the third case study discussed in this thesis, ODP Hole 735B, the relatively high core recovery meant reconstruction of the lithostratigraphy by logging data was rendered largely unnecessary, hence, other core-log integration techniques were discussed.

Several structural features are clearly shown on the downhole FMS logs, including fractures and bed boundaries. The Fe-Ti oxide gabbro horizons are particularly well-defined, due to their high conductivity relative to the more resistive massive olivine gabbros.

Most of the missing material in the core is from the more fractured and foliated horizons, these are probably underrepresented in the core therefore recovery is somewhat biased towards the massive olivine gabbros.

Reorientation and accurate location of individual core pieces can be achieved by integration of core image / log data by visual correlation of structures between FMS data and core images.

No conclusions have been reached at present concerning tectonic setting as insufficient core pieces have been positioned and orientated.

## **6.2. Suggested further work**

- reconstruction of lithological architecture of other “reference” boreholes 395A and 418A using log data. These may then be compared with Holes 896A and 504B to investigate whether the lithostratigraphy and geochemistry is different in crust formed at different spreading rates
- continued reorientation and location of core pieces in Hole 735B. This would ensure that it would be possible to accurately plot dips and strikes of veins, fractures and other structural features allowing the tectonic setting of Site 735B to be inferred.

# APPENDIX A

---

## *Acronyms used in this thesis*

### A.1. Logging tool acronyms

FMS	Formation MicroScanner <sup>1</sup>
DLL	Dual Laterolog <sup>1</sup>
SDT	Digital Sonic Tool <sup>1</sup>
NGT	Natural Gamma-ray Spectroscopy Tool <sup>1</sup>
TLT	Temperature Logging Tool <sup>2</sup>
GLT	Geochemical Logging Tool <sup>1</sup>
BHTV	Borehole Televiwer <sup>2</sup>
MCS	Multichannel Sonic Tool <sup>2</sup>
VSP	Vertical Seismic Profile
HLDS	High Temperature Lithodensity Sonde <sup>1</sup>
HLDT	High Temperature Lithodensity Tool <sup>1</sup>
APS	Accelerator Porosity Sonde <sup>1</sup>
HNGS	Hostile Environment Natural Gamma-ray Sonde <sup>1</sup>
DSI	Dipole Sonic Imager <sup>1</sup>
GPIT	General Purpose Inclinator Tool <sup>1</sup>

### A.2. Additional acronyms

LLD	Deep Laterolog
LLS	Shallow Laterolog
RHOB	Bulk Density
APLC	Array Porosity Limestone Corrected
FPLC	Formation Porosity Limestone Corrected
C1	FMS Caliper 1
C2	FMS Caliper 2

---

<sup>1</sup> Trade Mark of Schlumberger

<sup>2</sup> Trade Mark of LDEO-BRG

## APPENDIX B

---

### *Logging tools deployed on ODP Legs*

#### **B.1. Formation Microscanner™ (FMS)**

The Formation Microscanner<sup>1</sup> (FMS) is essentially an imaging device allowing for the visual representation of structural features near the borehole wall, (Alt, Kinoshita *et al.*, 1993). This is achieved by measurements which are related to the conductance of the formation. The conductance measurements are made by four pads containing electrodes, as the tool moves through the borehole these electrodes are pressed against the walls. The current from each electrode passes through the borehole wall to a depth of a few centimetres, measuring the conductance, (Alt, Kinoshita *et al.*, 1993). These conductance values are then processed as a high resolution image (Figure B1). On the image, areas with low conductance and, hence, high resistance, are represented by a light colour and those areas with high conductance are represented by a dark colour. This allows features such as bed boundaries, conductive / resistive fractures, and brecciated units to be identified on the FMS images.

The FMS tool string also includes a General Purpose Inclination Tool (GPIT). This contains a 3-component accelerometer and a 3-component magnetometer and measures both the orientation of the borehole and the orientation of the FMS sensors within the hole (Borehole Research Group, 1994).

The Formation Microscanner<sup>1</sup> has a number of applications including (Borehole Research Group, 1994):

- mapping and dip determination of formation structures, including bedding planes, fractures faults and foliations,
- correlation of logging and coring depths,

---

<sup>1</sup> Trade Mark of Schlumberger

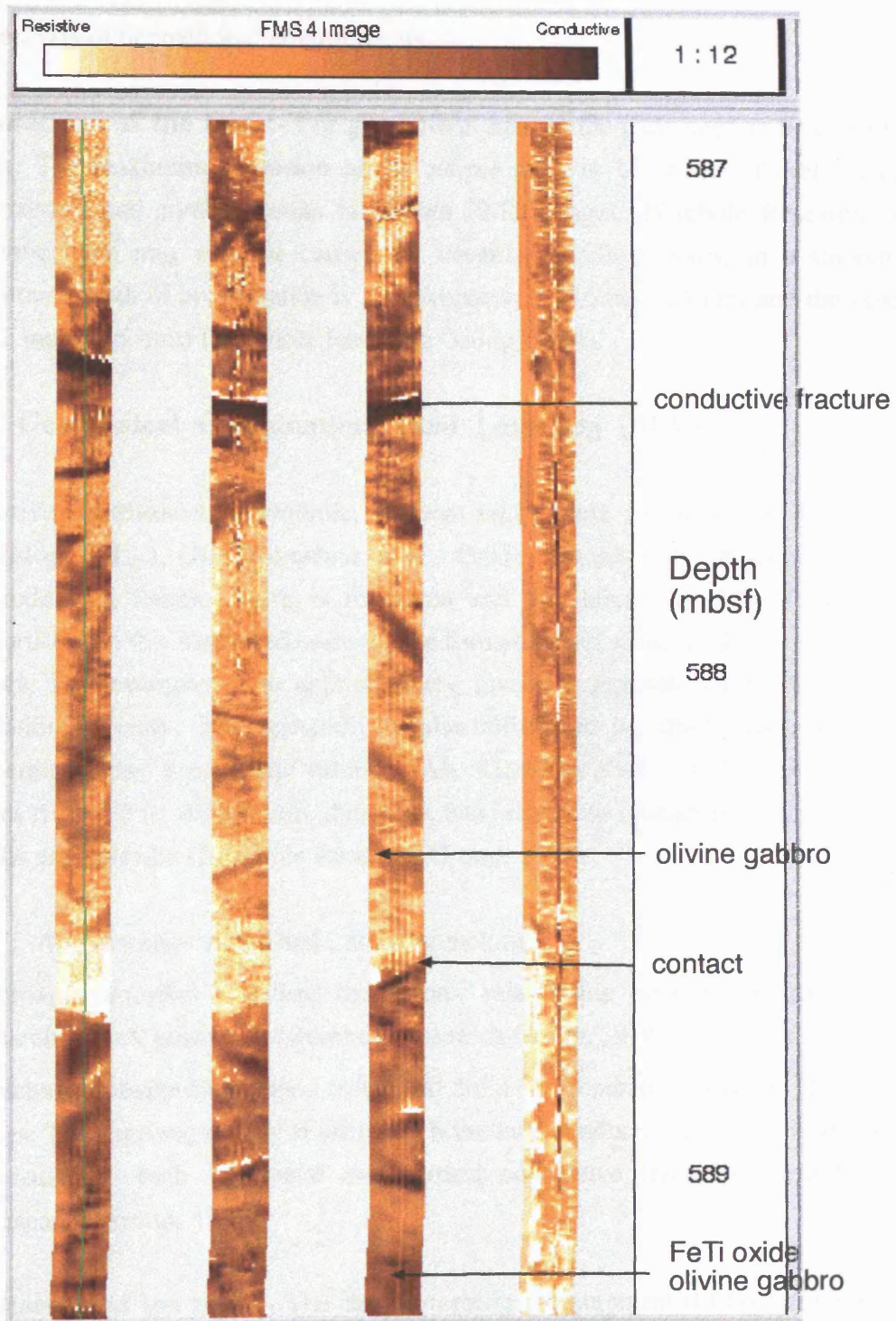


**Figure B.1.** Example of an FMS image from ODP Hole 735B (Southwest Indian Ridge) showing a contact between resistive olivine gabbro and conductive FeTi oxide olivine gabbro. The olivine gabbro contains a conductive fracture.

- accurate positioning of core sections in boreholes with low core recovery,
- analysis of depositional environments.

**Limitations of the tool :-** For good FMS images the pads need to be close to the borehole walls. The maximum extension of the caliper arms is 15 inches, therefore, in larger holes inconsistent pad contact results in blurred FMS images (Borehole Research Group, 1994). Complications may also be caused by irregular borehole walls, in a smooth borehole the maximum depth of investigation is approximately 10 inches (25 cm) and the vertical resolution is 0.2 inches (5 mm) (Borehole Research Group, 1994).

## **B.2. Geophysical Combination: Dual Laterolog (DLL)<sup>1</sup>**

Resistivity is measured downhole, at room temperature and pressure, by means of the Dual Laterolog<sup>1</sup> (DLL), (Alt, Kinoshita *et al.*, 1993). The intensity of the current flow from an electrode to a remote return is measured and the resistivity of the formation is inversely proportional to this measured current. The formation resistivity is closely related to a number of factors. For example, it is approximately inversely proportional to the square root of the formation porosity. The resistivity is also influenced by interconnectivity of pore spaces, temperature, clay content and salinity, (Alt, Kinoshita *et al.*, 1993). The response of the tool ranges from 0.2 to 40,000  $\Omega\text{m}$ , therefore, can be used to characterise resistive rocks, including basalts and gabbros (Borehole Research Group, 1994).

Applications of the Dual Laterolog include:

- porosity estimates - utilises the inverse relationship between resistivity and porosity to calculate rock porosities (Borehole Research Group, 1994).
- fracture porosity estimates - calculated from the separation between the shallow and deep logs. The deep log is only sensitive to horizontal conductive fractures whereas the shallow is sensitive to both horizontal and vertical conductive fractures (Pezard, 1990; Borehole Research Group, 1994).

**Limitations of the tool :-** The deep laterolog measurement (LLD) can be used in boreholes with up to 16 inch diameter whereas the shallow laterolog measurement (LLS) can be only used in boreholes up to 12 inches in diameter (Borehole Research Group, 1994). With corrections, the tool can be used in boreholes up to 20 ft in diameter. The depth of investigation is dependent on the wallrock resistivity and resistivity contrast between the drilling fluid and uninvaded zone.

---

<sup>1</sup> Trade Mark of Schlumberger

(Borehole Research Group, 1994). Vertical resolution of the tool is approximately 2 ft (Borehole Research Group, 1994).

### **B.3. Geophysical Combination: Array Sonic Tool (SDT)<sup>1</sup>**

This usually forms part of the Schlumberger Geophysical Combination along with the Dual Laterolog<sup>1</sup> (Alt, Kinoshita *et al.*, 1993). The SDT measures acoustic wave velocities. It consists of two acoustic transmitters and a receiver. The tool measures the time required for sonic waves to travel in the formation, the measurements obtained can then be used to calculate the velocity of compressional, sheer and surface waves within the formation (Borehole Research Group, 1994).

### **B.4. High Temperature Lithodensity Tool (HLDT)<sup>1</sup>**

The HLDT<sup>1</sup> comprises a Cs<sup>137</sup> gamma-ray source and 2 detectors (Borehole Research Group, 1994; Gonçalves, 1995). The gamma-rays emitted by the source interact with the electrons in the borehole formation in 2 ways, Compton scattering and photoelectric absorption (Borehole Research Group, 1994). Compton scattering provides the basis of the density measurements, the attenuation of the back scattered gamma-rays is controlled by the electron density of the formation which is in turn related to bulk density (Borehole Research Group, 1994; Gonçalves, 1995).

The tool has a number of applications including (Borehole Research Group, 1994):

- porosity estimations, porosity can be calculated from density if the grain density of the formation is known,
- if used with a neutron log, the density measurements can be used to aid the definition of lithological units and boundaries.

**Limitations of the tool :-** For accurate measurements, good contact with the formation is essential. This can be checked by the caliper measurement (Borehole Research Group, 1994). The depth of investigation is dependant on the density of the formation but usually ranges from 20 to 70 cm (Gonçalves, 1995). The vertical resolution of the tool is 38 cm (1.25 ft.; Borehole Research Group, 1994).

---

<sup>1</sup> Trade Mark of Schlumberger

## APPENDIX C

---

### *List of Core Samples*

The following tables comprise a list of both the ODP and lab numbers for the core samples taken from Holes 896A and 735B and used for thin-section descriptions.

#### C.1. Samples from Hole 896A

Lab Number	Approximate Depth	ODP Sample Number
896-1	195.89 mbsf	148-896A-1R-01 # 17 077 - 080 cm
896-2	230.08 mbsf	148-896A-5R-02 # 2 074 - 077 cm
896-3	268.51 mbsf	148-896A-9R-02 # 3 029 - 033 cm
896-4	316.90 mbsf	148-896A-14R-02 # 11B 089 - 091 cm
896-5	336.03 mbsf	148-896A-16R-02 # 1E 061 - 064 cm
896-6	354.89 mbsf	148-896A-18R-02 # 5 027 - 030 cm
896-7	356.37 mbsf	148-896A-19R-01 # 7 036 - 038 cm
896-10	364.76 mbsf	148-896A-20R-01 # 25 124 - 127 cm
896-11	373.04 mbsf	148-896A-21R-01 # 1 000 - 007 cm
896-12	374.46 mbsf	148-896A-21R-01 # 21 145 - 147 cm
896-13	376.13 mbsf	148-896A-21R-03 # 2 011 - 014 cm
896-14	382.73 mbsf	148-896A-22R-01 # 2 010 - 015 cm
896-15	384.25 mbsf	148-896A-22R-02 # 2 013 - 017 cm
896-16	386.49 mbsf	148-896A-22R-03 # 9 087 - 090 cm
896-17	394.97 mbsf	148-896A-23R-02 # 16 136 - 138 cm
896-19	401.94 mbsf	148-896A-24R-01 # 1 012 - 015 cm

896-20	402.96 mbsf	148-896A-24R-01 # 7	114-117 cm
896-21	404.01 mbsf	148-896A-24R-02 # 8	069 - 072 cm
896-22	408.43 mbsf	148-896A-24R-05 # 6	061 - 064 cm
896-25	415.00 mbsf	148-896A-25R-03 # 10	067 - 073 cm
896-27	431.53 mbsf	148-896A-27R-01 # 12B	101 - 104 cm
896-28	434.06 mbsf	148-896A-27R-03 # 6	053 - 058 cm
896-30	441.54 mbsf	148-896A-28R-02 # 1A	000 - 007 cm
896-31	449.75 mbsf	148-896A-29R-01 # 1	000 - 010 cm
896-32	450.69 mbsf	148-896A-29R-01 # 14	098 - 100 cm
896-33	460.14 mbsf	148-896A-30R-01 # 11C	081 - 086 cm
896-34	460.86 mbsf	148-896A-30R-2 # 1A	005 - 007 cm

### C.2. Samples from Hole 735B

Lab Number	Approximate Depth	ODP Sample Number	
735-1	33.9 mbsf	118-735B-8D-1 # 8	069 - 071 cm
735-2	43.48 mbsf	118-735B-12R-3 # 2J	107 - 109 cm
735-3	62.07 mbsf	118-735B-16R-1 # 2B	027 - 029 cm
735-4	97.84 mbsf	118-735B-22R-3 # 4	083 - 085 cm
735-5	169.57 mbsf	118-735B-35R-5 # 2B	026 - 028 cm
735-6	199.73 mbsf	118-735B-41R-4 # 1C	052 - 054 cm
735-7	214.47 mbsf	118-735B-44R-3 # 5D	086 - 088 cm
735-8	226.82 mbsf	118-735B-47R-1 # 5D	081 - 083 cm
735-9	238.82 mbsf	118-735B-50R-1 # 2B	031 - 033 cm
735-10	284.13 mbsf	118-735B-58R-3 # 1E	082 - 084 cm
735-11	387.93 mbsf	118-735B-75R-3 # 1C	067 - 069 cm
735-12	415.70 mbsf	118-735B-79R-1 # 10D	119 - 121 cm
735-13	461.77 mbsf	118-735B-83R-8 # 4	026 - 028 cm
735-14	479.41 mbsf	118-735B-85R-6 # 4A	095 - 097 cm
HAG-1	517.97 mbsf	176-735B-91R-1 # 2C	054 - 059 cm
HAG-2	534.52 mbsf	176-735B-93R-3 # 1A	009 - 014 cm

HAG-3	537.25 mbsf	176-735B-94R-1 # 1D 062 - 067 cm
HAG-4	670.65 mbsf	176-735B-115R-7 # 3A 022 - 027 cm
HAG-5	705.41 mbsf	176-735B-119R-4 # 9 078 - 083 cm
HAG-6	716.47 mbsf	176-735B-120R-5 # 4A 074 - 079 cm
HAG-7	719.90 mbsf	176-735B-121R-1 # 2B 017 - 022 cm
HAG-8	737.28 mbsf	176-735B-122R-6 # 3A 105 - 110 cm
HAG-9	799.53 mbsf	176-735B-130R-4 # 9 140 - 145 cm
HAG-10	823.62 mbsf	176-735B-133R-1 # 4 069 - 074 cm
HAG-11	871.79 mbsf	176-735B-139R-1 # 4 066 - 071 cm
HAG-12	891.48 mbsf	176-735B-141R-2 # 1B 075 - 080 cm
HAG-13	929.47 mbsf	176-735B-145R-6 # 8 094 - 099 cm
HAG-14	944.91 mbsf	176-735B-147R-4 # 1B 048 - 053 cm
HAG-15	962.20 mbsf	176-735B-149R-2 # 2 037 - 042 cm
HAG-16	1040.76 mbsf	176-735B-157R-5 # 4 053 - 058 cm
HAG-17	1083.83 mbsf	176-735B-162R-1 # 3B 120 - 125 cm
HAG-18	1111.84 mbsf	176-735B-165R-6 # 1C 081 - 086 cm
HAG-19	1173.38 mbsf	176-735B-172R-4 # 2 055 - 060 cm
HAG-20	1217.76 mbsf	176-735B-178-6 # 4 087 - 092 cm
HAG-21	1261.84 mbsf	176-735B-183R-2 # 2A 081 - 086 cm
HAG-22	1461.49 mbsf	176-735B-206R-2 # 2A 056 - 061 cm
HAG-23	1492.55 mbsf	176-735B-209R-3 # 6 132 - 137 cm

## APPENDIX D

---

### *Thin-section descriptions*

#### D.1. Hole 896A samples

<b>Specimen:</b> 896-1			
<b>Depth:</b> 195.89 mbsf			
<b>Lithology:</b> Pillow basalt			
<b>Texture:</b> Glomeroporphyritic			
<b>Grain Size:</b> fine to coarse (glomerocrysts)			
<b>Primary Mineralogy:</b>			
	%	Size Range	Crystal Shape
<b>Phenocrysts:</b>			
Plagioclase	5	0.5 - 1 mm	subhedral - euhedral
Olivine	1	0.5 - 1 mm	anhedral - subhedral
<b>Groundmass:</b> Microcrystalline groundmass consisting of acicular crystals of plagioclase and altered olivines			
<b>Alteration:</b>			
Olivine is replaced both as phenocrysts and in the groundmass by red / brown oxides.			
<b>Additional Notes:</b>			
Plagioclase often occurs as glomerocrysts			
<b>Additional Notes:</b>			

<b>Specimen:</b> 896-2			
<b>Depth:</b> 230.08 mbsf			
<b>Lithology:</b> Pillow Basalt			
<b>Texture:</b> Porphyritic			
<b>Grain Size:</b> fine to medium-grained			
<b>Primary Mineralogy:</b>			
	%	Size Range	Crystal Shape
<b>Phenocrysts:</b>			
Plagioclase	4	0.5 - 1 mm	euhedral
Olivine	1	< 1 mm	anhedral
<b>Groundmass:</b> Microcrystalline groundmass consisting of acicular crystals of plagioclase and altered olivines			
<b>Alteration:</b>			
Olivine is extensively replaced both in the groundmass and as phenocrysts by a brown amorphous material. The brown colour masks birefringence colours.			

<b>Specimen:</b> 896-3			
<b>Depth:</b> 268.51 mbsf			
<b>Lithology:</b> Pillow Basalt			
<b>Texture:</b> Glomeroporphyritic			
<b>Grain Size:</b> fine to coarse (glomerocrysts)			
<b>Primary Mineralogy:</b>			
	%	Size Range	Crystal Shape
<b>Phenocrysts:</b>			
Plagioclase	7	0.1 - 1 mm	euhedral
Olivine	2	< 1 mm	anhedral
<b>Groundmass:</b> contains altered olivines and plagioclase			
<b>Alteration:</b>			
Olivine is extensively replaced by a brown / yellow material.			
<b>Additional Notes:</b>			
Glomerocrysts occur consisting of 5 to 20 acicular plagioclase grains of variable size (0.1 to 1 mm).			

<b>Specimen:</b> 896-4			
<b>Depth:</b> 316.90 mbsf			
<b>Lithology:</b> Pillow Basalt			
<b>Texture:</b> Glomeroporphyritic			
<b>Grain Size:</b> fine to coarse (glomerocrysts)			
<b>Primary Mineralogy:</b>			
	%	Size Range	Crystal Shape
<b>Phenocrysts:</b>			
Plagioclase	5	0.5 - 0.75 mm	subhedral
Olivine	1	0.5 - 0.75 mm	anhedral
<b>Groundmass:</b> microcrystalline consisting of unaltered acicular crystals of plagioclase and altered olivines			
<b>Alteration:</b>			
Olivine is replaced in the groundmass and as phenocrysts by red / brown oxides.			

<b>Specimen:</b> 896-5			
<b>Depth:</b> 336.03 mbsf			
<b>Lithology:</b> Massive Basalt			
<b>Texture:</b> Glomeroporphyritic			
<b>Grain Size:</b> fine to coarse (glomerocrysts)			
<b>Primary Mineralogy:</b>			
	%	Size Range	Crystal Shape
<b>Phenocrysts:</b>			
Plagioclase	5	0.5 - 1 mm	subhedral - euhedral
Olivine	2	0.5 - 1 mm	anhedral
<b>Groundmass:</b> Groundmass has a coarser grain-size than pillow basalts but is of a similar composition, altered olivines and plagioclase			
<b>Alteration:</b>			
Extensive red / brown oxidative alteration occurs throughout the section. It occurs as "blebs" (<0.5 mm) in the groundmass and as haloes surrounding olivine grains.			
<b>Additional Notes:</b>			
Glomerocrysts consist exclusively of 10 to 20 plagioclase crystals approximately 0.1 to 1 mm in size.			

<b>Specimen: 896-6</b>			
<b>Depth: 354.89 mbsf</b>			
<b>Lithology: Basaltic Breccia</b>			
<b>Texture: Glomeroporphyritic</b>			
<b>Grain Size: fine to coarse (glomerocrysts)</b>			
<b>Primary Mineralogy:</b>			
	%	Size Range	Crystal Shape
<b>Phenocrysts:</b>			
Plagioclase	5	0.1 - 1.5 mm	subhedral - euhedral
Clinopyroxene	<1	< 1 mm	anhedral
<b>Additional Notes:</b>			
Glomerocrysts are ~ 4 mm in size with 5 to 30 phenocrysts of plagioclase ranging from 0.1 to 1.5 mm.			

<b>Specimen: 896-7</b>			
<b>Depth: 356.37 mbsf</b>			
<b>Lithology: Pillow Basalt</b>			
<b>Texture: Glomeroporphyritic</b>			
<b>Grain Size: fine to coarse (glomerocrysts)</b>			
<b>Primary Mineralogy:</b>			
	%	Size Range	Crystal Shape
<b>Phenocrysts:</b>			
Plagioclase	5	0.5 - 1 mm	subhedral - euhedral
Olivine	1	0.1 - 1 mm	anhedral
Clinopyroxene	<1	0.1 - 1 mm	anhedral - subhedral
<b>Groundmass: Microcrystalline groundmass consisting of acicular crystals of plagioclase and altered olivines</b>			
<b>Alteration:</b>			
Olivine in the groundmass is extensively replaced by oxides. A fine vein (~0.2 mm) cuts through the section. This is filled with a mineral with low birefringence, colourless in PPL (feldspar?).			

<b>Specimen:</b> 896-10			
<b>Depth:</b> 364.76 mbsf			
<b>Lithology:</b> Pillow Basalt			
<b>Texture:</b> Glomeroporphyritic			
<b>Grain Size:</b> fine to coarse (glomerocrysts)			
<b>Primary Mineralogy:</b>			
	%	Size Range	Crystal Shape
<b>Phenocrysts:</b>			
Plagioclase	4	0.5 - 1 mm	subhedral - euhedral
Olivine	1	0.5 - 1 mm	anhedral - subhedral
<b>Groundmass:</b> Microcrystalline groundmass consisting of acicular crystals of plagioclase and altered olivines			
<b>Alteration:</b>			
The section is heavily altered with all groundmass and phenocryst olivine replaced by red / brown oxides			
<b>Additional Notes:</b>			

<b>Specimen:</b> 896-11			
<b>Depth:</b> 373.04 mbsf			
<b>Lithology:</b> Pillow Basalt			
<b>Texture:</b> porphyritic			
<b>Grain Size:</b> fine to medium-grained			
<b>Primary Mineralogy:</b>			
	%	Size Range	Crystal Shape
<b>Phenocrysts:</b>			
Plagioclase	5	0.1 - 1 mm	subhedral - euhedral
Olivine	1	0.5 - 1 mm	anhedral
<b>Groundmass:</b> Microcrystalline groundmass consisting of acicular crystals of plagioclase and altered olivines			
<b>Alteration:</b>			
Olivine is altered to red / brown oxides both in the groundmass and as phenocrysts. In places olivine grains are rimmed by a bright green material.			
<b>Additional Notes:</b>			
Rare examples occur of a subhedral to anhedral mineral, colourless in PPL with moderate birefringence. This mineral has a strong cleavage and is simply twinned (pyroxene?).			

<b>Specimen:</b> 896-12			
<b>Depth:</b> 374.46			
<b>Lithology:</b> Pillow Basalt			
<b>Texture:</b> Glomeroporphyritic			
<b>Grain Size:</b> fine to coarse (glomerocrysts)			
<b>Primary Mineralogy:</b>			
	%	Size Range	Crystal Shape
<b>Phenocrysts:</b>			
Plagioclase	5	1 - 5 mm	subhedral - euhedral
Olivine	<1	0.1 - 1 mm	anhedral
<b>Groundmass:</b> Microcrystalline groundmass consisting of acicular crystals of plagioclase and altered olivines			
<b>Alteration:</b>			
The section is heavily altered with all groundmass and phenocryst olivine replaced by red / brown oxides			
<b>Additional Notes:</b>			
Phenocrysts of plagioclase often occur as glomerocrysts. These consist of exclusively of plagioclase 1 to 5 mm in size.			

<b>Specimen:</b> 896-13			
<b>Depth:</b> 376.13 mbsf			
<b>Lithology:</b> Basalt			
<b>Texture:</b> Glomeroporphyritic			
<b>Grain Size:</b> fine to coarse (glomerocrysts)			
<b>Primary Mineralogy:</b>			
	%	Size Range	Crystal Shape
Plagioclase			
Olivine			
<b>Alteration:</b>			
<b>Additional Notes:</b>			
Section has a lot of holes...mineralogy rather unclear			

<b>Specimen:</b> 896-14			
<b>Depth:</b> 382.73 mbsf			
<b>Lithology:</b> Pillow Basalt			
<b>Texture:</b> Glomeroporphyritic			
<b>Grain Size:</b> fine to coarse (glomerocrysts)			
<b>Primary Mineralogy:</b>			
	%	Size Range	Crystal Shape
<b>Phenocrysts:</b>			
Plagioclase	6	0.5 - 1 mm	subhedral - euhedral
Olivine	2	0.5 - 1 mm	anhedral - subhedral
Clinopyroxene	< 1		
<b>Groundmass:</b> Microcrystalline groundmass consisting of acicular crystals of plagioclase and altered olivines			
<b>Alteration:</b>			
Olivine is almost entirely replaced by clays / oxides both in the groundmass and as phenocrysts.			
<b>Additional Notes:</b>			
Rare occurrences of simply twinned clinopyroxene. Glomerocrysts consist of needles of 10 to 30 plagioclases, 1 to 1.5 mm in size, arranged in an apparently random pattern.			

<b>Specimen:</b> 896-15			
<b>Depth:</b> 384.25 mbsf			
<b>Lithology:</b> Pillow Basalt			
<b>Texture:</b> glomeropophyritic			
<b>Grain Size:</b> fine to coarse-grained			
<b>Primary Mineralogy:</b>			
	%	Size Range	Crystal Shape
<b>Phenocrysts:</b>			
Plagioclase		0.1 - 1.5 mm	subhedral - euhedral
Olivine		0.5 - 1 mm	anhedral
<b>Groundmass:</b> Microcrystalline groundmass consisting of acicular crystals of plagioclase and altered olivines			
<b>Alteration:</b>			
Olivine phenocrysts are partially altered to red / brown oxides, occur as "blebs" 0.5 to 1 mm in diameter. Olivine in the groundmass is extensively replaced by clays / oxides.			
<b>Additional Notes:</b>			
Plagioclase phenocrysts often form glomerocrysts, consist of crystals 1 to 5 mm in size.			

<b>Specimen:</b> 896-16			
<b>Depth:</b> 386.49 mbsf			
<b>Lithology:</b> Basalt			
<b>Texture:</b> porphyritic			
<b>Grain Size:</b> fine to medium-grained			
<b>Primary Mineralogy:</b>			
	%	Size Range	Crystal Shape
<b>Phenocrysts:</b>			
Plagioclase	6	0.5 - 1 mm	subhedral - euhedral
Olivine	1	0.5 - 1 mm	anhedral
Clinopyroxene	< 1	1 mm	subhedral
<b>Groundmass:</b> Microcrystalline groundmass consisting of acicular crystals of plagioclase and altered olivines			
<b>Alteration:</b>			
Olivine is completely replaced both in the groundmass and as phenocrysts to red / brown oxides.			
<b>Additional Notes:</b>			
One example of a compositionally zoned plagioclase crystal occurs.			

<b>Specimen:</b> 896-17			
<b>Depth:</b> 394.97 mbsf			
<b>Lithology:</b> Massive Basalt			
<b>Texture:</b> Intergranular			
<b>Grain Size:</b> medium-grained			
<b>Primary Mineralogy:</b>			
	%	Size Range	Crystal Shape
Plagioclase		0.75 - 1 mm	subhedral - euhedral
Olivine		0.75 - 1 mm	subhedral - euhedral
<b>Alteration:</b>			
Plagioclase crystals show little or no replacement or alteration. Olivines have been extensively (50-75%) replaced by Fe oxyhydroxides (red / brown in colour).			
<b>Additional Notes:</b>			
Plagioclase occurs as lath-shaped crystals often forming "flower-like" radial clusters.			

<b>Specimen:</b> 896-19			
<b>Depth:</b> 401.94 mbsf			
<b>Lithology:</b> Massive basalt			
<b>Texture:</b> Glomeroporphyritic			
<b>Grain Size:</b> fine to medium-grained			
<b>Primary Mineralogy:</b>			
	%	Size Range	Crystal Shape
Plagioclase	4.5	0.1 - 1 mm	subhedral - euhedral
Olivine	2	0.1 - 1 mm	subhedral
Clinopyroxene (?)	< 1	< 1 mm	subhedral
<b>Alteration:</b>			
Olivine grains are extensively fractured and replaced along these fractures by opaque minerals.			
<b>Additional Notes:</b>			
Rare occurrences of a green / brown pleochroic mineral with moderate birefringence (pyroxene?).			

<b>Specimen:</b> 896-20			
<b>Depth:</b> 402.96 mbsf			
<b>Lithology:</b> Massive Basalt			
<b>Texture:</b> Intergranular			
<b>Grain Size:</b> medium-grained			
<b>Primary Mineralogy:</b>			
	%	Size Range	Crystal Shape
Plagioclase		0.5 - 1 mm	subhedral - euhedral
Olivine		0.5 - 0.75 mm	subhedral - euhedral
<b>Alteration:</b>			
Olivine is patchily replaced by red / brown Fe oxyhydroxides.			
<b>Additional Notes:</b>			
Plagioclase and olivine frequently occur intergrown with one another.			

<b>Specimen:</b> 896-21		
<b>Depth:</b> 404.01 mbsf		
<b>Lithology:</b> Massive Basalt		
<b>Texture:</b> Intergranular		
<b>Grain Size:</b> fine to coarse (glomerocrysts)		
<b>Primary Mineralogy:</b>		
%	Size Range	Crystal Shape
Plagioclase	0.5 - 1 mm	subhedral - euhedral
Olivine	0.5 - 1 mm	subhedral - euhedral
<b>Alteration:</b>		
The section is cut by a vein 0.1 mm thick filled with red / brown material		
<b>Additional Notes:</b>		
Similar section to 896-20 but with more widespread replacement of olivine		

<b>Specimen:</b> 896-22		
<b>Depth:</b> 408.43 mbsf		
<b>Lithology:</b> Massive Basalt		
<b>Texture:</b> Intergranular		
<b>Grain Size:</b> medium-grained		
<b>Primary Mineralogy:</b>		
%	Size Range	Crystal Shape
Plagioclase	0.5 - 1 mm	subhedral - euhedral
Olivine	0.5 - 1 mm	subhedral - euhedral
Opaques	< 0.5 mm	
<b>Alteration:</b>		
Olivine is patchily altered to red / brown Fe oxyhydroxides. Many retain relatively unaltered cores.		
<b>Additional Notes:</b>		
Section consists of intergrown plagioclase and olivine crystals.		

<b>Specimen:</b> 896-25			
<b>Depth:</b> 415.00 mbsf			
<b>Lithology:</b> Pillow Basalt			
<b>Texture:</b> Glomeroporphyritic			
<b>Grain Size:</b> fine to coarse (glomerocrysts)			
<b>Primary Mineralogy:</b>			
	%	Size Range	Crystal Shape
<b>Phenocrysts:</b>			
Plagioclase	6	0.5 - 1 mm	subhedral - euhedral
Olivine	2	0.5 - 0.75 mm	subhedral
<b>Groundmass:</b> Microcrystalline groundmass consisting of acicular crystals of plagioclase and altered olivines			
<b>Alteration:</b>			
Olivine is altered to red / brown Fe oxyhydroxides at crystal edges with relatively unaltered cores preserved.			
<b>Additional Notes:</b>			

<b>Specimen:</b> 896-27			
<b>Depth:</b> 431.53 mbsf			
<b>Lithology:</b> Pillow Basalt			
<b>Texture:</b> Glomeroporphyritic			
<b>Grain Size:</b> fine to coarse (glomerocrysts)			
<b>Primary Mineralogy:</b>			
	%	Size Range	Crystal Shape
<b>Phenocrysts:</b>			
Plagioclase	3	0.5 - 1 mm	subhedral - euhedral
Olivine	1	1 - 2 mm	anhedral
<b>Groundmass:</b> Microcrystalline groundmass consisting of acicular crystals of plagioclase and altered olivines			
<b>Alteration:</b>			
Olivine is altered both in the groundmass and as phenocrysts to red / brown Fe oxyhydroxides. The section contains a small vein (0.1 mm) filled with a red / brown material with anomalous birefringent colours, Fe oxyhydroxides (?).			

<b>Specimen:</b> 896-28			
<b>Depth:</b> 434.06 mbsf			
<b>Lithology:</b> Pillow Basalt			
<b>Texture:</b> Porphyritic			
<b>Grain Size:</b> fine to medium-grained			
<b>Primary Mineralogy:</b>			
	%	Size Range	Crystal Shape
<b>Phenocrysts:</b>			
Plagioclase	5	0.5 - 1 mm	subhedral - euhedral
Olivine	1 - 2	0.5 - 1 mm	anhedral
<b>Groundmass:</b> Microcrystalline groundmass consisting of acicular crystals of plagioclase and altered olivines			
<b>Alteration:</b>			
The groundmass is extensively replaced by a red / brown material (Fe oxyhydroxides). Olivine phenocrysts are also replaced by Fe oxyhydroxides. Plagioclase crystals are mildly altered.			

<b>Specimen:</b> 896-30			
<b>Depth:</b> 441.54 mbsf			
<b>Lithology:</b> Pillow Basalt			
<b>Texture:</b> Porphyritic			
<b>Grain Size:</b> fine to medium-grained			
<b>Primary Mineralogy:</b>			
	%	Size Range	Crystal Shape
<b>Phenocrysts:</b>			
Plagioclase	6	0.5 - 1 mm	subhedral - euhedral
Olivine	1	0.5 - 0.75 mm	anhedral - subhedral
<b>Groundmass:</b> Microcrystalline groundmass consisting of acicular crystals of plagioclase and altered olivines			
<b>Alteration:</b>			
The groundmass is altered to a grey amorphous material (clay?).			
<b>Additional Notes:</b>			
Section contains rare examples of an anhedral brown / green mineral, non-pleochroic. In XPL this mineral has very low birefringence. Most olivine phenocrysts occur as radial or "flower-shaped" crystals.			

<b>Specimen:</b> 896-31			
<b>Depth:</b> 449.75 mbsf			
<b>Lithology:</b> Pillow Basalt			
<b>Texture:</b> Glomeroporphyritic			
<b>Grain Size:</b> fine to coarse (glomerocrysts)			
<b>Primary Mineralogy:</b>			
	%	Size Range	Crystal Shape
<b>Phenocrysts:</b>			
Plagioclase	6	0.5 - 1.5 mm	subhedral - euhedral
Olivine	2	0.5 - 1 mm	anhedral
<b>Groundmass:</b> Microcrystalline groundmass consisting of acicular crystals of plagioclase and altered olivines			
<b>Alteration:</b>			
Olivine is replaced by Fe oxyhydroxides both in the groundmass and as phenocrysts.			
<b>Additional Notes:</b>			
Plagioclase phenocrysts often occur clustered together as glomerocrysts. These are accumulations of 5 to 20 crystals.			

<b>Specimen:</b> 896-32			
<b>Depth:</b> 450.69 mbsf			
<b>Lithology:</b> Basalt			
<b>Texture:</b> Porphyritic			
<b>Grain Size:</b> fine to medium-grained			
<b>Primary Mineralogy:</b>			
	%	Size Range	Crystal Shape
<b>Phenocrysts:</b>			
Plagioclase	4	0.5 - 1 mm	subhedral - euhedral
Olivine	1	0.5 - 1 mm	anhedral - subhedral
<b>Groundmass:</b> Microcrystalline groundmass consisting of acicular crystals of plagioclase and altered olivines			
<b>Alteration:</b>			
Many olivine phenocrysts are unaltered. However some show patchy replacement by Fe oxyhydroxides.			
<b>Additional Notes:</b>			

<b>Specimen:</b> 896-33			
<b>Depth:</b> 460.14 mbsf			
<b>Lithology:</b> Pillow Basalt			
<b>Texture:</b> Glomeroporphyritic			
<b>Grain Size:</b> fine to coarse (glomerocrysts)			
<b>Primary Mineralogy:</b>			
	%	Size Range	Crystal Shape
<b>Phenocrysts:</b>			
Plagioclase	> 5	0.5 - 0.75 mm	subhedral - euhedral
Olivine	< 1	0.5 - 1 mm	anhedral - subhedral
<b>Groundmass:</b> Microcrystalline groundmass consisting of acicular crystals of plagioclase and altered olivines			
<b>Alteration:</b>			
Olivine phenocrysts and in groundmass have been replaced by Fe oxyhydroxides. The section contains a thin vein (0.1mm). This contains a dark grey material and a lime green material.			

<b>Specimen:</b> 896-34			
<b>Depth:</b> 460.86			
<b>Lithology:</b> Pillow Basalt			
<b>Texture:</b> Glomeroporphyritic			
<b>Grain Size:</b> fine to coarse (glomerocrysts)			
<b>Primary Mineralogy:</b>			
	%	Size Range	Crystal Shape
<b>Phenocrysts:</b>			
Plagioclase	5	0.5 - 1 mm	subhedral - euhedral
Olivine	1	0.5 - 1 mm	subhedral - euhedral
<b>Groundmass:</b> Microcrystalline groundmass consisting of acicular crystals of plagioclase and altered olivines			
<b>Alteration:</b>			
Olivine is extensively replaced by red / brown Fe oxyhydroxides.			
<b>Additional Notes:</b>			
Glomerocrysts in the section contain both olivine and plagioclase phenocrysts. They contain 10 to 30 crystals and are up to 5 mm in size.			

## D.2. Hole 735B samples

<b>Specimen:</b> 735-1			
<b>Depth:</b> 33.9 mbsf			
<b>Lithology:</b> Porphyroclastic Metagabbro			
<b>Texture:</b>			
<b>Grain Size:</b> fine to coarse-grained			
<b>Original Mineralogy:</b>			
	%	Size Range	Crystal Shape
Plagioclase	50	1 - 5 mm	subhedral - anhedral
Olivine	20	1 - 2 mm	anhedral
Clinopyroxene	30	1 - 3 mm	anhedral
<b>Alteration:</b>			
All mineral grains are extensively altered. Olivine is completely replaced by talc, serpentine and red brown iddingsite			
Clinopyroxene has been extensively replaced by green amphibole and biotite with a few rare remnant crystals remaining			
Plagioclase has been recrystallised in many cases. The remnant plagioclase grains have been deformed and show undulose extinction			

<b>Specimen:</b> 735-2			
<b>Depth:</b> 43.48 mbsf			
<b>Lithology:</b> Olivine-Bearing Gabbro			
<b>Texture:</b> granular			
<b>Grain Size:</b> very coarse-grained			
<b>Mineralogy:</b>			
	%	Size Range	Crystal Shape
Plagioclase	60	< 1 to > 10 mm	subhedral - anhedral
Clinopyroxene	40	< 1 to > 10 mm	anhedral
<b>Alteration and Deformation:</b>			
Clinopyroxene is extensively altered to a green - brown mineral with relatively high birefringence (amphibole?)			
A number of fine (0.1 - 0.5 mm) veins are present within the section. These are filled by a green - brown mineral similarly to that seen replacing clinopyroxene.			
<b>Additional Notes:</b>			
No olivine was observed in this section.			

<b>Specimen:</b> 735-3			
<b>Depth:</b> 62.07 mbsf			
<b>Lithology:</b> Massive Metagabbro			
<b>Texture:</b>			
<b>Grain Size:</b> fine to coarse-grained			
<b>Mineralogy:</b>			
	%	Size Range	Crystal Shape
Plagioclase		0.5 - 5 mm	anhedral
Clinopyroxene		0.5 - 5 mm	anhedral
<b>Alteration and Deformation:</b>			
<p>Both plagioclase and clinopyroxene have been extensively altered and recrystallised  Clinopyroxene has been extensively replaced by green amphibole. Some remnant crystals of clinopyroxene remain.  Recrystallisation of plagioclase has also occurred.  Small veins filled with amphibole also occur, these are, on average 0.5 to 1 mm wide.</p>			
<b>Additional Notes:</b>			
Rare opaque grains occur in this section.			

<b>Specimen:</b> 735-4			
<b>Depth:</b> 97.84 mbsf			
<b>Lithology:</b> Massive Olivine Gabbro			
<b>Texture:</b> granular			
<b>Grain Size:</b> coarse-grained			
<b>Mineralogy:</b>			
	%	Size Range	Crystal Shape
Plagioclase	55	0.5 - 2 mm	subhedral
Clinopyroxene	35	1 - 15 mm	subhedral - anhedral
Olivine	10	1 - 2 mm	anhedral
<b>Alteration and Deformation:</b>			
<p>Clinopyroxene is replaced at edges to a light green mineral with relatively high birefringence (amphibole?).  Olivine is replaced along edges and some fractures by a green / white fibrous material with high birefringence</p>			
<b>Additional Notes:</b>			
<p>The section is dominated by a large clinopyroxene crystal ~ 15 mm in size.  Some opaque grains occur in the section.</p>			

<b>Specimen: 735-5</b>			
<b>Depth: 169.57 mbsf</b>			
<b>Lithology: Olivine-Bearing Gabbro</b>			
<b>Texture: granular to sub-ophitic</b>			
<b>Grain Size: medium to coarse-grained</b>			
<b>Mineralogy:</b>			
	%	Size Range	Crystal Shape
Plagioclase	65	0.5 - 5 mm	subhedral
Clinopyroxene	30	1 - 3 mm	subhedral - anhedral
Olivine	5	1 - 2 mm	anhedral
<b>Alteration and Deformation:</b>			
<p>Clinopyroxene has been replaced at edges by a brown / green mineral (amphibole?)  Olivine is extensively replaced at edges by a white / green fibrous material with high birefringence.  Also get replacement of olivine by opaques particularly along fractures.  A fine vein (~ 0.2 mm) is present within the section, it is filled with amphibole.</p>			
<b>Additional Notes:</b>			
Clinopyroxene is partially enclosed by larger plagioclase crystals.			

<b>Specimen: 735-6</b>			
<b>Depth: 199.73 mbsf</b>			
<b>Lithology: Olivine Gabbro</b>			
<b>Texture: granular to sub-ophitic</b>			
<b>Grain Size: medium to coarse-grained</b>			
<b>Mineralogy:</b>			
	%	Size Range	Crystal Shape
Plagioclase	55	1 - 3 mm	anhedral
Clinopyroxene	35	1 - 3 mm	anhedral
Olivine	10	1 - 2 mm	anhedral
<b>Alteration and Deformation:</b>			
<p>The section is foliated, due to the alignment of clinopyroxene grains.  Clinopyroxene is replaced by a green mineral at the edges of some grains (amphibole?).  Olivine is replaced by opaque minerals along fractures and at the edges of grains.</p>			
<b>Additional Notes:</b>			
<p>Some clinopyroxene grains are simply twinned.  Small, rare, opaque grains occur. These range in size from 0.1 to 0.5 mm.</p>			

<b>Specimen: 735-7</b>			
<b>Depth: 214.47 mbsf</b>			
<b>Lithology: Olivine Gabbro - Ilmenite and Sulphide-Bearing</b>			
<b>Texture: granular to sub-ophitic</b>			
<b>Grain Size: medium to coarse-grained</b>			
<b>Mineralogy:</b>			
	%	Size Range	Crystal Shape
Plagioclase	50	1 - 10 mm	subhedral - anhedral
Clinopyroxene	35	1 - 10 mm	anhedral
Olivine	15	1 - 10 mm	anhedral
<b>Alteration and Deformation:</b>			
<p>Minor replacement of clinopyroxene by amphibole occurs at the edges of grains.  Olivine is replaced at edges by a colourless, relatively high relief mineral with very high birefringence colours.</p>			
<b>Additional Notes:</b>			
Some plagioclase grains are partially enclosed by clinopyroxenes and olivines.			

<b>Specimen: 735-8</b>			
<b>Depth: 226.82 mbsf</b>			
<b>Lithology: Iron-Titanium Oxide Gabbro (Olivine-Bearing)</b>			
<b>Texture: granular</b>			
<b>Grain Size: very coarse-grained</b>			
<b>Mineralogy:</b>			
	%	Size Range	Crystal Shape
Plagioclase	65	1 - 5 mm	anhedral
Clinopyroxene	30	up to 20 mm	anhedral
Opaques	5	1 - 2 mm	anhedral
<b>Alteration:</b>			
<p>The large clinopyroxene grain is extensively replaced by green amphibole, brown biotite (?) and opaque minerals both at the crystal edges and within the grain.  A thin vein (0.1 mm) cuts the large clinopyroxene vein. This contains a colourless mineral with low birefringence (feldspar?). The vein also cuts amphibole (altered clinopyroxene) therefore probably postdates alteration of clinopyroxene.</p>			
<b>Additional Notes:</b>			
The section is dominated by a large clinopyroxene grain > 20 mm in size.			

<b>Specimen:</b> 735-9			
<b>Depth:</b> 238.82 mbsf			
<b>Lithology:</b> Ilmenite-Bearing Gabbro			
<b>Texture:</b> granular			
<b>Grain Size:</b> coarse-grained			
<b>Mineralogy:</b>			
	%	Size Range	Crystal Shape
Plagioclase	60	3 - > 10 mm	anhedral
Clinopyroxene	35	3 - > 10 mm	anhedral
Opaques (ilmenite?)	5	1 - 5 mm	anhedral
<b>Alteration:</b>			
<p>Clinopyroxene is commonly replaced by green amphibole and brown biotite (?). This usually occurs at the edges of grains but in some cases extends into the centre of a grain.</p> <p>Opaque minerals (ilmenite?) occur rimmed with amphibole and a red non-pleochroic mineral (oxides?).</p>			
<b>Additional Notes:</b>			
Small opaque crystals $\leq$ 1 mm occur within plagioclase and clinopyroxene grains.			

<b>Specimen:</b> 735-10			
<b>Depth:</b> 284.13 mbsf			
<b>Lithology:</b> Olivine Gabbro			
<b>Texture:</b> granular to sub-ophitic			
<b>Grain Size:</b> medium to coarse-grained			
<b>Mineralogy:</b>			
	%	Size Range	Crystal Shape
Plagioclase	50	1 - 7 mm	anhedral
Clinopyroxene	40	1 - 5 mm	anhedral
Olivine	10	1 - 7 mm	anhedral
<b>Alteration and Deformation:</b>			
<p>Clinopyroxene is replaced by a pale green mineral (amphibole?) particularly at crystal edges.</p> <p>Edges of olivine grains are replaced by a colourless mineral with high relief and very high birefringence.</p> <p>Replacement by opaques along fractures also occurs.</p>			
<b>Additional Notes:</b>			
<p>Some plagioclase crystals are partially enclosed by larger clinopyroxene crystals.</p> <p>Rare opaque grains occur throughout the section.</p>			

<b>Specimen:</b> 735-11			
<b>Depth:</b> 387.93 mbsf			
<b>Lithology:</b> Olivine Gabbro			
<b>Texture:</b> granular to sub-ophitic			
<b>Grain Size:</b> medium to coarse-grained			
<b>Mineralogy:</b>			
	%	Size Range	Crystal Shape
Plagioclase	50	< 10 mm	subhedral
Clinopyroxene	43	< 7.5 mm	subhedral
Olivine	7	< 15 mm	anhedral
<b>Alteration:</b>			
Clinopyroxene is patchily altered to green amphibole at some crystal edges. Olivine is extensively replaced by opaque minerals along fractures, forming a mesh-like pattern.			
<b>Additional Notes:</b>			
Plagioclase is frequently partially enclosed by clinopyroxene crystals. Rare clinopyroxene grains show simple twinning.			

<b>Specimen:</b> 735-12			
<b>Depth:</b> 415.70 mbsf			
<b>Lithology:</b> Olivine Gabbro			
<b>Texture:</b> granular to sub-ophitic			
<b>Grain Size:</b> medium to coarse-grained			
<b>Mineralogy:</b>			
	%	Size Range	Crystal Shape
Plagioclase	45	1 - 10 mm	anhedral - subhedral
Clinopyroxene	50	1 - 10 mm	anhedral - subhedral
Olivine	5	1 - 10 mm	anhedral
<b>Alteration:</b>			
Olivine is replaced at edges of grains by a red / brown amorphous material with anomalous birefringence colours.			
<b>Additional Notes:</b>			
One large clinopyroxene crystal is simply twinned. Plagioclase sometimes occurs partially enclosed by clinopyroxene.			

<b>Specimen:</b> 735-13			
<b>Depth:</b> 461.77 mbsf			
<b>Lithology:</b> Troctolite			
<b>Texture:</b>			
<b>Grain Size:</b> medium to coarse-grained			
<b>Original Mineralogy:</b>			
	%	Size Range	Crystal Shape
Plagioclase	45	0.2 - 1.0 mm	anhedral
Olivine	45	0.5 - 1.0 mm	anhedral
Clinopyroxene	10	0.5 - 1.0 mm	anhedral
<b>Alteration:</b>			
The section has been extensively altered. Olivine grains are intensely fractured with opaque minerals filling the fractures			
Plagioclase has been extensively recrystallised			
Clinopyroxene has been replaced by green amphibole			

<b>Specimen:</b> 735-14			
<b>Depth:</b> 479.41 mbsf			
<b>Lithology:</b> Troctolite			
<b>Texture:</b> granular to sub-ophitic			
<b>Grain Size:</b> coarse-grained			
<b>Mineralogy:</b>			
	%	Size Range	Crystal Shape
Plagioclase	75	2 - 3 mm	anhedral - subhedral
Clinopyroxene	5	2 - 3 mm	anhedral
Olivine	15	< 2 mm	anhedral
<b>Alteration:</b>			
Olivine is patchily replaced at edges of grains by a colourless mineral with very high birefringent colours.			
Olivine is also replaced in patches by a red / brown mineral. Colour of this mineral is so strong it masks the birefringence (oxides?)			
<b>Additional Notes:</b>			
Plagioclase often occurs partially enclosed by olivine grains.			

<b>Specimen:</b> HAG-1			
<b>Depth:</b> 517.97 mbsf			
<b>Lithology:</b> Troctolite			
<b>Texture:</b> Granular			
<b>Grain Size:</b> fine to medium-grained			
<b>Mineralogy:</b>			
	%	Size Range	Crystal Shape
Plagioclase	65	0.5 - 2 mm	anhedral - subhedral
Clinopyroxene	5	0.5 - 1 mm	anhedral
Olivine	30	0.25 - 1 mm	anhedral
Opagues	< 1		
<b>Alteration and Deformation:</b>			
<p>Plagioclase is relatively fresh and unaltered. Some crystals show undulose extinction.  Olivine is replaced by opaque minerals along edges and fractures.  Some clinopyroxene grains are altered to a brown pleochroic mineral at edges.</p>			
<b>Additional Notes:</b>			
Rare opaque minerals occur in the section, these are usually < 0.2 mm in size.			

<b>Specimen:</b> HAG-2			
<b>Depth:</b> 534.52 mbsf			
<b>Lithology:</b> Olivine Gabbro			
<b>Texture:</b> Granular			
<b>Grain Size:</b> fine to medium			
<b>Mineralogy:</b>			
	%	Size Range	Crystal Shape
Plagioclase	50	up to 1 mm	anhedral
Clinopyroxene	40	0.1 - 3 mm	anhedral
Olivine	10	up to 1 mm	anhedral
<b>Alteration and Deformation:</b>			
<p>Plagioclase has undergone little or no alteration  Olivine is almost entirely replaced by opaques and a red-brown amorphous material  Clinopyroxene is altered to a green / brown pleochroic mineral  The section is cut by a network of fine green veins (&lt; 0.1 mm). These are filled with a dark to light green pleochroic mineral with high birefringence.  Alteration of mineral grains close to the veins has occurred this is accompanied in some cases by recrystallisation</p>			

<b>Specimen:</b> HAG-3			
<b>Depth:</b> 537.25 mbsf			
<b>Lithology:</b> Disseminated FeTi Oxide Gabbro			
<b>Texture:</b> Granular			
<b>Grain Size:</b> coarse-grained			
<b>Mineralogy:</b>			
	%	Size Range	Crystal Shape
Plagioclase	50	up to 1.5 mm	anhedral
Clinopyroxene	45	up to 2 mm	anhedral
Olivine	5	up to 1.5 mm	anhedral
<b>Alteration and Deformation:</b>			
<p>There is no foliation within the section</p> <p>The section is cross-cut by a number of small veins ~0.1mm wide. These are filled with a pleochroic (pale to deep green) material. Any crystals close to the veins have undergone some degree of alteration. Plagioclase is largely unaltered except where it occurs close to a vein</p> <p>Clinopyroxene is altered to a pale green-deep green pleochroic mineral especially close to the veining</p> <p>Olivine is largely replaced by opaque oxides, this is particularly common along the edges of crystals and along fractures</p>			

<b>Specimen:</b> HAG-4			
<b>Depth:</b> 670.65 mbsf			
<b>Lithology:</b> Gabbronorite			
<b>Texture:</b> Granular			
<b>Grain Size:</b> coarse-grained			
<b>Mineralogy:</b>			
	%	Size Range	Crystal Shape
Plagioclase	50	0.5 - 4 mm	subhedral - anhedral
Clinopyroxene	35	0.5 - 6 mm	anhedral
Orthopyroxene	5	0.5 - 4 mm	anhedral
Olivine	10	1 - 2 mm	anhedral
<b>Alteration and Deformation:</b>			
<p>The section is unfoliated.</p> <p>Plagioclase shows very little alteration.</p> <p>Some clinopyroxene crystals have been replaced by a pale to rich brown pleochroic mineral at edges and along fractures.</p> <p>Olivine is extensively replaced along fractures by opaque minerals.</p>			
<b>Additional Notes:</b>			
<p>Clinopyroxene crystals are usually rather large with a strongly-developed cleavage. Some examples show undulose extinction and have a "wavy" cleavage.</p>			

<b>Specimen:</b> HAG-5			
<b>Depth:</b> 705.41 mbsf			
<b>Lithology:</b> FeTi Oxide Gabbro			
<b>Texture:</b> granular			
<b>Grain Size:</b> coarse-grained			
<b>Mineralogy:</b>			
	%	Size Range	Crystal Shape
Plagioclase	50	3 - 7 mm	subhedral
Clinopyroxene	30	1 - 5 mm	anhedral
Orthopyroxene	5	1 - 3 mm	anhedral
Olivine	15	1 - 2 mm	anhedral
<b>Alteration and Deformation:</b>			
<p>This section shows no foliation but has suffered a higher degree of alteration than previous examples. Plagioclase crystals show undulose extinction.</p> <p>Both clinopyroxene and orthopyroxene have been extensively replaced by a green / brown pleochroic mineral (amphibole?) and are patchily replaced by a red / brown pleochroic mineral (biotite?).</p> <p>Olivines have been extensively altered and recrystallised. In many cases only the core of the original crystal remains. Olivine is replaced by a lime-green pleochroic mineral and a red / brown pleochroic material with anomalous birefringence colours.</p>			

<b>Specimen:</b> HAG-6			
<b>Depth:</b> 716.47 mbsf			
<b>Lithology:</b> Olivine Gabbro			
<b>Texture:</b> Granular			
<b>Grain Size:</b> medium			
<b>Mineralogy:</b>			
	%	Size Range	Crystal Shape
Plagioclase	55	<1 - 2 mm	subhedral - anhedral
Clinopyroxene	35	<1 - 3 mm	anhedral
Olivine	10	1 - 2 mm	anhedral
<b>Alteration:</b>			
<p>Plagioclase is rel. fresh</p> <p>Cpx is replaced at edges by brown pleochroic mineral (hornblende?)</p> <p>Olivines are replaced by opaques at edges and along fractures</p>			
<b>Additional Notes:</b>			
<p>No foliation / preferred orientation of crystals.</p> <p>Cpx is pale brown in colour with a strongly-developed cleavage (augite?)</p>			

<b>Specimen: HAG-7</b>			
<b>Depth: 719.90 mbsf</b>			
<b>Lithology: Olivine Microgabbro</b>			
<b>Texture: Granular</b>			
<b>Grain Size: fine-grained microgabbro</b>			
<b>Mineralogy:</b>			
	%	Size Range	Crystal Shape
Plagioclase	65	< 0.5 mm	subhedral - anhedral
Olivine	15	0.1 - 0.5 mm	anhedral
Clinopyroxene	20	0.2 - 0.4 mm	anhedral
<b>Alteration:</b>			
Plagioclase is relatively fresh.			
Clinopyroxene is often replaced by a red/brown pleochroic mineral with moderate/high birefringence			
Olivine is replaced along fractures by opaque minerals			
<b>Additional Notes:</b>			
Contact between a fine-grained microgabbro and a medium-grained olivine gabbro is seen in this section. The contact between the two lithologies is irregular.			

<b>Specimen: HAG-8</b>			
<b>Depth: 737.28 mbsf</b>			
<b>Lithology: Olivine Gabbro</b>			
<b>Texture: Granular</b>			
<b>Grain Size: coarse-grained</b>			
<b>Mineralogy:</b>			
	%	Size Range	Crystal Shape
Plagioclase	65	up to 6 mm	subhedral
Olivine	10	up to 4 mm	anhedral
Clinopyroxene	23	up to 6 mm	anhedral
Orthopyroxene	2		anhedral
<b>Alteration:</b>			
Plagioclase is relatively fresh and unaltered.			
Clinopyroxene is altered altered to a red/brown pleochroic mineral.			
Olivine is replaced by opaque minerals along fractures and at edges of grains.			
<b>Additional Notes:</b>			
Both clinopyroxene and orthopyroxene are present in the section, however, most is clinopyroxene.			
Plagioclase occurs as lath-shaped crystals.			

<b>Specimen:</b> HAG-9			
<b>Depth:</b> 799.53 mbsf			
<b>Lithology:</b> Disseminated FeTi Oxide Olivine Microgabbro			
<b>Texture:</b> Granular			
<b>Grain Size:</b> fine-grained (microgabbro)			
<b>Mineralogy:</b>			
	%	Size Range	Crystal Shape
Plagioclase	55	< 0.25 - 1.0 mm	anhedral
Olivine	35	0.25 - 2.0 mm	anhedral
Clinopyroxene	7	< 0.25 - 0.5 mm	anhedral
Opagues	3	< 0.25 - 0.5 mm	anhedral
<b>Alteration and Deformation:</b>			
<p>The section is foliated with a preferred orientation of plagioclase crystals  Plagioclase is relatively fresh and unaltered  Clinopyroxene is often altered to a reddish-brown material at crystal edges  Olivine is often replaced by opaque minerals along fractures and at xtal edges</p>			
<b>Additional Notes:</b>			
Clinopyroxene has a well-developed cleavage and is a dirty brown colour. Rare examples of crystals are up to 2mm in size			

<b>Specimen:</b> HAG-10			
<b>Depth:</b> 823.62 mbsf			
<b>Lithology:</b> FeTi Oxide Gabbro			
<b>Texture:</b> ophitic			
<b>Grain Size:</b> medium-grained			
<b>Mineralogy:</b>			
	%	Size Range	Crystal Shape
Plagioclase	40	0.1 - 1 mm	anhedral
Clinopyroxene	40	1 - 4 mm	subhedral - anhedral
Olivine	1	< 1 mm	anhedral
FeTi Oxides	20		
<b>Alteration and Deformation:</b>			
<p>Many of the plagioclase grains appear to have been recrystallised.  Clinopyroxene is patchily altered to a green to brown pleochroic mineral with moderate to high birefringence.  Olivine is replaced along fractures by opaques and a red / brown material.</p>			
<b>Additional Notes:</b>			
<p>Small plagioclase are often enclosed by larger clinopyroxene grains.  FeTi oxides predominantly occur between mineral grains.</p>			

<b>Specimen: HAG-11</b>			
<b>Depth: 871.79 mbsf</b>			
<b>Lithology: Olivine Gabbro</b>			
<b>Texture: granular</b>			
<b>Grain Size: medium to coarse-grained</b>			
<b>Mineralogy:</b>			
	%	Size Range	Crystal Shape
Plagioclase	65	0.1 - 5 mm	subhedral - anhedral
Clinopyroxene	28	0.5 - 2 mm	anhedral
Olivine	7	1 - 3 mm	anhedral
<b>Alteration and Deformation:</b>			
<p>There appears to have been some recrystallisation of plagioclase.  Clinopyroxene is patchily replaced by a brown pleochroic mineral (biotite?).  Olivine is replaced by opaque minerals along fractures.</p>			

<b>Specimen: HAG-12</b>			
<b>Depth: 891.48 mbsf</b>			
<b>Lithology: Disseminated FeTi Oxide Olivine Gabbro</b>			
<b>Texture: Granular</b>			
<b>Grain Size: coarse-grained</b>			
<b>Mineralogy:</b>			
	%	Size Range	Crystal Shape
Plagioclase	45	0.5 - > 7 mm	subhedral
Clinopyroxene	45	0.5 - > 7 mm	anhedral
Olivine	5	1 - 2 mm	anhedral
FeTi Oxides	5		
<b>Alteration:</b>			
<p>Clinopyroxene is patchily replaced by a red/brown pleochroic mineral with relatively high birefringence and replaced at edges by a green pleochroic mineral (amphibole?)  Olivine is altered at edges to a pale green/brown pleochroic mineral with moderate/high birefringence  The section is cut by a number of small veins 0.1 - 1 mm thick. These are infilled with a brown pleochroic material. Grains surrounding the veins are altered.</p>			
<b>Additional Notes:</b>			
<p>Fe Ti oxides occur filling fractures in olivines and between mineral grains.</p>			

<b>Specimen:</b> HAG-13			
<b>Depth:</b> 929.47 mbsf			
<b>Lithology:</b> Gabbro			
<b>Texture:</b> Granular			
<b>Grain Size:</b> coarse-grained			
<b>Mineralogy:</b>			
	%	Size Range	Crystal Shape
Plagioclase	~49	1 -3 mm	subhedral - anhedral
Clinopyroxene	50	1 - 7 mm	anhedral
Opaques	<1	< 1 mm	anhedral
<b>Alteration and Deformation:</b>			
There is no foliation / preferred alignment of crystals Plagioclase has undergone little or no alteration Clinopyroxene crystals are commonly replaced at their edges by a brown/green mineral (hornblende?)			
<b>Additional Notes:</b>			
The section mainly consists of clinopyroxene and plagioclase with no olivine and a few minor opaque grains			

<b>Specimen:</b> HAG-14			
<b>Depth:</b> 944.91 mbsf			
<b>Lithology:</b> Gabbro			
<b>Texture:</b> Granular			
<b>Grain Size:</b> fine to coarse-grained			
<b>Mineralogy:</b>			
	%	Size Range	Crystal Shape
Plagioclase	50	< 0.1 - 7 mm	anhedral
Clinopyroxene	48	1.5 - 7 mm	anhedral
Olivine	2	1 - 3 mm	anhedral
Opaques	<1	< 1 mm	anhedral
<b>Alteration and Deformation:</b>			
Some foliation can be observed in the section, there is a preferred alignment of clinopyroxene crystals Clinopyroxene is often replaced patchily by a brown pleochroic mineral (amphibole?) Olivine is often replaced by opaque minerals, particularly along fractures			
<b>Additional Notes:</b>			
The plagioclase crystals are smaller than the clinopyroxene crystals and appear to have crystallised very rapidly (recrystallisation?)			

<b>Specimen:</b> HAG-15			
<b>Depth:</b> 962.20 mbsf			
<b>Lithology:</b> Olivine Microgabbro			
<b>Texture:</b> Granular			
<b>Grain Size:</b> fine-grained (microgabbro)			
<b>Mineralogy:</b>			
	%	Size Range	Crystal Shape
Plagioclase	50	0.1 - 0.75 mm	anhedral
Clinopyroxene	45	0.1 - 1.0 mm	anhedral
Olivine	5	0.1 - 0.5 mm	anhedral
<b>Alteration and Deformation:</b>			
<p>The section is well-foliated - alignment of clinopyroxene, plagioclase and olivine crystals  Some clinopyroxene crystals have their edges replaced by a brown pleochroic mineral (hornblende?)  Plagioclase is relatively unaltered</p>			

<b>Specimen:</b> HAG-16			
<b>Depth:</b> 1040. 76 mbsf			
<b>Lithology:</b> Olivine Gabbro			
<b>Texture:</b> granular to ophitic			
<b>Grain Size:</b> coarse-grained			
<b>Mineralogy:</b>			
	%	Size Range	Crystal Shape
Plagioclase	45	0.1 - 2 mm	subhedral
Clinopyroxene	45	1 - 2 mm	anhedral
Olivine	10	0.5 - 5 mm	anhedral
<b>Alteration and Deformation:</b>			
<p>Plagioclase is relatively fresh and unaltered.  Olivine is replaced at edges by a pale to dark brown pleochroic mineral with moderately high birefringence.  Clinopyroxene is patchily (&lt; 0.1 mm) replaced by a pale to dark brown pleochroic mineral with moderate to high birefringence (amphibole?).</p>			
<b>Additional Notes:</b>			
<p>Some plagioclase crystals are partially or fully enclosed by large clinopyroxene grains.</p>			

<b>Specimen:</b> HAG-17			
<b>Depth:</b> 1083.83 mbsf			
<b>Lithology:</b> Olivine Gabbro			
<b>Texture:</b> granular			
<b>Grain Size:</b> medium to coarse-grained			
<b>Mineralogy:</b>			
	%	Size Range	Crystal Shape
Plagioclase	55	0.5 - 3 mm	anhedral - subhedral
Clinopyroxene	40	0.25 - 5 mm	anhedral
Orthopyroxene	< 1	1 - 2 mm	anhedral
Olivine	5	0.5 - 1 mm	anhedral
<b>Alteration and Deformation:</b>			
A slight foliation can be noted throughout the section, this is due to the alignment of clinopyroxene grains.			
Clinopyroxene is altered in small patches (0.1 mm) to a red / brown material with high birefringence.			
Olivine is replaced by opaques along fractures.			
<b>Additional Notes:</b>			
A small number of crystals of orthopyroxene occur within the section.			

<b>Specimen:</b> HAG-18			
<b>Depth:</b> 1111.84 mbsf			
<b>Lithology:</b> Olivine Gabbro			
<b>Texture:</b> Glomeroporphyritic			
<b>Grain Size:</b> fine to coarse (glomerocrysts)			
<b>Mineralogy:</b>			
	%	Size Range	Crystal Shape
Plagioclase	50	0.1 - 2 mm	anhedral
Clinopyroxene	40	0.1 - 2 mm	anhedral
Olivine	10	1 - 2 mm	anhedral
<b>Alteration:</b>			
Little or no alteration of plagioclase			

<b>Specimen:</b> HAG-19			
<b>Depth:</b> 1173.38 mbsf			
<b>Lithology:</b> Olivine Gabbro			
<b>Texture:</b> granular to sub-ophitic			
<b>Grain Size:</b> medium to coarse-grained			
<b>Mineralogy:</b>			
	%	Size Range	Crystal Shape
Plagioclase	45	0.1 - 4 mm	subhedral - anhedral
Clinopyroxene	50	0.5 - 5 mm	anhedral
Olivine	5	0.1 - 3 mm	anhedral
Opaques	1		
<b>Alteration and Deformation:</b>			
Clinopyroxene is patchily altered to a colourless to pale green pleochroic mineral (amphibole?). Olivine is replaced at edges by a colourless to brown pleochroic mineral with relative high birefringence.			
<b>Additional Notes:</b>			
Opaque minerals occur replacing olivine and in between mineral grains. Some plagioclase crystals are partially enclosed by larger clinopyroxene crystals.			

<b>Specimen:</b> HAG-20			
<b>Depth:</b> 1217.76 mbsf			
<b>Lithology:</b> Olivine Gabbro + Troctolitic Gabbro			
<b>Texture:</b> granular			
<b>Grain Size:</b> very coarse-grained			
<b>Mineralogy:</b>			
	%	Size Range	Crystal Shape
Plagioclase	50	0.75 - 5 mm	subhedral - anhedral
Clinopyroxene	48	1 - 7 mm	anhedral
Olivine	2	0.75 - 2 mm	anhedral
<b>Alteration:</b>			
Plagioclase relatively unaltered. Replacement of olivine and clinopyroxene.			
<b>Additional Notes:</b>			
Section is unfoliated and very coarse-grained with most grains > 1 mm.			

<b>Specimen:</b> HAG-21			
<b>Depth:</b> 1261.84 mbsf			
<b>Lithology:</b> Olivine Gabbro			
<b>Texture:</b> granular to sub-ophitic			
<b>Grain Size:</b> medium to coarse-grained			
<b>Mineralogy:</b>			
	%	Size Range	Crystal Shape
Plagioclase	45	0.1 - 2 mm	subhedral
Clinopyroxene	45	0.5 - 2 mm	anhedral
Olivine	10	1 - 2 mm	anhedral
<b>Alteration:</b>			
Plagioclase relatively unaltered. Replacement of olivine and clinopyroxene.			
<b>Additional Notes:</b>			
Similar to previous olivine gabbro sections			

<b>Specimen:</b> HAG-22			
<b>Depth:</b> 1461.49 mbsf			
<b>Lithology:</b> Olivine Gabbro			
<b>Texture:</b> granular to sub-ophitic			
<b>Grain Size:</b> medium to coarse-grained			
<b>Mineralogy:</b>			
	%	Size Range	Crystal Shape
Plagioclase	50	0.1 to 4 mm	subhedral - anhedral
Clinopyroxene	45	0.5 to 6 mm	anhedral
Olivine	5	1 to 2 mm	anhedral
<b>Alteration and Deformation:</b>			
Clinopyroxene crystals are relatively unaltered but some show small patches of replacement by a red / brown pleochroic mineral. Olivine is also replaced by a red / brown material, particularly along fractures.			
<b>Additional Notes:</b>			
Some plagioclase crystals are partially enclosed by larger clinopyroxene grains.			

<b>Specimen:</b> HAG-23			
<b>Depth:</b> 1492.55 mbsf			
<b>Lithology:</b> Olivine Gabbro			
<b>Texture:</b> granular to ophitic			
<b>Grain Size:</b> coarse-grained			
<b>Mineralogy:</b>			
	%	Size Range	Crystal Shape
Plagioclase	55	0.5 - 5 mm	subhedral - anhedral
Clinopyroxene	45	0.75 - 7 mm	subhedral - anhedral
<b>Alteration:</b>			
Clinopyroxene is altered at edges and in patches to pale green amphibole			
<b>Additional Notes:</b>			
Coarse-grained section containing no olivine			

## APPENDIX E

---

### *Geochemistry of Hole 735B core samples*

All major oxides are quoted in weight % and trace element abundances are given in parts per million (ppm). LOI is weight loss on ignition, quoted in weight %. Approximate depths are given in metres below seafloor (mbsf).

#### E.1. Leg 118 samples

Sample	735-1	735-2	735-3	735-4	735-5	735-6	735-7
Depth	33.9	43.48	62.07	97.84	169.57	199.73	214.47
SiO <sub>2</sub>	48.51	52.06	52.85	50.00	52.95	50.39	50.12
TiO <sub>2</sub>	0.22	0.30	0.75	0.51	0.51	0.26	0.23
Al <sub>2</sub> O <sub>3</sub>	15.00	20.69	15.31	6.20	16.42	14.63	19.72
Fe <sub>2</sub> O <sub>3</sub>	8.09	3.28	8.73	9.42	8.16	5.36	4.22
MnO	0.14	0.07	0.09	0.17	0.14	0.10	0.08
MgO	12.57	5.39	7.32	17.71	7.12	11.98	8.87
CaO	10.64	14.03	10.28	14.65	10.62	14.47	13.69
Na <sub>2</sub> O	2.40	3.23	3.80	1.03	3.58	1.99	2.45
K <sub>2</sub> O	0.26	0.10	0.13	0.09	0.11	0.08	0.08
P <sub>2</sub> O <sub>5</sub>	0.03	0.02	0.06	0.02	0.02	0.01	0.01
SO <sub>3</sub>	0.07	0.02	0.01	0.02	0.02	0.03	0.01
LOI	1.86	0.35	0.31	0.27	0.05	0.39	0.27
Ba	25	29	30	29	27	18	14
Ce	0	0	0	8	0	0	0
Co	45	12	39	49	28	35	19
Cr	433	461	66	366	591	0	725

<b>Sample</b>	<b>735-1</b>	<b>735-2</b>	<b>735-3</b>	<b>735-4</b>	<b>735-5</b>	<b>735-6</b>	<b>735-7</b>
<b>Depth</b>	33.9	43.48	62.07	97.84	169.57	199.73	214.47
<b>Cu</b>	12	11	7	43	56	42	87
<b>Ga</b>	12	14	18	7	10	18	13
<b>La</b>	0	0	0	0	0	0	0
<b>Nd</b>	8	5	5	4	0	4	7
<b>Ni</b>	239	54	79	208	201	38	157
<b>Pb</b>	4	8	7	8	5	4	5
<b>S</b>	191	146	137	669	738	793	797
<b>Sc</b>	22	39	56	65	44	37	27
<b>Sr</b>	122	190	175	54	126	186	173
<b>Th</b>	0	3	1	0	0	3	0
<b>U</b>	0	2	0	0	2	0	0
<b>V</b>	89	117	205	259	150	167	108
<b>Zn</b>	41	18	14	47	24	39	23
<b>Nb</b>	0	0	0	0	0	0	0
<b>Rb</b>	1	1	0	1	0	1	0
<b>Zr</b>	19	21	65	29	19	24	18
<b>Y</b>	6	6	35	15	6	10	4

<b>Sample</b>	<b>735-8</b>	<b>735-9</b>	<b>735-10</b>	<b>735-11</b>	<b>735-12</b>	<b>735-13</b>	<b>735-14</b>
<b>Depth</b>	226.82	238.83	284.13	387.93	415.7	461.77	479.41
<b>SiO<sub>2</sub></b>	35.88	44.80	49.66	48.38	50.53	41.90	52.32
<b>TiO<sub>2</sub></b>	13.67	5.32	0.24	0.15	0.27	0.08	0.44
<b>Al<sub>2</sub>O<sub>3</sub></b>	4.04	12.81	17.84	16.07	16.37	8.10	19.88
<b>Fe<sub>2</sub>O<sub>3</sub></b>	26.96	18.44	8.22	7.34	5.28	11.71	6.76
<b>MnO</b>	0.43	0.23	0.12	0.12	0.09	0.15	0.13
<b>MgO</b>	8.58	5.53	9.93	14.48	10.83	28.41	5.78
<b>CaO</b>	9.94	9.47	10.68	10.90	13.91	4.19	9.75
<b>Na<sub>2</sub>O</b>	1.00	3.14	2.86	2.02	2.14	0.83	3.77
<b>K<sub>2</sub>O</b>	0.13	0.14	0.11	0.08	0.09	0.71	0.22
<b>P<sub>2</sub>O<sub>5</sub></b>	0.04	0.01	0.02	0.01	0.02	0.02	0.14

<b>Sample</b>	<b>735-8</b>	<b>735-9</b>	<b>735-10</b>	<b>735-11</b>	<b>735-12</b>	<b>735-13</b>	<b>735-14</b>
<b>Depth</b>	226.82	238.83	284.13	387.93	415.7	461.77	479.41
<b>SO<sub>3</sub></b>	0.07	0.03	0.02	0.02	0.03	0.03	0.03
<b>LOI</b>	-0.76	-0.26	-0.04	-0.02	0.17	3.70	0.31
<b>Ba</b>	20	46	22	11	28	17	16
<b>Ce</b>	29	0	0	0	0	0	27
<b>Co</b>	108	68	42	39	27	74	27
<b>Cr</b>	0	0	132	221	932	344	163
<b>Cu</b>	228	80	36	82	54	18	35
<b>Ga</b>	11	21	13	9	11	6	19
<b>La</b>	0	0	0	0	0	0	6
<b>Nd</b>	5	2	3	1	0	3	22
<b>Ni</b>	59	17	142	224	190	968	103
<b>Pb</b>	8	5	7	14	4	6	4
<b>S</b>	7860	3153	537	802	891	446	640
<b>Sc</b>	81	49	24	19	35	9	22
<b>Sr</b>	51	177	186	148	126	24	175
<b>Th</b>	0	6	5	5	0	3	4
<b>U</b>	0	2	0	0	0	0	0
<b>V</b>	707	901	88	56	115	35	52
<b>Zn</b>	120	86	42	35	25	49	48
<b>Nb</b>	7	2	0	0	0	0	3
<b>Rb</b>	3	1	0	2	0	3	2
<b>Zr</b>	179	42	17	14	22	12	283
<b>Y</b>	44	16	5	2	6	0	53

### E.2. Leg 176 samples

<b>Sample</b>	<b>HAG-1</b>	<b>HAG-2</b>	<b>HAG-3</b>	<b>HAG-4</b>	<b>HAG-5</b>	<b>HAG-6</b>	<b>HAG-7</b>
<b>Depth</b>	517.97	534.52	537.25	670.65	705.41	716.47	719.9
<b>SiO<sub>2</sub></b>	45.43	51.04	50.10	51.94	55.15	51.07	50.38

<b>Sample</b>	<b>HAG-1</b>	<b>HAG-2</b>	<b>HAG-3</b>	<b>HAG-4</b>	<b>HAG-5</b>	<b>HAG-6</b>	<b>HAG-7</b>
<b>Depth</b>	517.97	534.52	537.25	670.65	705.41	716.47	719.9
<b>TiO<sub>2</sub></b>	0.25	0.46	0.40	0.51	0.90	0.39	0.41
<b>Al<sub>2</sub>O<sub>3</sub></b>	16.65	15.90	16.68	14.62	20.47	16.45	16.39
<b>Fe<sub>2</sub>O<sub>3</sub></b>	7.10	7.88	7.40	6.30	6.63	6.38	7.03
<b>MnO</b>	0.11	0.14	0.13	0.13	0.10	0.11	0.12
<b>MgO</b>	17.46	9.27	9.23	9.69	2.16	9.33	10.03
<b>CaO</b>	10.34	12.06	12.45	13.78	7.86	12.99	12.47
<b>Na<sub>2</sub>O</b>	1.53	2.99	2.98	2.68	5.96	2.80	2.82
<b>K<sub>2</sub>O</b>	0.09	0.12	0.10	0.10	0.23	0.09	0.10
<b>P<sub>2</sub>O<sub>5</sub></b>	0.02	0.07	0.05	0.05	0.27	0.02	0.03
<b>SO<sub>3</sub></b>	0.06	0.04	0.04	0.06	0.06	0.04	0.04
<b>LOI</b>	0.51	0.20	0.43	0.15	0.11	0.15	0.22
<b>Ba</b>	20	14	9	20	32	28	16
<b>Ce</b>	0	0	0	7	0	0	0
<b>Co</b>	35	25	36	55	27	35	30
<b>Cr</b>	182	57	12	4	57	99	234
<b>Cu</b>	86	47	40	60	68	55	33
<b>Ga</b>	14	15	17	19	14	15	15
<b>La</b>	5	0	0	0	0	0	0
<b>Nd</b>	7	4	0	3	0	6	6
<b>Ni</b>	113	82	33	45	70	84	96
<b>Pb</b>	6	2	5	6	3	0	3
<b>S</b>	883	601	789	2259	838	1196	393
<b>Sc</b>	35	29	35	44	34	47	43
<b>Sr</b>	169	190	181	169	180	149	170
<b>Th</b>	4	0	5	3	0	0	5
<b>U</b>	0	0	0	0	0	0	0
<b>V</b>	143	112	165	549	127	219	169
<b>Zn</b>	34	31	45	77	33	41	40
<b>Nb</b>	0	0	0	0	0	1	0
<b>Rb</b>	1	1	1	2	0	2	1
<b>Zr</b>	29	36	46	34	26	56	52
<b>Y</b>	11	10	19	17	9	19	16

Sample	HAG-8	HAG-9	HAG-10	HAG-11	HAG-12	HAG-13	HAG-14	HAG-15
<b>Depth</b>	737.28	799.53	823.62	871.79	891.48	929.47	944.91	962.2
<b>SiO<sub>2</sub></b>	51.28	52.45	48.88	51.36	51.02	51.07	51.62	51.88
<b>TiO<sub>2</sub></b>	0.37	0.67	2.44	0.40	0.89	0.63	0.61	0.43
<b>Al<sub>2</sub>O<sub>3</sub></b>	18.95	15.90	13.89	17.90	14.64	16.87	15.95	16.17
<b>Fe<sub>2</sub>O<sub>3</sub></b>	5.76	8.86	14.10	6.24	7.77	6.90	7.10	7.55
<b>MnO</b>	0.10	0.17	0.21	0.11	0.14	0.12	0.14	0.14
<b>MgO</b>	7.54	7.36	6.74	8.08	9.26	8.32	8.34	8.46
<b>CaO</b>	11.89	10.94	10.30	12.19	13.19	12.83	12.86	11.71
<b>Na<sub>2</sub>O</b>	3.47	3.67	3.31	3.17	2.82	3.15	3.08	3.21
<b>K<sub>2</sub>O</b>	0.11	0.13	0.13	0.10	0.15	0.17	0.11	0.10
<b>P<sub>2</sub>O<sub>5</sub></b>	0.04	0.02	0.02	0.02	0.04	0.03	0.03	0.02
<b>SO<sub>3</sub></b>	0.03	0.03	0.02	0.01	0.04	0.03	0.02	0.05
<b>LOI</b>	0.27	-0.06	-0.11	0.01	0.13	0.05	-0.02	-0.11
<b>Ba</b>	16	24	16	26	26	23	34	31
<b>Ce</b>	10	0	16	0	0	0	0	0
<b>Co</b>	30	37	34	31	31	28	28	37
<b>Cr</b>	53	7	85	50	51	154	108	142
<b>Cu</b>	66	48	58	55	67	44	50	93
<b>Ga</b>	17	16	14	15	14	13	14	12
<b>La</b>	0	0	4	0	0	0	0	0
<b>Nd</b>	6	4	14	0	3	4	2	7
<b>Ni</b>	55	51	73	70	75	72	93	129
<b>Pb</b>	3	3	3	3	2	7	5	5
<b>S</b>	828	726	770	693	684	644	696	1192
<b>Sc</b>	42	37	41	28	37	50	38	33
<b>Sr</b>	166	180	153	185	172	153	160	169
<b>Th</b>	0	1	0	2	3	4	0	0
<b>U</b>	0	0	0	0	0	0	1	1
<b>V</b>	190	160	152	131	126	189	116	119
<b>Zn</b>	35	38	39	31	35	33	30	37
<b>Nb</b>	1	1	2	0	0	0	0	0
<b>Rb</b>	0	0	1	0	0	2	0	2
<b>Zr</b>	38	23	82	24	23	47	30	21

<b>Sample</b>	<b>HAG-8</b>	<b>HAG-9</b>	<b>HAG-10</b>	<b>HAG-11</b>	<b>HAG-12</b>	<b>HAG-13</b>	<b>HAG-14</b>	<b>HAG-15</b>
<b>Depth</b>	737.28	799.53	823.62	871.79	891.48	929.47	944.91	962.2
<b>Y</b>	15	10	17	8	7	17	8	7
<b>Sample</b>	<b>HAG-16</b>	<b>HAG-17</b>	<b>HAG-18</b>	<b>HAG-19</b>	<b>HAG-20</b>	<b>HAG-21</b>	<b>HAG-22</b>	<b>HAG-23</b>
<b>Depth</b>	1040.76	1083.83	1111.84	1173.38	1217.76	1261.84	1461.49	1492.55
<b>SiO<sub>2</sub></b>	51.63	51.24	51.26	51.19	51.29	49.69	50.52	51.38
<b>TiO<sub>2</sub></b>	0.41	0.34	0.32	0.62	0.33	0.29	0.32	0.31
<b>Al<sub>2</sub>O<sub>3</sub></b>	15.01	17.25	17.44	15.46	17.23	16.72	17.10	18.23
<b>Fe<sub>2</sub>O<sub>3</sub></b>	7.11	6.17	6.47	6.09	5.96	7.34	6.12	4.77
<b>MnO</b>	0.12	0.11	0.11	0.12	0.11	0.12	0.10	0.09
<b>MgO</b>	9.89	9.15	8.74	9.14	9.18	10.98	10.05	8.19
<b>CaO</b>	12.54	12.36	12.17	14.32	12.69	11.81	12.39	12.80
<b>Na<sub>2</sub>O</b>	2.80	2.94	3.07	2.69	2.92	2.67	2.64	3.02
<b>K<sub>2</sub>O</b>	0.11	0.09	0.09	0.10	0.09	0.09	0.09	0.09
<b>P<sub>2</sub>O<sub>5</sub></b>	0.04	0.02	0.02	0.03	0.02	0.02	0.02	0.02
<b>SO<sub>3</sub></b>	0.02	0.01	0.01	0.00	0.02	0.02	0.02	0.01
<b>LOI</b>	0.07	0.16	0.03	0.18	0.25	0.26	0.18	0.58
<b>Ba</b>	10	22	9	18	24	29	42	28
<b>Ce</b>	0	0	0	0	0	0	26	0
<b>Co</b>	31	23	44	34	33	29	22	27
<b>Cr</b>	166	95	696	20	39	44	9	90
<b>Cu</b>	62	22	54	55	49	54	10	91
<b>Ga</b>	14	13	11	14	13	12	30	12
<b>La</b>	4	4	0	0	0	0	6	0
<b>Nd</b>	0	4	3	0	2	6	25	6
<b>Ni</b>	108	68	484	73	70	68	13	99
<b>Pb</b>	5	2	4	6	0	2	2	0
<b>S</b>	743	236	669	890	650	701	174	1072
<b>Sc</b>	33	29	24	38	41	47	18	38
<b>Sr</b>	163	179	131	154	164	145	257	156
<b>Th</b>	0	0	4	2	2	1	0	0

<b>Sample</b>	<b>HAG-16</b>	<b>HAG-17</b>	<b>HAG-18</b>	<b>HAG-19</b>	<b>HAG-20</b>	<b>HAG-21</b>	<b>HAG-22</b>	<b>HAG-23</b>
<b>Depth</b>	1040.76	1083.83	1111.84	1173.38	1217.76	1261.84	1461.49	1492.55
<b>U</b>	0	2	0	2	0	0	0	2
<b>V</b>	119	129	62	155	146	202	81	136
<b>Zn</b>	31	24	35	40	33	31	43	30
<b>Nb</b>	0	1	0	1	0	1	3	0
<b>Rb</b>	1	0	0	1	0	0	1	0
<b>Zr</b>	21	22	22	62	32	45	645	26
<b>Y</b>	7	6	4	16	10	14	56	9

# References

- Abers, G. A., Parsons, B., and Weissel, J. K. (1988). Seamount abundance and distribution in the SW Pacific. *Earth and Planetary Science Letters*, 87: 137-151.
- Adamson, A. C. (1985). Basement lithostratigraphy, Deep Sea Drilling Project Hole 504B. In Anderson, R. N., Honnorez, J., et al., *Initial Reports of the Deep Sea Drilling Project*, 83: Washington (U.S. Govt. Printing Office), 121-127.
- Allan, J. F., Batiza, R., Perfit, M. R., Fornari, D. J., and Sack, R. O. (1989). Petrology of lavas from the Lamont Seamount chain and adjacent East Pacific Rise 10°N. *Journal of Petrology*, 30 (5): 1245-1298.
- Allemendinger, R. W. and Riis, F. (1979). The Galapagos Rift at 86°W: 1. Regional morphological and structural analysis. *Journal of Geophysical Research*, 84 (B10): 5379-5389.
- Allerton, S., Worm, H.-U., Stokking, L. B. (1996). Palaeomagnetic and rock magnetic properties of Hole 896A. In Alt J. C., Kinoshita, H., Stokking, L. B., and Michael, P. J. (Eds.), *Proceedings of the Ocean Drilling Program, Scientific Results*, 148: College Station, TX (Ocean Drilling Program), 217-226.
- Alt, J. C., Kinoshita, H. et al. (1993). Site 896. In Alt, J. C., Kinoshita, H., et al., *Proceedings of the Ocean Drilling Program, Initial Reports*, 148: College Station, TX (Ocean Drilling Program).
- Alt, J. C., Teagle, D. A. H., Laverne, C., Vanko, D. A., Bach, W., Honnorez, J., Becker, K., Ayadi, M., and Pezard, P. A. (1996). Ridge flank alteration of upper oceanic crust in the Eastern Pacific: Synthesis of results for volcanic rocks of Holes 504B and 896A. In Alt J. C., Kinoshita, H., Stokking, L. B., and Michael, P. J. (Eds.), *Proceedings of the Ocean Drilling Program, Scientific Results*, 148: College Station, TX (Ocean Drilling Program), 435-450.
- Alt, J. C., Teagle, D. A. H., Brewer, T. S., Shanks, W. C., and Halliday, A. (1998). Alteration and mineralisation of an oceanic forearc and the ophiolite-ocean crust analogy. *Journal of Geophysical Research*, 103 (B6): 12,365-12,380.
- Anderson, R. N., McKenzie, D., and Sclater, J. G. (1973). Gravity, bathymetry and convection in the Earth. *Earth and Planetary Science Letters*, 18: 391-407.
- Anderson, D. L. (1981). Hotspots, basalts and the evolution of the mantle. *Science*, 213: 82-89.
- Anderson, R. N., McKenzie, D., and Sclater, J. G. (1973). Gravity, bathymetry and convection in the Earth. *Earth and Planetary Science Letters*, 18: 391-407.
- Anderson, R. N., Honnorez, J., et al. (1985). Hole 504B, Leg 83. In Anderson, R. N., Honnorez, J., et al., *Initial Reports of the Deep Sea Drilling Project*, 83: Washington (U.S. Govt. Printing Office), 13-118.
- Autio, L. K., and Rhodes, J. M. (1983). Costa Rica Rift basalts: Geochemical and experimental data from a possible example of multistage melting. In Cann, J. R., Langseth, M. G. et al. (Eds.), *Initial Reports of the Deep Sea Drilling Project*, 69: Washington (U.S. Govt. Printing Office), 729-745.
- Ayadi, M., Pezard, P. A., Laverne, C, and Bronner, G. (1998). Multi-scalar structure at DSDP / ODP Site 504, Costa Rica Rift; I, Stratigraphy of eruptive products and accretion processes.

In Harvey, P. K., and Lovell, M. A. (Eds.) *Core-Log Integration*, Geological Society, London, *Special Publications*, 136: 297-310.

Ballard, R. D., Bryan, W. B., Heirtzler, J. R., Keller, G., Moore, J. G., and van Andel, T. J. (1975). Manned submersible observations in the FAMOUS area: Mid-Atlantic Ridge. *Science*, 190 (4210): 103-108.

Ballard, R. D., Holcomb, R. T., and van Andel, T. H. (1979). The Galapagos Rift at 86°W: 3. Sheet-flows, collapse pits, and lava lakes of the rift valley. *Journal of Geophysical Research*, 84 (B10): 5407-5422.

Barany, I. and Karson, J. A. (1989). Basaltic breccias of the Clipperton Fracture Zone (East Pacific): Sedimentation and tectonics in a fast-slipping oceanic transform. *Geological Society of America Bulletin*, 101: 204-220.

Batiza, R. (1981). Lithospheric age dependence of off-ridge volcano production in the North Pacific. *Geophysical Research Letters*, 8 (8): 545-554.

Batiza, R. (1982). Abundances, distribution and sizes of volcanoes in the Pacific Ocean and the implications for the origin of non-hotspot volcanoes. *Earth and Planetary Science Letters*, 60: 195-206.

Batiza, R. (1984). Inverse relationship between Sr isotope diversity and rate of oceanic volcanism has implications for mantle heterogeneity. *Nature*, 309: 440-441.

Batiza, R. and Vanko, D. (1983). Volcanic development of small oceanic central volcanoes on the flanks of the East Pacific Rise inferred from narrow-beam echo-sounder surveys. *Marine Geology*, 54: 53-90.

Batiza, R., Melson, W. G., and O' Hearn, T. (1988). Simple magma supply geometry inferred beneath a segment of the Mid-Atlantic Ridge. *Nature*, 335: 428-431.

Batiza, R., Smith, T. L., and Niu, Y. (1989). Geological and petrological evolution of seamounts near the East Pacific Rise based on submersible and camera study. *Marine Geophysics Research*, 11: 169-236.

Batiza, R., Niu, Y., and Zayac, W. C. (1990). Chemistry of seamounts near the East Pacific Rise: Implications for the geometry of subaxial mantle flow. *Geology*, 18: 1122-1125.

Becker, K. (1990). Introduction to special section on logging and downhole measurements on DSDP / ODP deep crustal holes. *Journal of Geophysical Research*, 95 (B6): 9149-9151.

Becker, K., Foss, G., *et al.*, (1992). *Proceedings of the Ocean Drilling Program, Initial Reports*, 137: College Station, TX (Ocean Drilling Program).

Becker, K., Sakai, H., *et al.*, (1988). *Proceedings of the Ocean Drilling Program, Initial Reports*, 111: College Station, TX (Ocean Drilling Program).

Bellaiche, G., Cheminee, J. L., Francheteau, J., Hekinian, R., LePichon, X., Needham, H. D., and Ballard, R. D. (1974). Inner floor of the rift valley: First submersible study. *Nature*, 250: 558-560.

Binard, N., Hekinian, R., and Stoffers, P. (1992). Morphostructural study and type of volcanism of submarine volcanoes over the Pitcairn hotspot in the South Pacific. *Tectonophysics*, 206: 245-264.

Bloomer, S. H., Taylor, B., McLeod, C. J., Stern, R. J., Fryer, P., Hawkins, J. W., and Johnson, L. (1995). Early arc volcanism and the ophiolite problem: A perspective from drilling

in the Western Pacific. In *Active Margins and Marginal Basins of the Western Pacific: Geophysical Monograph*, 88: 1-25.

Bonatti, E. (1970). Deep sea volcanism. *Naturwissenschaften*, 57: 379-384.

Bonatti, E. and Harrison, C. G. A. (1988). Eruption styles of basalt in oceanic spreading ridges and seamounts: Effect of magma temperature and viscosity. *Journal of Geophysical Research*, 93(B4): 2967-2980.

Borehole Research Group. (1994). *Wireline Logging Services Guide: A brief description of logging tools*. Lamont-Doherty Earth Observatory. 22p.

Brewer, T. S., Lovell, M., Harvey, P., and Williamson, G. (1995). Stratigraphy of the ocean crust in ODP Hole 896A from FMS images. *Scientific Drilling*, 5: 87-92.

Brewer, T. S., Bach, W., and Furnes, H. (1996). Geochemistry of lavas from Hole 896A. In Alt, J. C., Kinoshita, H., Stokking, L. B., and Michael, P. J. (Eds.), *Proceedings of the Ocean Drilling Program, Scientific Results*, 148: College Station, TX (Ocean Drilling Program), 9-19.

Brewer, T. S., Harvey, P. K., Lovell, M. A., Haggas, S. L., Williamson, G., and Pezard, P. (1998). Ocean floor volcanism; constraints from the integration of core and downhole logging measurements. In Harvey, P. K., and Lovell, M. A. (Eds.), *Core-log Integration. Geological Society Special Publication*, 136: 341-362.

Brown, G. C., and Musset, A. E. (1993). *The Inaccessible Earth*, Chapman and Hall.

Bryan, W. B. and Moore, J. G. (1977). Compositional variations of young basalts in the Mid-Atlantic Ridge rift valley near latitude 36°49'N. *Geological Society of America Bulletin*, 88: 556-570.

Cann, J. R. (1970). New model for the structure of the ocean crust. *Nature*, 226 (5249): 928-930.

Cann, J. R. (1974). A model for oceanic crustal structure developed. *Geophysical Journal of the Royal Astronomical Society*, 39: 169-187.

Cann, J. R., Langseth, M. G., *et al.* (1983). Sites 501 and 504: Sediments and ocean crust in an area of high heat flow on the southern flank of the Costa Rica Rift. In Cann, J. R., Langseth, M. G. *et al.* (Eds.), *Initial Reports of the Deep Sea Drilling Project*, 69: Washington (U.S. Govt. Printing Office), 31-174.

Carlson, R. L. and Herrick, C. N. (1990). Densities and porosities in the oceanic crust and their variations with depth and age. *Journal of Geophysical Research*, 95 (B6): 9153-9170.

Chadwick, W. W., Embley, R. W., and Fox, C. G. (1991). Evidence for volcanic eruption on the southern Juan de Fuca Ridge between 1981 and 1987. *Nature*, 350: 416-418.

Chadwick, W. W. and Embley, R. W. (1994). Lava flows from a mid-1980s submarine eruption on the Cleft Segment, Juan de Fuca Ridge. *Journal of Geophysical Research*, 99 (B3): 4761-4776.

Christensen, N. I. (1970). Composition and evolution of the oceanic crust. *Marine Geology*, 8: 139-154.

Christensen, N. I. (1978). Ophiolites, seismic velocities and oceanic crustal structure. *Tectonophysics*, 47: 131-157.

Cox, K. G. (1988). Numerical modelling of a randomised RTF magma chamber : a comparison with continental flood basalt sequences. *Journal of Petrology*, 29: 681-697.

Detrick, R. S., Buhl, P., Vera, E., Mutter, J., Orcutt, J., Madsen, J., and Brocher, T. (1987). Multi-channel seismic imaging of a crustal magma chamber along the East Pacific Rise. *Nature*, 326:

Detrick, R. S., Mutter, J. C., Buhl, P., and Kim, I. I. (1990). No evidence from multichannel reflection data for a crustal magma chamber in the MARK area on the Mid-Atlantic Ridge. *Nature*, 347: 61-64.

Detrick, R., Collins, J., Stephen, R., and Swift, S. (1994). In situ evidence for the nature of the seismic layer 2/3 boundary in oceanic crust. *Nature*, 370: 288-290.

Dewey, J. F. and Kidd, W. S. F. (1977). Geometry of plate accretion. *Geological Society of America Bulletin*, 88: 960-968.

Dick, H. J. B., Meyer, P. S., Bloomer, S., Kirby, S., Stakes, D., and Mawer, C. (1991a). Lithostratigraphic evolution of an in-situ section of oceanic layer 3. In Von Herzen, R. P., Robinson, P. T., et al. (Eds.), *Proceedings of the Ocean Drilling Program, Scientific Results*, 118: College Station, TX (Ocean Drilling Program), 439-538.

Dick, H. J. B., Schouten, H., Meyer, P. S., Gallo, D. G., Bergh, H., Tyce, R., Patriat, P., Johnson, K. T. M., Snow, J., and Fisher, A. (1991b). Tectonic evolution of the Atlantis II Fracture Zone. In Von Herzen, R. P., Robinson, P. T., et al. (Eds.), *Proceedings of the Ocean Drilling Program, Scientific Results*, 118: College Station, TX (Ocean Drilling Program), 359-398.

Dick, H. J. B., Erzinger, J., Stokking, L. B., et al. (1992). *Proceedings of the Ocean Drilling Program, Initial Reports*, 140: College Station, TX (Ocean Drilling Program)

Dick, H. J. B., Natland, J. H., Miller, J. (1997). *Scientific Prospectus* 176: College Station, TX (Ocean Drilling Program).

Dick, H. J. B., Natland, J. H., Miller, J., et al. (in press). *Proceedings of the Ocean Drilling Program, Initial Reports*, 176: College Station, TX (Ocean Drilling Program).

Dilek, Y., Harper, G. D., Walker, J. E., Allerton, S., and Tartarotti, P. (1996). Structure of upper Layer 2 in Hole 896A. In Alt J. C., Kinoshita, H., Stokking, L. B., and Michael, P. J. (Eds.), *Proceedings of the Ocean Drilling Program, Scientific Results*, 148: College Station, TX (Ocean Drilling Program), 261-279.

DMT-GeoTec / Geo-Engineering. (1996). DMT Color CoreScan Users Manual - Acquisition and Evaluation Software.

Elthon, D. (1979). High magnesia liquids as the parental magma for ocean floor basalts. *Nature*, 278: 514-518.

Elthon, D. (1984). Plagioclase buoyancy in oceanic basalts: Chemical effects. *Geochimica Cosmochimica Acta*, 48: 753-768.

Embley, R. W., Chadwick, W., Perfit, M. R., and Baker, E. T. (1991). Geology of the northern Cleft Segment, Juan de Fuca Ridge: Recent lava flows, seafloor spreading and the formation of megaplumes. *Geology*, 19: 771-775.

Emmermann, R. (1985). Basement geochemistry, Hole 504B. In Anderson, R. N., Honnorez, J., et al., (Eds.), *Initial Reports of the Deep Sea Drilling Project*, 83: Washington (U.S. Govt. Printing Office), 183-200.

- Engel, A. E. J. and Engel, C. G. (1964a). Igneous rocks of the East Pacific Rise. *Science*, 146 (3643) : 477-485.
- Engel, A. E. J. and Engel, C. G. (1964b). Composition of basalts from the Mid-Atlantic Ridge. *Science*, 144: 1330-1333.
- Engel, A. E. J., Engel, C. G., and Havens, R. G. (1965). Chemical characteristics of oceanic basalts and the upper mantle. *Geological Society of America Bulletin*, 76: 719-734.
- Engel, C. G., Fischer, R. L., Engel, A. E. J. (1970). Igneous rocks of the Indian Ocean floor. *Science*, 170: 605-609.
- Ewing, J. and Ewing, M. (1959). Seismic refraction measurements in the Atlantic Ocean basins, in the Mediterranean Sea, on the Mid-Atlantic Ridge, and in the Norwegian Sea. *Geological Society of America Bulletin*, 70: 291-318.
- Fink, J. H. and Griffiths, R. W. (1992). A laboratory analog study of the surface morphology of lava flows extruded from point and line sources. *Journal of Volcanological and Geothermal Research*, 54: 19-32.
- Fisher, R. L., and Sclater, J. G. (1983). Tectonic evolution of the Southwest Indian Ocean since the Mid-Cretaceous: Plate motions and stability of the pole of Antarctica / Africa for at least 80 Myr. *Geophysical Journal of the Royal Astronomical Society*, 73: 553-576.
- Fisher, R. V., and Schmincke, H.-U. (1984). *Pyroclastic Rocks*, Springer-Verlag (Berlin), 472p.
- Fisk, M. R., Bence, A. E., and Schilling, J. G. (1982). Major element chemistry of Galapagos Rift Zone magmas and their phenocrysts. *Earth and Planetary Science Letters*, 61: 171-189.
- Fisk, M. R., Johnson, K. T. M., and Alt, J. C. (1995). Effect of assimilation of altered oceanic crust on magma chemistry: An experimental study. In Erzinger *et al.*, *Proceedings of Ocean Drilling Program, Scientific Results*, 137/140: College Station, TX (Ocean Drilling Program), 43-51.
- Fisk, M. R., McNeill, A. W., Teagle, D. A. H., Furnes, H., and Bach, W. (1996). Data Report: Major-element chemistry of Hole 896A glass. In Alt J. C., Kinoshita, H., Stokking, L. B., and Michael, P. J. (Eds.), *Proceedings of the Ocean Drilling Program, Scientific Results*, 148: College Station, TX (Ocean Drilling Program), 483-487.
- Fitton, J. G., Saunders, A. D., Larsen, L. M., Hardason, B. S., and Norry, M. J., (1997). Volcanic rocks of the southeast Greenland Margin at 63°N: Composition, petrogenesis, and mantle sources. In Saunders, A. D., Larsen, H. C., and Wise, S. W., Jr. (Eds.), *Proceedings of the Ocean Drilling Program, Scientific Results*, 152: College Station, TX (Ocean Drilling Program), 331-350.
- Fornari, D. J., Ryan, W. B. F., and Fox, P. J. (1985). Seafloor lava fields on the East Pacific Rise. *Geology*, 13: 413-416.
- Fornari, D. J., Perfit, M. R., Allan, J. F., Batiza, R., Haymon, R. M., Barone, A. M., Ryan, W. B. F., Smith, T., Simkin, T., and Luckman, M. (1988). Geochemical and structural studies of the Lamont Seamounts: Seamounts as indicators of mantle processes. *Earth and Planetary Science Letters*, 89: 63-83.
- Francheteau, J., Juteau, T., and Rangan, C. (1979). Basaltic pillars in collapsed lava pool on the deep ocean floor. *Nature*, 281: 209-211.

Francheteau, J. and Ballard, R. D. (1983). The East Pacific Rise near 21°N, 13°N and 20°S: Inferences for along-strike variability of axial processes of the mid-ocean ridge. *Earth and Planetary Science Letters*, 64: 93-116.

Fujii, T. and Bougalt, H. (1983). Melting relations of a magnesian abyssal tholeiite and the origin of MORBs. *Earth and Planetary Science Letters*, 62: 283-295.

Furnes, H. and Fridleifsson, I. B. (1979). Pillow block breccia: occurrences and mode of formation. *Neues Jahrbuch fur Geologie und Palaontologie (Monatshefte)*, 3: 147-154.

Gass, I. G. (1968). Is the Troodos Massif of Cyprus a fragment of Mesozoic ocean floor. *Nature*, 220: 39-42.

Gente, P., Auzende, J. M., Renard, V., Fouquet, Y., and Bideau, D. (1986). Detailed geological mapping by submersible of the East Pacific Rise axial graben near 13°N. *Earth and Planetary Science Letters*, 78: 224-236.

Gente, P., Ceuleneer, G., Dauteuil, O., Dymont, J., Honsho, C., Laverne, C., Le Turdu, C., Mitchell, N. C., Ravilly, M., and Thibaud, R. (1996). On- and off-axis submersible investigations of an highly magmatic segment of the Mid-Atlantic ridge (21°40'N): the TAMMAR cruise. *InterRidge News*, 5: 27-31.

Gonçalves, C., A. (1995). *Characterisation of formation heterogeneity*. Ph. D. Thesis. University of Leicester.

Green, D. H., Hibberson, W. O., and Jaques, A. L. (1979). Petrogenesis of mid-ocean ridge basalts. In McElhinny, M. W. (Ed.), *The Earth; Its origin, structure and evolution*, 265-295.

Gregg, T. K. P. and Fink, J. H. (1995). Quantification of submarine lava-flow morphology through analog experiments. *Geology*, 23 (1): 73-76.

Griffiths, R. W. and Fink, J. H. (1992). Solidification and morphology of submarine lavas: A dependence on extrusion rate. *Journal of Geophysical Research*, 97 (B13): 19,729-19,737.

Grove, T. L., Kinzler, R. J., and Bryan, W. B. (1992). Fractionation of mid-ocean ridge basalt. In Morgan, J. P., Blackman, D. K., and Sinton, J. M. *Mantle Flow and Melt Generation at Mid-Ocean Ridges*, American Geophysical Union. 71: 50-75.

Hale, L. D., Morton, C. J., and Sleep, N. H. (1982). Reinterpretation of seismic reflection data over the East Pacific Rise. *Journal of Geophysical Research*, 87 (B9): 7707-7717.

Harper, G. D. and Tartarotti, P. (1996). Structural evolution of upper layer 2, Hole 896A. In Alt J. C., Kinoshita, H., Stokking, L. B., and Michael, P. J. (Eds.), *Proceedings of the Ocean Drilling Program, Scientific Results*, 148: College Station, TX (Ocean Drilling Program), 245-259.

Harrison, C. G. A. and Bonatti, E. The oceanic lithosphere. In Emiliani, C. (Ed.), *The Sea*. (Wiley-InterScience), 7: 21-48.

Haymon, R. M., Fornari, D. J., Von Damm, K. L., Lilley, M. D., Perfit, M. R., Edmond, J. M., Shanks, W. C., Lutz, R. A., Grebmeier, J. M., Carbotte, S., Wright, D., McLaughlin, E., Smith, M., Beedle, N., and Olson, E. (1993). Volcanic eruption of the mid-ocean ridge along the East Pacific Rise crest at 9°45'-52'N: direct submersible observations of seafloor phenomena associated with an eruption event in April, 1991. *Earth and Planetary Science Letters*, 119: 85-101.

Herron, T. J., Stoffa, P. L., and Buhl, P. (1980). Magma chambers and mantle reflections - East Pacific Rise. *Geophysical Research Letters*, 7(11): 989-992.

Hey, R., Johnson, L., and Lowrie, A. (1977). Recent plate motion in the Galapagos Area. *Geological Society of America Bulletin*, 88: 1385-1403.

Hill, M. N. (1957). Recent geophysical exploration of the ocean floor. In Ahrens, L. H., et al., (Eds.), *Physics and Chemistry of the Earth*, 5 (2): 129-163.

Holden, J. C. and Dietz, R. S. (1972). Galapagos Gore, NazCoPac Triple Junction and Carnegie / Cocos Ridges. *Nature*, 235: 266-269.

Hon, K., Kauahikaua, Denlinger, J., R., and Mackay, K. A. (1994). Emplacement and inflation of pahoehoe sheet flows: Observations and measurements of active lava flows on Kilauea Volcano, Hawaii. *Geological Society of America Bulletin*, 106: 351-370.

Honnorez, J. and Kirst, P. (1975). Submarine basaltic volcanism: morphometric parameters for discriminating hyaloclastites from hyalotuffs. *Bulletin of Volcanology*, 39 (3): 441-465.

Honnorez, J., Laverne, C., Hubberten, H.-W., Emmermann, R., and Muehlenbachs, K. (1983). Alteration processes in layer 2 basalts from DSDP Hole 504B, Costa Rica Rift. In Cann, J. R., Langseth, M. G., et al., *Initial Reports of the Deep Sea Drilling Project*, 69: Washington (U.S. Govt. Printing Office), 509-546.

Houtz, R. and Ewing, J. (1976). Upper crustal structure as a function of plate age. *Journal of Geophysical Research*, 81 (14): 2490-2498.

Hubberten, H. -W., Emmermann, R., and Puchelt, H. (1983). Geochemistry of basalts from Costa Rica Rift Sites 504 and 505 (Deep Sea Drilling Project Legs 69 and 70). In Cann, J. R., Langseth, M. G., et al., *Initial Reports of the Deep Sea Drilling Project*, 69: Washington (U.S. Govt. Printing Office), 791-803.

Kay, R., Hubbard, N. J. and Gast, P. W. (1970). Chemical characteristics and origin of oceanic ridge volcanic rocks. *Journal of Geophysical Research*, 75(8): 1585-1613.

Kempton, P. D., Autio, L. K., Rhodes, J. M., Holdaway, M. J., Dungan, M. A., Johnson, P. (1985). Petrology of basalts from Hole 504B, DSDP Leg 83. In Anderson, R. N., Honnorez, J., et al. (Eds.), *Initial Reports of the Deep Sea Drilling Project*, 83: Washington (U.S. Govt. Printing Office), 129-164.

Kennish, M. J. and Lutz, R. A. (1998). Morphology and distribution of lava flows on mid-ocean ridges: A review. *Earth Science Reviews*, 43: 63-90.

Kidd, K. W. and Cann, J. R. (1974). Chilling statistics indicate an ocean-floor spreading origin for the Troodos Complex, Cyprus. *Earth and Planetary Science Letters*, 24: 151-155.

Kidd, R. G. W. (1977). A model for the process of formation of the upper oceanic crust. *Geophysical Journal of the Royal Astronomical Society*, 50: 149-183.

Klein, E. M. and Langmuir, C. H. (1987). Global correlations of ocean ridge basalt chemistry with axial depth and crustal thickness. *Journal of Geophysical Research*, 92(B4): 8089-8115.

Klein, E. M. and Langmuir, C. H. (1989). Local versus global variations in ocean ridge basalt composition: a reply. *Journal of Geophysical Research*, 94(B4): 4241-4252.

Kurnosov, V. B., Kholdkevich, I. V., Chubarov, V. M., and Schevchenko, A. Y. (1983). Secondary minerals in basalt from the Costa Rica Rift, Holes 501 and 504B, Deep Sea Drilling Project Legs 68, 69 and 70. In Cann, J. R., Langseth, M. G., et al., *Initial Reports of the Deep Sea Drilling Project*, 69: Washington (U.S. Govt. Printing Office), 573-583.

Kusznir, N. J. and Bott, M. H. P. (1976). A thermal study of the formation of oceanic crust. *Geophysical Journal of the Royal Astronomical Society* 47,: 83-95.

Langmuir, C. H. and Hanson, G. N. (1980). An evaluation of major element heterogeneity in the mantle sources of basalts. *Philosophical Transactions of the Royal Society London*, A297: 383-407.

de Larouziere, F. D., Pezard, P. A., Ayadi, M., and Becker, K. (1996). Downhole measurements and electrical images in Hole 896A, Costa Rica Rift. In Alt J. C., Kinoshita, H., Stokking, L. B., and Michael, P. J. (Eds.), *Proceedings of the Ocean Drilling Program, Scientific Results*, 148: College Station, TX (Ocean Drilling Program), 375-388.

Laverne, C., Belarouchi, A., and Honnorez, J. (1996). Alteration mineralogy and chemistry of the upper oceanic crust from Hole 896A (Costa Rica Rift). In Alt J. C., Kinoshita, H., Stokking, L. B., and Michael, P. J. (Eds.), *Proceedings of the Ocean Drilling Program, Scientific Results*, 148: College Station, TX (Ocean Drilling Program), 151-170.

Lewis, T. R. (1983). The process of formation of ocean crust. *Science*, 220 (4593): 151-156.

Lonsdale P. (1977). Abyssal pahoehoe with lava coils at the Galapagos Rift. *Geology*, 5: 147-152.

Lonsdale, P. (1983). Laccoliths (?) and small volcanoes on the flank of the East Pacific Rise. *Geology*, 11: 706-709.

Lonsdale, P. and Batiza, R. (1980). Hyaloclastite and lava flows on young seamounts examined with a submersible. *Geological Society of America Bulletin*, 91: 545-554.

Ludwig, W. J., Nafe, J. E., and Drake, C. L. (1970). Seismic refraction. In Maxwell, A. E. (Ed.), *The Sea* 4.1: (Wiley - InterScience), 53-84.

Luyendyk, B. P. and Macdonald, K. C. (1977). Physiography and structure of the inner floor of the FAMOUS rift valley: Observations with a deep-towed instrument package. *Geological Society of America Bulletin*, 88: 648-663.

Macdonald, G. A. (1967). Forms and structure of extrusive basaltic rocks. In Hess, H. H., and Poldervaart, A. (Eds.), *Basalts: The Poldervaart Treatise on Rocks of Basaltic Composition.*, InterScience: 66-87.

Macdonald, K. C. (1982). Mid-ocean ridges: Fine-scale tectonic, volcanic and hydrothermal processes within the plate boundary zone. *Annual Review of Earth and Planetary Science*, 10: 155-190.

Macdonald, K. C. and Fox, P. J. (1988). The axial summit graben and cross-sectional shape of the East Pacific Rise as indicators of axial magma chambers and recent volcanic eruptions. *Earth and Planetary Science Letters*, 88: 119-131.

Macdonald, K. C. and Luyendyk, B. P. (1977). Deep tow studies of the structure of the Mid-Atlantic Ridge crest near Lat. 37°N. *Geological Society of America Bulletin*, 88: 621-636.

Macdougall, J. D. and Lugmair, G. W. (1985). Extreme isotopic homogeneity among basalts from the southern East Pacific Rise: Mantle or mixing effect? *Nature*, 313: 209-211.

Marsh, N. G., Tarney, J., and Hendry, G. L. (1983). Trace element geochemistry of basalts from Hole 504B, Panama Basin, Deep Sea Drilling Project Legs 69 and 70. In Cann, J. R., Langseth, M. G., et al., *Initial Reports of the Deep Sea Drilling Project*, 69: Washington (U.S. Govt. Printing Office), 747-763.

Maxwell, A. E., *et al.* (1970). *Initial Reports of the Deep Sea Drilling Project, 3*: Washington (U.S. Govt. Printing Office).

McClain, J. S. and Lewis, B. T. R. (1982). Geophysical evidence for the absence of a crustal magma chamber under the northern Juan de Fuca Ridge: A contrast with ROSE results. *Journal of Geophysical Research*, 87 (B10): 8477-8489.

McCulloch, M. T. and Cameron, W. E. (1983). Nd-Sr isotopic study of primitive lavas from the Troodos ophiolite, Cyprus: Evidence for a subduction-related setting. *Geology*, 11: 727-731.

Miyashiro, A. (1973). The Troodos ophiolitic complex was probably formed in an island arc. *Earth and Planetary Science Letters*, 19: 218-224.

Miyashiro, A., Shido, F., and Ewing, M. (1970). Crystallisation and differentiation in abyssal tholeiites and gabbros from mid-ocean ridges. *Earth and Planetary Science Letters*, 7: 361-365.

Moore, J. G. (1975). Mechanisms of formation of pillow lavas. *American Scientist*, 63: 269-277.

Moores, E. M. and Vine, F. J. (1971). The Troodos Massif, Cyprus and other ophiolites as oceanic crust: Evaluation and implications. *Philosophical Transactions of the Royal Society, London*, A268: 443-466.

Natland, J. H., Adamson, A. C., Laverne, C., Melson, W. G., and O'Hearn, T. (1983). A compositionally nearly steady-state magma chamber at the Costa Rica Rift: Evidence from basalt glass and mineral data, DSDP Sites 501, 504 and 505. *In* Cann, J. R., Langseth, M. G., *et al.*, *Initial Reports of the Deep Sea Drilling Project*, 69: Washington (U.S. Govt. Printing Office), 811-858.

Natland, J. H., Dick, H. J. B., and Leg 176 Shipboard Scientific Party. (1998). A long gabbro section in the ocean crust: Results of Leg 176 drilling, Southwest Indian Ridge. *Joides Journal*, 24 (2): 11-14.

Nicholls, G. D., Nalwalk, A. J., and Hays, E. E. (1964). The nature and composition of rock samples dredged from the Mid-Atlantic Ridge between 22° and 52°N. *Marine Geology*, 1: 333-343.

Nisbet E. G. and Fowler, C. M. R. (1978). The Mid-Atlantic Ridge at 37 and 45°N: Some geophysical and petrological constraints. *Geophysical Journal of the Royal Astronomical Society*, 54: 631-660.

Noack, Y., Emmermann, R., and Hubberten, H.W. (1983). Alteration in Site 501 (Leg 68) and Site 504 (Leg 69) basalts: Preliminary results. *In* Cann, J. R., Langseth, M. G., *et al.*, *Initial Reports of the Deep Sea Drilling Project*, 69: Washington (U.S. Govt. Printing Office), 497-508.

Norris, R. D., Kroon, D., Klaus, A., *et al.* (1998). *Proceedings of the Ocean Drilling Program, Initial Reports*, 171B: College Station, TX (Ocean Drilling Program).

ODP (1998). *ODP's Greatest Hits*. (Ocean Drilling Program).

O'Hara, M. J. (1965). Primary magmas and the origin of basalts. *Journal of Geology*, 1 (1): 19-40.

O' Hara, M. J. (1968). Are ocean basalts primary magma? *Nature*, 220: 683-686.

- O'Hara, M. J. (1977). Geochemical evolution during fractional crystallisation of a periodically refilled magma chamber. *Nature*, 266: 503-507.
- Orcutt, J., Kennet, B., Dorman, L., and Prothero, W. (1975). A low velocity zone underlying a fast-spreading ridge crest. *Nature*, 256: 475-476.
- Pallister, J. S. and Hopson, C. A. (1981). Samail ophiolite plutonic suite: Field relations, phase variation, cryptic variation and layering, and a model of a spreading ridge magma chamber. *Journal of Geophysical Research*, 86 (B4): 2593-2644.
- Pearce, J. A. (1975). Basalt geochemistry used to investigate past tectonic environments on Cyprus. *Tectonophysics*, 25: 41-67.
- Pearce, J. A., Lippard, S. J., and Roberts, S. (1984). Characteristics and tectonic significance of supra-subduction zone ophiolites. In Kokelaar, B. P., and Howells, M. F. (Eds.) *Marginal Basin Geology: The Geological Society Special Publication*, 16: 77-94.
- Pelling, R. (1992). *Integrated geophysical-geochemical studies of the oceanic crust*. Ph.D. Thesis, University of Leicester.
- Pezard, P. A. (1990). *On electrical properties of rocks, with implications for the structure of the upper oceanic crust*. Ph.D. Thesis. University of Columbia.
- Presnall, D. C., Dixon, J. R., O'Donnell, T. H., and Dixon, S. A. (1979). Generation of mid-ocean ridge tholeiites. *Journal of Petrology*, 20 (1): 3-35.
- Presnall, D. C. and Hoover, J. D. (1987). High pressure phase equilibrium constraints on the origin of Mid-Ocean Ridge Basalt. In Mysen, B. O. (Ed.), *Magmatic Processes: Physiochemical principles*. *The Geochemical Society Special Publication*, 1: 75-89.
- Raitt, R. W. (1956). Seismic refraction studies of the Pacific Ocean Basin. *Geological Society of America Bulletin*, 67: 1623-1640.
- Rautenschlein, M., Jenner, G. A., Hertogen, J., Hofmann, A. W., Kench, R., Schmincke, H.-U., and White, W. M. (1985). Isotopic and trace element composition of volcanic glasses from the Akaki Canyon, Cyprus: Implications for the origin of the Troodos ophiolite. *Earth and Planetary Science Letters*, 75: 369-383.
- Reid, I. and Jackson, H.R. (1981). Oceanic spreading rate and crustal thickness. *Marine Geophysical Research*, 5: 165-172.
- Renard, V., Hekinian, R., Francheteau, J., Ballard, R. D., and Backer, H. (1985). Submersible observations at the axis of the ultra-fast spreading East Pacific Rise. *Earth and Planetary Science Letters*, 75: 339-353.
- Reynolds, J. R., Langmuir, C. H., Bender, J. F., Kastens, K. A., and Ryan, W. B. F. (1992). Spatial and temporal variability in the geochemistry of basalts from the East Pacific Rise. *Nature*, 359: 493-499.
- Reynolds, J. R. and Langmuir, C. H. (1997). Petrological systematics of the Mid-Atlantic Ridge south of Kane: Implications for ocean crust formation. *Journal of Geophysical Research*, 102 (87): 14,915-14,946.
- Robinson, P. T., Von Herzen, R., Adamson, A. C., et al. (1989). *Proceedings of the Ocean Drilling Program, Initial Reports*, 118: College Station, TX (Ocean Drilling Program).
- Robson, D. and Cann, J. R. (1982). A geochemical model of mid-ocean ridge magma chambers. *Earth and Planetary Science Letters*, 60: 93-104.

Schmincke, H., Rautenschlein, M., Robinson, P. T., and Mehegan, J. M. (1983). Troodos extrusive series of Cyprus: A comparison with oceanic crust. *Geology*, 11: 405-409.

Sempere, J. C., Purdy, G. M., and Schouten, H. (1990). Segmentation of the Mid-Atlantic Ridge between 24°N and 30°40'N. *Nature*, 344: 427-431.

Sempere, J. C., Lin, J., Brown, H. S., Schouten, H., and Purdy, G. M. (1993). Segmentation and morphotectonic variations along a slow-spreading centre: The Mid-Atlantic Ridge (24°00'N - 30°40'N). *Marine Geophysical Research*, 15: 153-200.

Shen, Y., Forsyth, D. W., Scheirer, D. S., and Macdonald, K. C. (1993). Two forms of volcanism: implications for mantle flow and off-axis crustal production on the west flank of the southern East Pacific Rise. *Journal of Geophysical Research*, 98 (B10): 17,875-17,889.

Sinton J. M. and Detrick, R. S. (1992). Mid-ocean ridge magma chambers. *Journal of Geophysical Research*, 97 (B1): 197-216.

Sleep, N. H. (1975). Formation of the oceanic crust, some thermal constraints. *Journal of Geophysical Research*, 80 (29): 4037-4042.

Sleep, N. H. (1984). Tapping of magmas from ubiquitous mantle heterogeneities: An alternative to mantle plumes? *Journal of Geophysical Research*, 89 (B12): 10,029-10,041.

Smith, D. K. (1988). Shape analysis of Pacific seamounts. *Earth and Planetary Science Letters*, 90: 457-466.

Smith, D. K. and Cann, J. R. (1990). Hundreds of small volcanoes on the median valley floor of the Mid-Atlantic Ridge at 24-30°N. *Nature*, 348: 152-155.

Smith, D. K. and Cann, J. R. (1992). The role of seamount volcanism in crustal construction at the Mid-Atlantic Ridge (24°-30°N). *Journal of Geophysical Research*, 97 (B2): 1645-1658.

Smith, D. K. and Cann, J. R. (1993). Building the crust at the Mid-Atlantic Ridge. *Nature*, 365: 707-715.

Smith, T. L. and Batiza, R. (1989). New field and laboratory evidence for the origin of hyaloclastite flows on seamount summits. *Bulletin of Volcanology*, 51: 96-114.

Sparks, R. S. J., Meyer, P., and Sigurdsson, H. (1980). Density variation amongst Mid-Ocean Ridge Basalts: Implications for magma mixing and the scarcity of primitive lavas. *Earth and Planetary Science Letters*, 46: 419-430.

Stakes, D. S., Shervais, J. W., and Hopson, C. A. (1984). The volcanic-tectonic cycle of the FAMOUS and AMAR valleys, Mid-Atlantic Ridge (36°47'N): Evidence from basalt glass and phenocryst compositional variations for a steady-state magma chamber beneath the valley mid-sections, AMAR 3. *Journal of Geophysical Research*, 89: 6995-7028.

Stolper, E. (1980). A phase diagram for Mid-Ocean Ridge Basalts: Preliminary results and implications for petrogenesis. *Contributions to Mineralogy and Petrology*, 74: 13-27.

Sun, S., Nesbitt, R. W., and Sharaskin, A. Y. (1979). Geochemical characteristics of mid-ocean ridge basalts. *Earth and Planetary Science Letters*, 44: 119-138.

Tazieff, H. (1972). About deep-sea volcanism. *Geologische Rundschau*, 61: 470-490.

Teagle, D. A. H., Alt, J. C., Bach, W., Halliday, A. N., and Erzinger, J. (1996). Alteration of upper oceanic crust in a ridge-flank hydrothermal upflow zone: mineral, chemical and isotopic

constraints from Hole 896A. In Alt J. C., Kinoshita, H., Stokking, L. B., and Michael, P. J. (Eds.), *Proceedings of the Ocean Drilling Program, Scientific Results*, 148: College Station, TX (Ocean Drilling Program), 119-150.

van Andel, T. H. and Ballard, R. D. (1979). The Galapagos Rift at 86°W: 2. Volcanism, structure and evolution of the rift valley. *Journal of Geophysical Research*, 84 (B10): 5390-5405.

Viereck, L. G., Flower, M. F. J., Hertogen, J., Schmincke, H.-U., and Jenner, G. A. (1989). The genesis and significance of N-MORB sub-types. *Contributions to Mineralogy and Petrology*, 102: 112-126.

Vuagnat, M. (1975). Pillow lava flows: Isolated sacks or connected tubes? *Bulletin of Volcanology*, 39: 581-589.

Walker G. P. L. (1973). Lengths of lava flows. *Philosophical Transactions of the Royal Society London*, A274: 107-118.

Walker G. P. L. (1992). Morphometric study of pillow-size spectrum among pillow lavas. *Bulletin of Volcanology*, 54: 459-474.

Wells, G., Bryan, W. B., and Pearce, T. H. (1979). Comparative morphology of ancient and modern pillow lavas. *Journal of Geology*, 87: 427-440.

Wilkinson, J. F. G. (1982). The genesis of mid ocean ridge basalt. *Earth Science Reviews*, 18: 1-57.

Worthington, P. F. (1994). Borehole measurements beneath the seafloor. *Oceanus*, 36 (4): 129-133.